Design and Synthesis of 3-Dimensional Fragments to Explore Pharmaceutical Space

Mary Christine Wheldon

Doctor of Philosophy

University of York

Chemistry

September 2016

Abstract

This thesis describes an approach to the design, analysis and synthesis of saturated nitrogen heterocyclic fragments to explore pharmaceutical space. Firstly, the development of a computational protocol for the shape analysis of fragments is described (Chapter 2). Principal moments of inertia (PMI) plots were used to generate a set of selection criteria to select compounds found in the 3-dimensional area of the PMI plot. The computational method was applied to different scaffolds, piperidine, pyrrolidine and azepane, to generate a 3-dimensional fragment library.

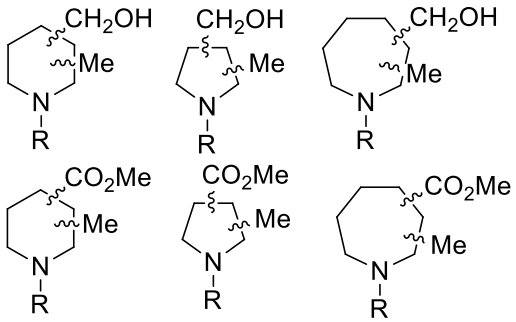

Structures of fragments analysed

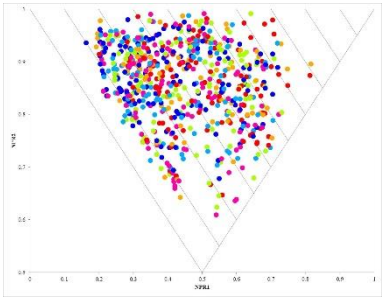

Example PMI plot

The computational analysis of a disubstituted piperidine fragment library provided a 20 compound sub-set library for synthesis. The progress of this synthesis is described (Chapter 3). Six final fragments (shown below) have been prepared and synthesis towards ten of the other fragments is reported. The synthesis was planned with careful consideration of synthetic routes to minimise the number of different steps and routes employed.

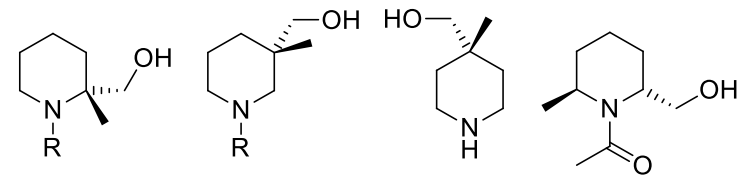

Finally, the application of our computational protocol to a virtually enumerated lead-like library is presented (Chapter 4). The shape diversity and physicochemical properties of 190 different lead-like compounds from six different saturated nitrogen heterocyclic scaffolds is described. The analysis of these data to select compounds with suitable lead-like properties and interesting 3-dimensional shapes is summarised.

List of contents

List of Tables

Acknowledgments

I would firstly like to thank my supervisor Professor Peter O'Brien. His help, encouragement and direction have been vital and without his support the research presented here would not have been possible. I would also like to thank Professor Richard Taylor for assistance and guidance as my independent panel member.

A special thank you must go to Paul Bond for his help and assistance with the development of the computational protocol, which wouldn't have been possible without our meetings in the pub.

For all their help and support, I would like to thank Heather for VT NMRs and the NMR service, Karl for mass spectrometry, Mike and Steve in stores, and Graeme McAllister for keeping the labs up and running.

Thank you to all the members of the POB group, past and present, for good discussions, laughs and support. In no particular order, Peter, Donald, Giacomo, Nah, Sarah, Alice, Josh, Adam, Mickey, Will, Masakazu, Paul, Tom, Ike, Laura D and Laura W. Thanks also to Joe who added a lot to D215, mainly glassware and chemicals but some fun too, and all the members of the Taylor group for interesting discussions and advice.

Thanks to all the members of "LunchSoc" who provided a welcome break from the lab most days, Matt, Ryan, Sarah, George, Tom and Aimee, as well as all my close friends who reminded me there is life outside of chemistry, especially Kirsty, Charlotte and Jess.

I would like to thank all of my family, especially my Mum and Dad, for their love and support throughout all of this and for looking after me when I needed it.

Finally, a very special thank you must go to Dave, who has not only had to deal with his own PhD but who has had to put up with my tears, stress and happiness over the last four years, I couldn't have done any of this without you!

Author's Declaration

The research presented in this thesis is, to the best of my knowledge, original except where due reference has been made to other authors. Computational protocol development was conducted in collaboration with Rod Hubbard and Paul Bond at York Structural Biology Laboratory. This work has not previously been presented for an award at this, or any other, University. All sources are acknowledged as References.

Chapter 1: Introduction

Drug discovery has changed and developed over many years to fit with the key needs and facilities of the time. There have been a number of methods developed to find suitable leads for drug development programmes. These have included discovery of drugs from natural products with known biological activity, development of drugs from existing leads or drugs, also known as patent busting and high-throughput screening (HTS), the screening of a very large number of lead-like compounds against a given target.[1] Each of these methods has had a significant impact on drug development over history, with many success stories.[2] However, each of these methods has pitfalls and there is a constant need to rethink and readjust drug discovery methods to drive forward programmes and discoveries of new leads for ever more challenging targets.

Recently, a shift in drug development has occurred with the drawbacks of screening lead-like molecules emerging. Rees and co-workers reported that hit rates are generally low in high throughput screens, with progression of only a small number of compounds.[2,3] There have also been a number of discussions relating to the increase in lipophilicity and molecular weight during lead optimisation as a result of the use of optimising against hydrophobic interactions to increase potency.[2,4] In addition, a number of reports link the high molecular weight and lipophilicity to drug attrition in later stages of drug development.[1,4,5] It was noted that compounds successful in clinical trials had, on average, a lower molecular weight than those at early stage development.[1,6] Less polar, more lipophilic compounds are also being linked to toxic effects and it was shown that a high molecular weight and lipophilicity have a significant effect on absorption, distribution and metabolism properties.[1,7] A reduction in the molecular weight and lipophilicity of screening collections might lessen or eliminate these issues.[1,2]

This is exemplified by the schematic diagram published by Rees (Figure 1.1). During optimisation, molecular weight and lipophilicity increases, as discussed above. It can be seen from Figure 1.1, that an increase in these properties for a smaller compound, or fragment, would give a final compound still within the desirable area of properties.

However, with a larger lead-like compound, a similar increase in molecular weight and lipophilicity would give a compound outside the desirable area.[3]

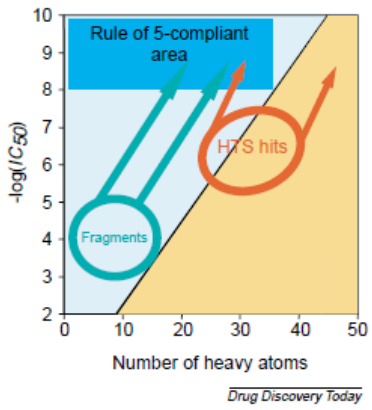

Figure 1.1: Figure showing the relationship between number of heavy atoms and potency. The number of heavy atoms increases as potency increases. Fragments have a better chance of remaining in the Rule of 5 compliant area as they start with a lower number of heavy atoms.[3]

This reduction in the size of compounds in screening libraries and the development of new libraries to investigate this paved the way for the introduction of fragment-based drug discovery (FBDD).

1.1 Fragment-based drug discovery

Fragment screening was first reported by Fesik and co-workers in 1996.[8] Here, small, low molecular weight ligands were screened against a protein target using NMR spectroscopy. After the initial ligand was found to bind, screening of close analogues provided an optimised ligand. Another ligand was then sought to bind in an adjacent site, repeating the optimisation process. After this, the two ligands, binding with 2 µM and 100 µM affinity respectively were linked to produce a compound with 19 nM affinity (Figure 1.2 and Figure 1.3).

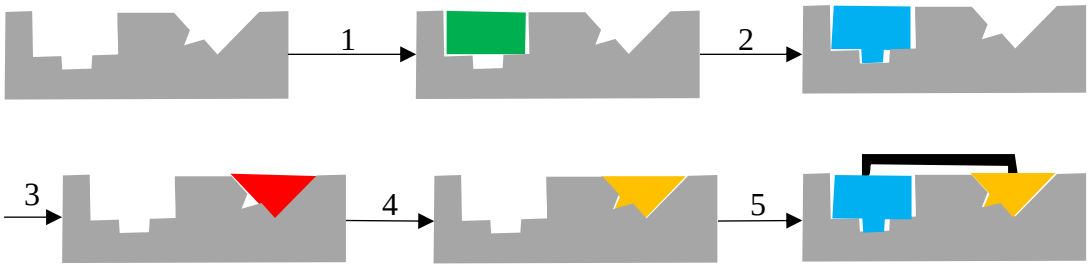

Figure 1.2: The premise of fragment-based drug discovery schematic; (1) Screen for first ligand, (2) Optimise first ligand, (3) Screen for second ligand, (4) Optimise second ligand, (5) Link Ligands

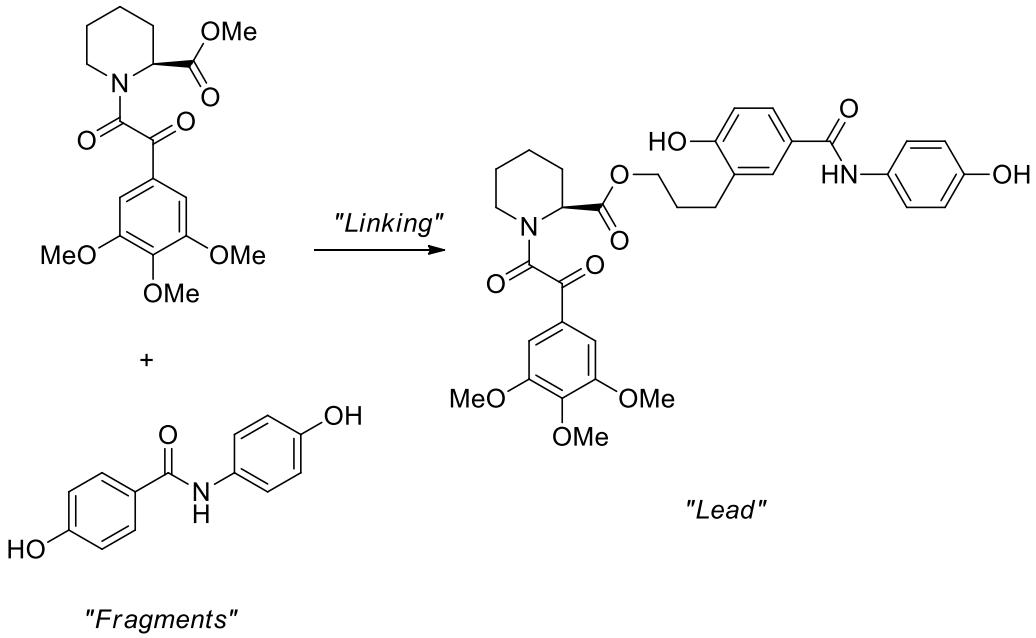

Figure 1.3: The premise of fragment-based drug discovery in chemical terms; finding, optimising and linking small molecules, "fragments", to develop lead compounds for drug development.[8]

Here, Fesik highlighted the benefit of this method: although the unlinked molecules have low affinity (micromolar to millimolar), after linking the binding affinity is the combined binding constants less the change for linking. Therefore, a compound in the micromolar binding range can be obtained from two millimolar binding range compounds.[8]

Since this publication, there has been significant growing interest in fragment screening and development of this method of drug discovery. Jhoti and colleagues noted that after analysis of fragments in the Astex screening library, the fragments generally had the same properties. Typically, they are small molecules of molecular weight less than 300 Da, have a *c*LogP less than 3 and have less than 3 hydrogen bond donors and acceptors. They also noted that the number of rotatable bonds is less than 3 and polar surface area is less than 60 $Å^2$.[9,10] As a result, these fragment properties were termed the "Rule of 3", in a similar vein to the "Rule of 5" outlined by Lipinski for orally available drugs.[11]

An advantage of screening small molecular weight fragments is that chemical space can be sampled more effectively. For larger, drug-like, compounds with around 30 heavy atoms or molecular weight around 500 Da, chemical space is covered by around 10^{60} compounds.[1,12,13] By reducing the size of the screened molecules to around 12 heavy atoms, the size of chemical space decreases to around 10^7.[12] This means that a lead-like screening library of 1 million compounds covers an infinitesimally small area of chemical space.[14] However, screening a library of compounds with less than 12 heavy atoms covers approximately 0.001% of the available chemical space.[5,13] A library of around 1000 fragments can have the same chemical diversity as a 10,000,000 compound lead-like library.[15,16]

Another advantage of small fragments over large lead-like compounds is the number of hits obtained from screening. Generally, the number of hits obtained from HTS is often considerably lower than would be expected and lower than with fragment screening. A number of reports have noted that as the size or complexity of a molecule

increases there is a greater probability of mis-matches with the binding site. This may be due to poor complementarity with the target protein and sub-optimal interactions and clashes.[1,3,5,12,13,17] Therefore, since smaller molecules or fragments have a lower chance of forming these clashes or mis-matches, hit rates are in fact higher.[2]

This view of complexity was, however, noted by Hann and Leach to be taken cautiously. As the complexity of the ligand decreases, the ability to detect binding decreases.[18] It has been well reported that although fragments have a higher hit rate, the binding affinity is much weaker.[4,12,13,19] Therefore, decreasing the complexity of compounds will only be beneficial if the binding can be detected.[18] This has been summarised well by Zartler and Shapiro.[4] Figure 1.4 shows how the chance of measuring binding increases with ligand complexity, although the probability of finding a match decreases, as there is an increased possibility of negative interactions with more complex ligands.[4] The chance of the binding mode being unique, however, increases with complexity. Ultimately, there is a better chance of finding a detectable and unique binding mode in a final compound if molecules start off simpler and smaller.[15]

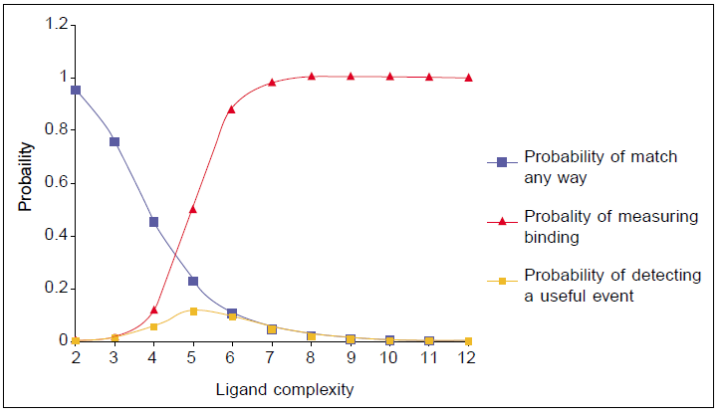

Figure 1.4: Graph showing the probability of a match with the target decreasing as the probability of measuring binding increases.[4]

Although binding affinity is low for smaller fragment-like molecules, when binding is detected, the interactions are generally as efficient and, if not, better quality than those formed by larger lead-like molecules.[5,12] Generally, all the available points of interaction are used in the binding of fragments and therefore fragments are more efficient binders. It was also noted in a report by Murray and Rees that for a fragment

with 100 μM affinity, the fragment binds with a free energy of –22.8 kJ mol^{-1}. This can be compared to a large drug-sized molecule with an affinity of 3 nM, which binds with a free energy of –63.6 kJ mol^{-1}. Clearly, the ratio of size to binding energy is much higher for that of the fragment. They conclude that it is this high energy binding compared to the molecular weight of the fragment that provides the key to such high quality binding.[1] This also forms the basis for ligand efficiency. Ligand efficiency is the binding free energy for a ligand divided by the number of heavy atoms in the ligand. This metric is useful to determine the impact of increasing molecular bulk on the activity of the compound. Generally fragments have very good ligand efficiency due to their small size and efficient interactions.[20] Therefore measuring ligand efficiency of fragment hits and through fragment development can ensure a high quality ligand with good potency for the given molecular weight.

Due to the weak binding, fragments generally need to be screened at a high concentration.[4,21] Therefore, screening methods need to be capable of detecting such interactions. Fragments generally bind with an affinity of between 10 mM and 100 μM, which is much weaker than the affinities usually observed in HTS and therefore normal biochemical *in vitro* receptor assays are not suitable.[1] A number of biophysical methods such as NMR spectroscopy, X-ray crystallography, surface plasmon resonance (SPR) and thermal shift that are used to screen fragments are detailed below.[2,19] These are often used orthogonally to generate a detailed picture of fragment binding.[19,22]

In the seminal paper on fragment screening by Fesik and co-workers,[8] NMR spectroscopy was used to detect binding and to aid development of selected fragments. NMR spectroscopy is a common method used in fragment screening as it is a relatively high throughput method. There are two general types of NMR spectroscopy screening methods, ligand-detected NMR spectroscopy and protein-detected NMR spectroscopy. For both of these methods, a large number compounds can be screened.[3] In ligand-detected NMR spectroscopy, information can be obtained to distinguish active site versus non-active site binders, whereas in protein-detected NMR spectroscopy, interactions between the ligand and the protein can be investigated.[3]

However, there are limitations to these methods. Ligand-detected NMR spectroscopy generally uses a large excess of ligand compared to protein, and therefore it is generally the effect on the bulk ligand population of interactions with the protein that is detected. This high concentration of ligand can also affect the pH of the screening media, which can lead to chemical shift changes.[22] Protein-detected NMR spectroscopy also requires labelled protein for detailed NMR spectroscopy experiments.[3] Nevertheless, NMR spectroscopy is a widely used method.

X-ray crystallography has become a potentially more popular method for fragment screening as methods and technologies have been developed recently. Typically, this method is less high throughput than NMR spectroscopy screening experiments. This method, however, gives very detailed, high resolution information about the binding site and mode.[3,4] The use of X-ray crystallographic information is key in the development and evolution of fragments.[4,22] There have been, however, a number of issues with X-ray crystallography noted. Davis and Erlanson highlighted the fact that the crystal structure obtained was a model based on an experimentally collected electron density map and therefore was subject to interpretation. It was also noted that these data provide no information on affinity and that some more potent fragments may not crystallise well in the given system.[22]

Surface plasmon resonance (SPR) has become one of the most popular methods of screening fragments in recent times. SPR involves an immobilised protein, generally on a chip, which is then subjected to varying concentrations of fragment solutions. If a fragment binds to the protein a change in reflective properties of the chip is observed which is dependent on the ratio of the fragment mass to the protein mass.[22] A very large number of compounds can also be screened by this method and quantitative dynamics data, such as binding constants, can be obtained.[23] This method, however, does not give detailed information on the ligand or binding mode and can suffer from a large number of false positives.[3]

Another very popular method for fragment screening is thermal shift. In this method, a protein and ligand are mixed and heated. The melting temperature of the protein is then measured. The melting temperature is thought to increase if the ligand stabilises the protein against thermal denaturation and this is classed as a hit as the ligand is clearly bound to the protein. This method is quick and cheap and therefore a very useful method of screening. However, Davis and Erlanson report that false negative results are possible with this method and the hit rate can be quite sporadic.[22] Abell and co-workers also noted that results of thermal shift screening are not always reproducible and that generally thermal shift should be used as a enrichment exercise before screening by other methods.[24]

Each of these methods have both positive and negative attributes. Therefore, it has been noted by a number of groups that fragment hits should be confirmed by at least two different methods before progression.[2,19,22]

1.2 Fragment library design

As FBDD has become a recognised method of drug discovery, the compounds in screening libraries have become particularly important and the design of fragment libraries has become a key focus for many groups. Mills highlighted the importance of designing a chemically diverse fragment library, as critical decisions on project initiation and continuation can be based on results from fragment screening.[15] Chen and Hubbard highlighted that a fragment library should be a resource that can be screened against a variety of targets and increase the number of distinct chemotypes in the screening output.[25] As discussed above (Section 1.1), fragment library compounds generally have similar properties, as described by the "Rule of Three". However, as FBDD developed, it became apparent that these were not the only desirable characteristics of fragments.

Since fragments bind relatively weakly, they require screening at high concentration [4,21] and therefore fragments need to have a high aqueous solubility. Ideally fragments should have a solubility of greater than 5 mM in 5% DMSO solution.[26,27] This can be imparted from low molecular weight, low lipophilicity and ionisable groups. Such properties can be an issue in the synthesis of fragments, where aqueous soluble polar compounds are difficult to make and isolate. Furthermore, very polar fragments are less likely to bind with the screening target.[21,27] With an increased aqueous solubility comes a need to ensure that the compounds are stable in various media. Davis and Erlanson discussed the need to ensure that compounds have good stability over long periods of time, not only as solid material, but also as solutions in DMSO and water.[22] The stability of the compounds in water is also important for storage in DMSO which is very hygroscopic. If compounds are stored below 0 °C the solutions may be subject to freeze-thaw cycles. This could cause dramatic changes to concentration and stability and dissolution of the compound, which could ultimately lead to false positives in screening data.[22]

Another problem associated with screening at high concentrations is the need to ensure the removal of low-level impurities. David and Erlanson noted that when screening at a high concentration, such as 1mM, a 1% impurity that is not normally detected would

be present at 10 μM and this could cause misleading and erroneous results.[22] Metals are also a common impurity found to cause false results in screens; for example, zinc has been detected in surface plasmon resonance screens.[22]

As well as addressing solubility issues and avoiding false results from impurities, there have been a number of investigations into compounds regularly found in screening libraries that cause false results or are repeat hitters. It has been suggested by a number of groups that these types of compounds should be avoided.[26,28] The first group of compounds to avoid are classed as reactive compounds. These compounds, for example, could react with biological targets to form covalent bonds and are related to toxicity.[22,28] Some examples of these types of groups are shown in Figure 1.5.

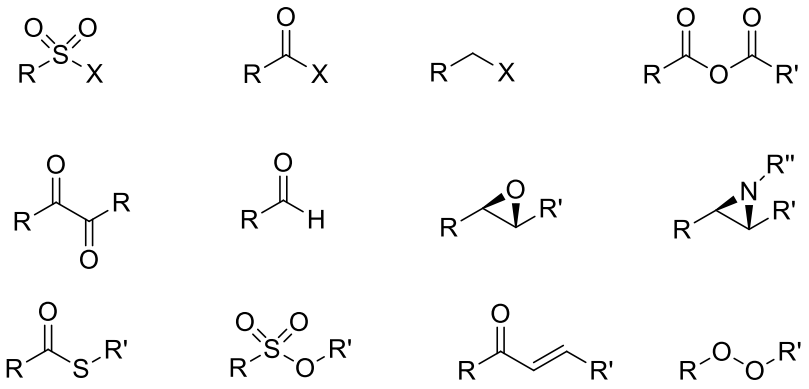

Figure 1.5: Moieties that could be potentially reactive and cause toxicity.[22]

Another group of compounds to avoid in screening libraries are termed pan-assay interference compounds (PAINS). Work by Baell and Holloway showed that a selection of the same compounds hit many different targets in HTS.[29] Generally, the compounds contain reactive features such as Michael acceptors. These can react reversibly or irreversibly with nucleophilic residues in the protein. PAINS have also been reported to bind covalently to targets which, although it can give them selectivity for a target, it can significantly affect interpretation of biology and development. Some PAINS may not necessarily be reactive but are strongly fluorescent or coloured, causing false data read-outs during fluorescence-based assays.[30] Examples of these moieties are shown in Figure 1.6.

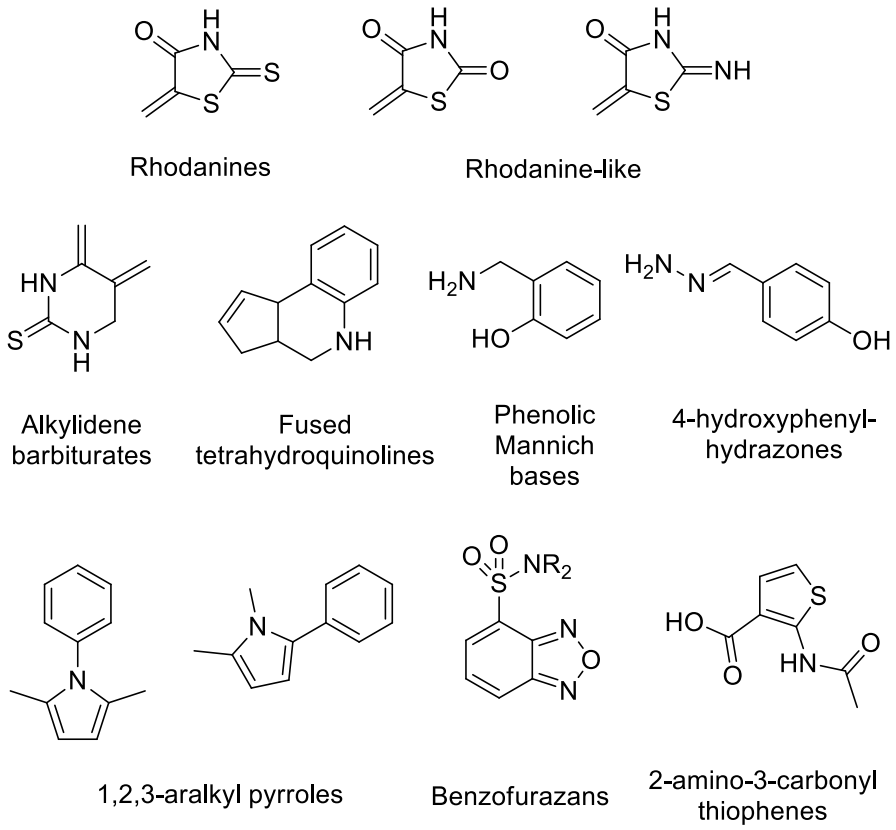

Figure 1.6: Example of pan-assay interference compounds.[22]

Another group of compounds noted for their tendency to affect assay and screening results are 2-amino thiazoles. Work by Scanlon and colleagues investigated whether this group of compounds should be eliminated from screening libraries due to their promiscuous behaviour. This behaviour was exemplified by phenylthiazol-2-amine (Figure 1.7) which when screened against 14 different protein targets was found to hit each of them. Although these data suggested that this type of compound should be eliminated from screening libraries, there are a number of example of this type of core in successful drug compounds, such as antibiotics, treatments for Parkinson's disease and leukemia. The work by Scanlon and colleagues, however, concluded that even though these promiscuous 2-aminothiazole (PrATs) fragments had desirable physicochemical properties the propensity to cause false hits suggested that these types of compounds should be avoided in fragment screening libraries.[31]

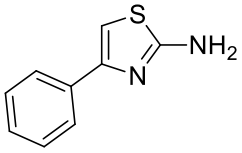

Figure 1.7: **Pr**omiscuous 2-**A**mino**T**hiazoles (PrATs)

Davis and Erlanson also highlighted that even if compounds pass through physicochemical property, stability, purity and reactivity screening, they may still cause problems through aggregation. Due to the high concentration of screening solutions, some small compounds can form microscopic aggregates in aqueous buffer.[19,22] These aggregates can then inhibit a range of assays, producing false results. A range of different compounds are known to produce this affect and work by Shoichet and co-workers went some way to predicting if a compound would be susceptible to aggregation, with the production of a free web-based tool to help understand assay results.[32] An alternative to avoid this is to add non-ionic detergents to the screening mixture to help reduce and eliminate aggregation. Some examples of aggregators are shown in Figure 1.8.[22]

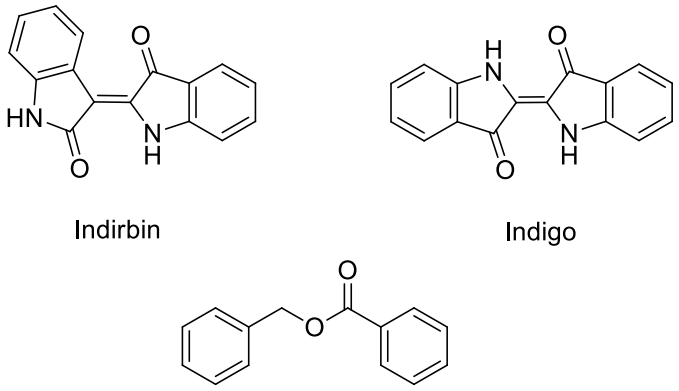

Figure 1.8: Compounds reported as aggregators that can inhibit enzymes and protein targets.

Although there has been discussion about the types of compounds that should be avoided in fragment libraries there has been substantial discussion in the literature relating to the desirable characteristics of fragments, libraries and how to populate

them.[15,21,22,28,33] A fragment library should also have certain characteristics as a whole such as synthetic tractability and molecular diversity.[2,9]

A number of groups have discussed the effect of the screening method on the size of a fragment library.[19,26] As described above, a fragment library does not need to be as large as a library for HTS, as chemical space is more efficiently sampled with smaller compounds. There does, however, need to be some indication on what would be a suitable size. Pickett discussed how the available screening method should determine how large the screening library should be. If a lower throughput technology is to be routinely used then a smaller library may be desirable to minimise the time and cost of screening.[19]

As the size of a library might be limited, it is essential to populate the library with desirable fragments. A diverse range of key pharmacophores that drive fragment binding should be present. The compounds should have suitable complexity as to encourage binding and not hinder it, but also not have too little complexity so detection becomes difficult. Fragment structure should be sufficiently varied so that the molecules represent different chemotypes and have novelty over other hits.[15,19] Kolmodin suggested that after acceptable compounds are identified, a screening library sub-set of these compounds should be selected. These selected compounds will provide good coverage of the acceptable compounds and would ensure that close structural analogues are available.[34] The need for close analogues has been highlighted by a number of groups and even the availability of solid material. Murray and Rees suggested that 50–100 mg of solid should be readily available.[27] The availability of close analogues could be used to facilitate fragment optimisation or to probe binding interactions between the fragment and protien.[15,27,34]

Closely related analogues are particularly important in the evolution of fragments towards lead compounds. A number of groups have suggested that fragments should have growth points or synthetic handles for quick and easy elaboration of fragments.[15,19,27,34] Murray and Rees highlighted the need to have the ability to

elaborate fragments from different points and in different directions and that the methodology to do this should be in place before the screening of fragments. This approach would help increase the chance of success in optimisation.[27] They suggested that groups such as amine and hydroxyl could offer potential as growth points as well as offering points of interaction.[27] Schultz and co-workers noted a similar point about growth vectors but aired caution about the fact that points for growth and synthetic handles should not be left too reactive that they may interfere with screening in a similar way to PAINS.[26] Kolmodin and co-workers suggested that synthetic handles such as hydroxyl groups and carboxylic acids could be masked as methyl ester or other less reactive functional groups.[34] Brennan was able to take this a step further and design a poised fragment library. This involves the identification of a "poised" bond in a fragment compound which can be deconstructed into two synthons, for which robust chemistry exists to re-join. For example, an amide group can be split into an acid chloride and an amine. In the event of an amide fragment hit, a range of synthons (acid chlorides and amines) can be reacted to rapidly product analogues for testing. This can allow for investigation of binding modes or elucidation of more potent hits.[35]

The availability of closely related analogues relies on commercial availability and synthetic tractability of the fragments. Murray noted that there is limited coverage of fragment space by commercial suppliers, even for very simple fragments, never mind for more complex heteroaromatic scaffolds.[13] Rees and Murray also noted that compounds in screening collections and closely related analogues should have robust methodology to support their synthesis and be available in less than 4 steps from commercially available compounds.[27] Inevitably, this has led to an increase in aromatic compounds in fragment libraries, which is supported by the robust chemistry available to build and functionalise aromatic compounds, as noted by Chan and co-workers.[36]

Work by other groups has shown that many fragment libraries are dominated by aromatic rings and planar compounds.[5,14,19,37] Baker commented that there are considerably more stereocentres and saturated carbon atoms in approved drugs and natural products compared to screening libraries.[14] Waldmann and co-workers

highlighted that this may be because most fragment libraries have been delineated from already known drug molecules and hence already cover identified areas of chemical space.[38] This is a problem that has not only been recognised in fragment libraries but also in lead-like compound libraries.[39,40] A selection of typical fragments taken from a report by Murray and Rees, is shown in Figure 1.9 and highlights that small aromatic compounds dominate fragment libraries.[1]

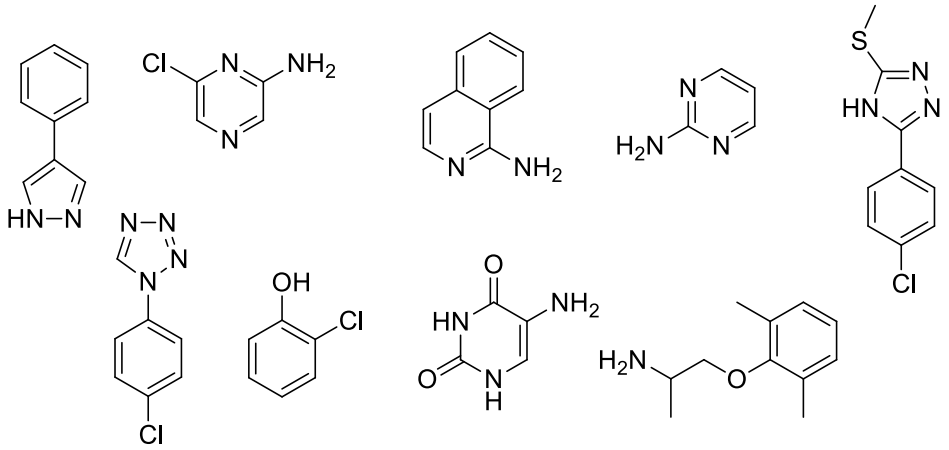

Figure 1.9: Example fragment compounds: generally low molecular weight, aromatic compounds.

The number of aromatic and planar fragments has led groups to suggest that increasing the number of diversely shaped fragments could be a method to introduce complexity and diversity into fragment libraries and explore new areas of chemical space.[14,37-39,41]

1.3 Success of fragment-based drug discovery

Since the seminal paper by Fesik,[8] a number of groups have reported clinical candidates derived from fragment screens. These were summarised in a report by Jhoti and co-workers.[42] Here, it was highlighted that there have been compounds that have entered the clinic, with two being approved by the FDA, as summarised below.

Vemurafenib was the first compound derived from a fragment hit to be approved.[5,43,44] This drug is used to treat late-stage melanoma and was passed for use in the clinic in August 2011. Plexxicon screened 20,000 fragment compounds with a molecular weight between 150 and 350 Da. From these 20,000 compounds, 238 were found to bind to a number of kinase targets and inhibited their activity by at least 30%. After cocrystalisation, around 100 compounds showed bound structures. From these compounds, 7-azaindole derivative **1** was selected. This fragment offered a number of hydrogen bonding interactions as well as a number of positions for substitution and derivatisation.[44] Structure-guided optimisation was used to develop the fragment and major developments are shown in Scheme 1.1. The final compound PLX4032 (Vemurafenib) has superior pharmacokinetic properties and excellent efficacy in patients.[5,44]

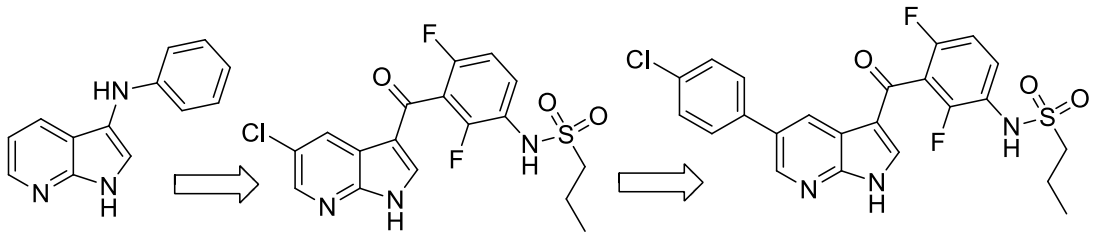

Scheme 1.1

The other compound approved for treatment derived from a fragment screen is Venetoclax, an anti-cancer agent. The therapeutic target was the Bcl-2 family of proteins, which are over-expressed in cancer cells. The specific target was a protein-protein interaction which had proved difficult to target with small molecules in the conventional way. Therefore, Rosenberg and colleagues employed an NMR

spectroscopy based screen of fragment molecules. This furnished two hits, **2** and **3**, with reasonable potency (0.30 mM and 4.3 mM respectively) (Figure 1.10).[45]

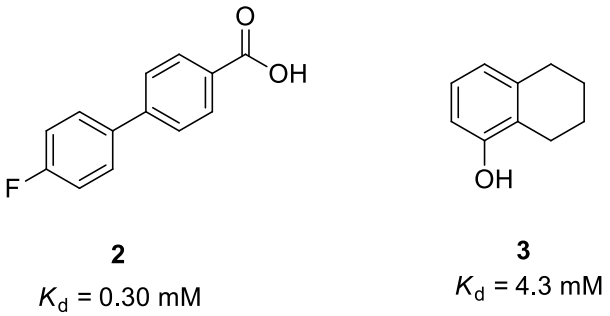

Figure 1.10: Two fragment hits that target Bcl-2.

Manipulation of these fragments and structure-based design of new targets led to the highly potent compound **4** (ABT-737).[45] This compound however, lacked good oral bioavailability and therefore further optimisation was undertaken.[46] Development gave compound **5** (ABT-263)[46], which was further developed to give the final compound **6** (ABT-199, Venetoclax) (Figure 1.3). This compound has proved very efficacious in the clinic causing tumour lysis within 24 hours of treatment.[47]

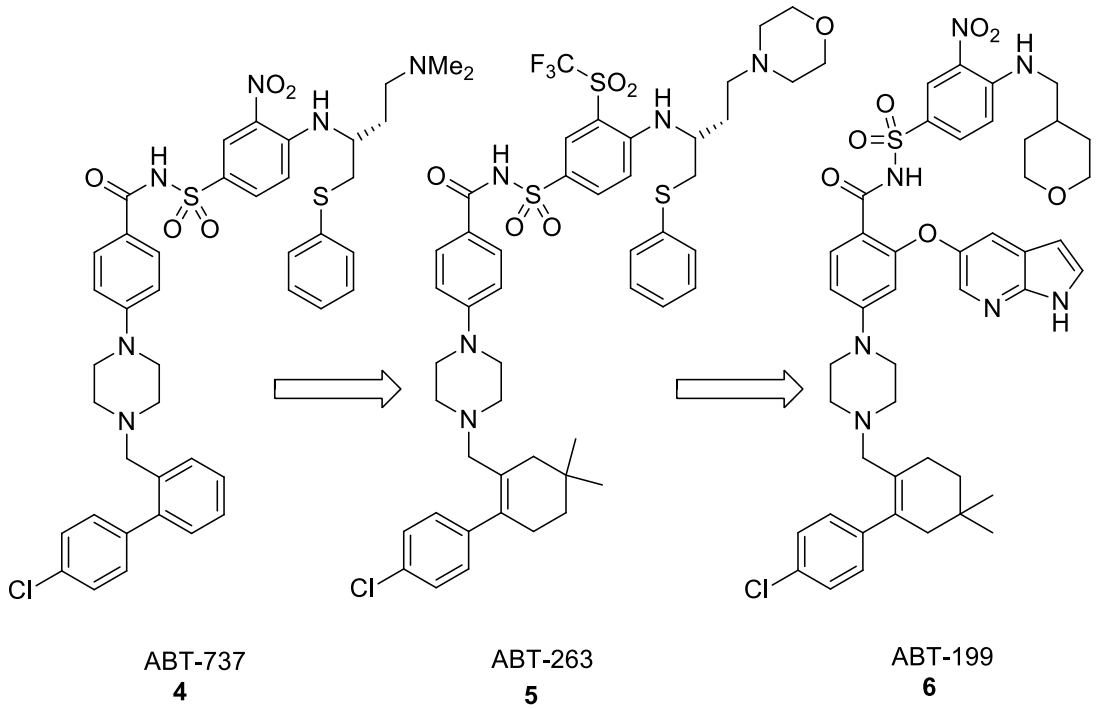

Scheme 1.2

A number of other FBDD-derived compounds are in stage III clinical trials, of particular note is the BACE inhibitor MK-8931, used in the treatment of Alzheimer's

disease. Scientists at Merck/Schering-Plough carried out fragment screening, using 2D NMR spectroscopy and structure determination by X-ray crystallography to find BACE inhibitors. This approach led to the discovery of thioamidine fragment **7**.[5,48,49] Subsequent fragment combination and structure-based drug design led to a series of iminothiadiazine dioxide derivatives.[48,50] Further work and optimisation led to the discovery of Verubecestat (MK-8931) (Scheme 1.3). This compound is one of the most advanced BACE1 inhibitors with high selectivity, which limit off-target effects.[48] The discovery of this inhibitor also highlights the benefits of the alternative screening approach offered by fragment-based drug discovery, as this target had proved very difficult to work with in conventional high throughput screens.[5]

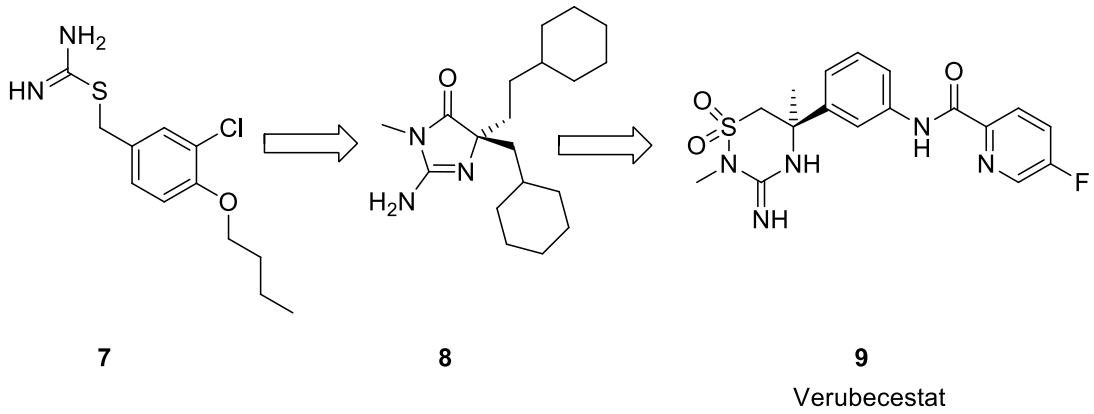

7 **8** **9**

Verubecestat

Scheme 1.3

These success stories, as well as numerous others,[42] highlight the impact of fragment-based drug discovery in such a short period of time.

1.4 3-Dimensional fragment libraries

The need to increase molecular complexity and diversity in fragment libraries has become more important with the increasing need to explore new areas of chemical space and with the desire to investigate more challenging targets. In a report by Chan and co-workers, it was highlighted that FBDD was generally focussed on aromatic, sp^2 rich, planer compounds. These types of molecules can impair the shape diversity of the library and hinder the exploration of chemical and pharmaceutical space.[36] This has led to an interest in more 3-dimensional fragments that can access new areas of chemical space. A further benefit to more 3-dimensional fragments was emphasised by Young. Nature generally recognises molecules in a 3-dimensional fashion and therefore it is intuitive that more 3-dimensional ligands will gain the best interaction and broad biological activity.[41]

With the increasing interest in 3-dimensional fragments, the 3D fragment consortium was assembled from several UK not-for-profit drug discovery groups.[37] The consortium's aim was to build a shared library of between 300 and 500 fragments, which would particularly focus on architecturally diverse fragments. It was noted that the "flatness" of current fragments could be responsible for the low success rates with certain targets. To highlight this, current fragment libraries and fragments from compounds successful in the clinic were compared. Two principal moment of inertia (PMI) plots[51] for the fragments in current screening libraries and fragments found in drug molecules are shown in Figure 1.11. PMI plots are a 2-dimensional way to represent 3-dimensional chemical space, where each corner of the graph represents a different extreme area of chemical shape; rod (*e.g.* an alkyne), spherical (*e.g.* adamantane) and disc-like (*e.g.* benzene).[37,41] Further information on PMI plots is provided in Section 1.5.5.

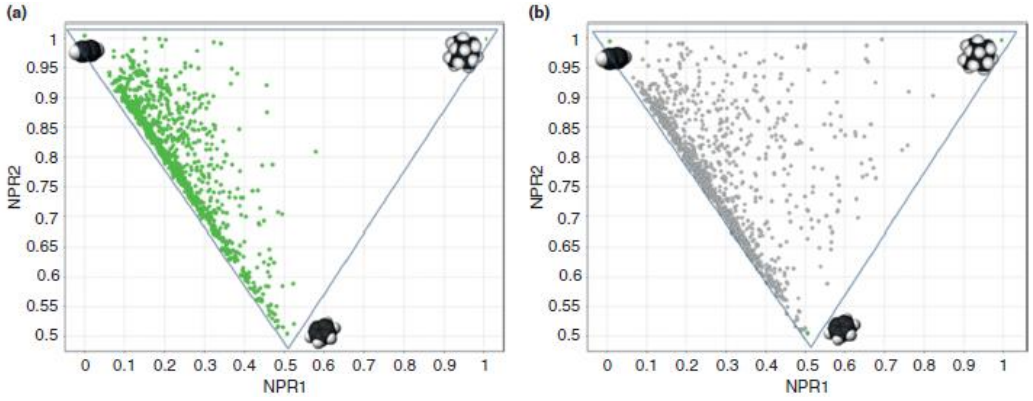

Figure 1.11: PMI plot (a) shows fragments in current screening libraries, which lie close to the rod-disc line. PMI plot (b) shows fragments found in drug molecules which have a much larger spread across the plot.[51]

The PMI plot in Figure 1.11(a) shows the fragments from current screening libraries. The points lie close to the rod-disc line, with only a limited spread across the whole plot. This is contrasted by the fragments found in drug molecules in the PMI plot in Figure 1.11(b). This has a much larger spread across the plot, with a number of compounds towards the top right of the plot. This illustrates the need to broaden the structural diversity of current fragment libraries.

As discussed, Nature recognises compounds in a 3-dimensional manner, and therefore natural products would be an excellent starting point for designing fragment compounds. Natural products have played a pivotal role in drug discovery and development and these types of compounds often occupy new and different areas of chemical space.[38,41] For this reason, Waldmann reported a natural-product-derived fragment library. This involved the fragmentation of known natural products into smaller fragment-like molecules, taking into consideration some of the rules outlined earlier such as the "Rule of 3" and elimination of toxic moieties. An example of fragment generation form the natural product Renieramycin P is shown in Scheme 1.4.[38]

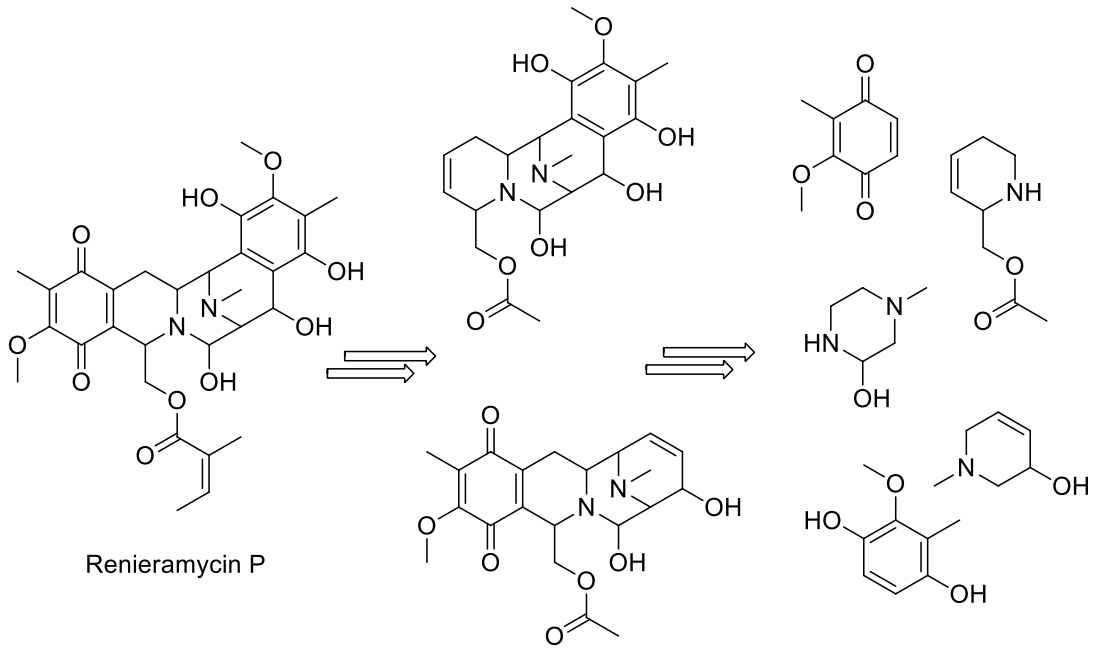

Scheme 1.4

The fragment library generated from this process was found to have high structural diversity compared to commercial fragment libraries and was found to occupy a considerably different area of chemical space. The library generated also represented the starting natural product library well, suggesting that the architectural diversity and 3-dimensionality desired from the natural products had not been lost.[38]

A paper entitled "Escape from Flatland" by Lovering draws together the problem of 2-dimensionality in screening collections and drug compounds and suggests methods to analyse and rectify the issue.[40] Lovering highlighted that saturation and number of stereocentres is an effective method to determine architectural diversity. This was exemplified with the isomers of dimethylpyridine and dimethylpiperidine (Figure 1.12). Dimethylpyridine is a flat, unsaturated aromatic compound and only has a total of 6 different isomers. However, the fully saturated dimethylpiperidine allows for methyl groups to be placed on the same carbon or on different carbons with *cis/trans* relative stereochemistry and gives an increased number of isomers, 32 in total. Examples are shown in Figure 1.12.*

* Lovering incorrectly calculated the number of isomers of both dimethylpyridine (5) and dimethylpiperidine (34).

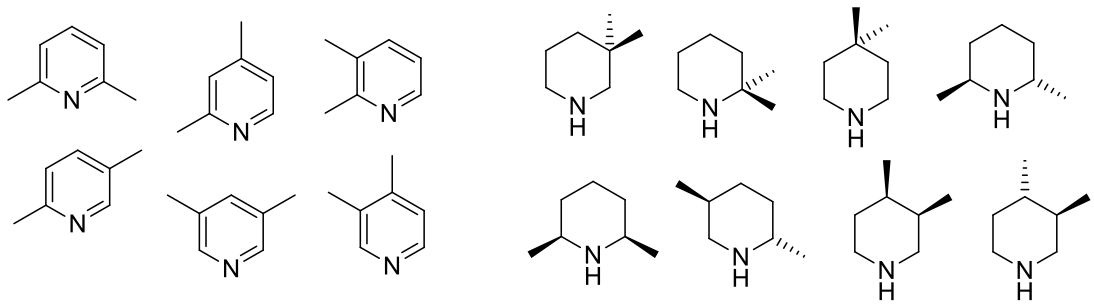

Figure 1.12: Comparison of only 6 isomers of dimethylpyridine, a saturated aromatic heterocycle and 8 of the possible 32 isomers of dimethylpiperidine, a saturated heterocycle.

Lovering's rationale for this increase in saturation was that molecular complexity and diverse chemical space can be accessed by compounds without increasing the molecular weight significantly, and that saturated compounds already have a greater level of 3-dimensionality. Another benefit of increasing saturation and decreasing aromatic character is the possible increase in solubility linked to increased saturation, a factor that had already been identified as leading to drug attrition. In addition, with increased opportunity to install out-of-plane substituents, the possibility of receptor/ligand complementarity and some elimination of off-target activity is increased.[40]

Investigating the change in saturation and number of stereocentres across drug development processes emphasised the benefit of architectural complexity and saturation. It was shown that, from discovery to drug, saturation increased by 31% as did the number of stereocentres (by 21%). The complexity of a possible drug compound is key to its success and therefore should be an important part of drug screening and development.[40]

Diversity-oriented synthesis has also been identified as a method to increase the architectural diversity of compound collections, and was first investigated for HTS libraries.[40,41] This method was used by Young and co-workers to generate compounds with different properties for better biological target interrogation. Ideally, diversity oriented synthesis uses short and efficient pathways to obtain structurally and physically diverse compounds. Young and co-workers developed the build-couple-pair algorithm to generate structurally and stereochemically diverse compounds. A

stereochemically diverse starting material was obtained, such as **10**, which was then "coupled" to the same (or different) starting material to give **11**. It is at this stage that the stereogenicity of the final fragment was installed. In the last stage, the compound was "paired". In this example, intramolecular reaction using ruthenium-catalysed ring-closing metathesis gave the final, rigid, architecturally-interesting fragment **12**. An example of this approach is shown in Scheme 1.5. A selection of fragments synthesised using the build/couple/pair approach are shown in Figure 1.13.[41]

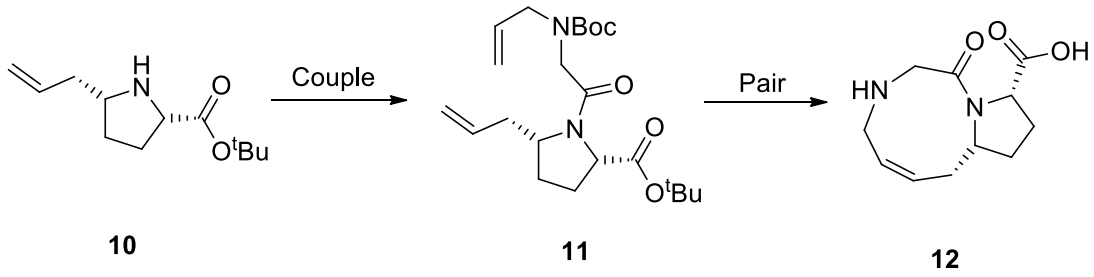

Scheme 1.5

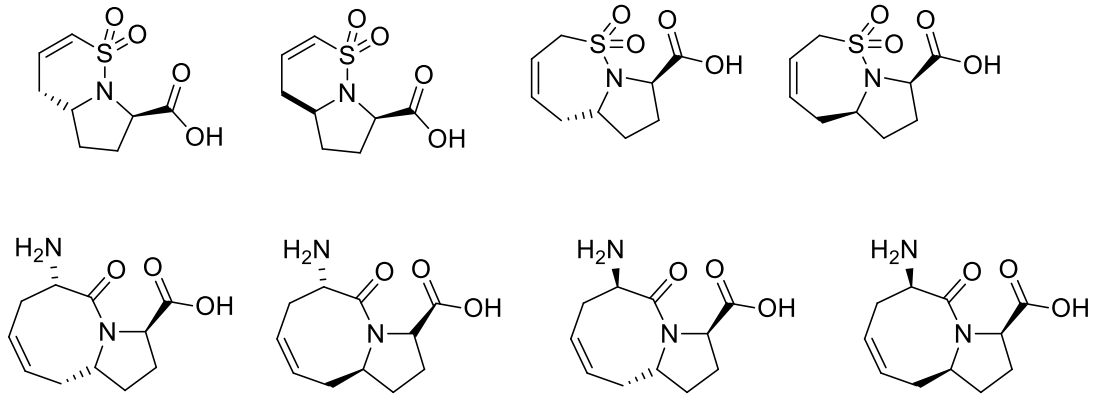

Figure 1.13: Examples of fragments synthesised using the diversity-oriented synthesis build/couple/pair method.

The introduction of more 3-dimensional compounds into screening libraries and the methods to do this has received some attention. Not only do these types of compounds help to explore new areas of chemical space, but they correlate with more desirable properties such as increased solubility, lower lipophilicity and decreased albumin-binding and cytochrome P450 inhibition.[36] Murray and Rees highlighted the need to develop the synthesis of 3-dimensional fragments and the significant lack of

methodology to functionalise and synthesise small fragments without having to devise new routes.[27]

Despite the significant interest in 3-dimensional fragments and numerous benefits to having these compounds in a fragment library, there have been some comments on the effectiveness of 3-dimensional fragments and their ability to bind. Chan and co-workers reported that binding frequency and selectivity increased on introduction of more 3-dimensional sp^3-hybridised compounds into the screening collection.[36] However, this is not a result mirrored in other reports. Pickett and colleagues noted that an increase in 3-dimensionality could increase the complexity of the fragments and, as discussed earlier, this could lead to a lower hit rate as there is more chance of mis-match or clashes.[37] With an increased structural complexity there is also a reduced probability of the shape matching that of the receptor. They noted that in order to take advantage of more 3-dimensional fragments, there needs to be a careful balance between complexity, size, shape and diversity of fragments.[19] Murray and co-workers highlighted this point, with a comparison of the similar sized planar and 3-dimensional fragments. Functionalised molecules with more shape diversity are obviously more complex than a relatively planar undecorated fragment of the same weight. This led them to conclude that if more complex and diverse fragments are to be included in fragment libraries then they should be smaller in mass than other more 2-dimensional fragments in the library, generally with less than 16 heavy atoms.[13]

Despite the concerns with the added complexity of 3-dimensional fragments, evidence suggests that more 3-dimensional fragments are having positive results in drug development programmes, such as the success targeting protease β-secretase (BACE). There is definitely a need to explore more 3-dimensional areas of pharmaceutical space.[14,37]

1.5 3-Dimensional shape analysis of compounds

As the assessment of the shape of compounds has become increasingly more important in medicinal chemistry, a number of methods have been developed to generate and analyse the shapes and conformations of compounds. Bender and colleagues highlighted the importance of computational analysis in drug design and that development of novel computational methods would allow for better and more efficient exploration of therapeutically-relevant space.[52] It has also been noted that the analysis of shape is one way to assess the diversity of a set of compounds.[51-53] A number of methods have been developed and are discussed below.

1.5.1 Fraction of sp^3 centres

In 2009, Lovering disclosed a new method to assess the molecular complexity of compounds by investigating the number of saturated sp^3 carbon centres.[40] Lovering developed this method as a simpler alternative to the method developed by Badertscher, which involved a much more mathematically demanding calculation of the saturation in a compound. Lovering's formula is shown in Equation (1).

$$F\mathrm{sp}^3 = \frac{\text{number of sp}^3\text{hybridised carbons}}{\text{total carbon count}} \qquad (1)$$

As part of Lovering's paper, compounds from development and marketed drugs were analysed using a Pipeline Pilot protocol with the ability to calculate the Fsp^3. This method provided a good indication that compounds closer to market had a higher value of Fsp^3 and therefore had more molecular complexity.

There have, however, been criticisms of this method. Firth, Brown and Blagg noted that Fsp^3 poorly characterises whether the sp^3 carbon atoms are connected to extended vectors out of the main plane (which would offer more varied shape and structure). They exemplified this with the comparison of two compounds, **13** and **14**, with the same Fsp^3 but quite different computationally-determined conformations (Figure 1.14).[53]

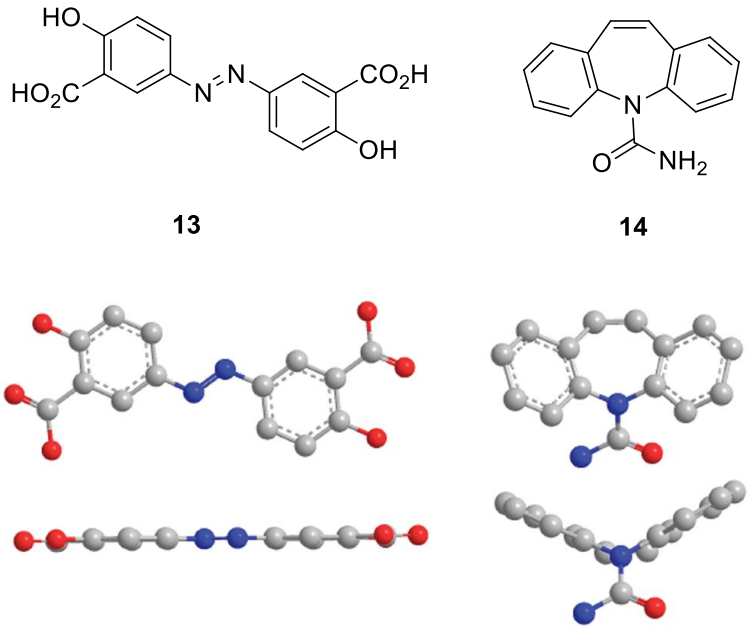

Figure 1.14: Comparison of two compounds with the same Fsp^3 value (0).

Both compounds, **13** and **14**, have an Fsp^3 of zero which suggests that the compound should be planer. However, this is clearly not the case for compound **14** which has a V-like shape, with the pseudo-sp^3 nitrogen substituent coming out below the main scaffold. Compound **13** is flat as predicted from the Fsp^3 value. This shape difference, however, is likely to be predicted by other computational shape analysis methods.[53]

1.5.2 Rapid Overlay of Chemical Structures (ROCS)

This method in general assesses the atom-centred overlapping Gaussians and calculates the maximal intersection of the volume between molecules and then compares molecules based on these molecular shapes. Grant reported this method as a further improvement on the simple method of treating a molecule as a set of intersecting spheres, with the exposed surface of these spheres giving the boundary of molecular volume. Since this method does not take into account the quantum nature and the electron charge distribution of molecules, Grant and co-workers developed a revised method.[54]

The revised method involves a Gaussian description of molecular shape, using a generalised coalescence theorem to generate molecular volumes, areas and nuclear coordinates. This method specifically deals with the electron charge distributions in a

simple manner and without the need for complex, computationally demanding quantum mechanical calculations.[54] These calculations consider the chemical similarity and atom types, not just the molecular shape.[52]

1.5.3 Molecular Globularity

The term "globularity" or "globular compounds" was first introduced by Timmerman in 1954.[55] Meyer further developed this term and applied it to a computational analysis of compounds in 1986.[56] This method of determining shape and size starts with the optimisation of geometry and conformation using molecular mechanics. Next, the molecule is treated as a solid in space, where spheres are traced around the atomic nuclei.[56] In this case of globularity measurement, van der Waals radii are used which subsequently give the van der Waals volume (V_w) and surface area (S_w). These values can then be used to provide a quantitative measure of globularity or deviation from sphericity. It can be imagined that branching is likely to change these values away from a perfect spherical value. A compound will have the volume V_w, from which the radius and surface area can be calculated (Equation (2) and (3)).

$$r_{e,w} = \left(\frac{3V_w}{4\pi}\right)^{1/3} \qquad (2)$$

$$S_{e,w} = 4\pi {r_{e,w}}^2 \sim 4.836 {V_w}^{2/3} \qquad (3)$$

For a perfect sphere, the calculated $S_{e,w}$ will be equivalent to the van der Waals surface area S_w ($S_{e.w}$ / S_w = 1). Therefore, measuring the ratio of these values (Equation (4)) gives a measure of globularity (G_w).

$$G_w = \frac{S_{e,w}}{S_w} \qquad (4)$$

If one axis was to become longer compared to the others, the S_w value will be out of proportion to $S_{e,w}$ and the G_w will decrease. [57]

1.5.4 Plane of Best Fit (PBF)

An alternative method for analysing shape has recently been developed by Firth, Brown and Blagg.[53] This method was expected to deliver quick, unambiguous and quantitative characterisation of shape diversity. The method determines the how far removed molecules are from a 2-dimensional plane and was termed "plane of best fit" (PBF). This involved fitting a plane across the heavy atoms of a molecule and subsequently calculating the average of the distance away from this plane of the other heavy atoms. In order to carry this out, the conformation of a given compound is computationally calculated and the plane fitted to the shape. This is exemplified by cyclohexane shown in Figure 1.15.

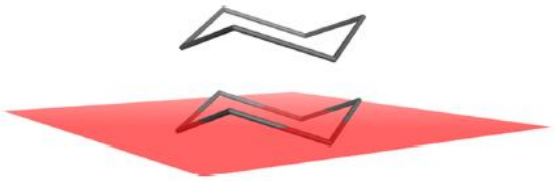

Figure 1.15: Plane fitted to the lowest energy conformation of cyclohexane.

It was highlighted in the paper that this analysis was carried out on a single conformer of a compound. This is similar to other methods (e.g. PMI analysis), although the method is amenable to the analysis of a number of conformations.[53]

The conformation is generated computationally with salts removed and hydrogens omitted. Then, the plane of best fit is calculated using the least squares method from the generated coordinates. The plane of best fit is given by Equation (5).

$$Ax + By + Cz + D = 0 \qquad (5)$$

This equation can then be manipulated to calculate the distance, Δ, of each heavy atom away from the plane, which is given by Equation (6).

$$\Delta = \frac{|Ax_i + By_i + Cz_i + D|}{\sqrt{A^2 + B^2 + C^2}} \qquad (6)$$

It was noted that the PBF score has a theoretical range of 0 to ∞. However, in general, drug-like molecules have a score of less than 2.[53]

In order to assess the applicability of the method, a number of compound set analyses were carried out and compared to other current methods of shape analysis. In general, for all of the compound collections, the PBF method was comparable to molecular globularity and PMI, but differed significantly from Fsp^3. As discussed earlier (Section 1.5.1), Fsp^3 is not a good descriptor of shape, as the Fsp^3 value does not determine whether the sp^3 centre leads to out of plane shapes. This method is comparable to currently employed methods and offers a high-throughput rapid method of shape analysis, the only rate-limiting factor being the generation of conformations This method also allows comparison of compounds as values are irrespective of molecular size as the PBF score is normalised according to the number of heavy atoms.[53]

1.5.5 Principal Moments of Inertia (PMI)

An alternative method of shape and diversity analysis was developed by Saur and Schwarz.[51] Initially, they set out to investigate how small multiple-scaffold libraries compared to large single-scaffold libraries. A molecular descriptor to help with this analysis needed to fulfil three criteria: correlate with and be predictive for biological activity, be translatable into chemical structure, and be rapid to calculate. It was decided that the molecular shape fitted well with these criteria.[51] Generally, compound shape can be rationalised and modified if desired and other examples of shape calculation exemplify the ability to calculate this property quickly.

Saur and Schwarz proposed that the evaluation of normalised ratios of principal moments of inertia would be a suitable method to describe molecular shape.[51] In order to obtain the normalised principal moments of inertia, a 3-dimensional structure must be derived and from this the three principal moments of inertia can be calculated computationally using molecular mechanics. These values are sorted into ascending size to give I_1, I_2 and I_3. From these values the normalised ratios are obtained (Equation

(7)). The two lower values (I_1 and I_2) are divided by the largest value (I_3). By choosing to normalise the ratios, the dependence on the size of the compound under analysis is eliminated.

$$\text{NPR1} = \frac{I_1}{I_3} \text{ and NPR2} = \frac{I_2}{I_3} \qquad (7)$$

These values can then be plotted easily on a 2-dimensional graph. This graph is triangular in shape, where the corners are defined as rod [0,1], disc [0.5,0.5], and sphere [1,1]. This is shown in Figure 1.16.

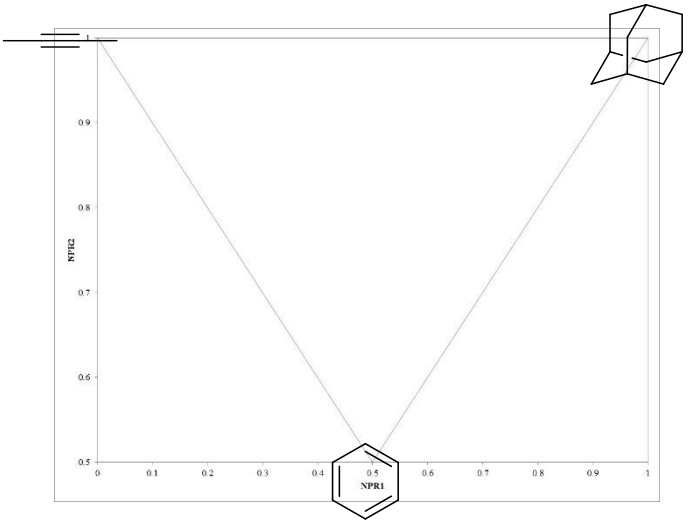

Figure 1.16: The triangular shaped PMI plot with the three extreme shapes.

As alternative methods for shape and diversity analysis have been developed, the methods have been scrutinised and investigated further. Bender and colleagues compared PMI to a number of other methods and noted that PMI behaved quite differently.[52] This could be attributed to this method comparing molecular shapes to archetypal shapes, rod, disc and sphere and disregarding size. It was also noted that although the shape properties of a chemical library can be analysed using PMI, there is generally no correlation of these values with diversity of coverage in bioactivity space. It was noted by Bender that compounds binding to different proteins fall in the similar areas of chemical space according to their normalised principal moments of inertia.[52]

In summary, each of the 3-dimensional shape analysis methods has a number of positives and are often quick, rapid and quantitative methods to analyse compound shape and assess shape diversity of a compound set. For best results, methods could be combined and compared to give the full representation and analysis of compound libraries, bearing in mind the use of molecular mechanics to generate conformations and structural shapes. More computationally demanding methods may give a more realistic representation, but would inevitably be more low-throughput.

1.6 Project outline

This project aims to design, analyse and synthesise 3-dimensional fragments for ultimate use in fragment-based drug discovery. Our approach will focus on the use of different sized saturated nitrogen heterocycles as a way to introduce structural and shape diversity into a fragment library. We hope to demonstrate that architecturally interesting, 3-dimensional fragments can be obtained from such simple building blocks. Saturated scaffolds are generally more 3-dimensional and offer access to different binding vectors and globular shapes. These also offer more complexity than the aromatic counterpart for only a small increase in molecular weight.[36] The prevalence of saturated nitrogen heterocycles in current drug molecules was highlighted by Chan, with 5- and 6-membered rings being the most common. Piperidine is the second most frequently found saturated heterocycle with pyrrolidine coming fifth.[36] A report by Lawson also highlighted that piperidine was the third most common ring, after benzene and pyridine in FDA-approved small molecule drugs.[58] Therefore, pyrrolidine, piperidine and azepane scaffolds will be investigated.

We decided that our three different heterocycles would be substituted with two different substituents: methyl/hydroxymethyl and methyl/methyl ester. The hydroxymethyl and ester groups offer a handle for further functionalisation as well as hydrogen bonding capabilities. The methyl group is commonly used in medicinal chemistry; it can alter the lipophilicity and solubility as well as bioavailability and metabolism of a drug molecule[59] and appears in 67% of the top selling drugs of 2011.[60] This will give us six different libraries as shown in Figure 1.17. To offer more variation in our fragments, the nitrogen will be functionalised in four different ways: NH, NMe, NC(O)Me (amide) and NSO_2Me (sulfonamide).

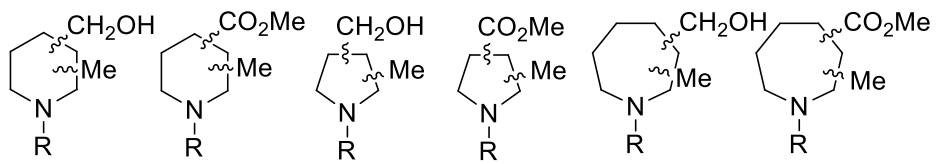

Figure 1.17: The different scaffolds with hydroxymethyl and ester substituents, where R is NH, NMe, NC(O)Me (amide) and NSO_2Me (sulfonamide).

Our plan was to use shape analysis to assess the shape diversity of all of the enumerated isomers (not including enantiomers) of these six different scaffolds. In order to carry out unbiased and efficient shape analysis a computational method will be developed. Principal moments of inertia (PMI) plots will be used to assess shape diversity and develop criteria to select compounds that focus on the under-represented, 3-dimensional area of chemical space. The results of our efforts in this area are described in Chapter 2.

The compounds identified by the selection criteria will form six sub-set libraries. We will focus on the synthesis of the hydroxymethyl piperidine sub-set fragments (Figure 1.18). The synthesis will be carefully designed so as to minimise the number of different routes used to obtain all the fragments. It will also be important to ensure that within these routes the number of steps to access the final fragments are minimised and it is hoped that methodology allowing the flexible installation of different groups will be used. Our synthetic efforts on 3-dimensional fragment synthesis are discussed in Chapter 3.

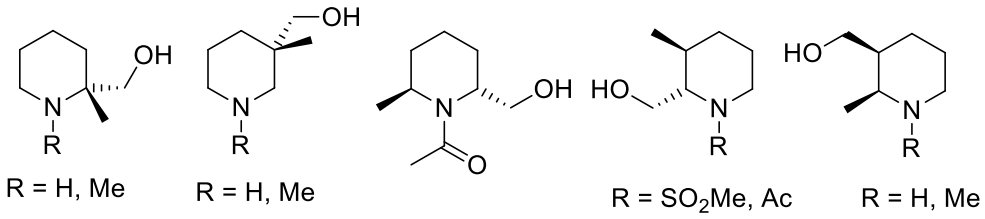

Figure 1.18: Some of the hydroxymethyl piperidine fragments

In addition, we also briefly explored the use of shape analysis to characterise the 3-dimensional shape diversity of a virtual lead-like library generated from compounds accessible using O'Brien group lithiation methodology. This is described in Chapter 4.

Chapter 2: Design, Analysis and Selection of 3-Dimensional Fragments

Design and assessment of fragments are both fundamental to building a diverse and useful fragment library. In our planned project, it is key to ascertain how 3-dimensional and structurally diverse a set of compounds are in order to select suitable compounds for synthesis. As discussed in Section 1.5.5, the area of 3-dimensional chemical space covered by a compound library can be assessed using a PMI plot.[41,61] In order to do this, the different conformations of a compound are generated and energies for each are calculated computationally. These can then be normalised and the lowest energy conformations plotted on a PMI plot. All the isomers (not including enantiomers) of six different scaffolds Figure 2.1 were enumerated and functionalised with four different nitrogen substituents (Figure 2.1).

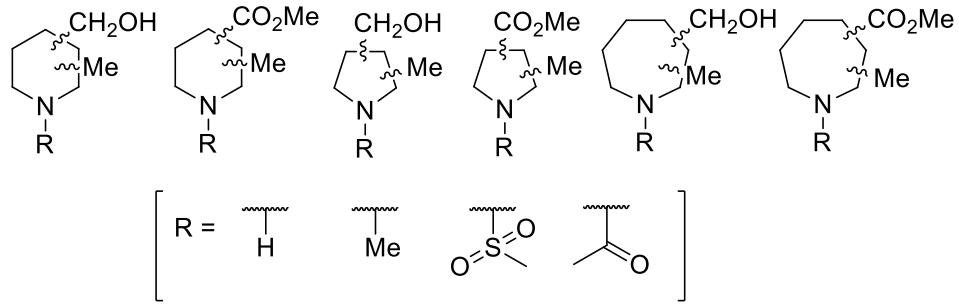

Figure 2.1: The six different scaffolds and nitrogen substituents.

These compounds were then computationally analysed and the conformations generated. We describe the development of the computational protocol using the hydroxymethyl piperidine library in Section 2.1 – 2.4. The use of the PMI plots to generate selection criteria is also described and these criteria are used to analyse the other scaffolds (Section 2.5). The analysis, selection of sub-set libraries and combination to give a fragment library focussed on the under-represented, 3-dimensional area of the PMI plot is also described in Section 2.5.

Once the computational protocol had been developed the physicochemical properties of our selected fragments were analysed and this is presented in Section 2.6. The comparison of our selected fragments to a commercial library is described in Section 2.7.

2.1 Enumeration of hydroxymethyl piperidine scaffold

To start, we decided to investigate the design, analysis and selection of fragments approach with a disubstituted piperidine scaffold. Disubstituted piperidines bearing two different substituents, methyl and hydroxymethyl, provide a total of 23 isomers (excluding enantiomers). In order to create interesting fragments and architectural diversity, the nitrogen was functionalised in four different ways: NH, NMe, NC(O)Me and NSO_2Me. These groups offer a variety of properties, such as hydrogen bonding capabilities, give different shapes and offer a different hybridisation of the nitrogen (sp^2 versus sp^3) and it is expected that they have suitable fragment-like physicochemical properties. This gives a total of 92 different compounds. All of the 23 different isomers are shown in Figure 2.2.

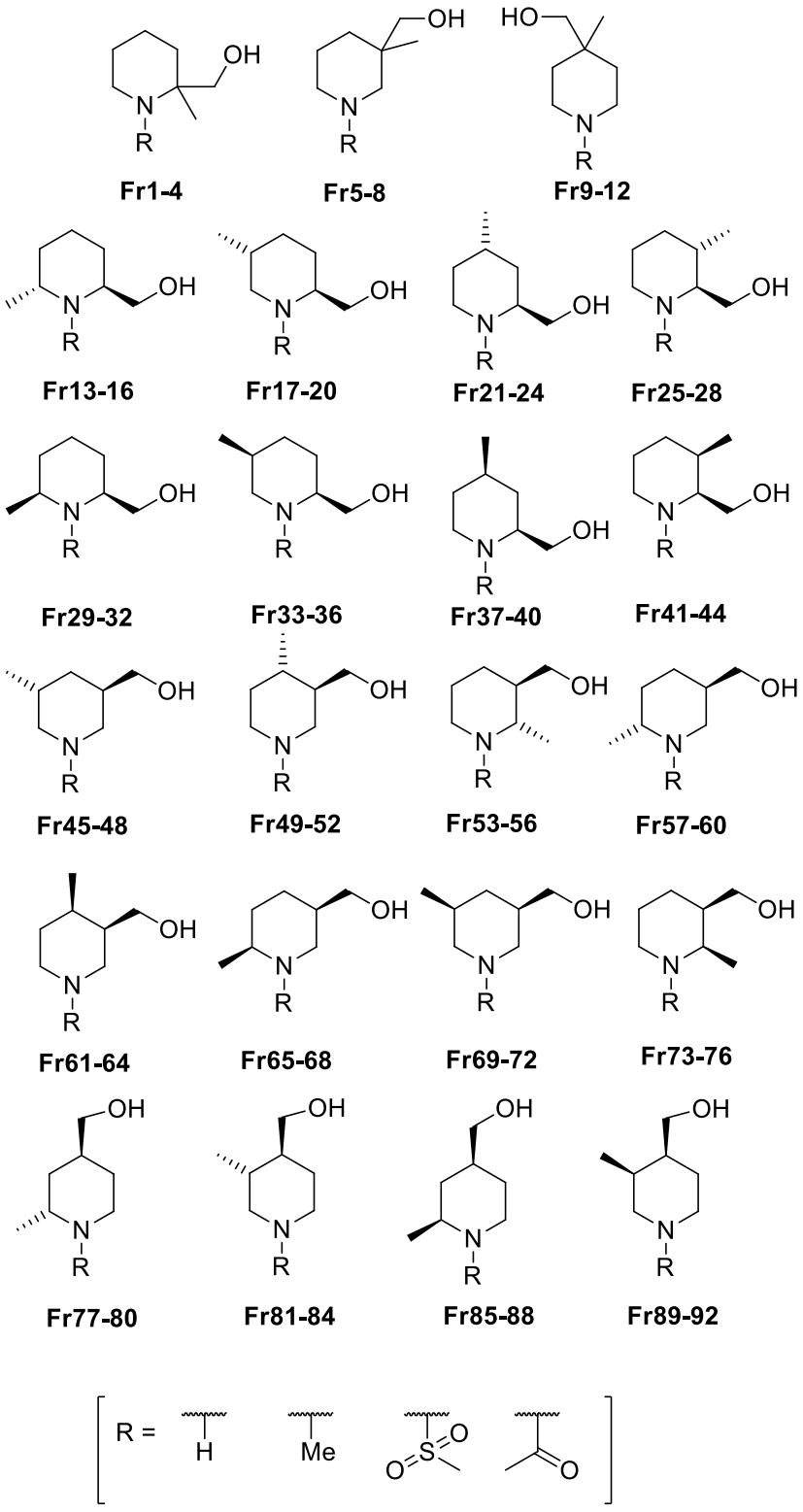

Figure 2.2: All 23 different isomers of disubstituted piperidine. The four different nitrogen substituents are also shown.

We propose that it is not necessary to synthesise all of the 92 possible fragments. Therefore, a sub-set library will be selected. This will have a fraction of the original 92 fragments and will focus on more spherical shapes and the under-represented 3-

dimensional area of the PMI plot. PMI data on the 92-member library was generated and subsequently analysed to select suitable compounds. The importance of an unbiased, efficient and unlimited analysis led to the development of a computational approach to this analysis.

2.2 Introduction to the computational protocol

Conformation generation and PMI data were obtained through a collaboration with Rod Hubbard and Paul Bond at York Structural Biology Laboratory.[62] Paul Bond provided the initial Pipeline Pilot protocol from which I obtained the data, this data was analysed, if issues or development was needed this was fed back to Paul Bond and a new iteration of the protocol was produced with my input. Data was obtained and tested again and the process repeated until the protocol gave satisfactory data. Conformer generation used Pipeline Pilot 8.5 (see Section 6.1 for further details). The BEST algorithm was used to generate conformers as this algorithm ensures the best coverage of conformational space. During conformation generation, constraints can be applied to reduce the number of conformers generated. Two of these constraints are the conformational energy difference and the RMSD. The conformational energy difference gives the difference in energy between each conformer and the lowest energy conformer of that particular compound. Therefore, the larger this number the more conformers that will be generated. The RMSD indicates the difference in Å between atoms, or points of a conformer and the standard. If the RMSD is 0 Å, a conformer that only varies slightly from the standard will be kept, whereas if the RMSD is 1 Å, only very different conformers will be kept. Hence, the larger the RMSD, the fewer conformers that will be selected.

The influence of these constraints was investigated in more detail. It was decided to select the two different energy cut offs of 7.0 and 20.0 kcal mol^{-1} and three different values of RMSD to give a range in the amount of conformers that would be generated. Table 2.1 shows how the number of conformations generated were affected by the constraints. All of the 92 compounds **Fr1** – **Fr92** were analysed, with all possible conformations generated within the constraints. The conformations were generated without an implicit solvent model, under vacuum conditions (See Section 6.1 for further details).

Entry	Conformational energy difference / kcal mol^{-1}	RMSD / Å	Total number of conformations
1	20.0	1.0	589
2	20.0	0.5	1740
3	20.0	0.0	2609
4	7.0	1.0	279
5	7.0	0.5	533
6	7.0	0.0	702

Table 2.1: Data for each conformer generation run and the total number of conformers generated from the analysis of the 92 piperidine fragments **Fr1** – **Fr92**.

As can be seen in Table 2.1, changing the conformational energy difference and RMSD constraints significantly affects the number of conformers generated from the 92 fragments. The largest number of conformers was generated when the conformational energy difference cut off was 20.0 kcal mol^{-1} and the RMSD 0.0 Å (Entry 3). This was to be expected, as no restrictions had been applied. It can be seen, also as expected, that the largest RMSD gave the fewest number of conformers (Entries 1 and 4), and that having a conformational energy difference cut off of 7.0 kcal mol^{-1} (Entries 4 to 6) reduced the number in comparison to the 20.0 kcal mol^{-1} cut off (Entries 1 to 3). The number of conformers generated by not applying constraints still gives a manageable data set size, especially for use with computational analysis. Therefore, further analysis of different scaffolds used a protocol with no constraints.

After initial exploration of the protocol and constraints, the protocol was further optimised to give the best conformational data. This was to ensure that conformations were generated in the most relevant model system. For example, the system calculated the conformations with an approximation for solvation. All conformations of each of the 92 piperidine fragments **Fr1** – **Fr92** were generated using the BEST algorithm with no RMSD or energy constraints. This gave a total number of 2848 conformations. It was this version of the protocol and data that was used for further analysis.

PMI plots in the current literature generally show just the lowest energy conformer of a given compound.[37,63] However, the protocol generates numerous different energy conformations of a given compound. The generation of all conformations can offer a

good insight into how the 3-dimensionality of a given compound can vary due to different conformations. This information can then be used to give the library 3-dimensional conformational diversity as well as architectural diversity. This is exemplified in Figure 2.3, where the lowest energy conformations of each of the piperidine fragments **Fr1** – **Fr92** in the 92-member library (Figure 2.3 (a)) is compared to the PMI plot of all the different conformers for the 92-member library (Figure 2.3 (b)). It is clear that there is a much larger spread across the plot by investigating the different conformations.

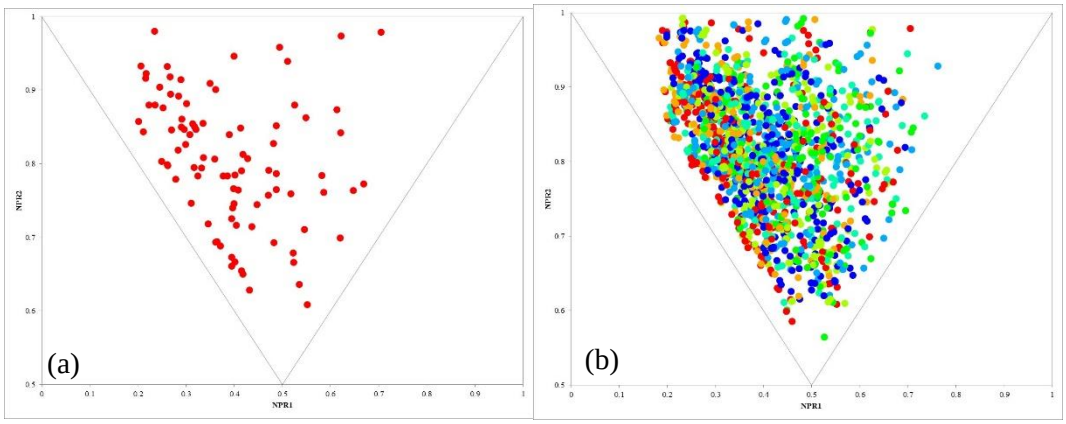

Colour							
Conformational energy difference / kcal mol^{-1}	< 1	< 2	< 3	< 4	< 5	< 6	< 7

Figure 2.3: (a) PMI plot of the lowest energy conformer for all piperidine fragments **Fr1** – **Fr92**. There is a good spread across the plot, but conformations are weighted towards the rod-disc axis. b) PMI plot of all the conformations (with a conformational energy difference of less than 7.0 kcal mol^{-1}) for all piperidine fragments **Fr1** – **Fr92**. This shows a good coverage of all of the plot, with a number of conformers in the top right, more spherical area of the plot, there will be however a number of high energy conformations that might not be truly accessible.

The PMI plot with all the conformations seemed a suitable starting point for analysis and selection of compounds for a smaller sub-set library. Our plan was to use Figure 2.3 (b) and devise selection rules, so that conformations in the under-represented area of 3-dimensional space in the PMI plot were prioritised. It was hoped that the selected compounds will have 3-dimensional and conformational diversity and would be focussed away from the rod-disc axis.

The large number of data points on the PMI plot in Figure 2.3 (b) meant that a method to segment the plot was required. We chose to divide the plot into 10 areas, using

diagonal lines as shown in Figure 2.4. The position of each conformer on the plot is determined by the *npr1* and *npr2* values, which are effectively the (*x*,*y*) coordinates, obtained from the normalisation of the 3-dimensional axis coordinates of a compound's conformation. The number of conformers in each area or "category" can easily be determined computationally. The more spherical, or 3-dimensional compounds will be in the lowest value category (e.g. 1 or 2).

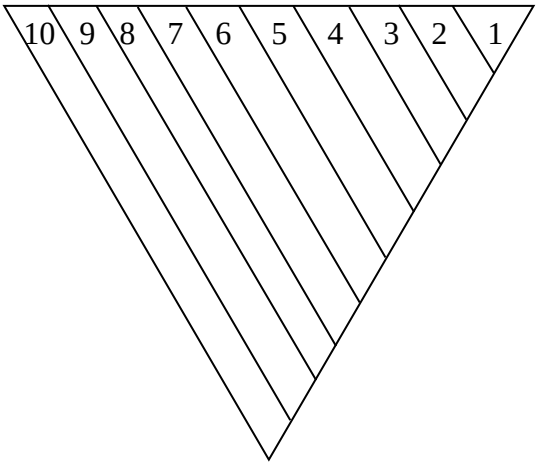

Figure 2.4: PMI plot showing the 10 different categories.

The 2848 conformations of the piperidine fragments **Fr1** – **Fr92** shown in Figure 2.3 (b) was analysed further to determine the spread of conformers across the plot. These results are shown in Table 2.2 and Figure 2.5.

Conformational energy difference / kcal mol^{-1}	RMSD / Å	PMI Category									
		1	**2**	**3**	**4**	**5**	**6**	**7**	**8**	**9**	**10**
20.0	0.0	0	0	0	8	41	172	336	904	1150	237

Table 2.2: The total number of conformers in each PMI category for the 2848 conforations generated for all of the 92 piperidine fragmetns **Fr1** – **Fr92**.

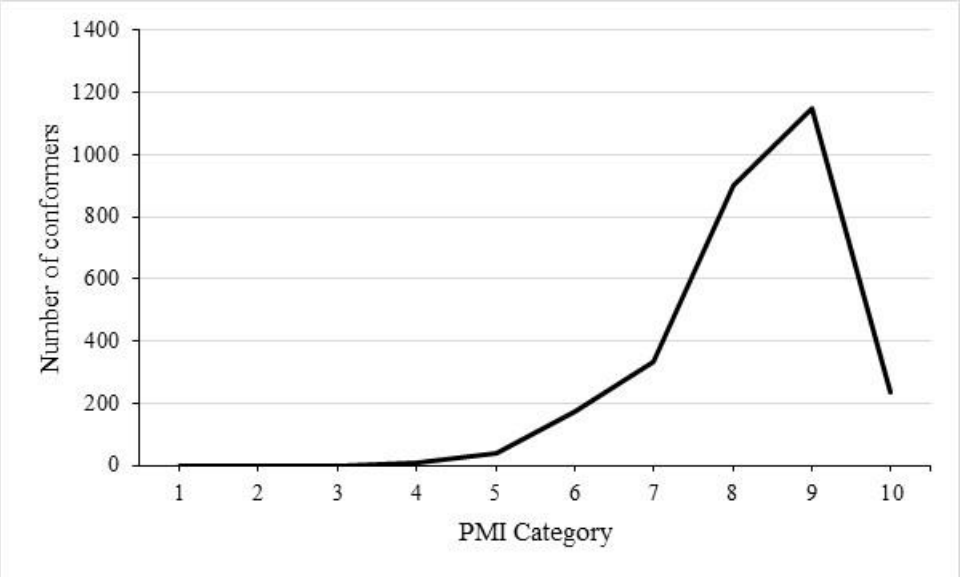

Figure 2.5: Graph showing the number of conformers in each of the PMI categories 1 to 10.

Figure 2.5 clearly shows that the spread of conformers varies across the plot. The most spherical area of the plot, categories 1–3, contains no conformers, but there are some in category 4 and increasing numbers in categories 5 and 6. The most interesting result is that there are relatively few conformers in category 10. This is the area closest to the rod-disc line of a PMI plot and is associated with very flat molecules. This result indicates that the conformations of the compounds in this data set have a high degree of 3-dimensionality. This clearly shows that it is possible to obtain shape diversity from very simple scaffolds.

It was our intention that the selection of compounds for the sub-set library would be based on the position of the conformations on the PMI plot and the energy of each of these conformations. Analysis of all of the 2848 conformations was carried out to investigate the spread of conformational energy differences across the different categories of the PMI plot. The conformational energy difference gives the difference in energy between each conformer and the lowest energy conformer, for a given

fragment. Two analyses were carried out. Firstly, the energy levels were divided into 1.0 kcal mol^{-1} groups (Table 2.3) and secondly, the lowest energy levels were split into 0.5 kcal mol^{-1} groups (Table 2.4).

PMI Category	Conformational Energy Difference / kcal mol^{-1}							
	0 - 1	**1 - 2**	**2 - 3**	**3 - 4**	**4 - 5**	**5 - 6**	**6 - 7**	**7-20**
4	1	0	1	1	1	1	0	3
5	3	3	0	4	4	8	5	14
6	15	9	20	23	21	19	11	54
7	20	13	29	34	23	33	30	154
8	48	46	70	66	64	78	103	429
9	135	103	103	62	67	114	134	432
10	52	23	18	20	22	21	22	59
Total	274	197	241	210	202	274	305	1145

Table 2.3: Data showing the distribution of conformers by PMI category and conformational energy.

PMI Category	Conformational Energy Difference / kcal mol^{-1}				
	<0.5	**0.5 – 1.0**	**1.0 – 1.5**	**1.5 – 2.0**	**2.0 – 2.5**
4	1	0	0	0	0
5	3	0	1	2	0
6	10	5	5	4	9
7	13	7	7	6	10
8	31	17	17	29	46
Total	58	29	30	41	65

Table 2.4: Data showing the distribution of conformers by PMI category and conformational energy.

The lower conformational energy difference values 0-2.5 kcal mol^{-1} were split into 0.5 kcal mol^{-1} groups as these energy differences will give the most energetically accessible conformations. This is exemplified with the two conformations of disubstituted piperidine **Fr16**. The lowest energy conformation of **Fr16** (Figure 2.6 (a)) has a chair conformation with an axial methyl group and an equatorial hydroxymethyl group. In contrast, the conformation with an energy difference of 11.1 kcal mol^{-1} (Figure 2.6 (b)) has a twisted 6-membered ring, producing unfavourable interactions.

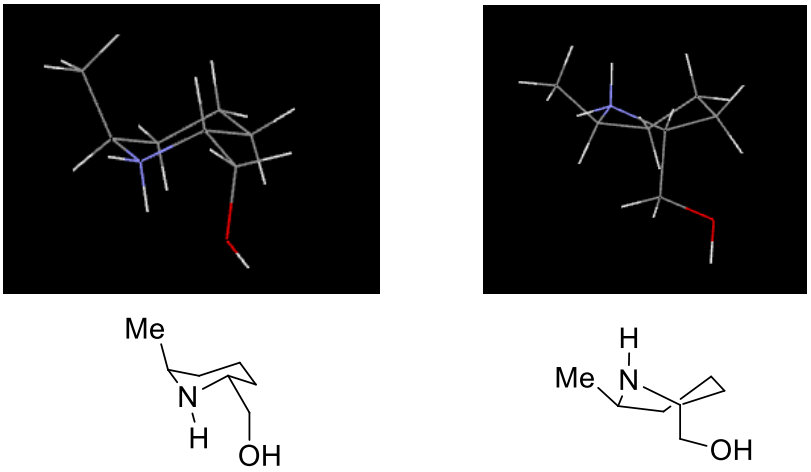

Figure 2.6: Comparison of two different conformations of the same piperidine **Fr16**.

From the data in Table 2.3 and Table 2.4, it is possible to see that there are a large number of conformers with a low conformational energy difference. It is also clear that in the more 3-dimensional areas of the PMI plot (PMI categories 4, 5 and 6), the conformations generally have a lower conformational energy difference. This is a promising result, suggesting that these more 3-dimensional conformations are accessible.

In order to select a suitable subset focussed on the under-represented area of the PMI plot, with suitable conformational energy difference, the data set was analysed further. The number of compounds at a given conformational energy difference and PMI category are shown in Figure 2.7. The number of compounds is given by the size of the graph point (numbers adjacent). As we were aiming to select between 20 and 30 compounds for the sub-set, this graph provides a useful insight into the factors that govern the selection of a suitable number. The trade-off between conformational energy difference and PMI category can clearly be seen in Figure 2.7.

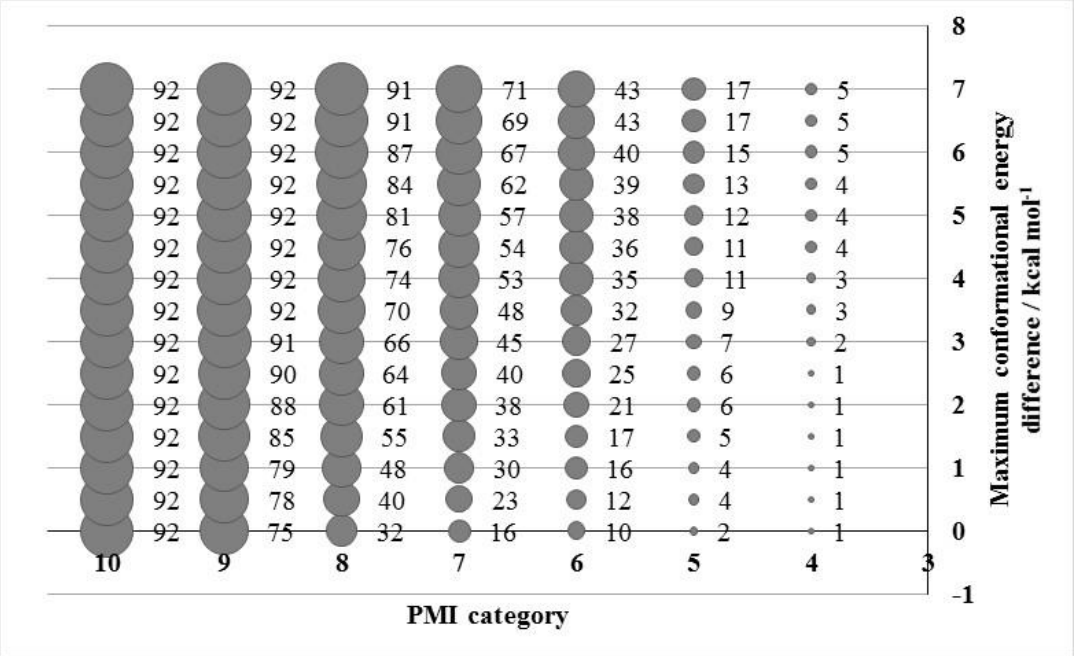

Figure 2.7: Graph showing the number of compounds selected at different conformational energy difference and PMI categories.

As expected, the higher the conformational energy cut off and the more PMI categories included then the higher the number of compounds that would be selected. Likewise, the lower the conformational energy cut off, and the fewer PMI categories chosen, then the lower the number of compounds that would be selected. In order to obtain a suitable number of compounds, there has to be a balance between the energy cut off and PMI category cut off. For a large spread across the plot (e.g. all PMI categories), the energy cut off must be low, otherwise the number of compounds becomes too large. However, the energy cut off should not be so low as to eliminate compounds that might have conformers with accessible energies. This is best exemplified with an example: if the PMI category goes up to 8 and the conformational energy difference is 1.0 kcal mol^{-1}, 48 compounds would be identified; this is over half the number of starting compounds. Similarly, when the PMI category is reduced to 3, 4, 5 and 6 and the conformational energy difference cut off is at 4.0 kcal mol^{-1}, 35 compounds would be identified. Both are beyond our target numbers for the sub-set library. The most promising results comes from the area around a conformational energy cut off of between 1.0 and 2.0 kcal mol^{-1} and selecting compounds from categories 1-6 and 1-7. We planned that the number of different isomers selected would be no more than 15 out of the possible 23. Therefore, closer analysis of conformers with an energy of less than 1.5 kcal mol^{-1} in PMI category 7 was undertaken. As with the plot as a whole,

PMI category 7 can be further segmented into 10 smaller categories. The number of conformations, compounds and isomers given in each of these sub-categories is shown in Table 2.5.

Entry	Energy / kcal mol^{-1}	Category	Number of Conformers	Number of Compounds	Number of Isomers
1	< 1.5	1 to 6	25	17	11
2	< 1.5	1 to 6.1	26	18	11
3	< 1.5	1 to 6.2	26	18	11
4	< 1.5	1 to 6.3	32	22	14
5	< 1.5	1 to 6.4	38	26	14
6	< 1.5	1 to 6.5	41	27	14
7	< 1.5	1 to 6.6	46	30	15

Table 2.5: Analysis of the library between PMI cateogories 6 and 7 to determine suitable compounds for the library by varying energy cut off and PMI categories.

From Table 2.5, we can see that the most suitable number of compounds and isomers would be obtained by selecting from categories 1 to 6.3 (Entry 4). It was our plan that the 22 compounds selected would form the sub-set library of compounds. The compound numbers of these 22 compounds can now be associated with the structure, which to this point has remained anonymous. The structures of the 22 selected compounds for the sub-set library (out of the starting 92) are shown in Figure 2.8.

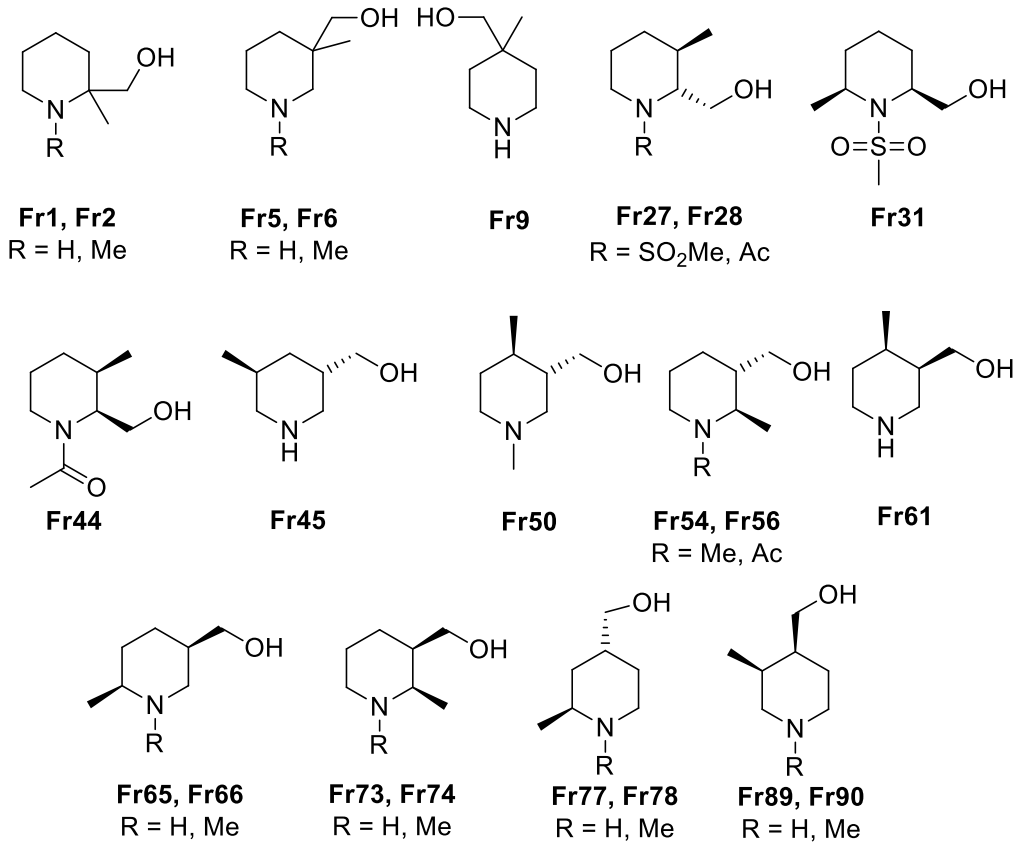

Figure 2.8: The 22 selected compounds, shown as 14 isomers. The R groups are shown where one isomer has different nitrogen functionalisation.

The selected 22 compounds have at least one low energy conformer (conformational energy difference < 1.5 kcal mol^{-1}) in the top right of the PMI plot (PMI categories 3, 4, 5 and 6), and are therefore appropriate to explore as 3-dimensional fragments. Although the compounds were selected based on conformations at the top right of the PMI plot, it is likely that the compounds will also have conformations that fall in categories outside 3 to 6 and this can be considered a bonus. Therefore, all of the conformers that have a conformational energy difference of <1.5 kcal mol^{-1} for the selected 22 compounds are shown in Figure 2.9(a). For comparison, the conformers of all the 92-member library compounds with energy <1.5 kcal mol^{-1} are shown in Figure 2.9(b). Figure 2.9 (b) has 386 conformers for the 92 compounds and is effectively the PMI plot that was used to select the fragments. The conformations in Figure 2.9 (b) are weighted towards the rod-disc axis, whereas the selected compounds (Figure 2.9 (a)) have a higher percentage of conformers in the more interesting, under-represented, 3-dimensional area of the PMI plot.

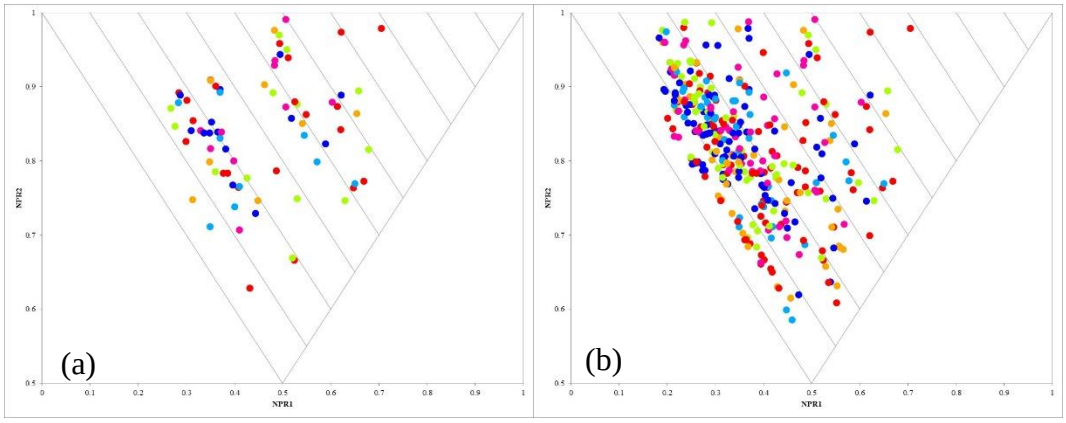

Colour						
Conformational energy difference / kcal mol^{-1}	0	< 0.3	< 0.6	< 0.9	< 1.2	< 1.5

Figure 2.9: PMI (a), shows conformers with an energy of less than 1.5 kcal mol^{-1} for all 22 final compounds. This is contrasted by PMI (b), which shows conformers with an energy of less 1.5 kcal mol^{-1} for all 92 starting compounds. There are a total of 386 conformers on PMI (b), compared to 76 conformers on PMI (a).

It may be concluded that the compounds selected for the sub-set library are focussed on the more interesting 3-dimensional area of the plot and access under-represented areas of fragment chemical space. These conformers are low in conformational energy difference and are therefore expected to be readily accessible.

2.3 "Enantiomer problem"

In carrying out further analysis of the piperidine hydroxymethyl fragments, an unexpected anomaly between different enantiomers of some of the compounds was noted from the output of data from Pipeline Pilot. It was found that, for some compounds, if the enantiomers of a given disubstituted piperidine fragment were input and analysed, the conformations generated computationally were not the same. As a result the different enantiomers had different positions on the PMI plot. This was not expected as different enantiomers should have mirror image conformations and would therefore give the same PMI result. These difference are presented in more detail below.

At this point, it was decided that a systematic approach to drawing the compounds should be formulated as this would help comparisons between different systems. These guidelines are detailed below.

- The group with lowest priority (R^1) is drawn "up".
- The "up" wedge gets larger away from the molecule, the "down" wedge gets smaller away from the molecule.
- Nitrogen substituent order is always NH, NMe, NSO_2Me and NC(O)Me.
- Any geminal disubstituted fragments come first.
- Start with lowest priority group (R^1) in the 2-position, and R^2 opposite.
- The diastereomer order is always *trans* then *cis*.
- R^2 then moves around the ring to the position of R^1.
- Then move R^1 to the 3-position and then repeat.
- Continue until all isomers are drawn.
- Different scaffolds will have a new letter assigned to the name and enantiomers, where required, will be defined as (a) for R^1 = "up" and (b) for R^1 = "down".

These guidelines also help to ensure investigation of all isomers and aims to avoid error. The newly drawn isomers are shown in Figure 2.10. It must be noted that the fragments described in Section 2.2 have a different numbering system. From here onwards, the new numbering system will be adopted.

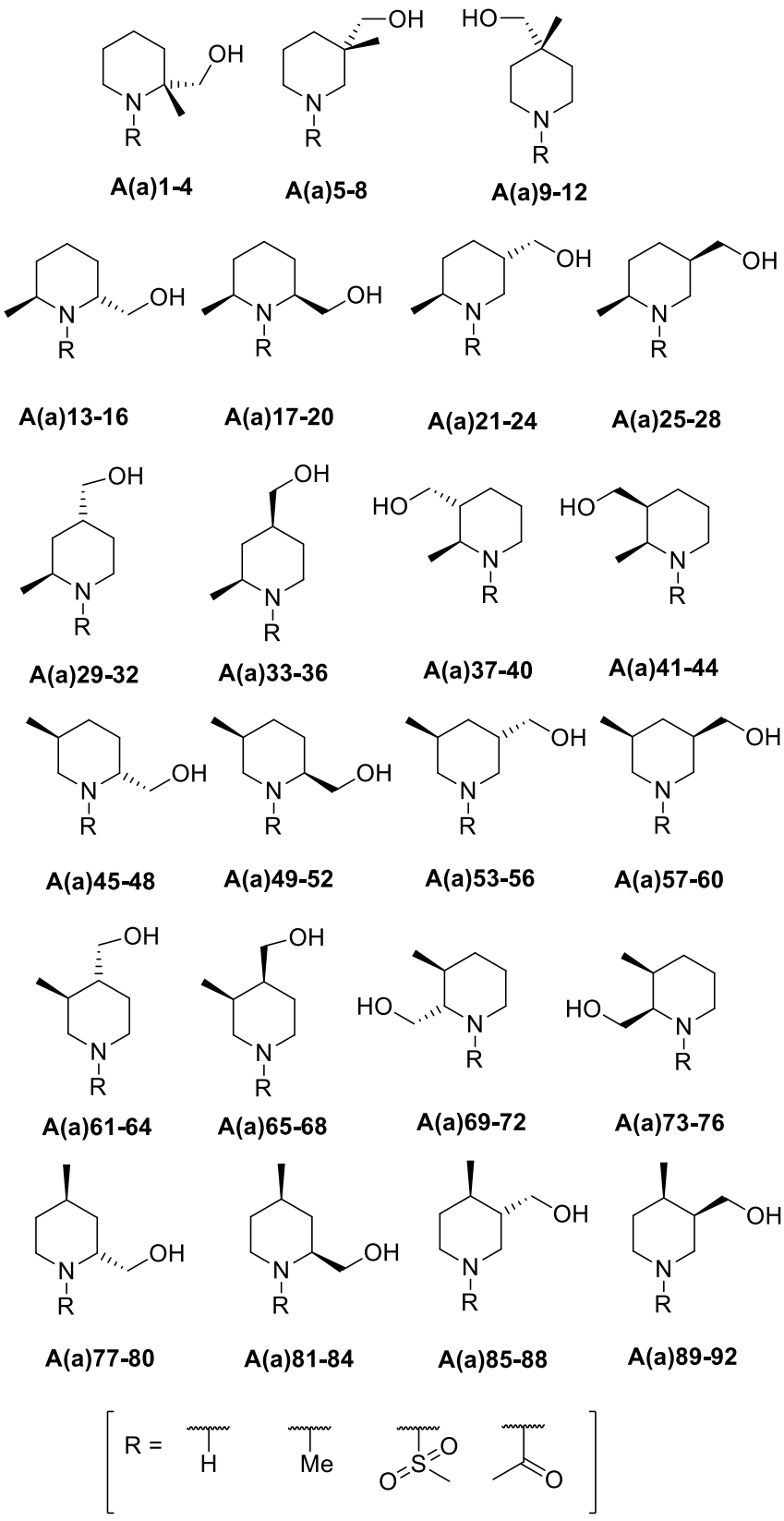

Figure 2.10: All 23 isomers of piperidine hydroxymethyl fragments drawn using the new guidelines, where the methyl group is “up”.

The guidelines were then repeated to give the enantiomers of the 92-compounds, in which R^1 was drawn in the "down" position. Separate conformer generation and PMI analysis were carried out on the two sets of enantiomers (Me "up" and Me "down"). Initial analysis considered the difference in conformations generated for the whole set (Table 2.6) and how this varied across the PMI plot.

	Data Set	PMI Category										Total
		1	2	3	4	5	6	7	8	9	10	
1	Me "up"	0	0	0	6	44	180	326	889	1155	240	2840
2	Me "down"	0	0	0	8	33	168	351	900	1110	218	2788

Table 2.6: Number of conformers in each of the PMI categories for the two different hydroxymethyl piperidine enantiomer data sets.

From Table 2.6, it can be seen that there is a noticeable difference in the two different data sets and the total number of conformations generated for each 92-member library. It is also clear that there is a variation in the spread of the conformations across the plot. For a more simple comparison, the lowest energy conformations are shown plotted on a PMI plot (Figure 2.11). Figure 2.11 (a) shows the R^1 = "up" data set, Figure 2.11 (b) shows the R^1 = "down" data set and Figure 2.11 (c) shows the two different data sets overlaid.

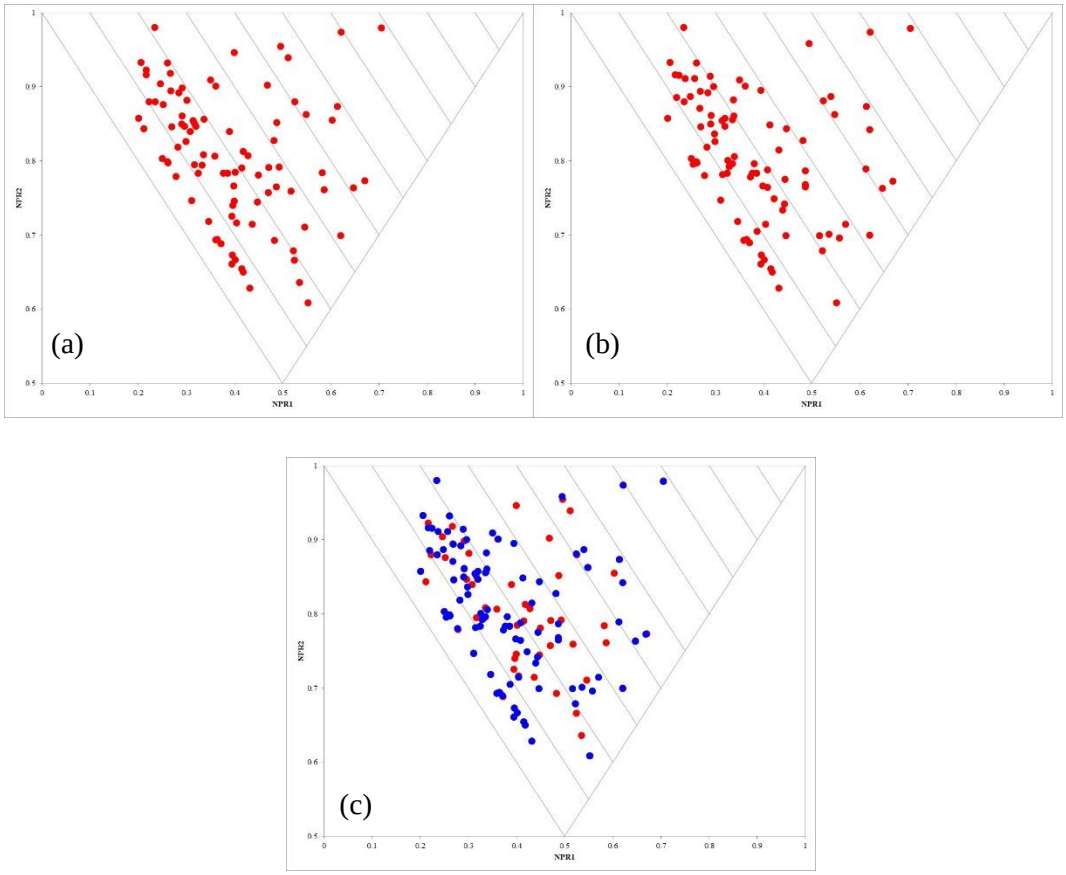

Figure 2.11: Three different PMI plots showing the two different enantiomer data sets (R^1 = "up" (a) and R^1 = "down" (b)). The two enantiomer data sets are overlaid in (c), R^1 = "down" blue. All plots show the lowest energy conformer.

The results in Figure 2.11 show how some data points have very similar PMI positions and others are significantly different. Some of the most significantly different pairs of enantiomers are shown in Figure 2.12. Unfortunately, the observation of difference between enantiomers is quite random, and no real correlation could be worked out.

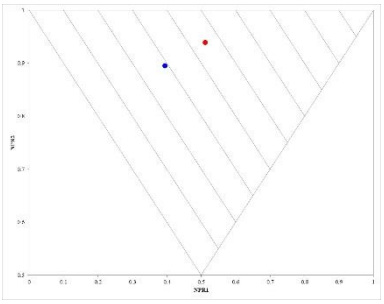

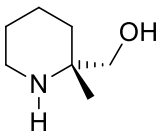

A1

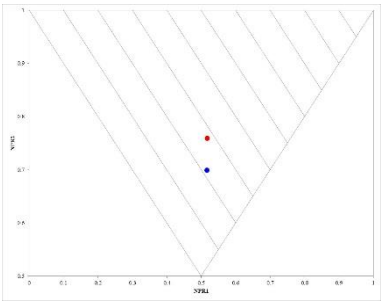

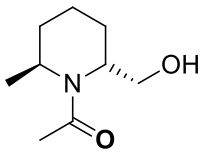

A15

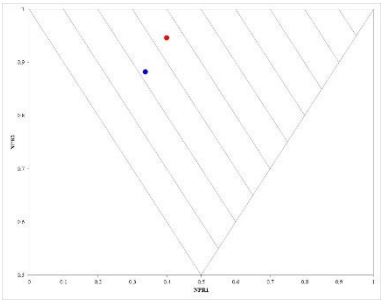

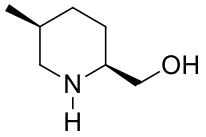

A49

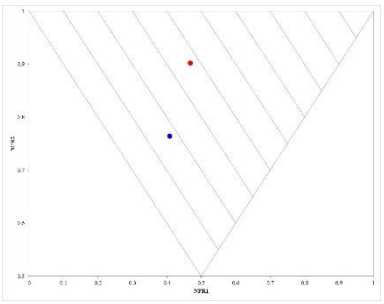

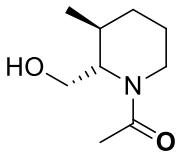

A71

Figure 2.12: Some of the compounds where the calculated conformations of enantiomers are significantly different.

At this point, we had to decide how to treat the "enantiomer problem". In the end, we decided that each enantiomeric data set should be fully evaluated in the way described previously and then the results of the two sub-sets could be combined to identify the final sub-set of compounds. This was considered the best approach as the drawn structures in the previously described approach effectively had "mixtures" of the two enantiomeric series.

The number of compounds that would be selected at each of the conformational energy difference cut offs was analysed for the R^1 = "up" data set. This is summarised in Figure 2.13. There is a trade-off between conformational energy difference and PMI category. The most suitable number of compounds would be selected from a conformational energy difference of <1.5 kcal mol^{-1} and between PMI categories 6 and 7. Further analysis of PMI category 6 and the number of conformers, compounds and isomers obtained is given in Table 2.7.

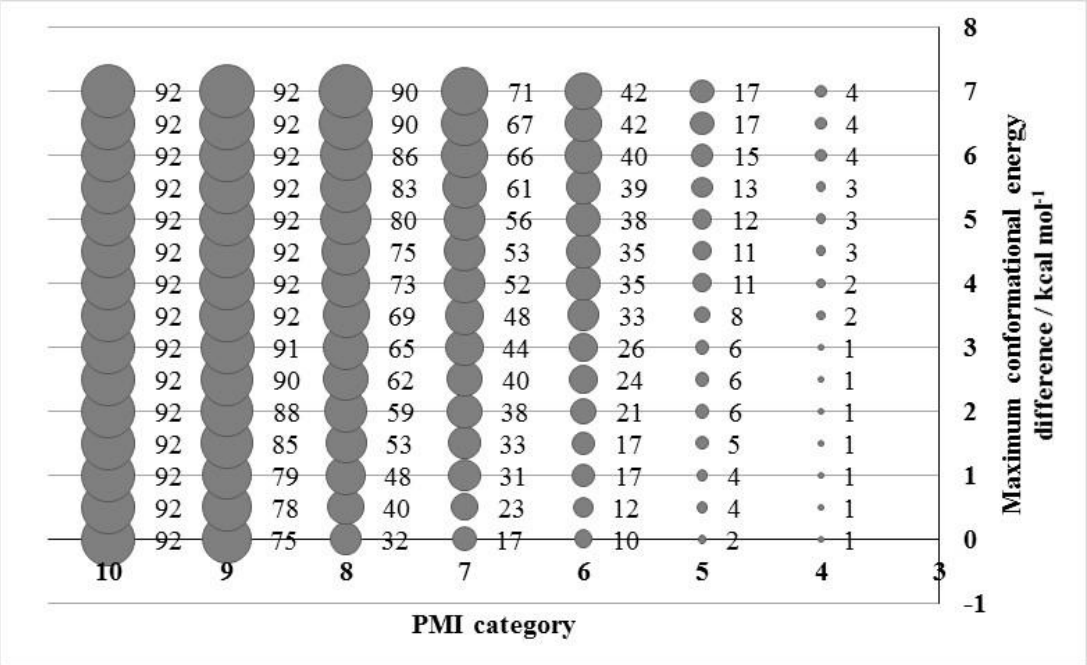

Figure 2.13: Graph showing the number of compounds selected at different conformational energy difference and PMI categories.

Entry	Energy / kcal mol^{-1}	PMI Category	Number of Conformers	Number of Compounds	Number of Isomers
1	< 1.5	1 to 6	23	17	11
2	< 1.5	1 to 6.1	24	18	11
3	< 1.5	1 to 6.2	24	18	11
4	< 1.5	1 to 6.3	30	22	14
5	< 1.5	1 to 6.4	37	26	14

Table 2.7: Analysis of the library between PMI categories 6 and 7 to determine suitable compounds for the library by varying energy cut off and PMI categories.

The same analysis was then carried out on the R^1 = "down" data set. The number of compounds selected at each of the conformational energy difference cut offs was analysed and are shown in Figure 2.14. As with the R^1 = "up" data set, there is a trade-off between conformational energy difference and PMI category. The most suitable number of compounds would be selected from a conformational energy difference of

<1.5 kcal mol^{-1} and between PMI categories 6 and 7. Further analysis of PMI category 6 is given in Table 2.8.

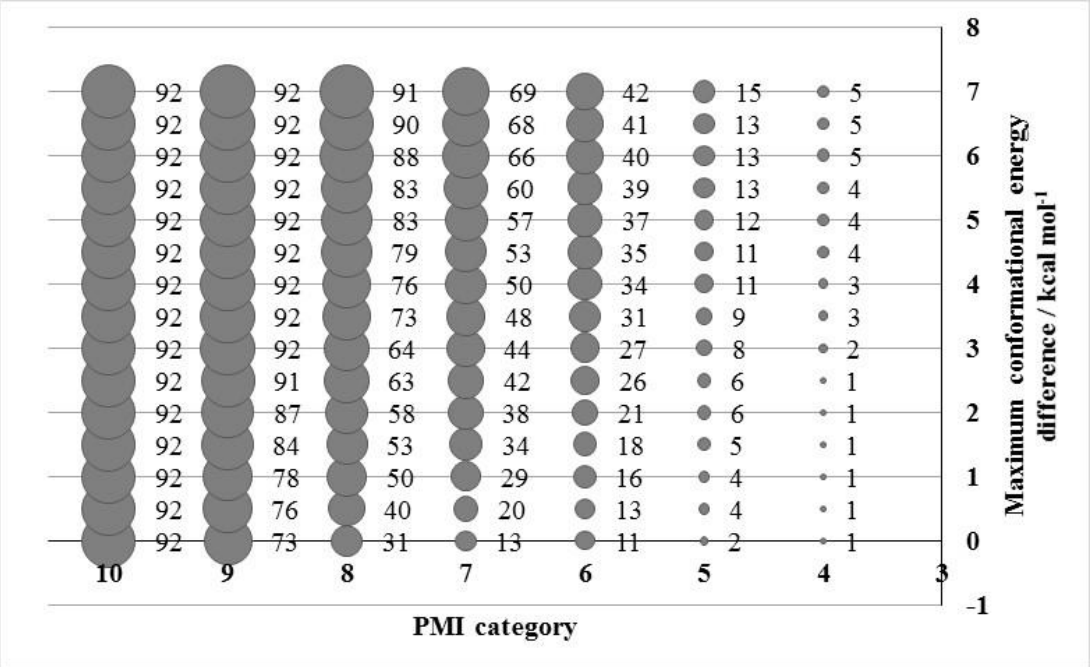

Figure 2.14: Graph showing the number of compounds selected at different conformational energy difference and PMI categories.

Entry	Energy / kcal mol^{-1}	Category	Number of Conformers	Number of Compounds	Number of Isomers
1	< 1.5	1 to 6	27	18	11
2	< 1.5	1 to 6.1	29	19	11
3	< 1.5	1 to 6.2	32	20	12
4	< 1.5	1 to 6.3	37	24	15
5	< 1.5	1 to 6.4	39	25	15

Table 2.8: Analysis of the library between PMI cateogories 6 and 7 to determine suitable compounds for the library by varying energy cut off and PMI categories.

Comparing data sets for the enantiomeric pairs of the 92 compounds and information in Table 2.7 and Table 2.8, it can be seen that the number of conformers, compounds and isomers differ for the two different enantiomer data sets. However, these differences are not that significant when we analysed the compounds and isomers that were selected. The compound numbers for the compounds that would be selected from an energy <1.5 kcal mol^{-1} and up to 6.2 PMI category are detailed in Table 2.9.

	Data set	Selected Compound Numbers																			
1	**Me "up"**	1	2	5	6	9		19		25	26	38	40	41	42	53	65	66	71	72	89
2	**Me "down"**	1	2	5	6	9	16	19	20	25	26	38	40	41	42	53	65	66	71	72	89
3	**Isomer**	1		2		3	4	5		7		10		11		14	17		18		23

Table 2.9: Fragments selected from the individual analysis of both enantiomer data sets, with the relevant isomer number.

There is little difference in the compounds selected from each data set, with only two variations in compounds and only one variation in isomer. As this difference is small, it was decided that the two compound selections could be combined to give the final compound sub-set. The structures of these compounds are shown in Figure 2.15.

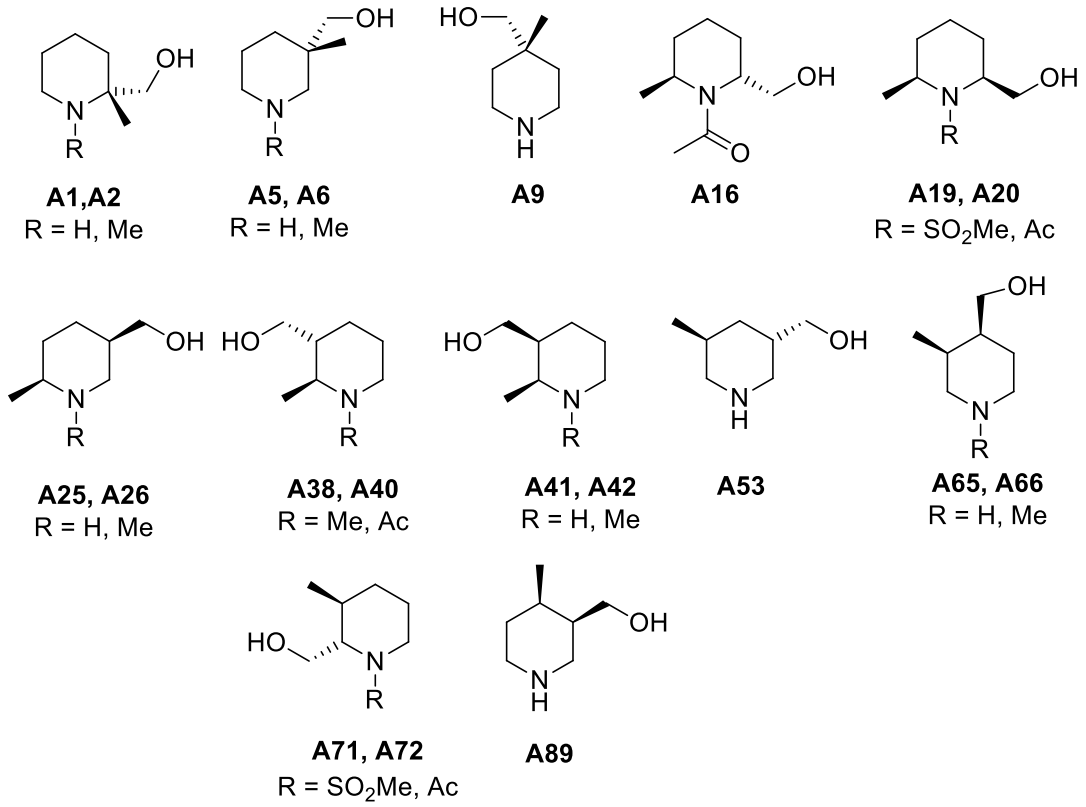

Figure 2.15: The 20 fragment selected sub-set, combined from both enantiomer data set analyses.

The PMI plot with the selected 20 compounds was generated. This plot includes the two different enantiomer data set points and shows 121 conformations covering the whole of the PMI plot (Figure 2.16 (a)). This can be compared to the PMI plot showing the 777 conformers of both enantiomers of all 92 compounds, with a conformational energy difference of < 1.5 kcal mol^{-1} (Figure 2.16 (b)).

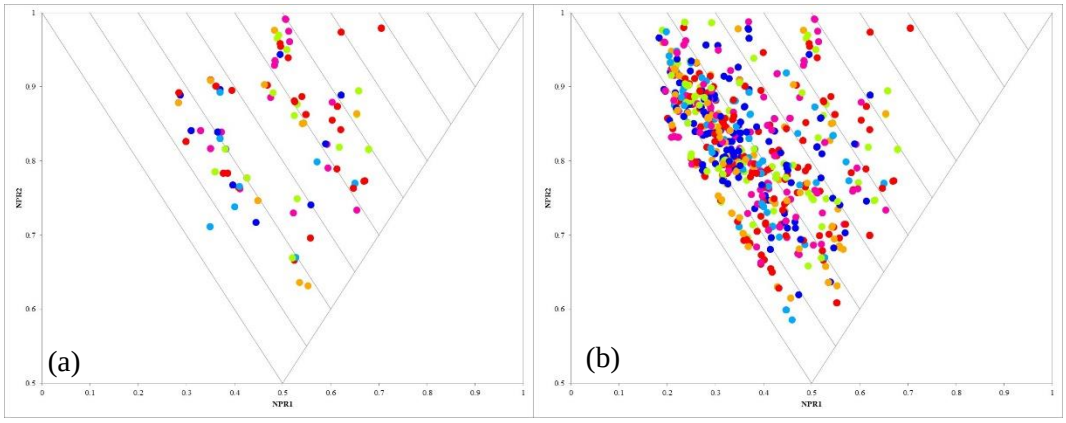

Colour						
Conformational energy difference / kcal mol^{-1}	0	< 0.3	< 0.6	< 0.9	< 1.2	< 1.5

Figure 2.16: PMI (a), shows conformers with an energy of < 1.5 kcal mol^{-1} for all 20 selected fragments. This is contrasted by PMI (b), which shows conformers with an energy of less 1.5 kcal mol^{-1} for both enantiomer conformers for all 92 starting compounds.

This comparison shows that the new sub-set compounds compares well to the original 92-member library. There is a good spread of conformations across the plot with focus on the more 3-dimensional area of the plot. There are a large number of conformers with a low energy conformational energy difference which suggests a large number of accessible conformations. There are a range of different compounds and isomers which give the sub-set library architectural and conformational diversity.

2.4 New protocol analysis: overview of selection process and results

Due to the "enantiomer problem" observed in the previous analysis, the protocol was further developed with the aim to reduce or eradicate any further issues. In particular this would remove the need to analyse two sets of data separately and combine them. The protocol was developed to calculate the mirror image of the input compound and run both data sets through the program and then combine both data sets at the end, see Section 6.1.4. The 92 compounds, as drawn in Section 2.3, were passed through this new protocol. The data generated from these compounds was then analysed in the same way as previously described. A PMI plot of the 92 lowest energy conformations is shown in Figure 2.17.

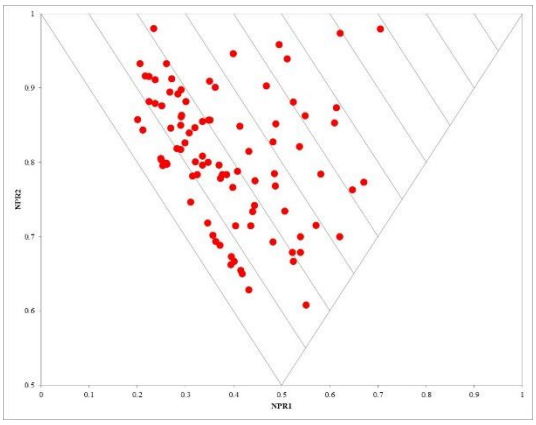

Figure 2.17: PMI plot showing the lowest energy conformations of the hydroxymethyl piperidine fragments generated using the new protocol.

All the conformations generated were then analysed to determine the spread of conformers across the plot and the energy of these conformers was analysed (Table 2.10).

PMI Category	Conformational Energy Difference / kcal mol^{-1}							
	0 - 1	**1 - 2**	**2 - 3**	**3 - 4**	**4 - 5**	**5 - 6**	**6 - 7**	**7-20**
4	1	0	0	1	1	1	0	3
5	3	3	1	5	4	10	3	15
6	16	8	12	26	23	21	14	58
7	16	15	30	28	29	44	37	173
8	41	42	60	64	76	88	119	481
9	130	114	96	79	75	128	158	471
10	49	20	14	22	21	22	25	63
Total	256	202	213	225	229	314	356	1264

Table 2.10: Table showing the number of conformers in each PMI category and their conformational energy differences.

The total number of conformers in each of the PMI categories are shown in Table 2.11 below. The enantiomer data set for Me "down" is also presented. This data set was analysed to confirm that there was no difference in enantiomers with the new protocol.

	Data Set	PMI Category										Total
		1	2	3	4	5	6	7	8	9	10	
1	Me "up"	0	0	0	7	44	178	372	971	1251	236	3059
2	Me "down"	0	0	0	7	44	178	372	971	1251	236	3059

Table 2.11: Comparison of the number of conformers in each PMI category for both enantiomer data sets, there is clearly no difference between enantiomers.

The data showed the same general trend as the previous analysis in the spread of conformers across the plot with an increasing number in 4, 5 and 6. There are a large number of conformers in category 9, but a significant drop off in category 10, suggesting that there are a few conformers that have a more rod/disc like shape. This shows that the 92-member library has shape diversity. Information in Table 2.10 shows that the conformers in more 3-dimensional areas of the plot (PMI categories 4,5,6) have low conformational energy differences which suggest that these more 3-dimensional conformations are accessible.

As with previous iterations, the number of compounds selected based on conformational energy difference and position on the PMI plot was analysed. This is shown in Figure 2.18. The most suitable number of compounds for the sub-set library are obtained from a conformational energy difference of < 1.5 kcal mol^{-1} and between category 6 and 7. Further analysis of this is shown in Table 2.12.

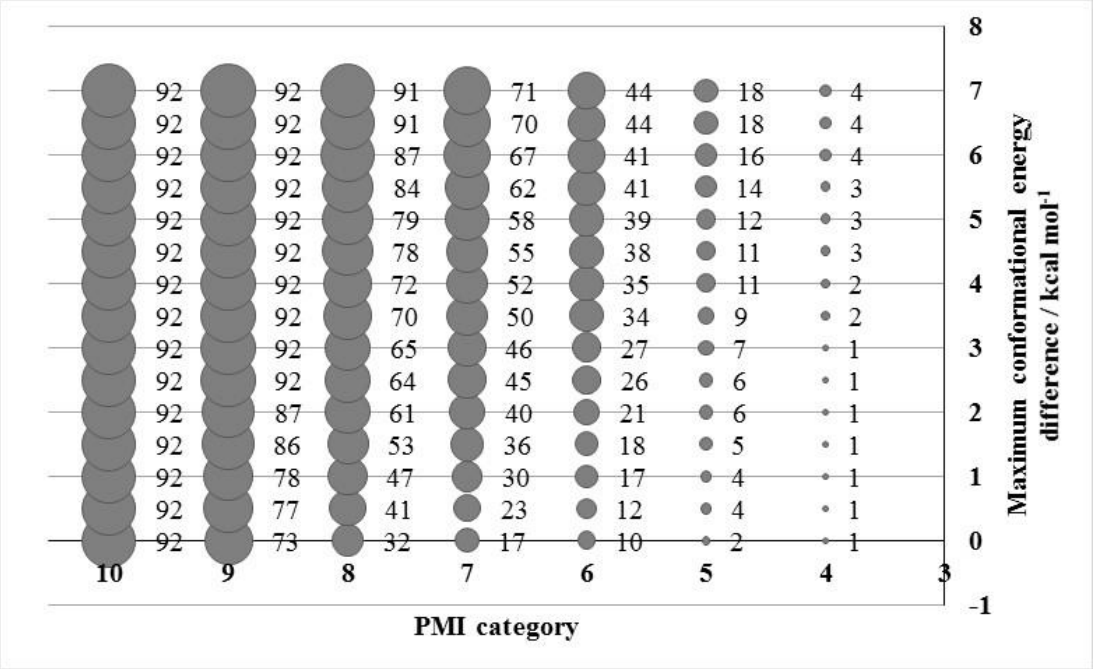

Figure 2.18: Graph showing the number of compounds selected at different conformational energy difference and PMI categories.

Entry	Energy / kcal mol^{-1}	Category	Number of Conformers	Number of Compounds	Number of Isomers
1	< 1.5	1 to 6	26	18	11
2	< 1.5	1 to 6.1	27	19	11
3	< 1.5	1 to 6.2	27	19	11
4	< 1.5	1 to 6.3	33	23	14
5	< 1.5	1 to 6.4	37	24	14

Table 2.12: Analysis of the library between PMI cateogories 6 and 7 to determine suitable compounds for the library by varying energy cut off and PMI categories.

The data in Table 2.12 shows that as with the previous analysis (Section 2.3), the most suitable number of compounds and isomers for the sub-set library is given by categories 1 to 6.2. With the new protocol, 19 compounds would be selected and the compound numbers for these are given in Table 2.13 ("New"). These can be compared to the compounds selected from the previous iteration, labelled "Old".

	Data set	Selected Compound Numbers																			
1	**New**	1	2	5	6	9		19	20	25	26	38	40	41	42	53	65	66	71	72	89
2	**Old**	1	2	5	6	9	*16*	19	20	25	26	38	40	41	42	53	65	66	71	72	89
3	**Isomer**	1		2		3	*4*	5		7		10		11		14	17		18		23

Table 2.13: The fragment number for the selected sub-set of fragments compared to the fragments selected in the previous analysis; there is only one compound different.

It can be seen that the new sub-set only varies by one compound, **A16**. This is ideal as synthesis of some of the original sub-set had already been started (See Chapter 3 for fragment synthesis). It is these 19 compounds that represent the final selection of

compounds for the hydroxymethyl piperidine library sub-set. The structures of these 19 compounds are shown in Figure 2.19.

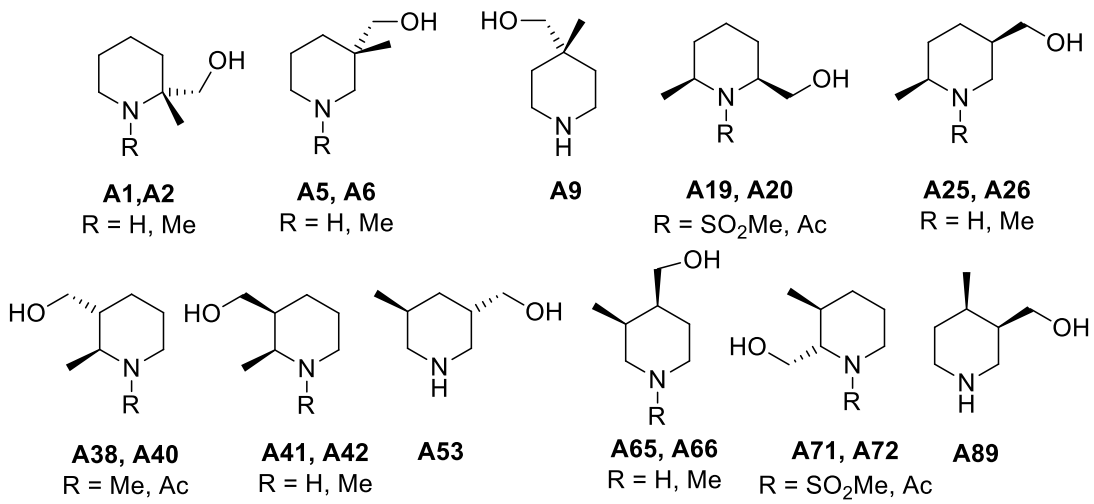

Figure 2.19: The selected hydroxymethyl piperidine19 fragment sub-set.

The PMI plot showing all the conformers of these 19 compounds with a conformational energy difference of < 1.5 kcal mol^{-1} is shown in Figure 2.20 (a). This can be compared to the PMI plot of the original 92-member library (Figure 2.20 (b)). This again shows that the selected sub-set of compounds focusses on the under-represented, 3-dimensional area of the plot, with less conformations falling close to the rod-disc axis which is more heavily weighted in the original 92-member library. These plots show that the hydroxymethyl piperidine scaffold produce a fragment library with interesting shape and conformational diversity.

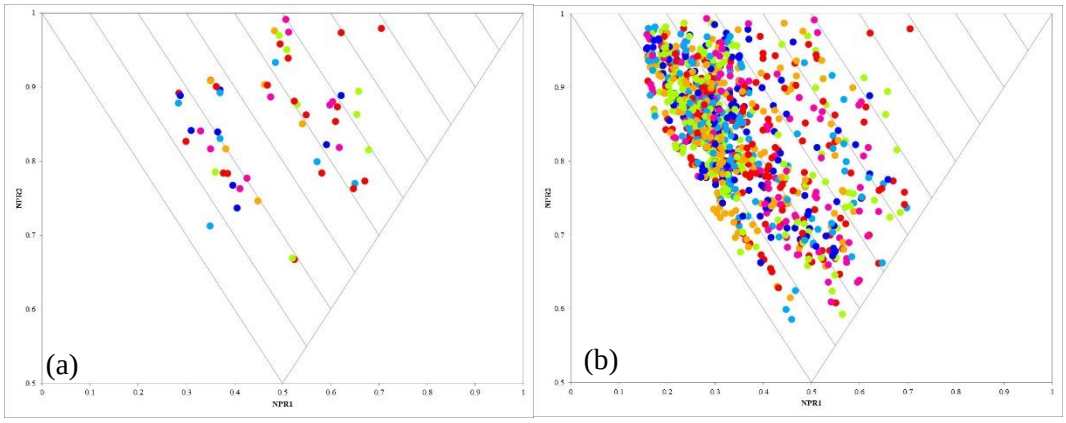

Colour						
Conformational energy difference / kcal mol^{-1}	0	< 0.3	< 0.6	< 0.9	< 1.2	< 1.5

Figure 2.20: PMI (a), shows conformers with an energy of less than 1.5 kcal mol^{-1} for all 19 selected fragments. This is contrasted by PMI (b), which shows conformers with an energy of less 1.5 kcal mol^{-1} for all 92 starting compounds.

2.5 Computational selection from different scaffolds and substituents

As the Pipeline Pilot protocol had now been optimised and the analysis investigated with the hydroxymethyl piperidine library, it is possible to summarise the process and apply this method to different scaffolds and substituents. The steps for the analysis are as follows:

- All fragments are drawn according to the rules defined in Section 2.3.
- The structures are converted into SMILES strings.
- The SMILES strings are input into the new Pipeline Pilot protocol to generate conformations with an energy up to 20 kcal mol^{-1} and an RMSD cut off of 0.1.
- All the conformations are analysed for the number of conformers in each PMI category at different conformational energy cut offs.
- All the conformations are then analysed to determine the number of compounds selected at different PMI category cut offs and conformational energy cut offs.
- The conformational energy difference cut off will always be < 1.5 kcal mol^{-1}, but the PMI category may vary, therefore the number of conformers, compounds and isomers are selected at different PMI categories are analysed further.
- The most suitable number of compounds and isomers for the sub-set library is selected and the compound numbers are associated with the structures.
- A PMI plot of these selected compounds is then generated.

This method of compound analysis and sub-set selection was then applied to a number of different nitrogen heterocycles with varying substituents.

2.5.1 Methyl ester, methyl-disubstituted piperidine library

Firstly, the closely related methyl and methyl ester disubstituted piperidine was analysed. The similarity in the substituents of the ester and hydroxymethyl could make synthesis of selected compounds simpler, as simple reduction of the ester would provide the hydroxymethyl group. The 92 different compounds provided from the 23 different isomers of the disubstituted piperidine were drawn based on the guidelines set out previously (Section 2.3) and are shown in Figure 2.21.

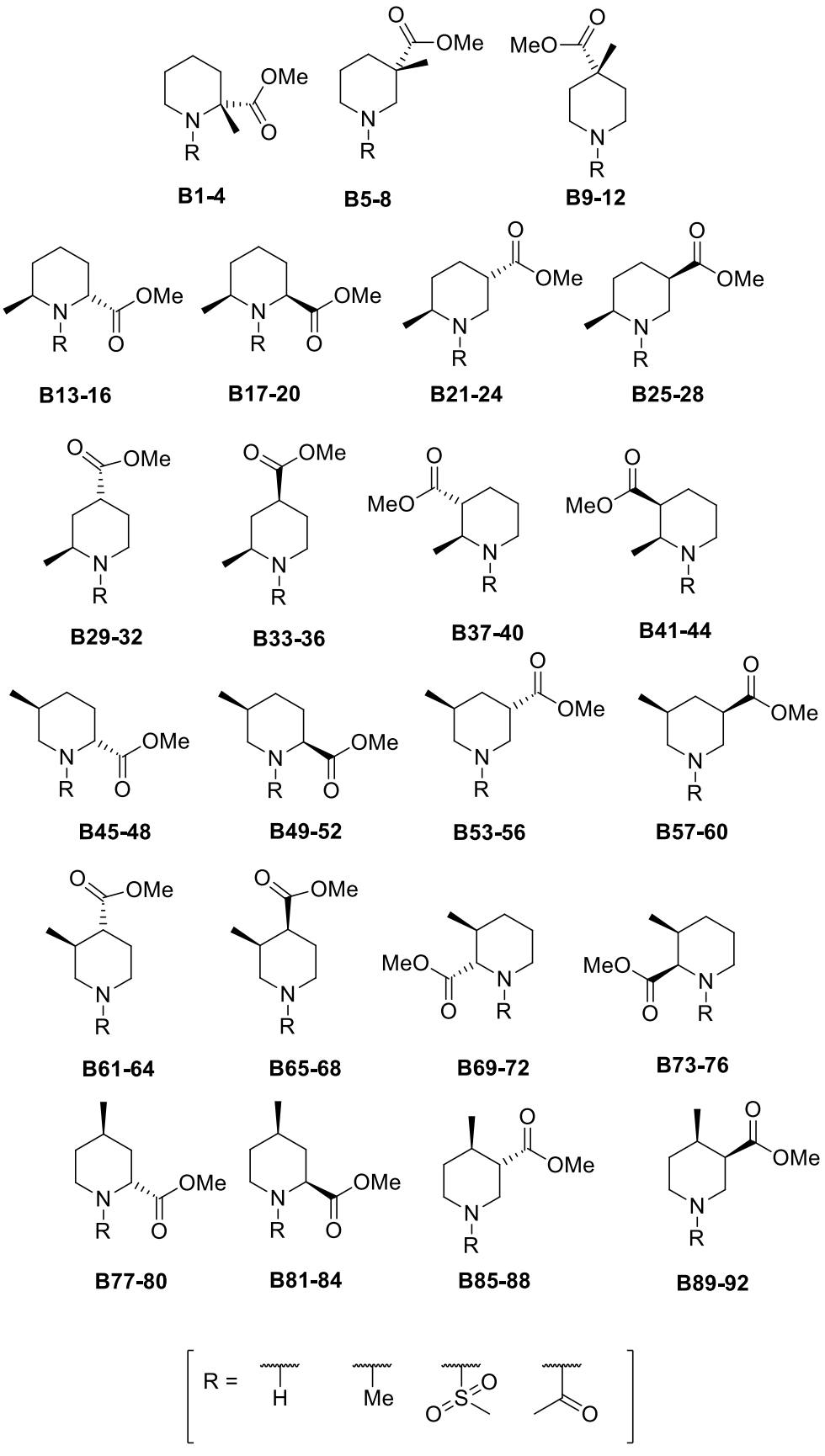

Figure 2.21: The 23 different isomers of ester, methyl disubstituted piperidine. The four different nitrogen substituents are also shown.

These 92 compounds were then subjected to the standard analysis. The PMI plot of the lowest energy conformers of the 92 compounds is shown in Figure 2.22. There is a relatively small spread of conformers across the PMI plot and most lie towards the rod-disc axis compared to the hydroxymethyl piperidine library (See Figure 2.16). This is perhaps surprising given that they look like they should be 3-dimensional in shape.

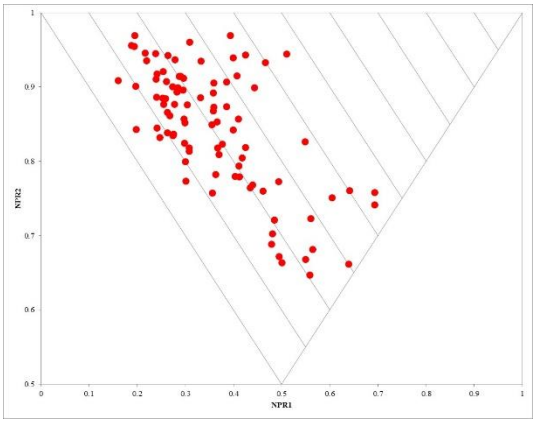

Figure 2.22: PMI plot of the lowest energy conformations of the 92 ester piperidine fragments.

As with the previous analyses, all the conformations generated for the 92 compounds were analysed to determine the spread of conformers across the different PMI categories and their relative conformational energies was analysed (Table 2.14).

Category	**Conformational Energy Difference / kcal mol^{-1}**								**Total**
	1	**2**	**3**	**4**	**5**	**6**	**7**	**8**	
3	0	0	0	0	0	0	0	1	1
4	0	0	0	0	1	0	0	2	3
5	1	0	2	1	5	8	4	25	46
6	15	6	13	10	16	18	30	105	213
7	38	16	24	29	49	49	73	430	708
8	115	79	68	73	92	146	179	905	1657
9	276	107	104	67	100	163	195	692	1704
10	88	17	25	18	15	13	17	48	241
Total	533	225	236	198	278	397	498	2208	4573

Table 2.14: Table showing the number of conformers in each PMI category and their conformational energy differences.

These data show that there is a similar trend to that seen for the hydroxymethyl piperidine library. There are no conformers in the most spherical area of the PMI plot (PMI categories 1 to 3), but some in the 3-dimensional categories 3, 4, 5 and 6. There

is a drop-off from the most populated category 9 to category 10, showing that this simple scaffold has few conformers that have the flattest shapes.

A sub-set of compounds could now be selected from the original 92-member library. The analysis in Figure 2.23 shows how the number of compounds selected varies with conformational energy difference and PMI category, with closer analysis of the 6 to 7 category shown in Table 2.15.

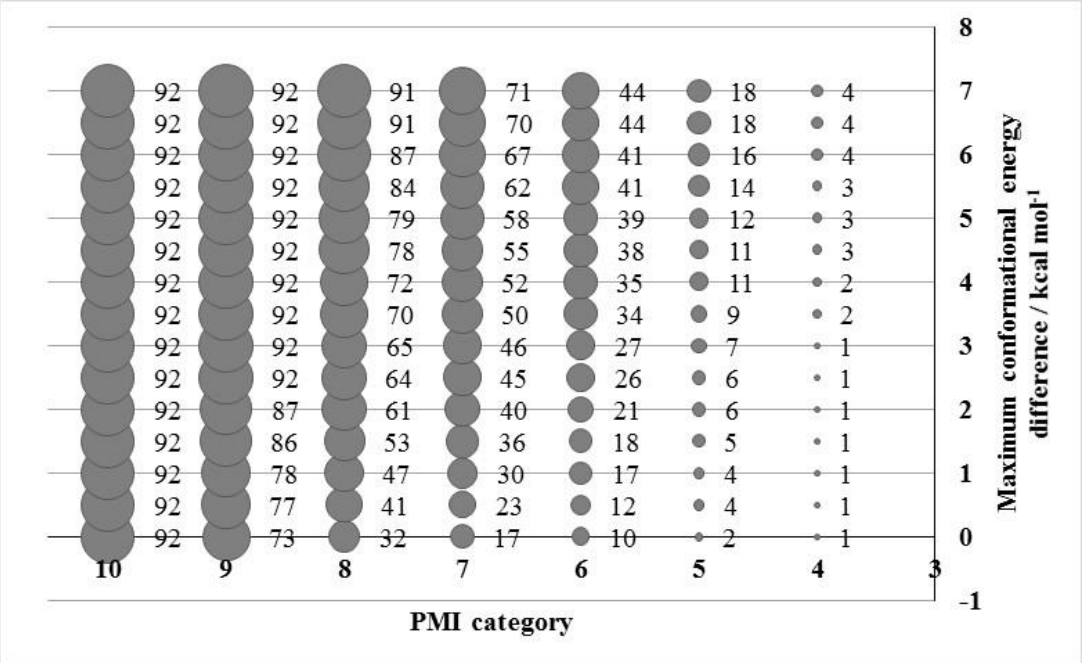

Figure 2.23: Graph showing the number of compounds selected at different conformational energy difference and PMI categories.

Entry	Energy / kcal mol^{-1}	Category	Number of Conformers	Number of Compounds	Number of Isomers
1	< 1.5	1 to 6	19	13	7
2	< 1.5	1 to 6.1	26	17	11
3	< 1.5	1 to 6.2	29	18	12
4	< 1.5	1 to 6.3	31	19	13
5	< 1.5	1 to 6.4	35	20	13

Table 2.15: Analysis of the library between PMI cateogories 6 and 7 to determine suitable compounds for the library by varying energy cut off and PMI categories.

A suitable number of compounds is given when the PMI categories selected go up to 6.2. This is also the same PMI categories as selected in the hydroxymethyl piperidine

analysis. This gives 18 compounds and 12 isomers, the compound numbers associated with these are given in Table 2.16. The structures of the 18 compounds are shown in Figure 2.24.

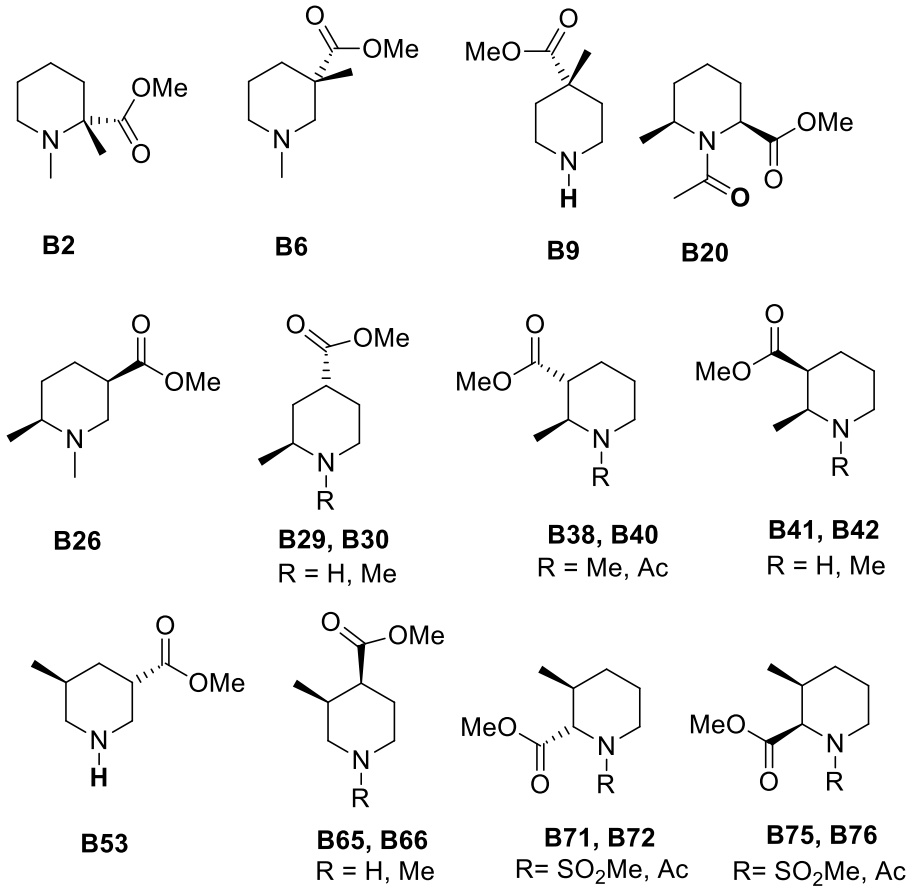

Figure 2.24: The selected methyl ester piperidine18 fragment sub-set.

	Data set	Selected compound numbers											
1	Ester		2		6	9		20		26	29	30	
2	OH	1	2	5	6	9	19	20	25	26			
3	Isomer	1		2		3	5		7		8		
4	Ester	38	40	41	42	53	65	66	71	72	75	76	
5	OH	38	40	41	42	53	65	66	71	72			89
6	Isomer	10		11		14	17		18		19		23

Table 2.16: The fragment number for the selected sub-set of fragments compared to the fragments selected in the hydroxymethyl piperidine analysis.

The PMI plot of the all the conformers with a conformational energy difference of < 1.5 kcal mol^{-1} is in Figure 2.25 (a). This can be compared the full 92 member library PMI plot, showing conformers with conformational energy difference of < 1.5 kcal mol^{-1} (Figure 2.25 (b)).

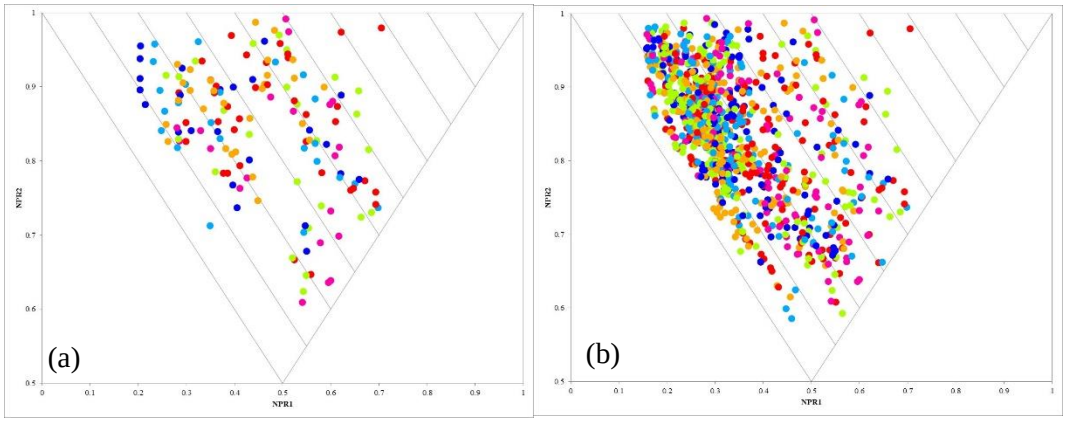

Colour						
Conformational energy difference / kcal mol^{-1}	0	< 0.3	< 0.6	< 0.9	< 1.2	< 1.5

Figure 2.25: PMI (a), shows conformers with an energy of less than 1.5 kcal mol^{-1} for all 18 selected fragments. This is contrasted by PMI (b), which shows conformers with an energy of less 1.5 kcal mol^{-1} for all 92 starting compounds.

These plots show that the sub-set library has a good coverage of the under-represented 3-dimensional fragment space. Table 2.16 also details the compound numbers associated with the methyl, hydroxymethyl piperidine sub-set. Interestingly, there is a significant overlap in compound numbers. These are associated with the same isomer and only differ in the hydroxymethyl/ester substituent. In fact, fourteen compounds are duplicated in the library. This could significantly simplify the amount of synthesis that would be required if the same synthetic route could be used to access both compounds. The two PMI plots of the hydroxymethyl and ester piperidine selected sub-sets are shown in Figure 2.26 (a) and (b). Figure 2.26 (c) shows the PMI plot of an overlay of the two different selected libraries with colours representing the substituent (See key).

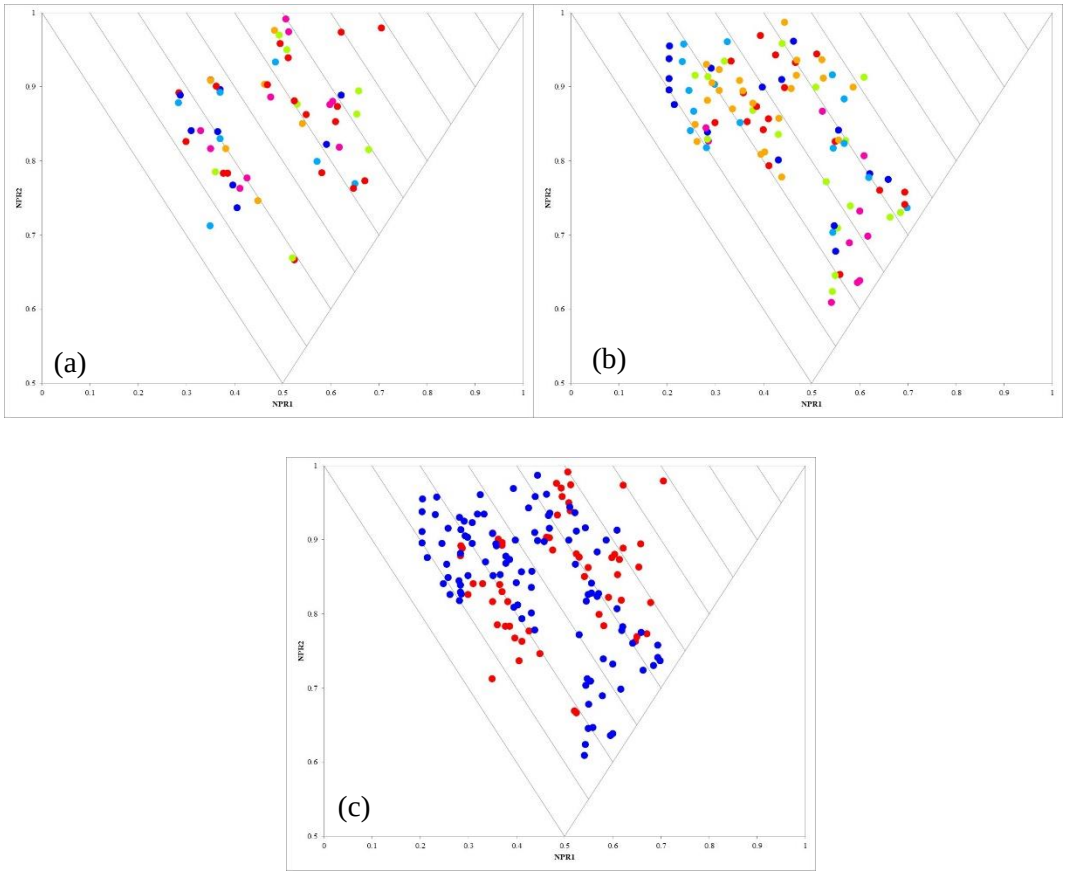

Plot (a) and (b)	Colour						
	Conformational energy difference / kcal mol^{-1}	0	< 0.3	< 0.6	< 0.9	< 1.2	< 1.5
Plot (c)	Colour						
	R^2	CH_2OH			CO_2Me		

Figure 2.26: PMI (a), shows conformers with an energy of less than 1.5 kcal mol^{-1} for all 19 selected hydroxymethyl piperidine fragments. This is contrasted by PMI (b), which shows conformers with an energy of less 1.5 kcal mol^{-1} for all 18 selected methyl ester piperidine fragments. PMI (c) shows both libraries overlaid.

The comparison of methyl/hydroxymethyl with methyl/methyl ester really highlight that even small changes to a molecule can produce quite different shaped conformations. It is evident that the ester piperidine sub-set focuses more on the area towards the rod-disc axis, contrasting with the hydroxymethyl which covers more of the spherical area of the plot. The combined sub-sets cover a large area of the plot and show that the piperidine scaffold has both shape and conformational diversity.

2.5.2 Hydroxymethyl, methyl-disubstituted pyrrolidine library

It is desirable to also populate our fragment library with different scaffolds. Therefore, we decided to analyse other simple saturated nitrogen heterocycles for their shape diversity and with a desire to select compounds that are more 3-dimensional. Thus disubstituted pyrrolidine with hydroxymethyl and methyl substituents was selected for analysis. Disubstituted pyrrolidine gives 14 different isomers and functionalising the nitrogen with H, Me, SO_2Me and Ac gives a 56-member library. These compounds are shown in Figure 2.27.

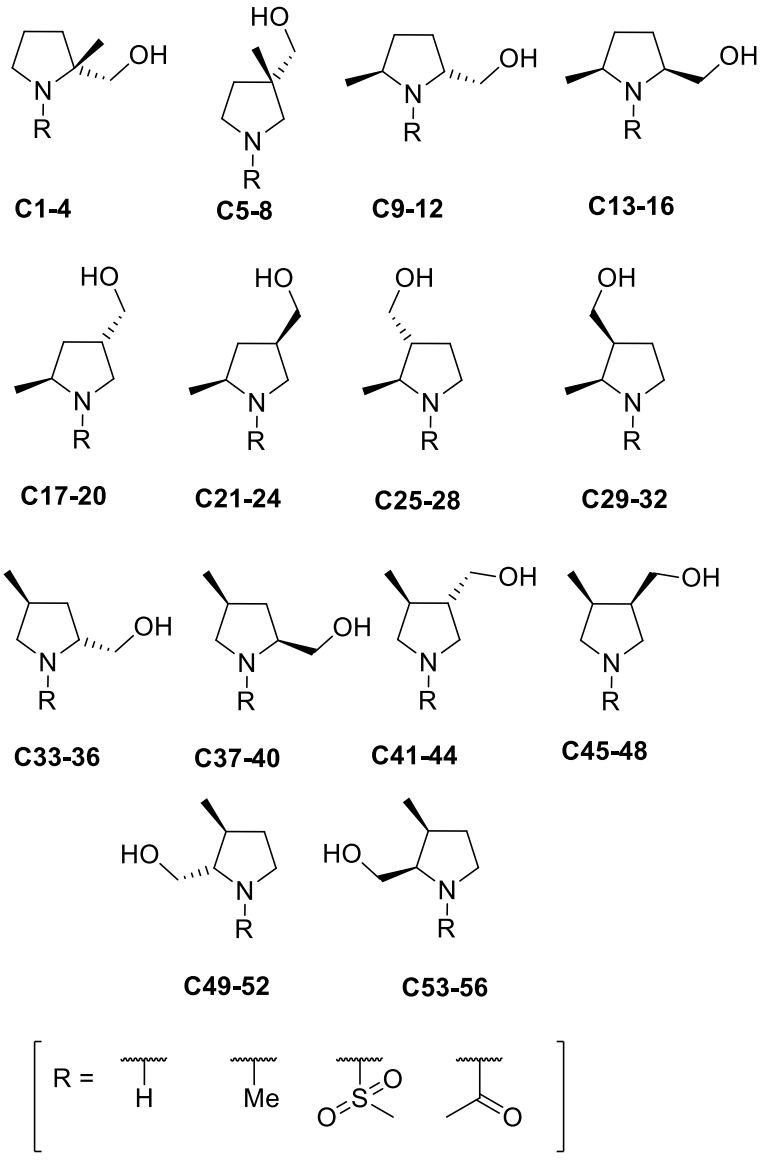

Figure 2.27: The 14 different isomers of hydroxymethyl, methyl disubstituted pyrrolidine. The four different nitrogen substituents are also shown.

The 56 compounds were then subjected to the same analysis as the piperidine compounds. The PMI plot of the lowest energy conformers of the 56 compounds is shown in Figure 2.28. This shows a small spread of conformers across the plot, with a few compounds reaching out into the more spherical area of the plot.

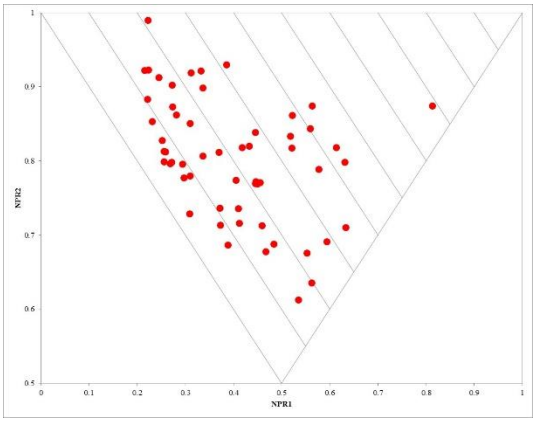

Figure 2.28: PMI plot of the lowest energy conformations of the 56 hydroxymethyl pyrrolidine fragments.

All the conformations and PMI data were then generated computationally for these 56 compounds. Analysis was carried out in the same way as for the piperidines. The number of conformers, their position on the plot and their conformational energy was analysed and is detailed in Table 2.17.

Category	**Conformational Energy Difference / kcal mol^{-1}**								**Total**
	1	**2**	**3**	**4**	**5**	**6**	**7**	**8**	
2	0	0	0	0	0	1	0	1	**2**
3	0	0	0	0	1	0	0	0	**1**
4	2	0	1	0	0	0	0	0	3
5	0	2	0	3	0	0	0	1	6
6	10	7	7	8	2	3	3	1	41
7	16	26	17	15	12	11	4	3	104
8	50	51	47	48	24	28	18	32	298
9	84	65	76	47	55	41	26	28	422
10	49	17	15	12	2	1	0	0	96
Total	211	168	163	133	96	85	51	66	973

Table 2.17: Data showing the distribution of conformers by PMI category and conformational energy.

The data in Table 2.17 show that there is a large spread of conformers across the plot, although the most spherical conformers (PMI categories 2 to 5) have a high conformational energy difference. There are increasingly more in PMI categories 6

and 7, some with lower energy suggesting accessible 3-dimensional conformers. There is a lower number of conformers in category 10, which suggest a low amount of flat conformations. This information shows that the simple pyrrolidine scaffold has both shape and conformational diversity.

For our fragment library, we did not plan to synthesise all compounds and so a sub-set library was be selected. Disubstituted pyrrolidine provides 14 isomers and 56 compounds and therefore a suitable size for the sub-set library would be no more than 7 isomers and 15 compounds. The data set was then analysed to determine the number of compounds obtained from different areas of the plot and with different energies. The full library analysis is show in Figure 2.29. It can be seen that there is a trade-off in PMI category and conformational energy. In order to select compounds from the most spherical area of the plot, a conformational energy difference cut off of 1.5 kcal mol^{-1} was selected. The most suitable number of compounds is provided between categories 6 and 7. Therefore, this category was further analysed (Table 2.18).

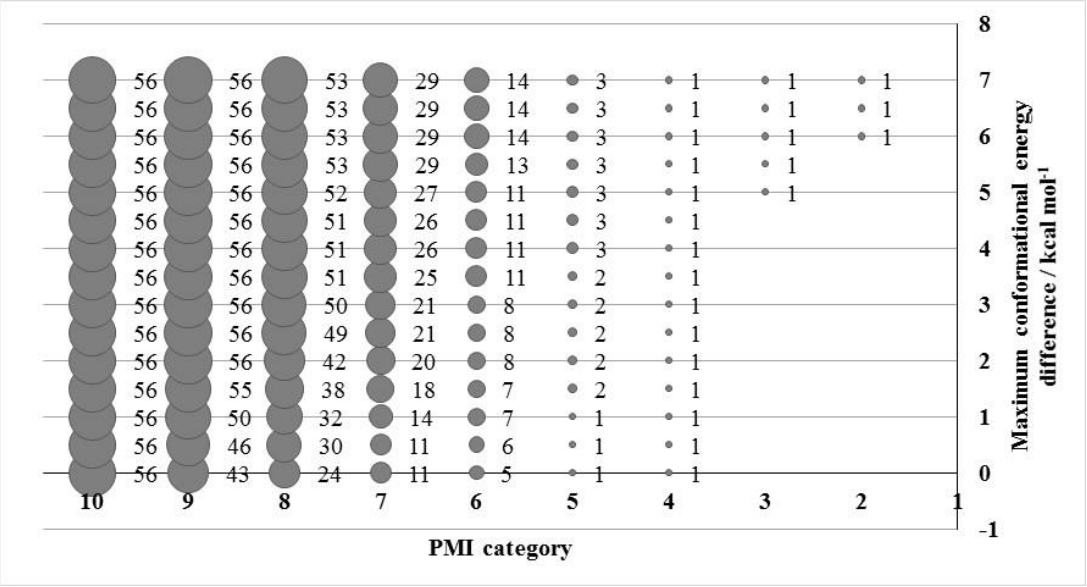

Figure 2.29: Graph showing the number of compounds selected at different conformational energy difference and PMI categories.

Entry	Energy / kcal mol^{-1}	Category	Number of Conformers	Number of Compounds	Number of Isomers
1	< 1.5	1 to 6	18	7	4
2	< 1.5	1 to 6.1	18	7	4
3	< 1.5	1 to 6.2	23	10	5
4	< 1.5	1 to 6.3	25	10	5
5	< 1.5	1 to 6.4	27	10	5
6	< 1.5	1 to 6.5	33	11	5
7	< 1.5	1 to 6.6	34	11	5
8	< 1.5	1 to 6.7	37	13	6
9	< 1.5	1 to 6.8	39	14	7
10	< 1.5	1 to 6.9	42	15	8
11	< 1.5	1 to 7	48	18	9

Table 2.18: Analysis of the library between PMI categories 6 and 7 to determine suitable compounds for the library by varying energy cut off and PMI categories.

Table 2.18 shows that a suitable number of compounds is selected from category 6.2 and a conformational energy difference < 1.5 kcal mol^{-1}. These 10 compounds are shown in Figure 2.30.

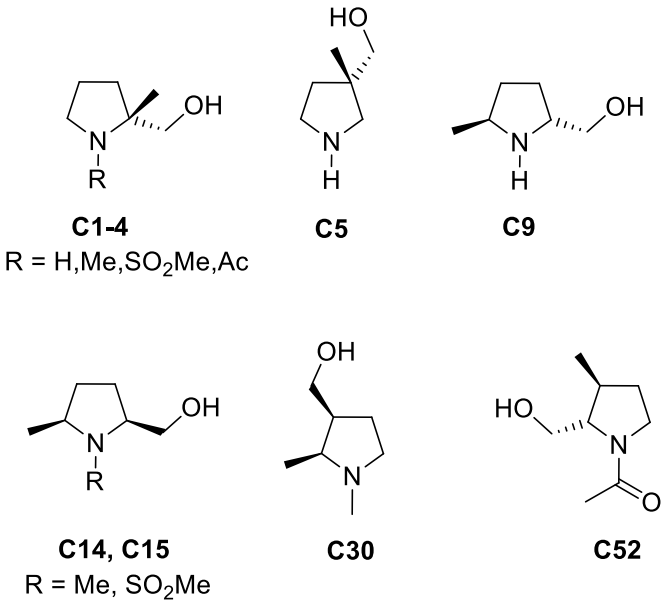

Figure 2.30: The selected hydroxymethyl pyrrolidine 10 fragment sub-set.

The PMI plot of these 10 compounds (Figure 2.31 (a)) can be compared to the original 56-member library (Figure 2.31 (b)). Both of these plots show conformers with a conformational energy difference of < 1.5 kcal mol^{-1}. The selected sub-set has a clear

focus on the under-represented part of the plot. There are a number of low energy 3-dimensional fragments. These plots clearly show that both the sub-set and original library have conformational and shape diversity.

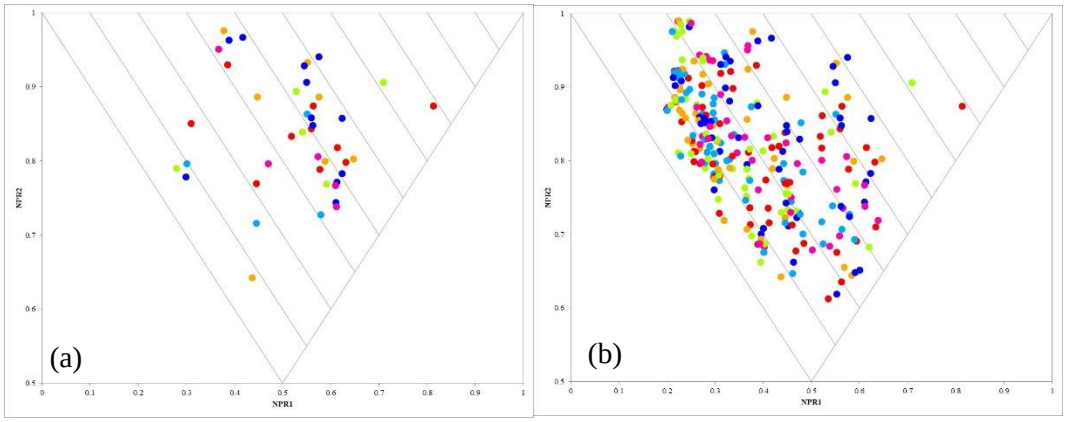

Colour						
Conformational energy difference / kcal mol^{-1}	0	< 0.3	< 0.6	< 0.9	< 1.2	< 1.5

Figure 2.31: PMI (a), shows conformers with an energy of less than 1.5 kcal mol^{-1} for all 10 selected fragments. This is contrasted by PMI (b), which shows conformers with an energy of less 1.5 kcal mol^{-1} for all 56 starting compounds.

2.5.3 Methyl ester, methyl-disubstituted pyrrolidine library

Next, a set of disubstituted pyrrolidine compounds with methyl ester and methyl substituents was analysed. The 56 compounds are shown in Figure 2.32 and the PMI plot of the lowest energy conformations is shown in Figure 2.33.

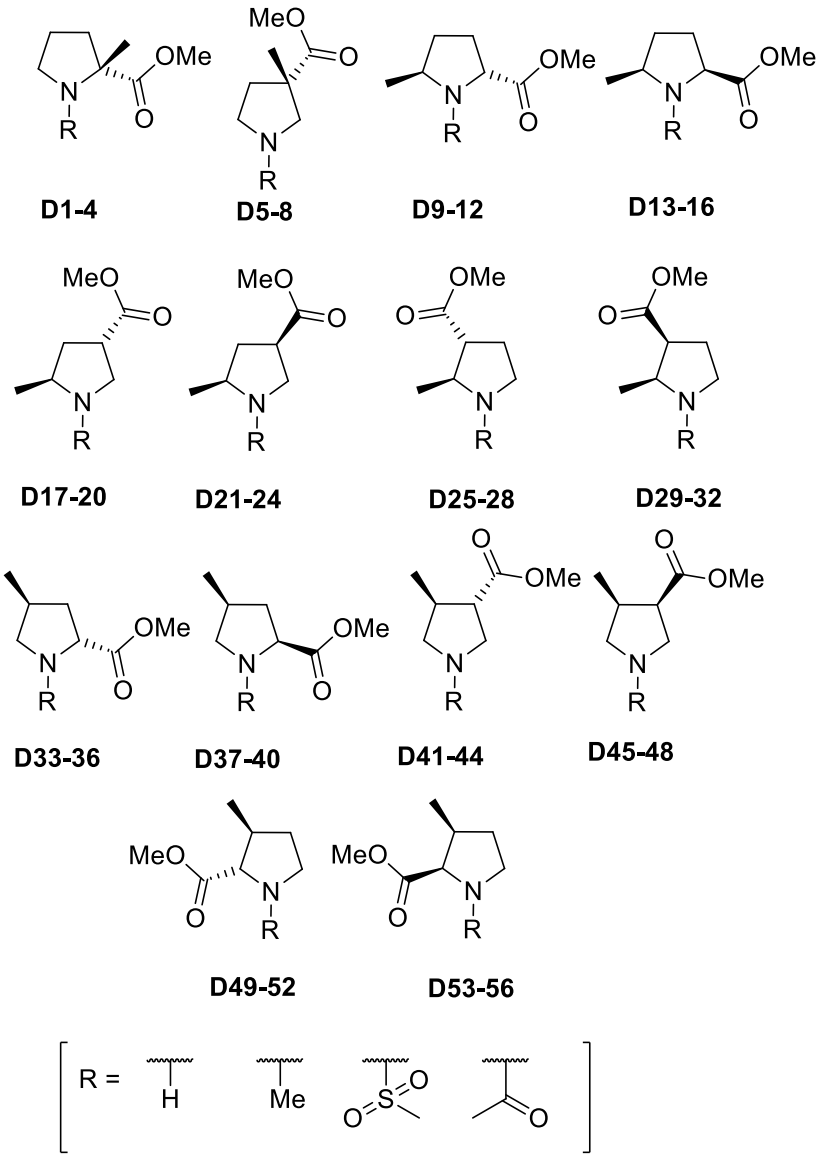

Figure 2.32: The 14 different isomers of ester, methyl disubstituted pyrrolidine. The four different nitrogen substituents are also shown.

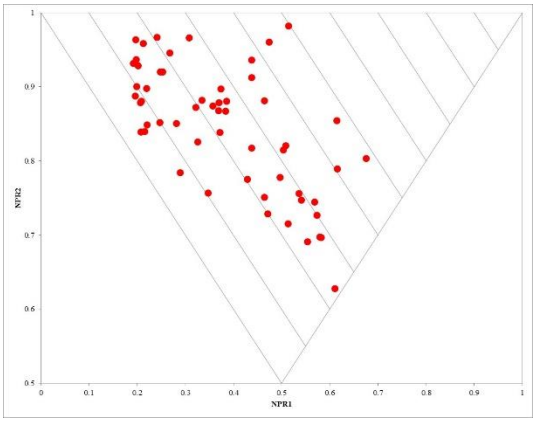

Figure 2.33 PMI plot of the lowest energy conformations of the 56 ester pyrrolidine fragments.

The spread of conformers across the plot and the relative conformational energies were then analysed and the results are shown in Table 2.19.

Category	**Conformational Energy Difference / kcal mol^{-1}**								**Total**
	1	**2**	**3**	**4**	**5**	**6**	**7**	**8**	
3	0	0	0	0	0	0	0	0	0
4	0	0	0	0	0	0	0	0	0
5	5	1	1	1	0	0	2	7	17
6	12	1	2	0	4	3	4	26	52
7	42	27	10	8	5	17	22	74	205
8	103	81	39	28	44	60	37	174	566
9	197	80	62	52	78	44	48	75	636
10	95	27	8	1	15	2	5	0	153
Total	454	217	122	90	146	126	118	356	1629

Table 2.19: Data showing the distribution of conformers by PMI category and conformational energy.

The data in Table 2.19 show that there are no conformers in the most spherical part of the plot but increasing numbers towards the centre of the plot, with most conformers in categories 8 and 9. This is different to the hydroxymethyl pyrrolidines, which had conformers more towards the top right of the plot. There are low numbers in category 10 suggesting few flat, 2-dimensional conformers. There is a large spread of low energy conformations, and those conformers in the middle to top right of the plot (categories 5, 6 and 7) have lower conformational energy differences and are therefore likely to be accessible.

In order to select a suitable number of compounds for the sub-set library, the whole data set was analysed and the number of compounds selected from different PMI categories and conformational energies was determined. The results are shown in Figure 2.34. Similarly to the hydroxymethyl pyrrolidines, a suitable number of compounds is selected between categories 6 and 7, with an energy difference of less than 1.5 kcal mol^{-1}. Further analysis is shown in Table 2.20.

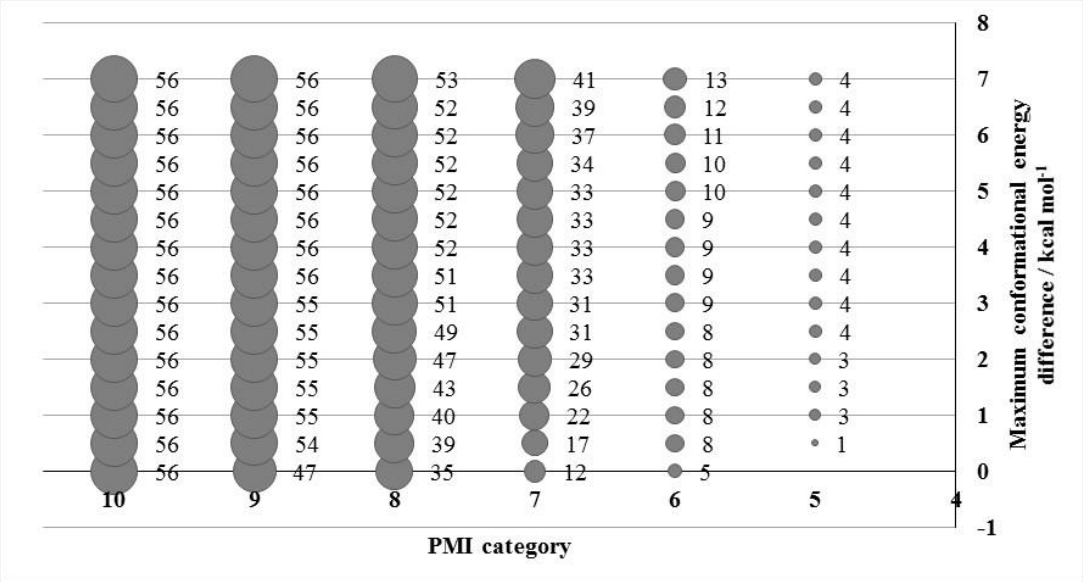

Figure 2.34: Graph showing the number of compounds selected at different conformational energy difference and PMI categories.

Entry	Energy / kcal mol^{-1}	Category	Number of Conformers	Number of Compounds	Number of Isomers
1	< 1.5	1 to 6	18	8	5
2	< 1.5	1 to 6.1	19	9	6
3	< 1.5	1 to 6.2	20	9	6
4	< 1.5	1 to 6.3	23	10	7
5	< 1.5	1 to 6.4	28	14	9
6	< 1.5	1 to 6.5	30	15	9
7	< 1.5	1 to 6.6	34	17	10
8	< 1.5	1 to 6.7	40	19	11
9	< 1.5	1 to 6.8	52	22	12
10	< 1.5	1 to 6.9	58	23	12
11	< 1.5	1 to 7	75	27	13

Table 2.20: Analysis of the library between PMI cateogories 6 and 7 to determine suitable compounds for the library by varying energy cut off and PMI categories.

Table 2.20 shows that a suitable number of compounds and isomers is selected from category 6.2 with a conformational energy difference of <1.5 kcal mol^{-1}. This is also

the same selection point as the hydroxymethyl pyrrolidine library. The 9 selected compounds are shown in Figure 2.35 .

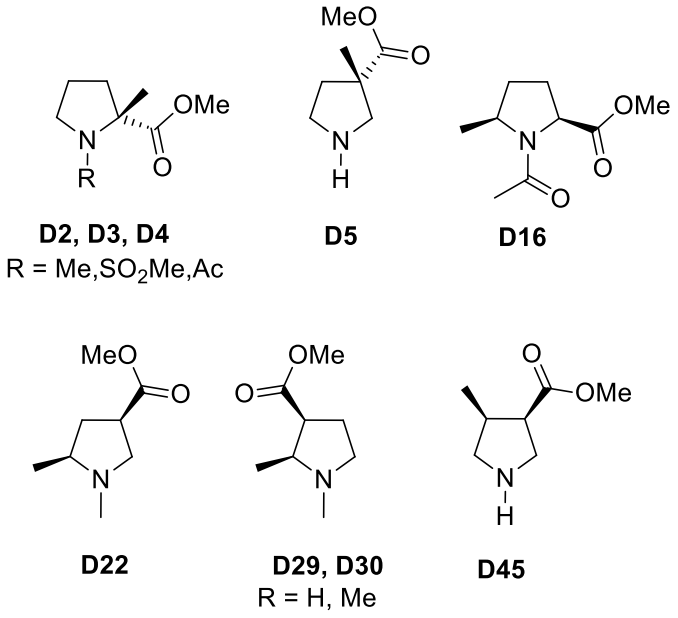

Figure 2.35: The selected ester pyrrolidine 9 fragment sub-set.

The PMI plots showing all conformers with a conformational energy difference of < 1.5 kcal mol^{-1} for the 9 compound sub-set (Figure 2.36 (a)) and the original 56-member library (Figure 2.36 (b)) can be compared. It can be seen that there the selected sub-set library has a good spread across the plot, selecting more 3-dimensional conformers, and shows that both the sub-set and original library have shape and conformational diversity.

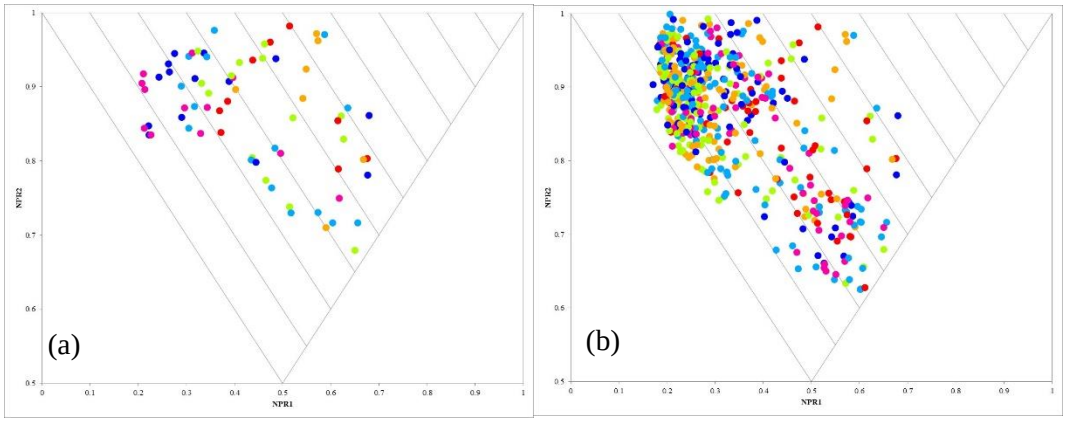

Colour						
Conformational energy difference / kcal mol-1	0	< 0.3	< 0.6	< 0.9	< 1.2	< 1.5

Figure 2.36: PMI (a), shows conformers with an energy of less than 1.5 kcal mol^{-1} for all 9 selected fragments. This is contrasted by PMI (b), which shows conformers with an energy of less 1.5 kcal mol^{-1} for all 56 starting compounds.

Comparing the ester pyrrolidine selected sub-set to the hydroxymethyl pyrrolidine sub-set highlights some similarities in the isomers that would be selected for synthesis. The fragment numbers from both sub-sets are shown in Table 2.21. It can be seen that five compounds are the same, only varying in the hydroxymethyl/ester substituent. This means that with careful synthetic planning both the ester and hydroxymethyl may be accessible from the same route, hence minimising the number of different synthetic routes.

	Data set	**Selected Compound Numbers**													
1	OH	1	2	3	4	5	9	14	15				30		52
2	Ester		2	3	4	5				16	22	29	30	45	
3	Isomer	1				2	3	4			6	8		12	13

Table 2.21: The fragment number for the ester pyrrolidine selected sub-set of fragments compared to the fragments selected in the hydroxymethyl pyrrolidine analysis.

The PMI plots of the selected sub-set libraries for hydroxymethyl and ester pyrrolidine are shown in Figure 2.37, as well as the overlaid plot of the two selected pyrrolidine libraries. Colouring is based on the substituent type (see Key). The comparison of these two sub-sets demonstrates that even small changes to a molecule can produce quite different shaped conformations. Both sub-set libraries focus on the more spherical area of the plot, although the ester pyrrolidine library has more conformations closer to the unfavourable rod-disc axis. This plot shows that this

library has good conformational diversity and accesses new areas of 3-dimensional chemical space.

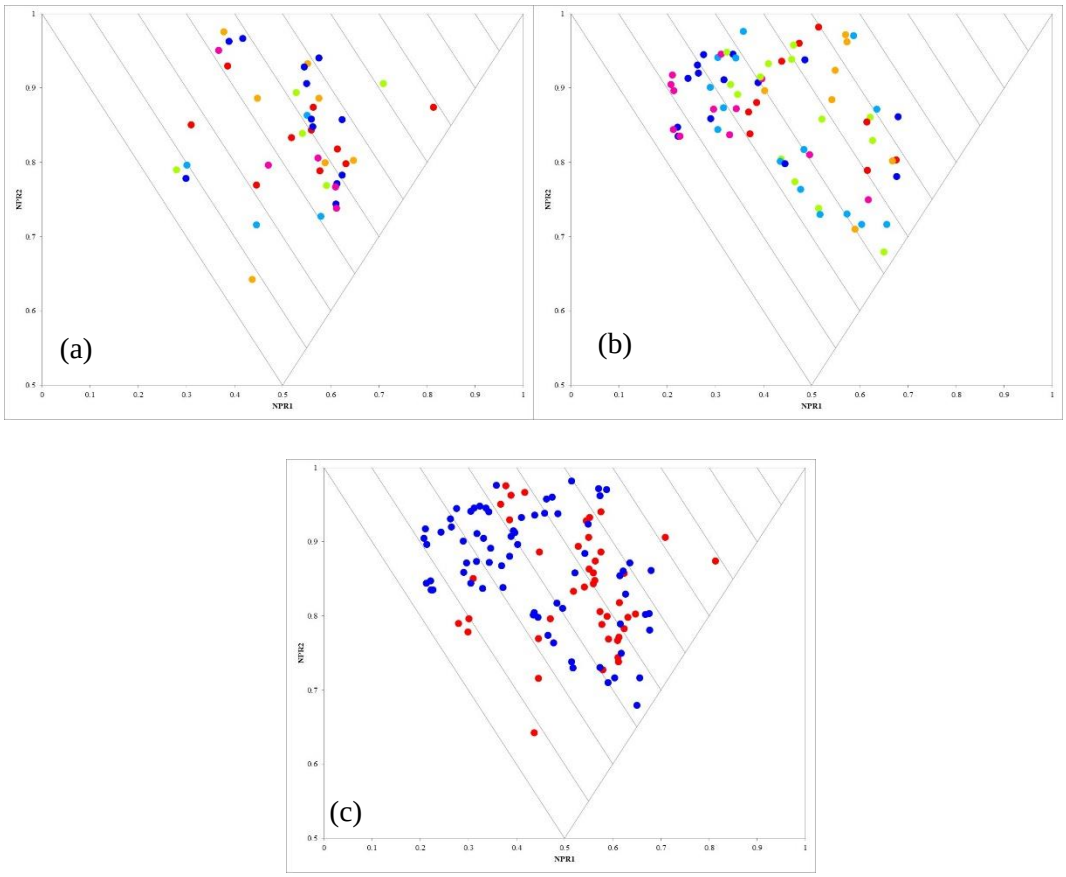

Plot (a) and (b)	Colour						
	Conformational energy difference / kcal mol^{-1}	0	< 0.3	< 0.6	< 0.9	< 1.2	< 1.5
Plot (c)	Colour						
	R^2	CH_2OH			CO_2Me		

Figure 2.37: PMI (a), shows conformers with an energy of less than 1.5 kcal mol^{-1} for all 10 selected hydroxymethyl pyrrolidine fragments. This is contrasted by PMI (b), which shows conformers with an energy of less 1.5 kcal mol^{-1} for all 9 selected methyl ester pyrrolidine fragments. PMI (c) shows both libraries overlaid.

It is also possible to compare the combined selected hydroxymethyl and ester pyrrolidine sub-set library with the original hydroxymethyl and ester pyrrolidine library. Figure 2.38 shows that the sub-set library covers a large area of chemical space, some of the bulk has been removed from the areas closer to the rod-disc axis, highlighting that the more 3-dimensional fragments have been selected for the library.

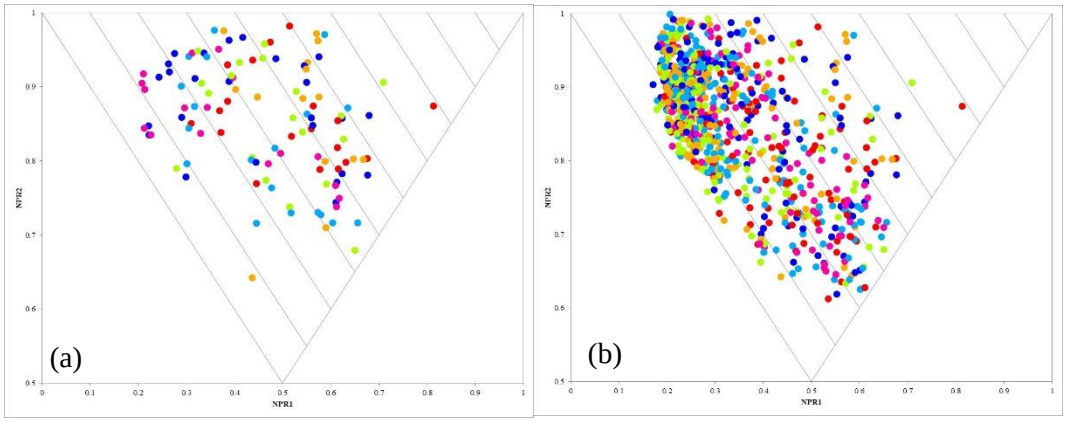

Colour						
Conformational energy difference / kcal mol-1	0	< 0.3	< 0.6	< 0.9	< 1.2	< 1.5

Figure 2.38: PMI (a), shows conformers with an energy of less than 1.5 kcal mol^{-1} for the combined 19 selected hydroxymethyl and ester fragments. This is compared to PMI (b), which shows all the conformers with an energy of less 1.5 kcal mol^{-1} for both 56 original pyrrolidine fragments.

2.5.4 Hydroxymethyl, methyl- and methyl ester, methyl-disubstituted azepane libraries

The azepane heterocycle is another simple saturated scaffold that could be considered for the fragment library. It is anticipated that the 7-membered ring would be more conformationally flexible due to the larger ring size compared to the pyrrolidine and piperidine scaffolds. As with the previous heterocycles, there will be two different azepane systems, hydroxymethyl and methyl-disubstituted azepane and methyl ester, methyl-disubstituted azepane. Disubstituted azepane has 33 different isomers (not including enantiomers), which when functionalised 4 different ways, with H, Me, SO_2Me and Ac, gives 132 different compounds, shown generally in Figure 2.39. Full analysis will not be presented.

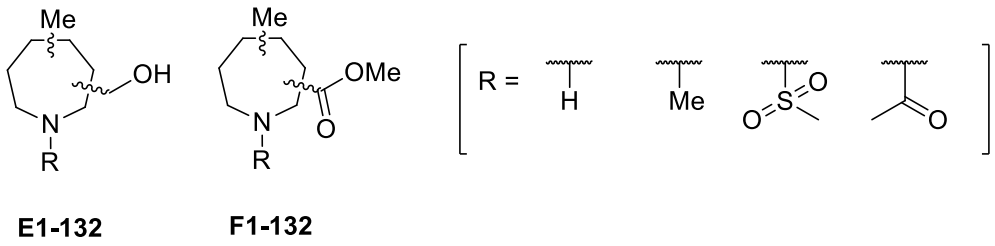

Figure 2.39: The hydroxymethyl, methyl disubstituted azepane and methyl ester, methyl disubstituted azepane scaffolds. The four different nitrogen substituents are also shown.

The 132 compounds from both systems were computationally analysed. All conformations were generated and relevant data obtained using our Pipeline Pilot protocol. These data were then analysed to determine the structural diversity of the scaffold. The PMI plot showing the lowest energy conformation of both hydroxymethyl and methyl ester libraries are shown in Figure 2.40. This shows that there is a significant spread of compounds across the plot and that the scaffold clearly demonstrates structural diversity. The scaffold accesses new areas of 3-dimensional space well.

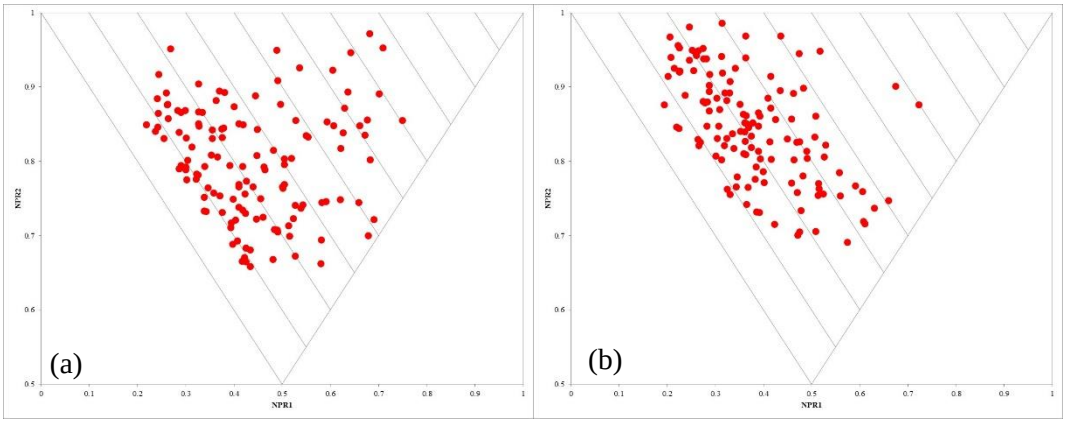

Figure 2.40: PMI (a) the lowest energy conformations of the 132 hydroxymethyl azepane fragments. PMI (b) the lowest energy conformations of the 132 methyl ester azepane fragments.

The data for both systems was then further analysed to ascertain the number of compounds selected at each energy level and PMI category. As with previous analysis, not all compounds need to be synthesised and therefore a smaller sub-set is selected focussing on the more 3-dimensional fragments.

For the hydroxymethyl azepane library, it was found that a suitable number of compounds is selected from PMI categories 1 to 5.3 with a conformational energy difference of < 1.5 kcal mol^{-1} to give a total of 27 compounds and 16 isomers. The 27 member sub-set library fragments are shown in Figure 2.41.

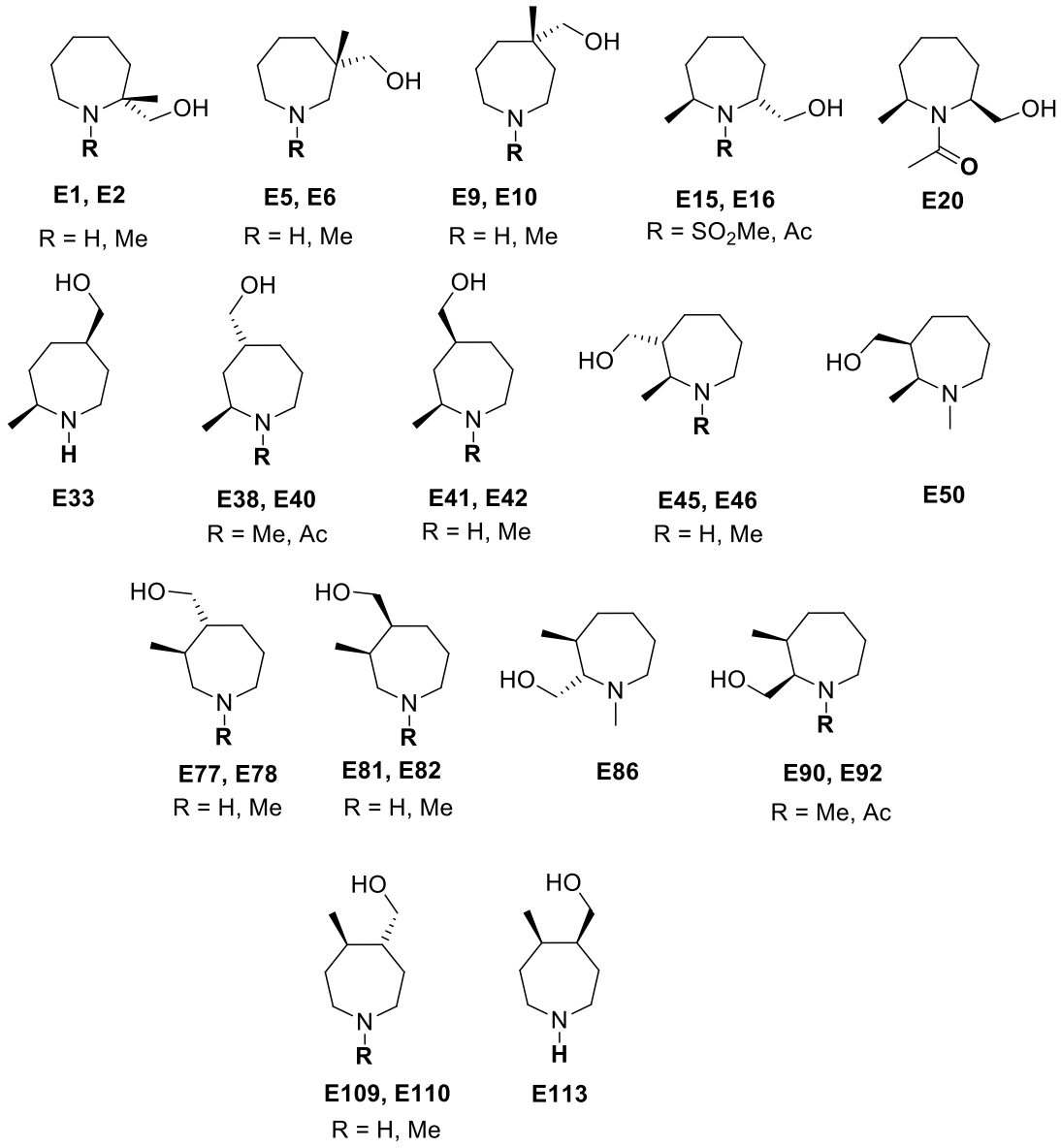

Figure 2.41: The selected hydroxymethyl azepane 27 fragment sub-set.

A PMI plot of the 27 selected fragments can be generated and is shown in Figure 2.42 (a). This shows that the sub-set has very good coverage of chemical space, with a number of low energy fragments reaching into the more 3-dimensional area of chemical space. This plot can be compared to a plot of the full 132 member hydroxymethyl library (Figure 2.42 (b)). Here it can be noted that the selected sub-set

has very good coverage of the top right of the plot with only a small percentage of conformations towards to the rod-disc axis.

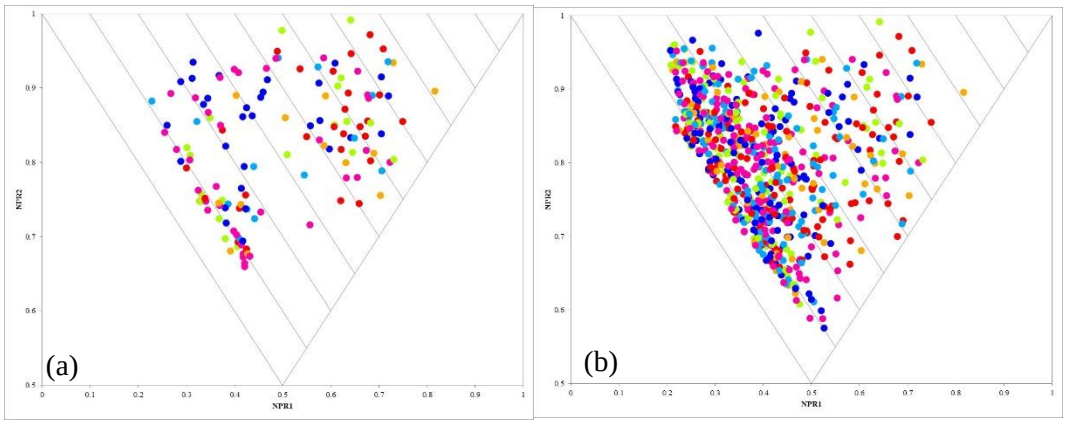

Colour						
Conformational energy difference / kcal mol-1	0	< 0.3	< 0.6	< 0.9	< 1.2	< 1.5

Figure 2.42: PMI (a), shows conformers with an energy of less than 1.5 kcal mol^{-1} for all 27 selected fragments. This is contrasted by PMI (b), which shows conformers with an energy of less 1.5 kcal mol^{-1} for all 132 starting compounds.

The same analysis on the methyl ester azepane library showed that selection from PMI categories 1 to 6, with a conformational energy difference < 1.5 kcal mol^{-1}, gave 29 compounds and 17 isomers. These compounds are shown in Figure 2.43 below.

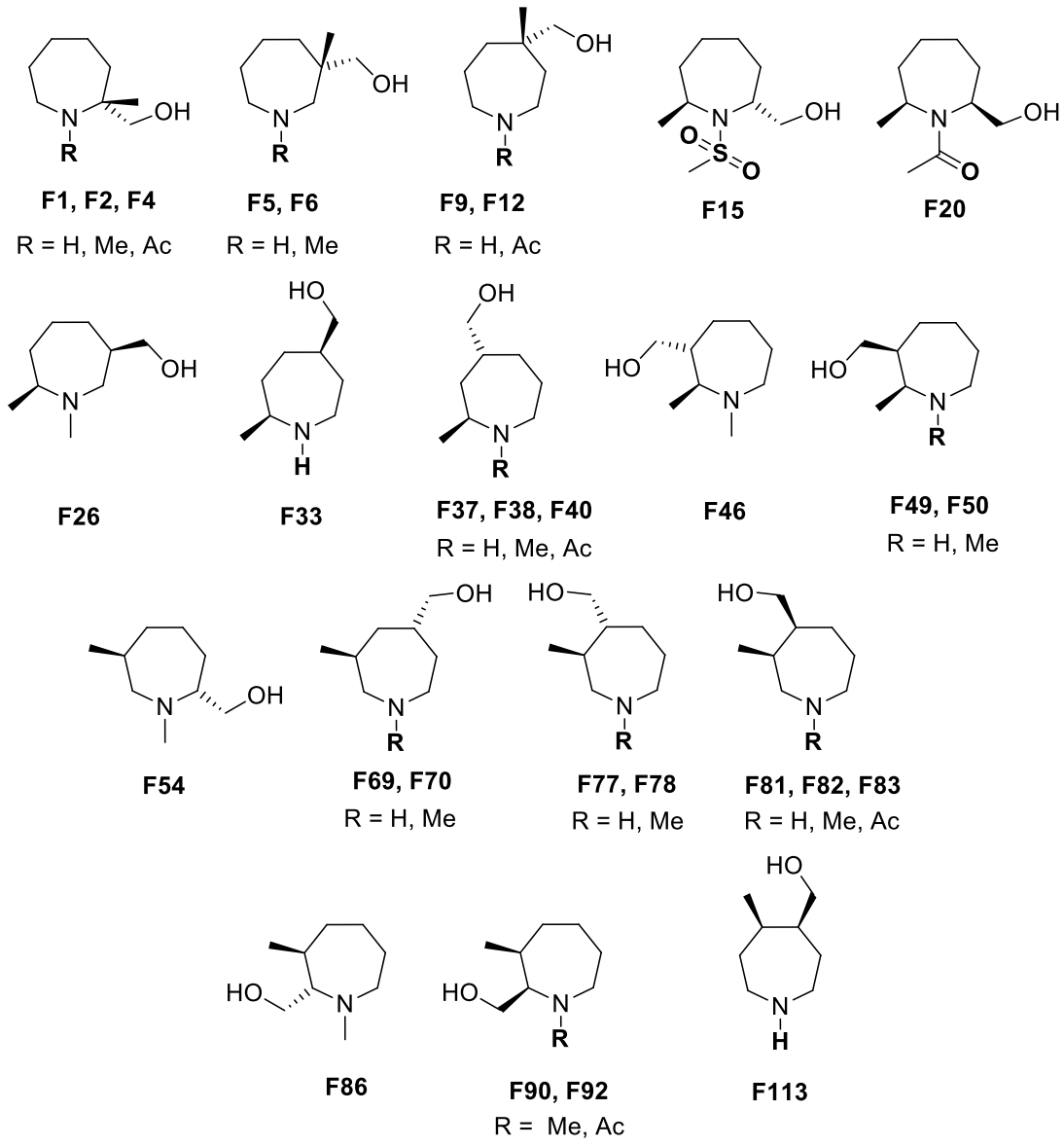

Figure 2.43: The selected ester azepane 29 fragment sub-set.

The PMI generated for all the conformations with less than 1.5 kcal mol^{-1} conformational energy difference of the 29 selected compound sub-set is shown in Figure 2.44 (a). Comparing this to the original 132-member library with conformations less than 1.5 kcal mol^{-1} conformational energy difference (Figure 2.44 (b)) shows that there is good conformational diversity and shape diversity. The ester substituent, however, does not produce a large number of conformations in the top right of the plot; the conformations are more evenly spread across the plot. The sub-set has selected the most 3-dimensional compounds which can be seen by the lower

percentage of compounds near the rod-disc axis compared to the original library.

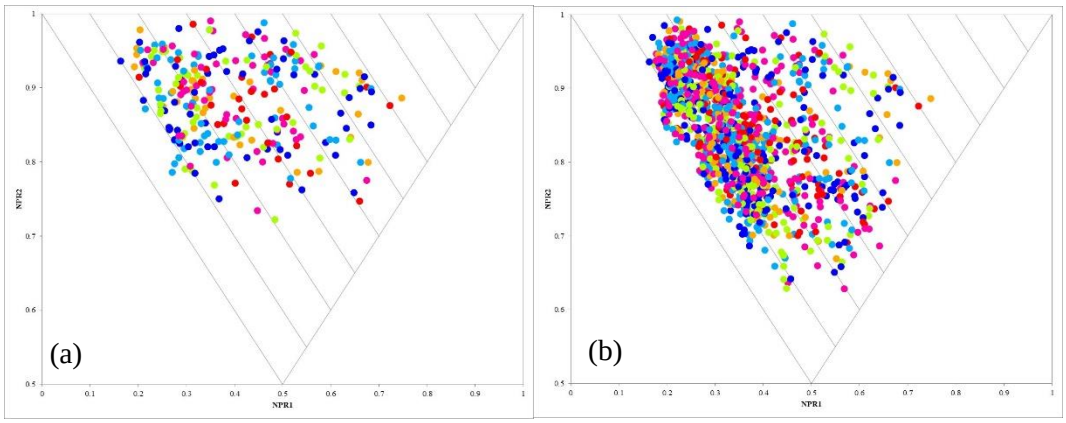

Colour						
Conformational energy difference / kcal mol-1	0	< 0.3	< 0.6	< 0.9	< 1.2	< 1.5

Figure 2.44: PMI (a), shows conformers with an energy of less than 1.5 kcal mol^{-1} for all 29 selected ester azepane fragments. This is contrasted by PMI (b), which shows conformers with an energy of less 1.5 kcal mol^{-1} the original 132 member methyl ester azepane fragments.

It is now possible to collect together the selected hydroxymethyl azepane sub-set and the ester azepane sub-set to investigate any similarities and differences between the two sets. The fragment numbers of both sets are shown in Table 2.22. This also highlights the similar and different isomers in both data sets.

	Data set	**Compound Numbers**													
1	OH	1	2		5	6	9	10		15	16	20		33	
2	Ester	1	2	4	5	6	9		12	15		20	26	33	
3	Isomer	1			2		3			4		5	7	9	
4	OH		38	40	41	42	45	46		50				77	78
5	Ester	37	38	40				46	49	50	54	69	70	77	78
6	Isomer	10			11		12		13		14	18		20	
7	OH	81	82		86	90	92	109	110	113					
8	Ester	81	82	83	86	90	92			113					
9	Isomer	21			22	23		28		29					

Table 2.22: The fragment number for the ester azepane selected sub-set of fragments compared to the fragments selected in the hydroxymethyl azepane analysis.

Table 2.22 shows that there are a number of the same isomer and some with similar nitrogen functionalisation, these only vary in the R^2 substituent. In total there are 20 isomers which are the same, and this should significantly reduce the quantity of

synthetic methods to develop. A comparison of the two different sub-sets PMI plot is shown in Figure 2.45 with an overlaid PMI plot with both data sets on Figure 2.45 (c), where spots are coloured based on substituent.

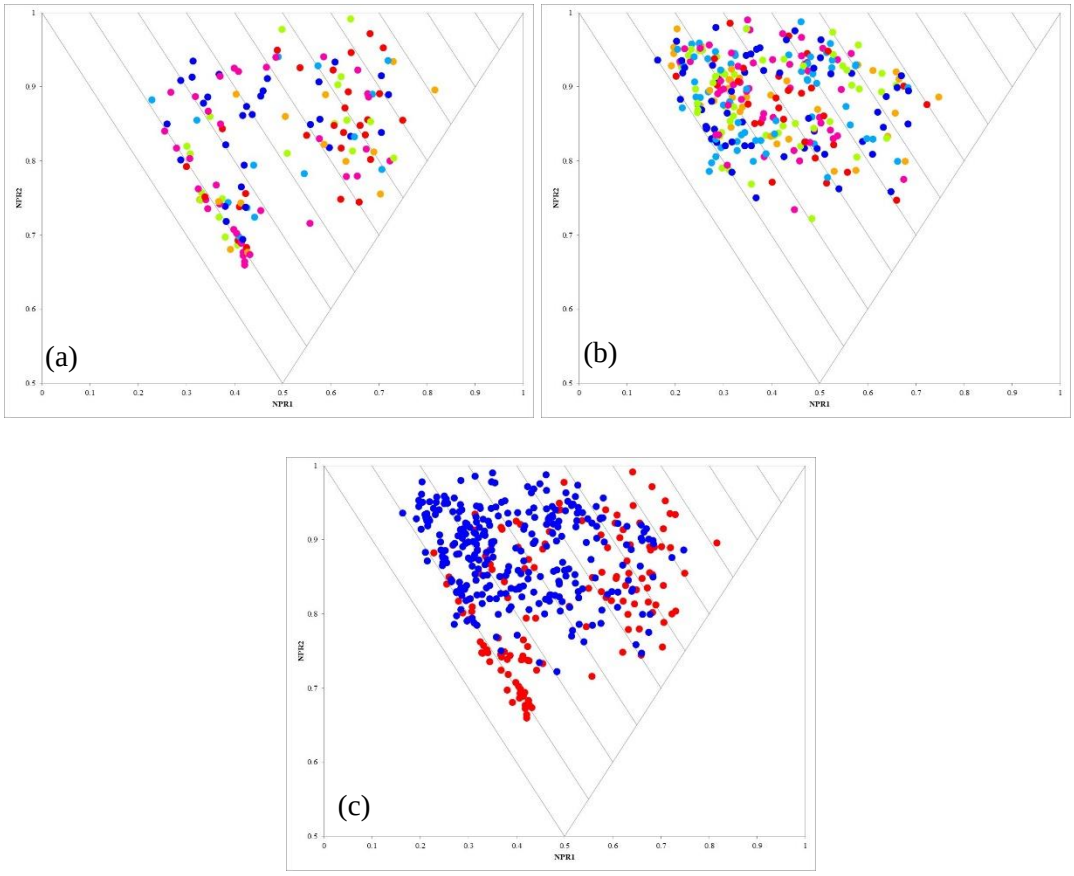

Plot (a) and (b)	Colour						
	Conformational energy difference / kcal mol^{-1}	0	< 0.3	< 0.6	< 0.9	< 1.2	< 1.5
Plot (c)	Colour						
	R^2	CH_2OH			CO_2Me		

Figure 2.45: PMI (a), shows conformers with an energy of less than 1.5 kcal mol^{-1} for all 27 selected hydroxymethyl azepane fragments. This is contrasted by PMI (b), which shows conformers with an energy of less 1.5 kcal mol^{-1} for all 29 selected methyl ester azepane fragments. PMI (c) shows both libraries overlaid.

These plots also show how the two different sub-sets cover slightly different areas of the plot. Both scaffolds have a number of conformers in the top right of the plot, but the left of the plot seems to vary slightly between scaffold. The hydroxymethyl azepane fragments have more coverage in the lower area of the plot towards the disc area, whereas the ester fragments have greater population of fragments in the top left of the plot. The gap in the middle of the hydroxymethyl plot is well covered by the ester fragments. A combined PMI plot of the two azepane fragment sub-sets is shown

in Figure 2.46 (a). This can be compared to the plot of the combined azepane original libraries with all conformations of less than 1.5 kcal mol^{-1} (Figure 2.46 (b). This shows that the azepane scaffold produces fragments which have shape and conformational diversity and a large area of chemical space is covered by this simple scaffold.

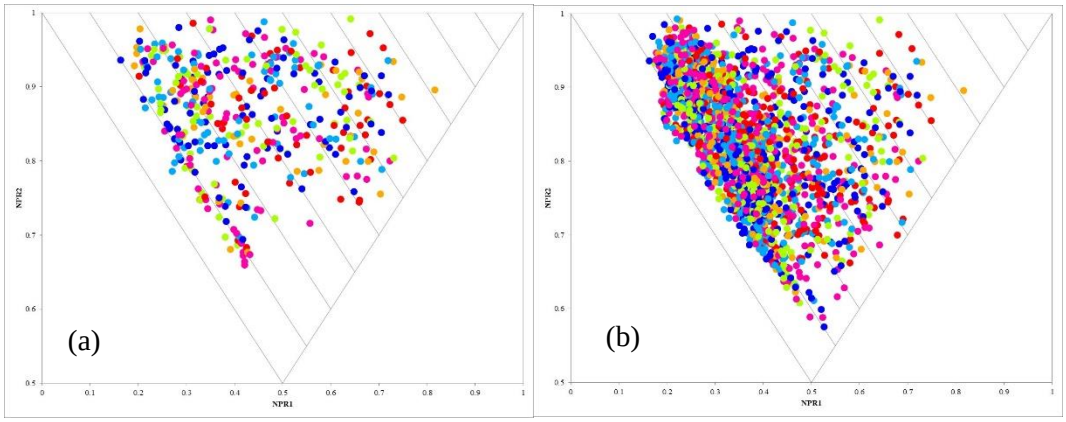

Colour						
Conformational energy difference / kcal mol-1	0	< 0.3	< 0.6	< 0.9	< 1.2	< 1.5

Figure 2.46: PMI (a), shows conformers with an energy of less than 1.5 kcal mol^{-1} for the combined 56 selected hydroxymethyl and ester fragments. This is compared to PMI (b), which shows all the conformers with an energy of less 1.5 kcal mol^{-1} for both 132 original azepane fragments.

2.5.5 Combined piperidine, pyrrolidine and azepane library

Each of the six analyses presented so far has provided a smaller sub-set of compounds suitable for a 3-dimensional fragment library. These analyses can now be combined to give an overall picture of the selected fragment library. The PMI plots showing each of the two combined libraries, (PMI (a) showing the 19 pyrrolidine fragments, PMI (b) showing the 37 piperidine fragments and PMI (c) showing 56 azepane fragments) is shown as well as the combined PMI plot of the 112 fragments (Figure 2.47 (d)) of all the pyrrolidine, piperidine and azepane conformers with less than 1.5 kcal mol^{-1} conformational energy difference.

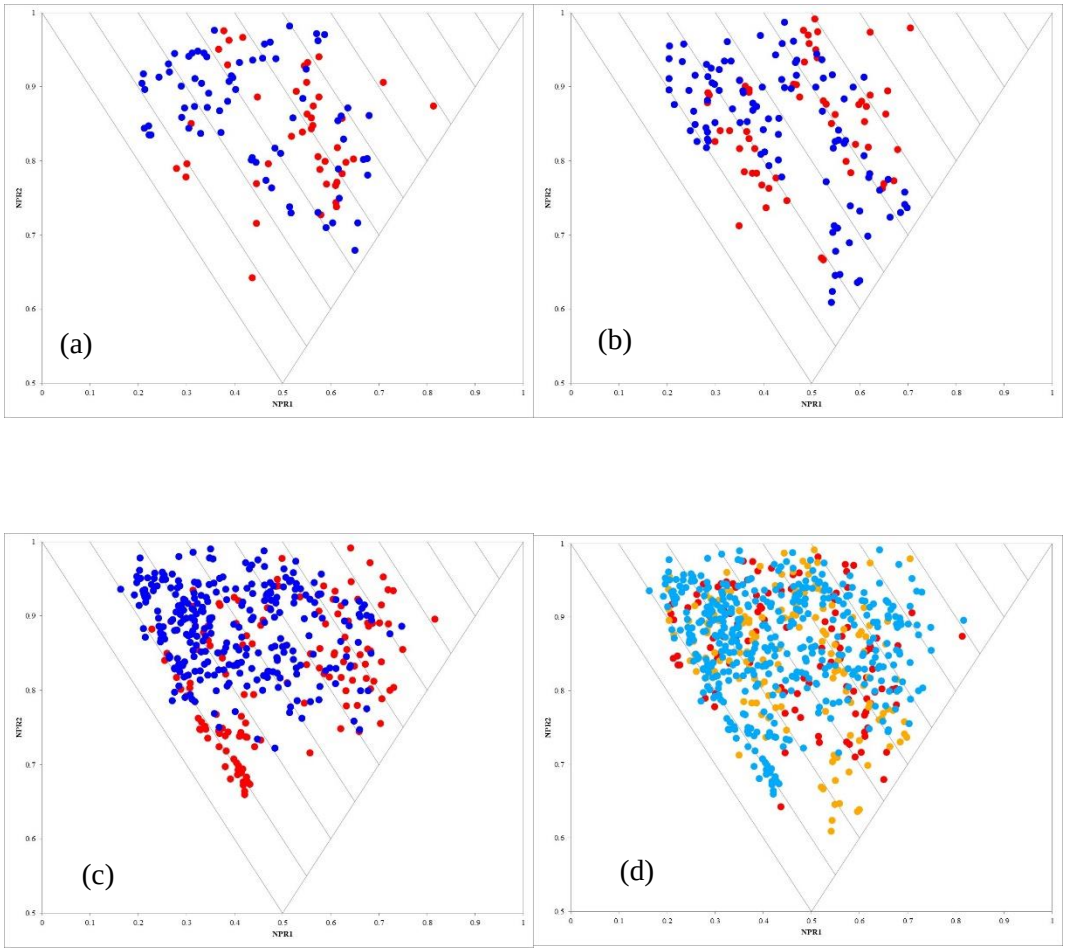

Plot (a), (b) and (c)	Colour			
	R^1	CH_2OH		CO_2Me
Plot (d)	Colour			
	Scaffold	Pyrrolidine	Piperidine	Azepane

Figure 2.47: All plots show conformers with an energy of less than 1.5 kcal mol^{-1} for both hydroxymethyl and ester substituted fragments. PMI (a) shows 19 pyrrolidine fragments, PMI (b) shows 37 piperidine fragments, PMI (c) shows 56 azepane fragments and PMI (d) combined plot of all three scaffolds (112 fragments).

These plots show how each of the different scaffolds contribute to the library. It can be seen that the azepane library has the greatest spread of conformers across the plot and is the scaffold with the most spherical conformers. However, there is quite a bit of difference between the piperidine and pyrrolidine scaffolds. Each of the two libraries seems to occupy a space left by the other, for example the bottom of the plot, is sparsely populated by the pyrrolidine fragments (red), but is covered by a number of piperidine fragments (orange). The coverage is shared by the two scaffolds at the top right of the plot, where a larger area is covered by the two different scaffolds. The more sparsely populated area at the top right contains more azepane conformers. It can

also be noted that category 10 has only a few conformers. This is ideal as this area of the plot is already well covered by existing fragment libraries, and shows that our fragments have shape diversity despite the simple nature of the scaffold.

In summary, this combined sub-set library of 112 compounds demonstrates that it is possible to generate shape diversity from simple scaffolds. Furthermore, by introducing conformational diversity, a large area of the plot can be covered, giving access to new areas of 3-dimensional chemical space.

2.6 Physicochemical properties of selected library

To date, we have analysed the shape diversity of the simple heterocyclic fragments and selected the more 3-dimensional fragments to form the basis for our 3-dimensional fragment library. However, it is important to analyse the physicochemical properties of both the original library and the selected sub-set. By doing this we are able to check that the properties are "fragment like". As discussed in Section 1.1, fragments generally have similar properties and are said to follow a certain set of criteria or "Rule of 3". These data as well as other properties not encompassed in the "Rule of 3" can be calculated for each of the compounds in the library. The values can be computationally generated using Pipeline Pilot 8.5 built-in components and the data for each full library of each scaffold and set of substituents was generated (See Section 6.1.1 for details).

2.6.1 Physicochemical properties of piperidine fragments

It is important to determine if all the members of the full library fit with desirable criteria. Taking piperidine as our initial example, each compound in the 92-member library was analysed for their physicochemical properties. As the analysis occurs after the run to generate all conformations, the data is generated for all of conformations of a given compound. However, the physicochemical properties do not vary based on conformation. Therefore, only the lowest energy conformation data was used. The data in Table 2.23 summarises the piperidine data set as a whole including the breakdown for the two different piperidine substituents.

	R^2		ALogP	MW (HAC)	H Bond Acceptor	H Bond Donor	Molecular PSA / Å^2
1	CH_2OH	Average	-0.44	163.24 (11)	1.75	1.5	42.01
2		Smallest	-1.18	130.21 (9)	1	1	24.67
3		Largest	0.363	207.29 (13)	3	2	65.99
4	Ester	Average	0.0176	191.20 (13)	2.80	0.5	47.83
5		Smallest	-0.733	157.21 (11)	2	0	30.74
6		Largest	0.716	235.30 (15)	4	1	72.06
7	Full	Average	-0.212	177.22 (12)	2.28	1	44.92
8		Smallest	-1.18	130.21 (9)	1	0	24.67
9		Largest	0.716	235.30 (15)	4	2	72.06

Table 2.23: Table showing analysis of the physicochemical properties of the piperidine fragments.

These data (Table 2.23) show that in each of the 92-member substituent libraries and the full 184-member combined library the average molecular weight falls well below the guidelines provided by the "Rule of 3" (< 300 Da). The highest values also fall below the limit. This is also the case for the number of hydrogen bond donors, although not for acceptors, where the ester library provides some compounds with more than 3 hydrogen bond acceptors. The average value, however, falls below the three maximum suggestion. The range in the number of donor and acceptor sites varies slightly showing that the fragments have a good range of sites to provide hydrogen bond handles. The ALogP value falls well below the guideline of 3. Even the highest values of ALogP in the libraries is still two log units lower than the maximum. This suggests that our fragments are very polar and offer a huge potential for adding more lipophilic groups during fragment development. The polar surface area is more mixed. Generally a polar surface area of less than 60 Å^2 is desirable for fragments, this is to allow for an increase during development, generally an orally bioavailable drug has a polar surface of around 120 Å^2, however this is considerably smaller (< 60 Å^2) for drugs requiring brain penetration. For our fragments on average the polar surface area is less than the 60 Å^2 value, although the largest value of each substituent library is greater. These data show that we are not only designing compounds with shape diversity, but also suitable physicochemical properties for a fragment library.

It is expected that the selected sub-set library will also follow the "Rule of 3" guidelines as the parent library does, but it is important to check that the properties of

the selected fragments are varied and that selection has not given a narrow range of physicochemical properties. Table 2.24 shows the data for the selected sub-set libraries.

	R^2		ALogP	MW (HAC)	H Bond Acceptor	H Bond Donor	Molecular PSA / Å^2
1	CH_2OH	Average	-0.660	149.23 (10.2)	1.37	1.74	36.65
2		Smallest	-1.18	130.21 (9)	1	1	24.67
3		Largest	0.363	207.29 (13)	3	2	65.99
4	Ester	Average	-0.0367	181.00 (12.5)	2.61	0.667	41.50
5		Smallest	-0.665	157.21 (11)	2	0	30.74
6		Largest	0.716	235.30 (15)	4	1	72.06
7	Full	Average	-0.321	164.78 (11.3)	1.97	1.22	39.00
8		Smallest	-1.18	130.21 (9)	1	0	24.67
9		Largest	0.716	235.30 (15)	4	2	72.06

Table 2.24: Table showing analysis of the physicochemical properties of the selected sub-set library of piperidine fragments.

These data show that the selected library follows a similar trend to that of the original library with only subtle differences in values. The selected library has lower values than the original library for molecular weight and the polar surface area, but the selected sub-set represents original library well. The selected sub-set library has a good range of values and fits the desirable physicochemical properties for a fragment library.

2.6.2 Physicochemical properties of pyrrolidine and azepane fragments

A similar analysis of the physicochemical properties can also be carried out for the other fragment library scaffolds, pyrrolidine and azepane. Although the data for all compounds and conformers was generated, only the lowest energy conformation was considered.

Analysis of both full 56-member pyrrolidine hydroxymethyl and methyl ester libraries have been undertaken, and show that these pyrrolidine fragments fit within the "Rule of 3" guidelines. This was also the case for the selected sub-sets for both of these fragment scaffolds, with analysis summarised in Table 2.25.

	R^2		ALogP	MW (HAC)	H Bond Acceptor	H Bond Donor	Molecular PSA / Å^2
1	CH_2OH	Average	-0.839	144.01 (9.7)	1.6	1.6	39.76
2		Smallest	-1.48	116.18 (8)	1	1	24.67
3		Largest	-0.151	193.26 (12)	3	2	65.99
4	Ester	Average	-0.568	167.00 (11.4)	2.44	0.667	42.90
5		Smallest	-1.12	144.19 (10)	2	0	30.74
6		Largest	0.26	221.27 (14)	4	1	72.06
7	Full	Average	-0.710	154.69 (10.5)	2	1.16	41.25
8		Smallest	-1.48	116.18 (8)	1	0	24.67
9		Largest	0.260	221.27 (14)	4	2	72.06

Table 2.25: Table showing analysis of the physicochemical properties of the selected sub-set library of pyrrolidine fragments.

The pyrrolidine sub-set library provides compounds with suitable characteristics for a successful fragment library, with all following the "Rule of 3" guidelines. The fragments have a low average ALogP value, suggesting a larger proportion of polar fragments. This low ALogP value and the moderate average molecular weight provides a good starting point to build on to the fragment without the risk of generating an unfavourably high ALogP value.

The physicochemical properties of the azepane library were also computationally generated and analysed. Analysis of the hydroxymethyl azepane library and the methyl ester azepane library showed that the fragments generally obey the criteria outlined in the "Rule of 3". Therefore, the selected sub-sets also showed good fragment properties, as outlined in Table 2.26

	R^2		ALogP	MW (HAC)	H Bond Acceptor	H Bond Donor	Molecular PSA / Å^2
1	CH_2OH	Average	-0.258	159.40 (11.0)	1.22	1.81	33.06
2		Smallest	-0.728	144.23 (10)	1	1	24.67
3		Largest	0.819	221.32 (14)	3	2	65.99
4	Ester	Average	0.167	190.0 (13.2)	2.31	0.759	40.5
5		Smallest	-0.411	172.24 (12)	2	0	30.74
6		Largest	1.17	249.33 (16)	4	1	72.06
7	Full	Average	-0.0380	175.47 (12.2)	1.79	1.27	36.92
8		Smallest	-0.728	144.23 (10)	1	0	24.67
9		Largest	1.17	249.33 (16)	4	2	72.06

Table 2.26: Table showing analysis of the physicochemical properties of the selected sub-set library of azepane fragments.

Both hydroxymethyl and ester selected libraries fit within the "Rule of 3" guidelines. Comparing the azepane selected sub-set to the piperidine and pyrrolidine selected libraries it should be noted that the azepane fragments have a lower polar surface area and a higher ALogP. This suggests that the library contains fragments with a range of physicochemical properties. An analysis of the combined full and selected libraries was then undertaken. Table 2.27 compares the properties for the selected 112 compound combined sub-set library and the full library.

	Data set		ALogP	MW (HAC)	H Bond Acceptor	H Bond Donor	Molecular PSA / Å^2
1	Selected	Average	-0.246	168.4 (11.6)	1.88	1.23	38.34
2		Smallest	-1.48	116.18 (8)	1	0	24.67
3		Largest	1.17	249.33 (16)	4	2	72.06
4	Full	Average	-0.116	181.05 (12.3)	2.26	1	45.00
5		Smallest	-1.57	116.18 (8)	1	0	24.67
6		Largest	1.17	249.33 (16)	4	2	72.06

Table 2.27: Table showing analysis of the physicochemical properties of combined selected library and the combined full library.

These data show that there is a small difference in the selected library and the full library. The average size of fragments in the selected library is smaller, although the average heavy atom count is closer. The lower ALogP of the selected library suggests that more polar compounds have been selected. This allows for addition of lipophilic groups in fragment development without approaching an unfavourable ALogP level. In conclusion, the compounds in the selected library meet all the criteria outlined in the "Rule of 3" and have favourable properties to allow for fragment development.

2.7 Comparison of library with a commercial fragment library

Our selected fragment library was specifically designed to explore more 3-dimensional areas of chemical space and introduce more simple saturated scaffolds into fragment libraries. To show this, we compare our library to a commercial fragment library. The Maybridge Rule of 3, core 1000 fragment[64] library is a commercially library available to purchase and screen. This library of compounds was subjected to our PMI analysis protocol to generate conformations of these compounds and determine their position on the PMI plot.

Figure 2.48 (a) shows the lowest energy conformation of each of the 1000 compounds in the Maybridge library. This is compared to our full 560-member (Figure 2.48 (b)) and the 112-member sub-set library (Figure 2.48 (c)).

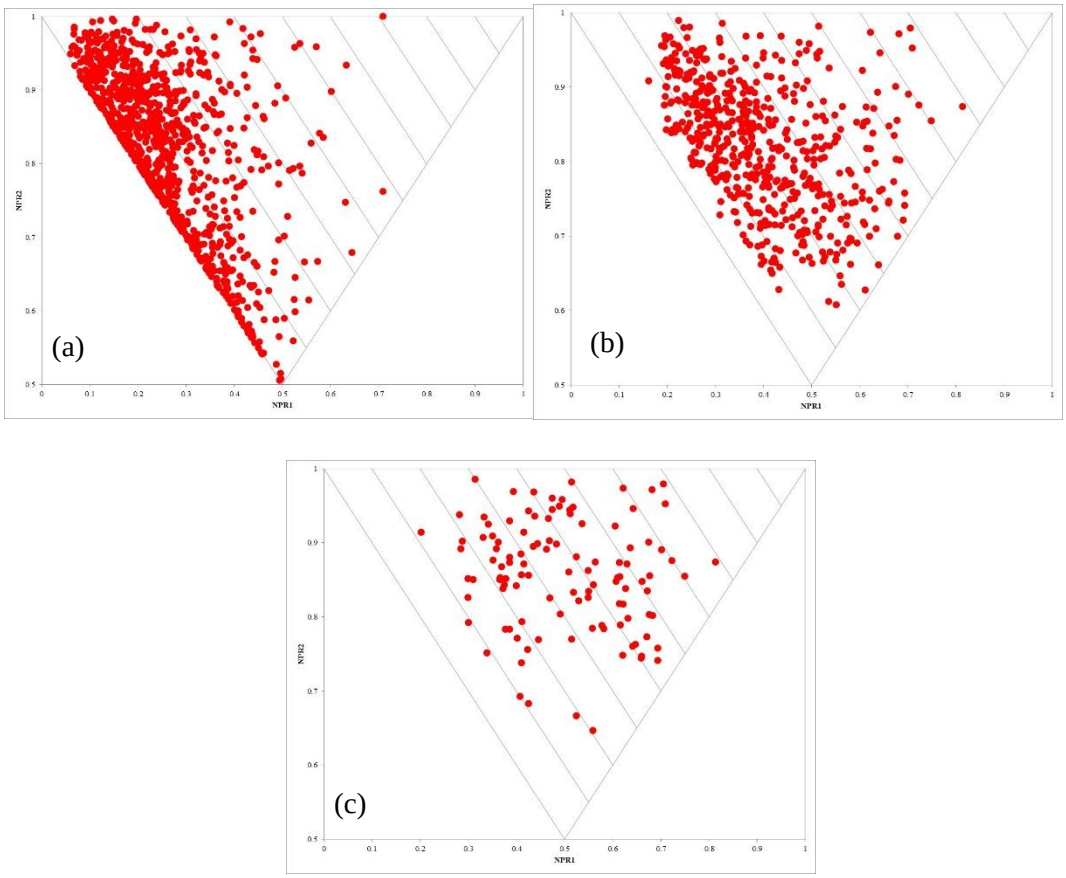

Figure 2.48: PMI (a), shows compounds from the Maybridge Rule of 3 fragment library, PMI (b) shows the combined pyrrolidine, piperidine and azepane libraries and PMI (c) shows the combined selected sub-set library for all three scaffolds. Each plot only shows the lowest energy conformer for each compound.

The Maybridge library clearly contains more flat molecules as shown by the number of compounds close to the rod-disc axis of the PMI plot. This can be more closely analysed and it is found that 69% of compounds are in PMI category 10, with only 3.6% of compounds in the more spherical part of the plot (PMI categories 1 to 7). It is clear that there are considerably less compounds in this category of our library (1.8%) and more compounds covering the more 3-dimensional areas of chemical space. The full library has 20% of compounds in PMI categories 1 to 7 and the selected library 61.6%. These data are also presented in Figure 2.49 which shows the percentage of each compound in each of the PMI categories for each library.

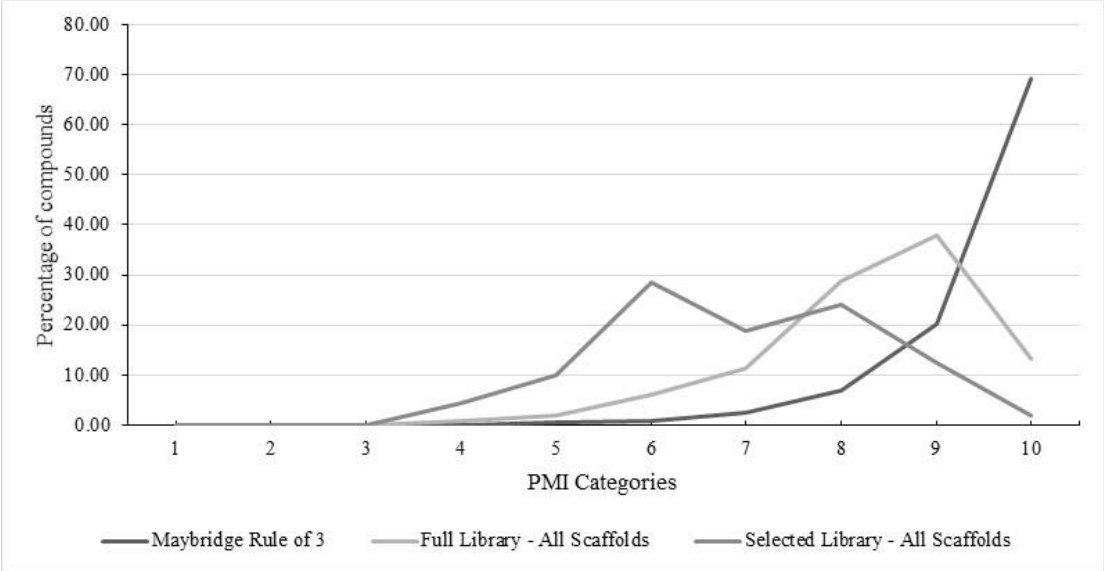

Figure 2.49: Graph showing the percentage of compounds in each category of the PMI plot for each library.

The graph shows that we have succeeded in selecting compounds with particular focus on the more interesting, under-represented, 3-dimensional area of the PMI plot and have less compounds in the area closest to the rod-disc axis.

For full comparison, the physicochemical properties of the Maybridge library were analysed. The key properties are summarised in Table 2.28.

	Data set		ALogP	MW (HAC)	H Bond Acceptor	H Bond Donor	Molecular PSA / Å^2
1	Selected	Average	-0.246	168.4 (11.6)	1.88	1.23	38.34
2		Smallest	-1.48	116.18 (8)	1	0	24.67
3		Largest	1.17	249.33 (16)	4	2	72.06
4	Full	Average	-0.116	181.05 (12.3)	2.26	1	45.00
5		Smallest	-1.57	116.18 (8)	1	0	24.67
6		Largest	1.17	249.33 (16)	4	2	72.06
7	Maybridge Rule of 3	Average	1.30	180.1 (12.5)	1.94	0.787	45.92
8		Smallest	-2.68	82.1 (6)	0	0	3.24
9		Largest	3.95	295.8 (21)	4	3	117.5

Table 2.28: The physicochemical properties of the selected sub-set fragment library, the full fragment library and the Maybridge Rule of 3, core 1000 library.

As expected, the Maybridge Rule of 3 average is within the desired criteria for all of the properties. The most extreme values, however, vary considerably and some lie quite far away from the general desirable criteria. The Maybridge library values compare well to the full and selected libraries. Molecular weight is very similar between all of the libraries, as is polar surface area. There is, however, a considerable difference in the average ALogP for the Maybridge library. The much higher ALogP for the Maybridge library may suggest that there is a lower proportion of very polar compounds in the Maybridge library. Further analysis shows that 58% of the Maybridge library compounds contain one aromatic ring, compared to none in ours. This may be where our selected library falls down, as very polar compounds can have issues further into development and issues with too polar compounds struggling to cross cell membranes.[65] However, this may not be a major issue if the fragments are diversified and further functionalised later in development. This data shows that our selected library covers a different range of physical properties, which may not be efficiently sampled by the commercial library.

2.8 Conclusions and Overview

We have been able to develop a computational approach for the analysis and selection of a range of saturated nitrogen heterocycles. This computational protocol has been optimised and provides reliable conformational data. We have demonstrated that shape diversity can be obtained from simple scaffolds and that by analysing the different conformations of a compound, we have been able to access new and interesting areas of pharmaceutical space. It has been possible to develop criteria to select fragments focused on the under-represented, 3-dimensional area of the PMI plot and new areas of pharmaceutical space and move away from the undesirable rod-disc axis. Introducing different synthetically accessible substituents gave additional fragments that cover different areas of chemical space and this highlights that simple modifications can open up new interesting areas of chemical space. Comparison of our full and selected sub-set libraries highlight that our scaffolds and compound collections cover more 3-dimensional space than current libraries and access new areas of chemical space. Our fragments also fit with the "Rule of 3" desirable criteria for fragment compounds and have suitable properties that could be further developed in the drug development process. The selection of a smaller sub-set of these compounds has made synthesis more amenable.

Chapter 3: Synthesis Towards Selected Disubstituted Piperidines

The analysis of different heterocycles in Chapter 2 yielded a number of smaller subset libraries that we wished to synthesise. As the main focus and development centred on disubstituted piperidines, it was the synthesis of these that was tackled. It was important to minimise the number of different routes and steps used to synthesise the final fragments and therefore the synthetic strategy is presented in Section 3.1. The use of these compounds as valuable building blocks also highlights the importance of simple and efficient synthesis. The use of a model piperidine system to optimise the installation of the different nitrogen substituents (Figure 3.1) is described in Section 3.2.

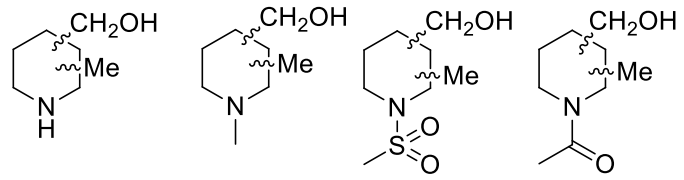

Figure 3.1: Four different nitrogen substituents

A range of synthetic methods were employed in the preparation of the piperidine fragments. These included enolate alkylation methodology (Section 3.3), lithiation-trapping of *N*-Boc piperidines (Section 3.4), amino zinc enolate carbocyclisation methodology (Section 3.5 and 3.6), a condensation and aza-annulation approach (Section 3.7) and reduction of disubstituted pyridines (Section 3.8).

3.1 Synthetic strategy

The computational analysis in Section 2.4 selected 20 fragments for synthesis (Figure 3.2). Fragment and building block synthesis should be tractable in order to make suitable amounts (~ 100-200 mg) of a given compound available for testing, analysis and further development. It would therefore be beneficial to try and group similar fragments to minimise the number of synthetic routes.

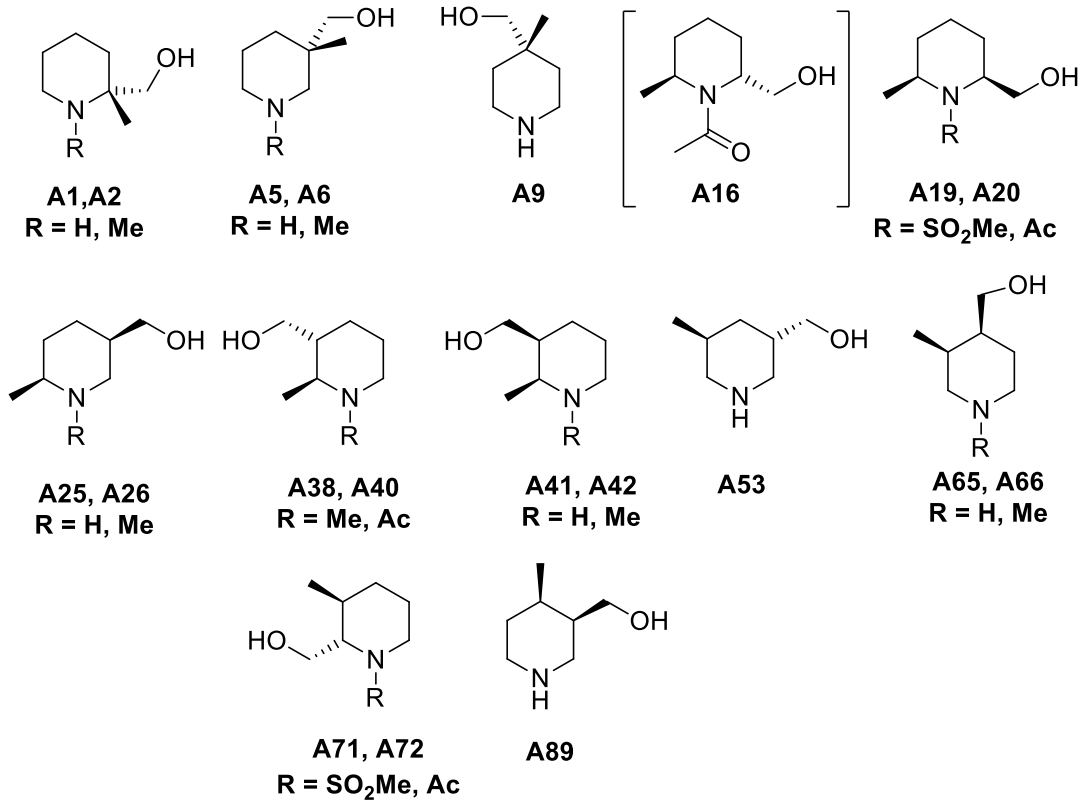

Figure 3.2: The 20 fragments selected for synthesis using our analysis protocol.

It was envisaged that the fragments could be grouped based on the position of the substituents. Therefore, the following groupings were devised.

- **A1** – **A9** – geminal disubstituted piperidines
- **A16**, **A19** and **A20** – 2,6-disubstituted piperidines
- **A38**, **A40**, **A41** and **A42** – 2,3-disubsituted piperidines

In addition, some of the fragments have similar substitution patterns, such as **A65**, **A66**, **A71**, **A72** and **A89**, with adjacent methyl and ester arrangement. It could be imagined that these fragments may be synthesised using related methodology. The synthesis towards the selected fragments is described below.

3.2 Optimisation of *N*-functionalisation methods using a model piperidine

In order to vary the structures within the sub-set library, four different nitrogen substituents will be used to functionalise the compounds (Figure 3.3). These are NH, *N*-methyl, *N*-methanesulfonyl and *N*-acetyl groups. It would be desirable to develop a synthetic sequence that can be used to install these groups in the minimum number of steps and in good yield. It is also essential to ensure that the synthetic sequence is carried out in a suitable order to prevent the formation of any undesirable by-products.

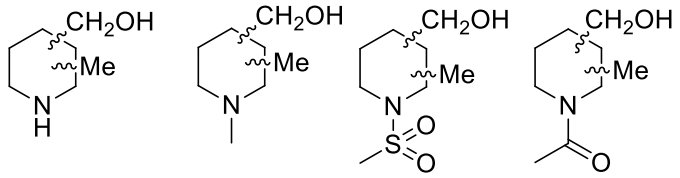

Figure 3.3: The four different nitrogen substituents installed to give the final fragments.

It was decided that a model piperidine would be used to investigate suitable methods and conditions for *N*-functionalisation. Thus, *N*-protected, methyl ester piperidine **16** was selected. Using a literature method,[66] treatment of pipecolic acid **15** with thionyl chloride and methanol and subsequent Boc protection gave methyl ester **16** in 94% yield (Scheme 3.1).

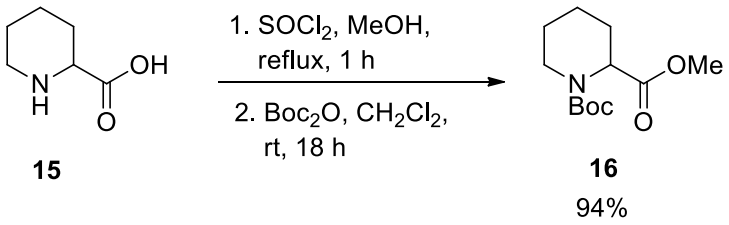

Scheme 3.1

The first nitrogen substituent would simply be the free amine. Before deprotection, it is desirable to reduce the ester. If the deprotection was carried out first, the isolation and purification of the amino alcohol may be difficult. This synthetic order avoids this complication. Alcohol **17** was obtained through the treatment of methyl ester **16** with lithium aluminium hydride in 88% yield. We planned to remove the Boc group using HCl in Et_2O, a procedure that allows for evaporation of solvent under reduced pressure after reaction completion to give clean deprotected amine as the hydrochloride salt. Treatment of piperidine alcohol **17** with commercially available 2 M HCl in Et_2O gave deprotected amino alcohol **18.HCl** in 100% yield (Scheme 3.2).

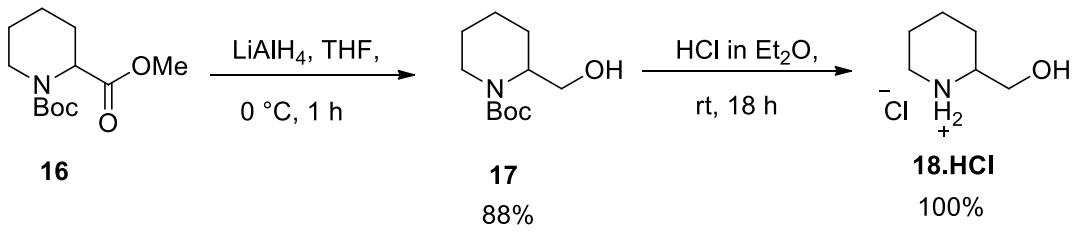

Scheme 3.2

Next, a reliable route to the *N*-methyl substituent was needed. It was proposed that direct reduction of the Boc group of methyl ester **16** using lithium aluminium hydride would yield the *N*-methyl group, as shown by Bowen and co-workers in the synthesis of various piperidines.[67] Treatment of piperidine ester **16** with lithium aluminium hydride at reflux gave piperidine **19** in 82% yield (Scheme 3.3). As hoped, the simultaneous reduction of the ester group to give the hydroxymethyl occurred, negating the need for separate steps. The clean reaction also meant that purification was not required.

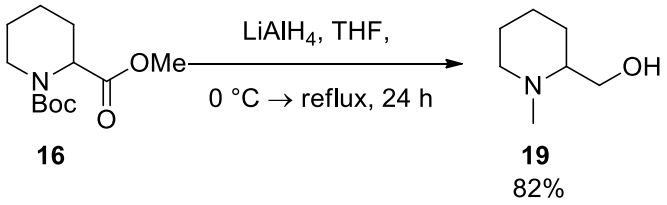

Scheme 3.3

We expected that the other two model fragments containing *N*-sulfonyl and *N*-acetyl groups could be made by functionalisation of the deprotected amino ester **20** followed by reduction to give the alcohol. The ester would be reduced after *N*-functionalisation to prevent unwanted reaction of the alcohol with acetyl chloride or methanesulfonyl chloride. In effect, the ester is acting as a protecting group for the hydroxymethyl substituent. The Boc group was removed from methyl ester **16** using HCl formed *in situ* from the reaction of acetyl chloride and ethanol. This gave deprotected methyl ester **20.HCl** as the hydrochloride salt in 82% yield (Scheme 3.4).

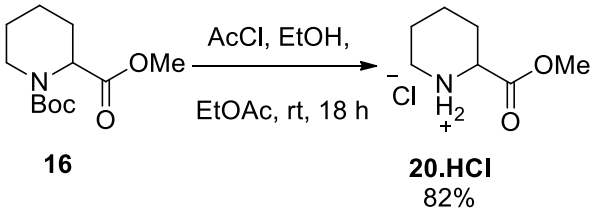

Scheme 3.4

From here, the nitrogen substituent was installed. Treatment of hydrochloride salt **20.HCl** with acetyl chloride gave acetamide **21** in 99% yield. Subsequent reduction of acetamide ester **21** using lithium aluminium hydride gave a poor 19% yield of acetamide amino alcohol **22**. This could be due to over-reduction of the acetamide, but by-products were obtained in too low yield to be identified. Due to the poor results from the reduction using lithium aluminium hydride, lithium borohydride was investigated as a milder reducing agent. The reduction of piperidine ester **21** with lithium borohydride was carried out in THF at room temperature to give a 29% yield of acetamide alcohol **22** (Scheme 3.5).

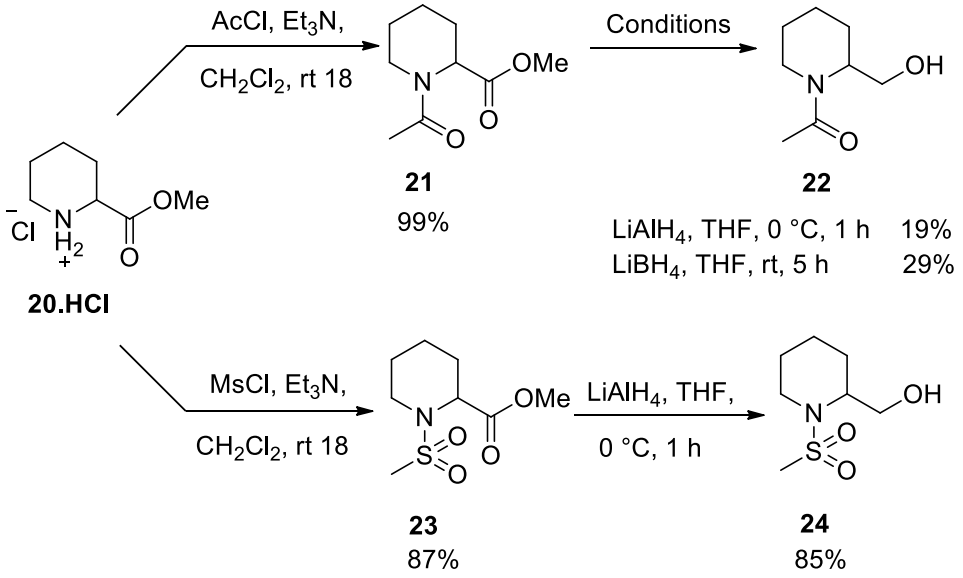

Scheme 3.5

Sulfonamide **24** can also be prepared from the deprotected methyl ester hydrochloride salt **20.HCl**. Reaction of **20.HCl** with methanesulfonyl chloride gave sulfonamide ester **23** in 87% yield. Subsequent reduction of the ester **23** with lithium aluminium hydride was much more straightforward than the amide and gave sulfonamide alcohol **24** in 85% yield (Scheme 3.5).

These reactions demonstrate that if we had access to the *N*-Boc methyl ester precursors of fragments then we have reactions in place to introduce all the *N*-groups in a few simple and mild steps and in good yield.

3.3 Synthesis of geminal disubstituted piperidines

The fragments **A1**, **A2**, **A5**, **A6** and **A9** (Figure 3.4) have geminal substituents and therefore it was envisaged that the same methodology could be used to synthesise each group of isomers.

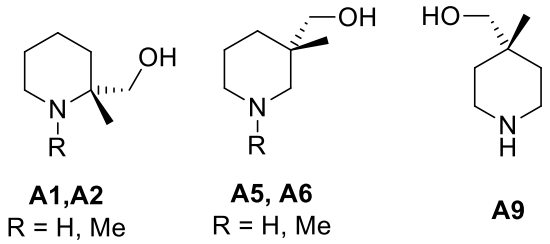

Figure 3.4: The five geminal disubstituted piperidines selected for synthesis.

The previous syntheses of these types of compound in the literature have focused on enolate alkylation chemistry, starting from the different piperidine esters to give disubstituted piperidine esters. For example, work by Ikeda and co-workers in the synthesis of 2-(but-3-ynyl)-1-(*o*-iodobenzoyl) piperidines used lithium bis(trimethylsilyl)amide to deprotonate *N*-Boc piperidine ester **16** in THF at –78 °C for 15 min. Subsequent trapping with methyl iodide gave methylated ester **25** in quantitative yield (Scheme 3.6).[68]

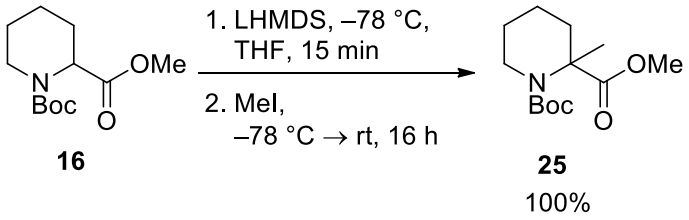

Scheme 3.6

Onomura and colleages reported the racemic synthesis of 2,2-disubstituted piperidine **27** by the methylation of enantiomerically pure piperidine ester **26** using sodium hexamethyldisilazide and three equivalents of methyl iodide in 89% yield (Scheme 3.7). The deprotonation in this case was started at –78 °C and warmed to –20 °C for 30 min.[69]

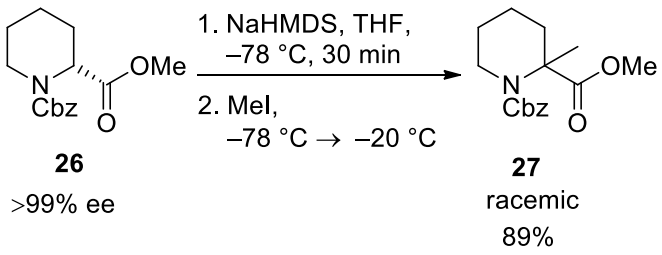

Scheme 3.7

The synthesis of a 3,3-disubstituted piperidine also using 1.2 equivalents of sodium hexamethyldisilazide was reported by McNamara and co-workers. Here the enolate of free piperidine **28** was alkylated with MeI (Scheme 3.8). It was reported that enolate alkylation occurred preferentially over *N*-alkylation, but the yield was not given.[70]

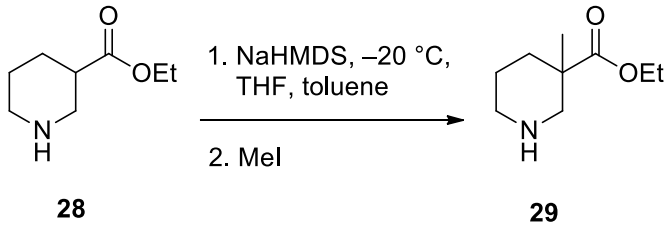

Scheme 3.8

Paterniti and co-workers also reported the synthesis of 3,3-disubsituted piperidines. However, in this case, *N*-Boc protection was used and the enolate formation was carried out with LDA at –78 °C. Alkylation was then carried out with methyl iodide to give piperidine **32** in 90% yield (Scheme 3.9).[71] LDA was also employed as the base in the enolate alkylation of 4-ester piperidine **31** as reported by Gordeev and colleagues.[72] Alkylation with methyl iodide gave 4,4-disubstituted piperidine **33** in 70% yield.

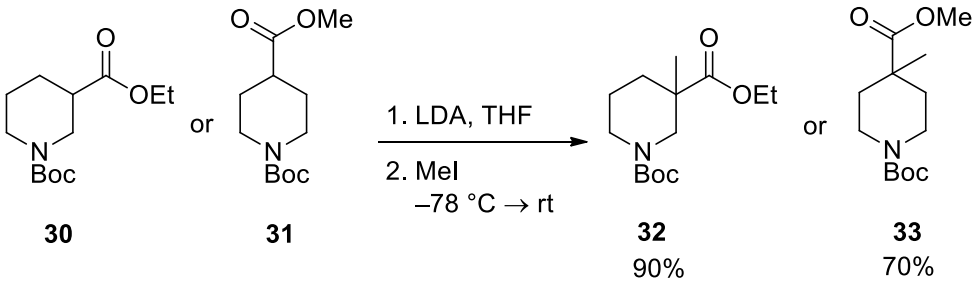

Scheme 3.9

As there have been a number of different bases used in the literature with varying conditions, the enolate alkylation of *N*-Boc piperidine **16** was undertaken using lithium bis(trimethylsilyl)amide in THF at –78 °C for 1 h and methyl iodide in our hands, due mainly to availability of reagents. Starting with 2-ester substituted piperidine **16**, these conditions gave a 91:9 mixture of product **25** and starting material **16**, which could not be separated by column chromatography (Table 3.1, Entry 1). The ratio of **25**:**16** was determined by integrating the δ 3.71 and δ 3.70 signals in the ^{1}H NMR spectrum of the crude product. In order to increase conversion to product, other conditions were explored. DMPU was added to the lithium bis(trimethylsilyl)amide reaction. DMPU is known to increase the nucleophilicity and basicity of reagents which is believed to be due to it breaking apart aggregates.[73] This was also compared with potassium bis(trimethylsilyl)amide. The results are summarised in Table 3.1.

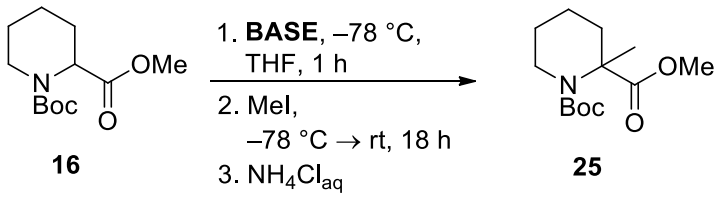

Entry	Base	Product:Starting material[a]	Yield[b]
1	LHMDS	91:9	68%
2	LHMDS + DMPU	42:58	72%
3	KHMDS	98:2	96%

Table 3.1: Comparison of different bases and conditions used in the enolate alkylation of piperidine methyl ester **16**. [a] Obtained from the ^{1}H NMR spectrum of the crude product. [b] % yield of crude product.

It appeared that addition of DMPU to the LHMDS reaction had a detrimental effect on conversion to product **25**, with only a small increase in yield (Entry 2). The best result was obtained with KHMDS, giving a 98:2 mixture of product **25** and starting material **16** and a crude yield of 96% (Entry 3). These conditions were carried forward for use in a large-scale synthesis of methylated ester **25**. Treatment of methyl ester piperidine **16** (5.0 mmol) with KHMDS and subsequent trapping with methyl iodide gave a 95:5 mixture (by ^{1}H NMR spectroscopy) of methylated ester **25** and starting methyl ester piperidine **16** (94% and 5% yield of methylated ester **25** and piperidine **16** respectively) after column chromatography (Scheme 3.10). These inseparable compounds were carried forward as a mixture.

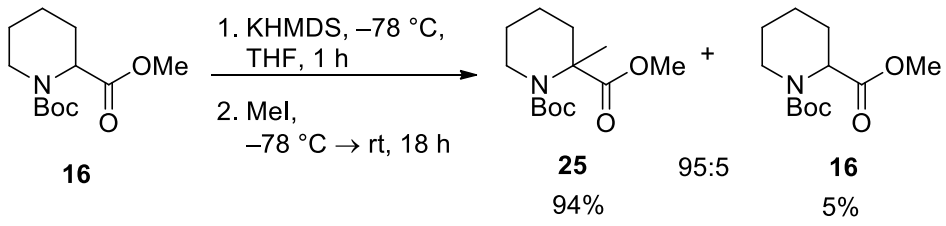

Scheme 3.10

Our hope was that after reduction of the mixture of **25** and **16**, the resulting alcohols would be separable. For the synthesis of fragment **A1**, the methylated ester **25** needed to be reduced and the Boc group deprotected. Thus, the 95:5 mixture of methylated piperidine **25** and starting ester **16** was treated with lithium aluminium hydride. This gave a separable mixture of methylated amino alcohol **34** and amino alcohol **17**, which were obtained in a 65% yield and quantitative yield from **25** and **16** respectively (Scheme 3.11).

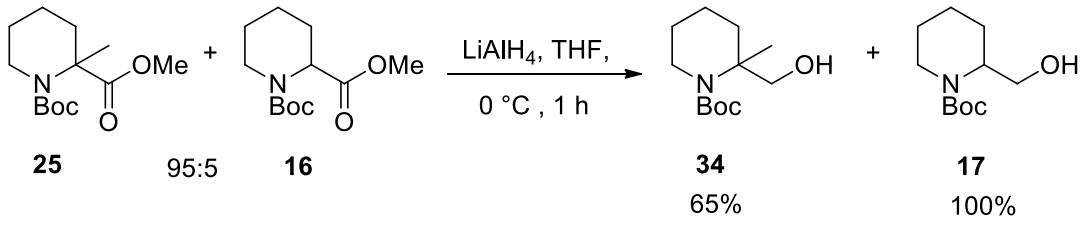

Scheme 3.11

The pure amino alcohol **34** was then taken on and treated with HCl in Et_2O to obtain the deprotected methylated piperidine **A1.HCl** as a hydrochloride salt in 58% yield (Scheme 3.12). The methylated fragment **A2** could be synthesised from the already reduced piperidine alcohol **34**. Reduction straight from the mixture of **25** and **16** would lead to two very polar, difficult to separate products. Therefore, reduction from piperidine alcohol **34** negates the need for purification. The reduction of the Boc group using lithium aluminium hydride gave the methylated disubstituted piperidine **A2** in 76% yield (Scheme 3.12).

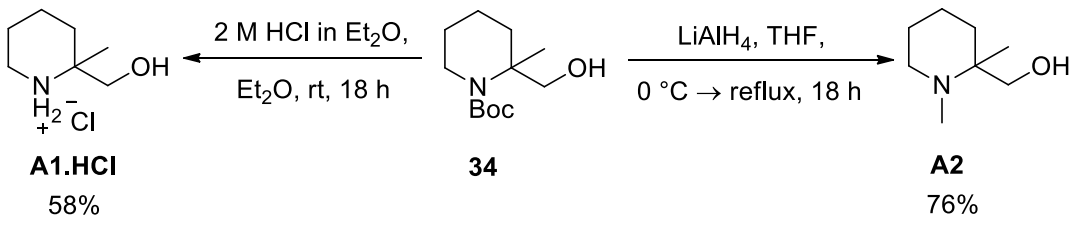

Scheme 3.12

The enolate alkylation methodology used above was then applied to the synthesis of fragments **A5**, **A6** and **A9**. Fragments **A5** and **A6**, were prepared from nipecotic acid **35**. Reaction of nipecotic acid **35** with thionyl chloride in methanol followed by Boc protection gave piperidine ester **36** in 81% yield (Scheme 3.13). The new enolate alkylation conditions were then employed on piperidine ester **36**. Deprotonation with KHMDS followed by trapping with methyl iodide gave methylated piperidine ester **37** in 97% yield after column chromatography (Scheme 3.13). In this case, methylated piperidine ester **37** was obtained as a single product and there was no remaining starting material.

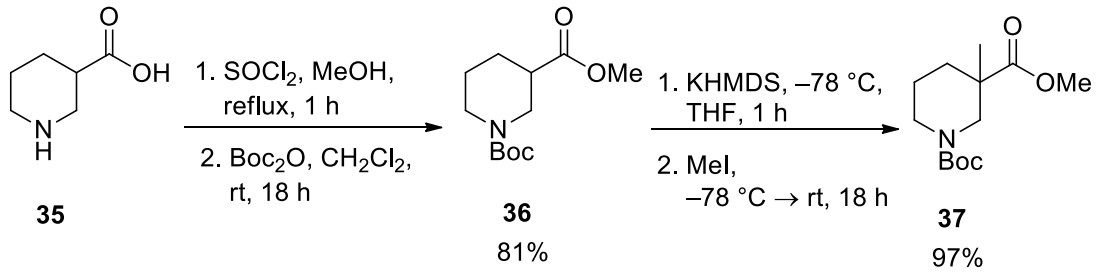

Scheme 3.13

The methylated piperidine ester **37** was then reduced using lithium aluminium hydride to give amino alcohol **38** in 91% yield. Subsequent deprotection of this substrate with HCl in Et_2O gave the final fragment **A5.HCl** in 94% yield (Scheme 3.14). Fragment **A6** was prepared by direct reduction of piperidine ester **37** using lithium aluminium hydride. This gave methyl amino piperidine **A6** in 96% yield (Scheme 3.14).

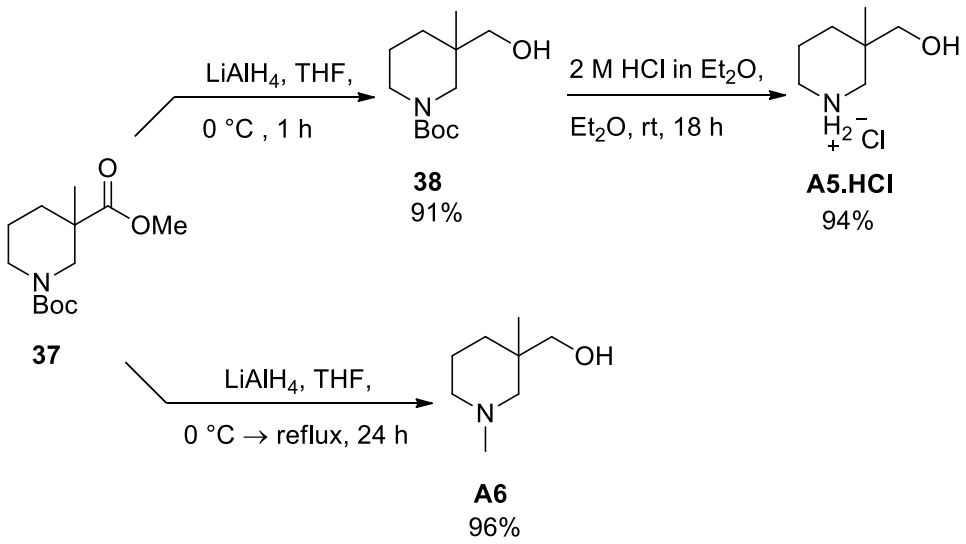

Scheme 3.14

The final fragment in this group is 4,4-disubstituted piperidine **A9**. The starting methyl ester **31** for this synthesis was prepared from isonipecotic acid **38**. Reaction with thionyl chloride in methanol and subsequent Boc protection gave the methyl ester **31** in 85% yield (Scheme 3.15). Enolate alkylation of piperidine ester **31** using our standard conditions gave disubstituted piperidine **33** in quantitative yield (Scheme 3.15).

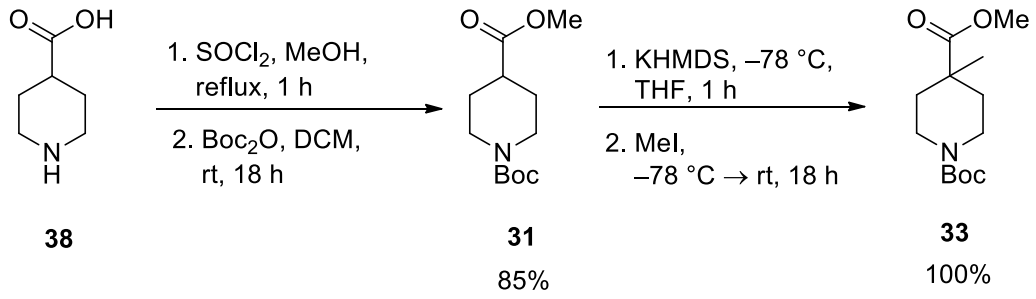

Scheme 3.15

Methylated piperidine ester **33** was then reduced using lithium aluminium hydride to give amino alcohol **39** in quantitative yield (Scheme 3.16). Deprotection of amino alcohol **39** using HCl in Et_2O gave a quantitative yield of 4,4-disubstituted piperidine **A9.HCl** (Scheme 3.16).

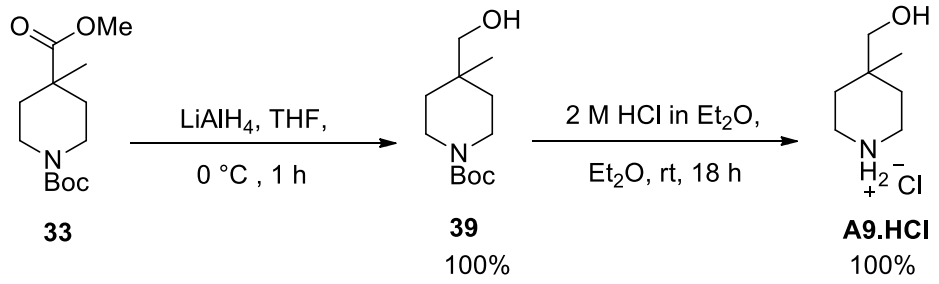

Scheme 3.16

3.4 Synthesis of 2-hydroxymethyl, 6-methyl disubstituted piperidines

Our next set of targets were fragments **A16**, **A19** and **A20**, which bear a 2,6-disubstitution pattern in both *cis* and *trans* configurations (Figure 3.5). It must be noted that fragment **A16** was selected in a previous version of the protocol (Section 1.2). The synthesis of this fragment had already started and was therefore completed despite not being selected by our current version of the protocol. A number of routes to different 2,6-disubstituted piperidines have been previously reported in the literature and a selection of the main approaches will be briefly summarised. The methods described focus on methyl, ester and some hydroxymethyl substituted piperidines as these are the most relevant to the synthesis of **A16**, **A19** and **A20**.

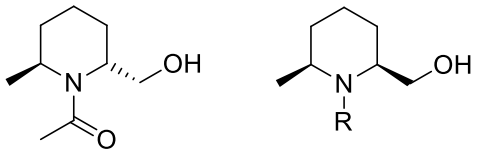

A16 **A19, A20**

R = SO_2Me, Ac

Figure 3.5: The three 2,6-disubstituted fragments selected for synthesis.

Blechert and colleagues reported a route to *cis*-**43** via ruthenium-catalysed cross metathesis of alkyl-substituted olefins and subsequent reductive amination.[74] First, cross-coupling of *N*-protected homoallylic amine **40** with enone **41** in the presence of the ruthenium catalyst **44** gave amino enone **42** in 85% yield. Then, reaction with H_2 and Pd/C provided disubstituted piperidine ester *cis*-**43** in 85% yield, selectively as the *cis* diastereomer (Scheme 3.17). Hydrogenation of the intermediate iminium ion on the face opposite the ester group explains the diastereoselectivity.[74]

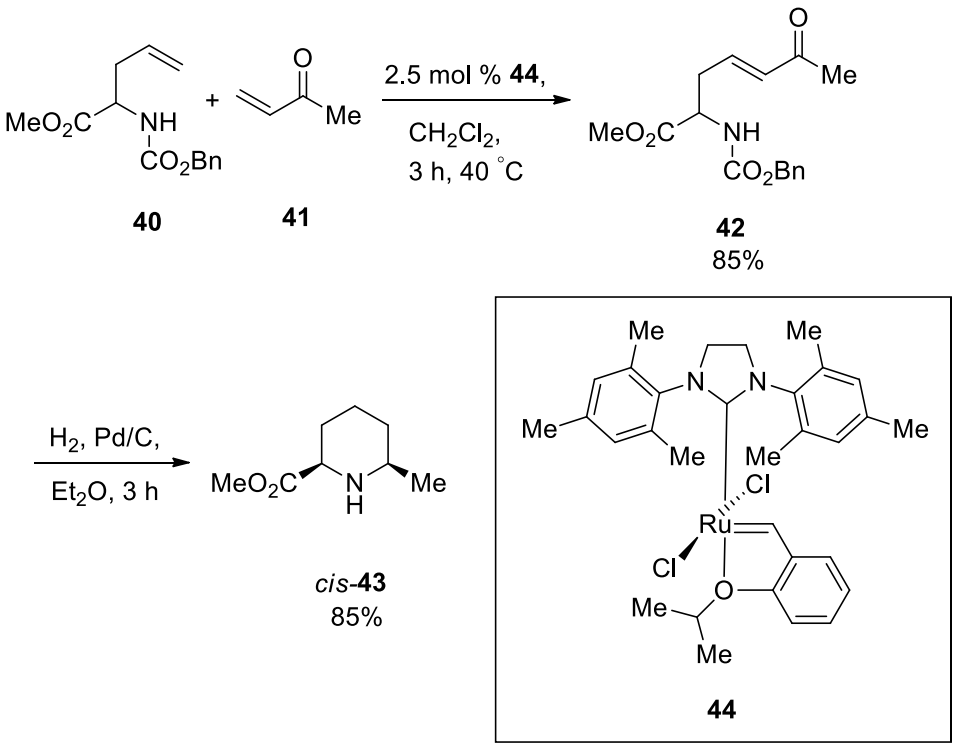

Scheme 3.17

A four-step synthesis of 2,6-disubstituted piperidines was reported by Lubell and co-workers.[75] This route from aspartic acid features an aldol condensation, dehydration and reductive amination. Initially, methyl alkyl ketone was treated with LDA to give the lithium enolate, which was then reacted with an aldehyde in an aldol condensation to give amino-ester **45** in 68% yield (Scheme 3.18). Amino-ester **45** was then treated with methansulfonyl chloride and triethylamine in CH_2Cl_2 to give the enone **46** in 86% yield by an elimination reaction of the methansulfonate (Scheme 3.18). Diastereoselective hydrogenation of enone **46** subsequently gave pipecolate *tert*-butyl ester *cis*-**47** in 90% yield (Scheme 3.18).[75]

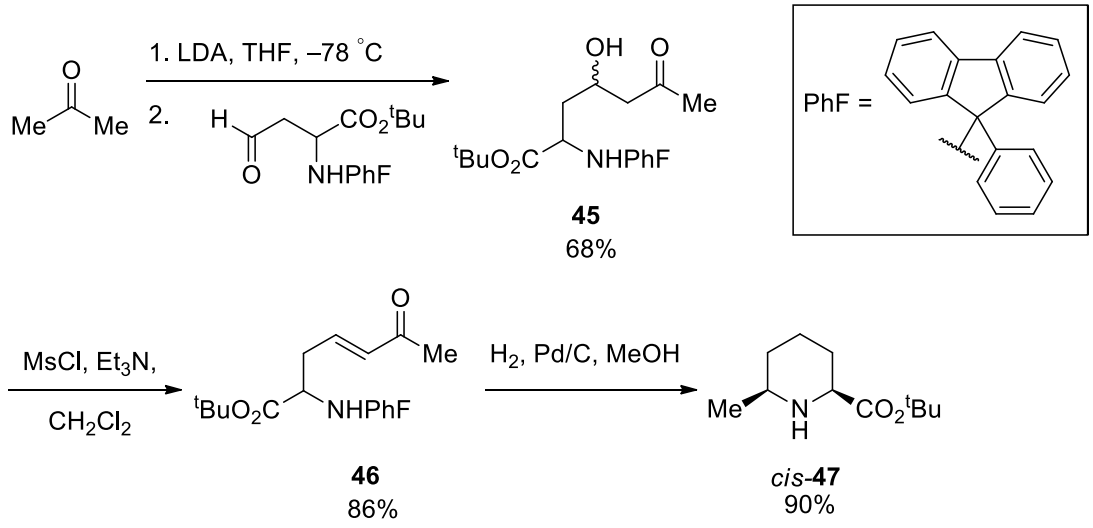

Scheme 3.18

The lithiation-trapping of *N*-Boc nitrogen heterocycles, first reported by Beak[76], has been reported by a number of groups as a method to synthesise 2,6-disubsituted piperidines. Hart and Wu reported the lithiation of protected hydroxymethyl *N*-Boc piperidine **48** using *s*-BuLi/TMEDA and trapping with methyl iodide to give disubstituted piperidine *trans*-**50** in 71% yield (Scheme 3.19). The product was then used in their preparation of the natural product (+)-Himbacine.[77] In a similar process, Pissarnitski reported the lithiation of *N*-Boc methylpiperidine **49** and trapping with DMF as a method to obtain 2,6-disubstituted piperidine *trans*-**51** (Scheme 3.19). Aldehyde **51** was used in the synthesis of γ-sectretase inhibitors.[78] An explanation of the *trans*-diastereoselectivity of both of these reactions is presented later.

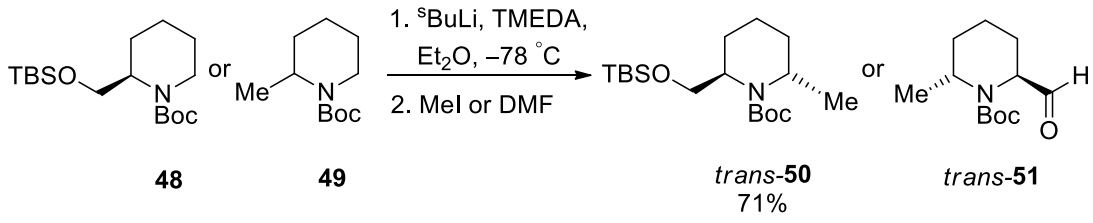

Scheme 3.19

Both of these synthetic routes follow the conditions originally outlined by Beak in 1989.[76] It involves the treatment of an *N*-Boc heterocycle with *s*-BuLi and a ligand such as TMEDA followed by trapping with a suitable electrophile to give α-substituted *N*-heterocycles. Investigation into the lithiation-trapping of mono-substituted *N*-Boc heterocycles is well precedented.[79-81] The lithiation-trapping of 2-substituted *N*-Boc

piperidines preferentially gives *trans* stereochemistry, as shown in the lithiation-trapping of 2-methyl *N*-Boc piperidine **49** with dimethylsulfate (Scheme 3.20).[82]

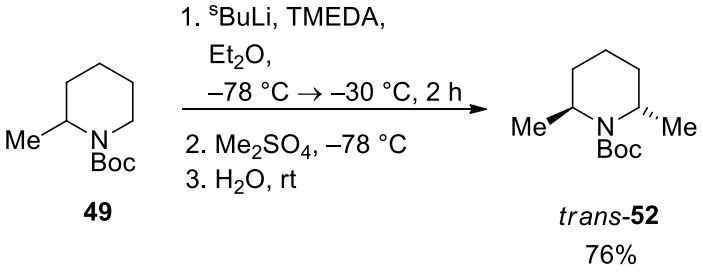

Scheme 3.20

Our plan was to use Beak's methodology to access fragment **A16**. Using lithiation-trapping gives us the opportunity to use a range of electrophiles to introduce the different substituents and could also open up synthetic variation in the future.

There are two alternative routes to furnish disubstituted piperidine **54**. Piperidine methanol **53** can undergo lithiation-trapping with a methylating agent to give disubstituted piperidine or methyl piperidine **49** can undergo lithiation-trapping with DMF, subsequent reduction would give the disubstituted piperidine **54** (Scheme 3.21). Each of these methods are presented in turn below.

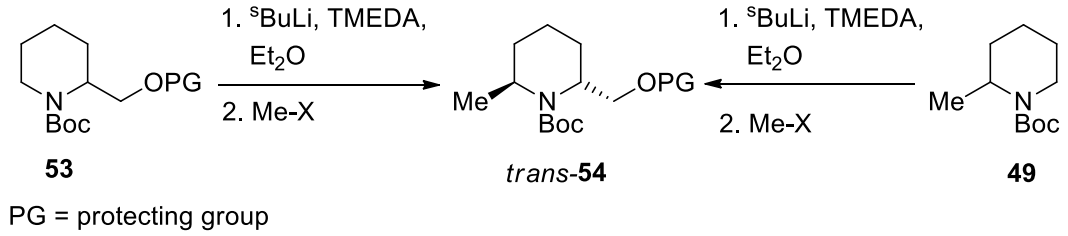

Scheme 3.21

To start with, protected *N*-Boc piperidine **55** was prepared. Boc protection with Boc_2O gave protected piperidine **17** in 80% yield. This was followed by reaction with triisopropylsilyl chloride to give fully protected *N*-Boc piperidine **55** in 92% yield (Scheme 3.22).

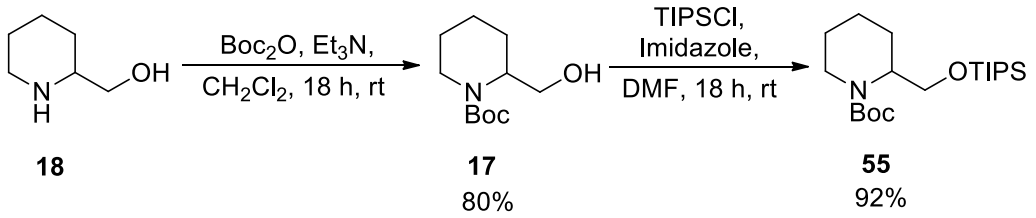

Scheme 3.22

An important factor to consider before the lithiation-trapping is the rotamer interconversion of the Boc group. The lithiation time can be affected by the orientation of the Boc group. In order for lithiation to occur the carbonyl of the Boc group must be oriented correctly to direct the organolithium to the site of lithiation (**B**) in Figure 3.6.

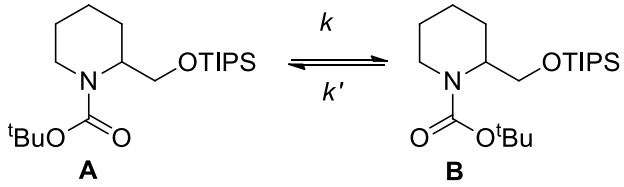

Figure 3.6

If there is a slow rate of interconversion of rotamers **A** and **B** at the reaction temperature, only some of the compound will be in the correct orientation for lithiation and therefore the yield of the reaction will be limited. The α-proton of rotamer **A** is too sterically hindered to undergo lithiation, reaction only occurs on rotamer **B**.[83,84] In order to calculate the rate of interconversion, VT NMR spectroscopic studies were carried out on *N*-Boc piperidine **55**. The rate for the interconversion of the two rotamers (**A** and **B**), *k*, can be calculated using the Eyring equation (1).

$$k = (k_B \cdot T/h) \cdot e^{(-\Delta G‡/RT)} \qquad (1)$$

where k_B is Boltzmann's constant, h is Planck's constant, R is the gas constant and $\Delta G^‡$ is the Gibbs free energy of activation.

In the low temperature NMR spectrum, there will be two distinct signals corresponding to the two rotamers. As the temperature the spectrum is run at increases, the signals move together. When the signals finally merge into one signal, this is the coalescence temperature (See Figure 3.7). At the coalescence temperature, T_c, the rate constant, *k*, is given by equation (2).

$$k = (\pi \cdot \Delta v_0)/\sqrt{2} \qquad (2)$$

where Δv_0 is the separation in Hertz between the peaks of **A** and **B** at the slow rate of interconversion. From this, $\Delta G^{\ddagger}$ can be calculated using equation (3).

$$\Delta G^{\ddagger} = \mathrm{RT}[\ln(\mathrm{k_B} \cdot \mathrm{T/h}) - \ln k] \qquad (3)$$

Using this value of $\Delta G^{\ddagger}$, it is possible to calculate the rate constant *k* at different temperatures using the Eyring equation (1). This uses the assumption that the change in entropy is zero on changing temperature. Once *k* is known, it is possible to calculate the half-life at a particular temperature using equation (4)

$$t_{1/2} = \ln 2/k \qquad (4)$$

Using ^{1}H NMR spectroscopy of *N*-Boc piperidine **55** in toluene-d_8 at different temperatures, it was possible to calculate the rate constant *k* at the coalescence temperature. The NCH signals at δ 2.68 and δ 2.47 were selected. At –60 °C, Δv_0 = 82.4 Hz (Figure 3.7, a). This gave the rate constant k = 183 s^{-1} and a half life $t_{1/2} \approx$ 0.003 s at T_c. The two signals coalesced at approximately 10 °C (283 K) (Figure 3.7, e). At a temperature of –78 °C (195 K), the half-life can be calculated using equation (4). At –78 °C, $t_{1/2} \approx$ 5 minutes, whereas at –50 °C, $t_{1/2} \approx$ 3 seconds.

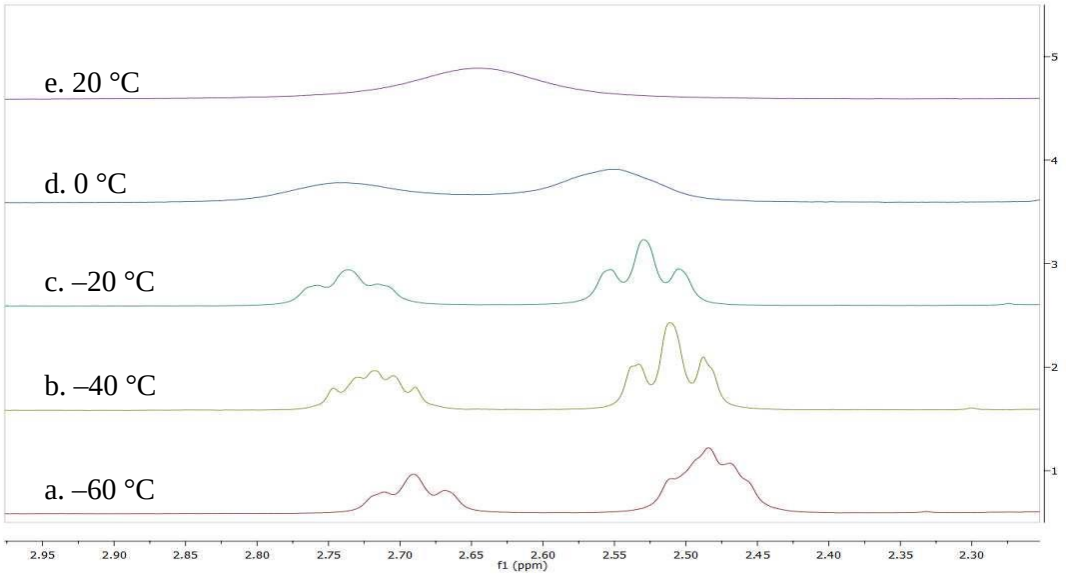

Figure 3.7: ^{1}H NMR spectra of *N*-Boc piperidine **55** at different temperatures.

Using this information, it was possible to identify a suitable temperature for lithiation. The results suggest that the rotamer interconversion is rapid enough at both –78 °C and –50 °C for lithiation of *N*-Boc piperidine **55.**

The lithiation reaction of *N*-Boc piperidine **55** was carried out at these two different temperatures for different lengths of time using *s*-BuLi and TMEDA in Et_2O. Dimethylsulfate was chosen as the electrophile for trapping to give disubstituted piperidine *trans*-**56** (Scheme 3.23 and Table 3.2).

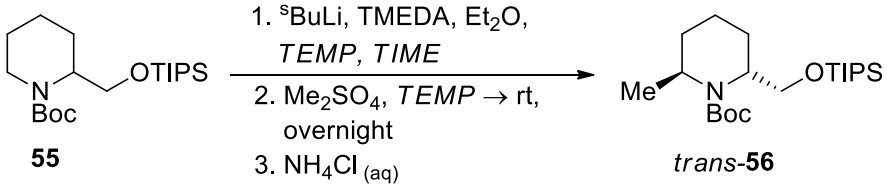

Scheme 3.23

Entry	Temperature	Time	Result
1	–50 °C	1 h	41% product, 57% starting material
2	–78 °C	3 h	29% product, 52% starting material

Table 3.2: The different conditions used for the lithiation-trapping of *N*-Boc piperidine **55**.

The most promising result was obtained using lithiation at –50 °C for 1 hour, which gave disubstituted piperidine *trans*-**56** in 41% yield (Entry 1). The ^{1}H NMR spectrum

of the crude product indicated that only one diastereomer was obtained. Literature precedent would suggest that the *trans* diastereomer is obtained preferentially.[85] The CH_2OTIPS group preferentially sits in the axial position to avoid $A^{1,3}$ strain between the substituent and the Boc group, shown in Figure 3.8. Due to this well-established literature precedent it has been assumed that the *trans*-diastereomer is the major product in all the lithiation-trapping reactions in this section.

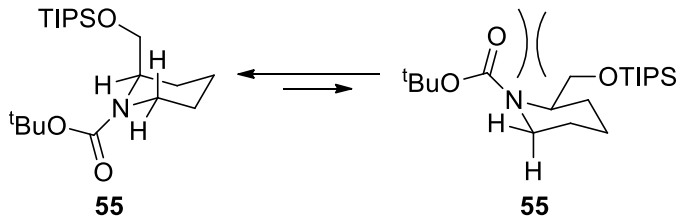

Figure 3.8

The carbonyl of the Boc group then directs the deprotonation of the 6-equatorial proton, by coordination to the lithium, to give intermediate **57**. The electrophile then adds with retention of stereochemistry of the lithium to give *trans*-**56** as shown in Scheme 3.24.

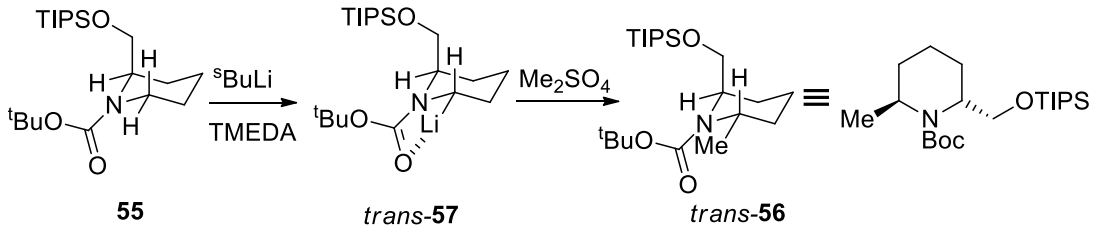

Scheme 3.24

It was surprising that such a large amount of starting material was recovered from these two reactions, especially in light of the interconversion of rotamers at –50 and –78 °C. A possible explanation is the incomplete trapping by dimethylsulfate as other work in the O'Brien group had shown that this electrophile is one of the slowest to trap.[86] As the yield of this lithiation-trapping sequence was low and there would also be a need for protecting group removal in the synthesis, it was decided to investigate the alternative lithiation-trapping sequence.

It was proposed that the lithiation trapping of *N*-Boc methyl piperidine **49** should be investigated. The lithiation-trapping chemistry of this substrate benefits from the

range of different electrophiles that could be used to install the CH_2OH group. These include DMF, methylchloroformate and CO_2 to give the aldehyde, methyl ester and carboxylic acid respectively. Although each of these electrophiles would require reduction after installation to obtain the desired hydroxymethyl group, this route opens up synthetic flexibility.

Although the lithiation-trapping of 2-methyl piperidine **49** is precedented,[82,87-89] it was desired to optimise the lithiation conditions in our hands. *N*-Boc 2-methyl piperidine **49**, was synthesised from 2-methyl piperidine **58** and Boc_2O in 82% yield (Scheme 3.25). Trimethylsilyl chloride was chosen as the electrophile for the initial optimisation study. The lithiation temperature and time were varied, as shown in Table 3.3.

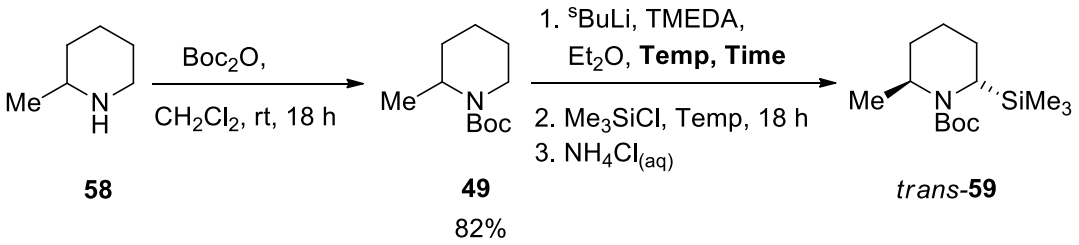

58 **49** 82% *trans*-**59**

Scheme 3.25

Entry	Temperature / °C	Time / h	Product yield / %	Recovered starting material / %
1	–78	3	63	15
2	–78	1	30	26
3	–50	1	70	2
4	–40	1	68	17
5	–40	1.5	85	2

Table 3.3: Different lithiation conditions used in the lithiation-trapping of 2-methyl piperidine **49** and trimethylsilylchloride.

To start, a lithiation at –78 °C for 3 hours was selected, based on Beak's literature precedent.[76,81] This gave a 63% yield of *trans*-**59** (Entry 1). A shorter lithiation time (1 h) gave a lower yield (30%, Entry 2). Other reports have suggested that at a higher temperature, a shorter lithiation time is possible.[82,90,91] Therefore, –40 °C and –50 °C were also chosen. The promising result shown at –40 °C for 1 hour (Entry 4) led to attempting the lithiation at –40 °C for 1.5 hours which gave the highest yield (85%) of disubstituted piperidine *trans*-**59** (Entry 5). Hence, these conditions were used in all subsequent lithiation-trapping reactions of 2-methyl piperidine **49**.

Trapping with DMF as the electrophile allows for installation of an aldehyde α to the nitrogen. Following this transformation with a reduction would then give the desired hydroxymethyl substituted piperidine. The optimised lithiation conditions were then used for the lithiation-trapping of *N*-Boc 2-methyl piperidine **49** with DMF and subsequent reduction of the aldehyde gave disubstituted piperidine *trans*-**61** (Scheme 3.26). Electrophile trapping was carried out at –78 °C for 10 minutes before quenching with water, which gave an 80:20 mixture of disubstituted aldehydes *trans*-**60** and *cis*-**60** by ^{1}H NMR spectroscopy of the crude reaction mixture. Reduction of the crude aldehyde mixture with sodium borohydride gave an 80:20 mixture of inseparable disubstituted alcohols *trans*-**61** and *cis*-**61**, isolated in 81% yield over the two steps from piperidine **49** (Scheme 3.26).

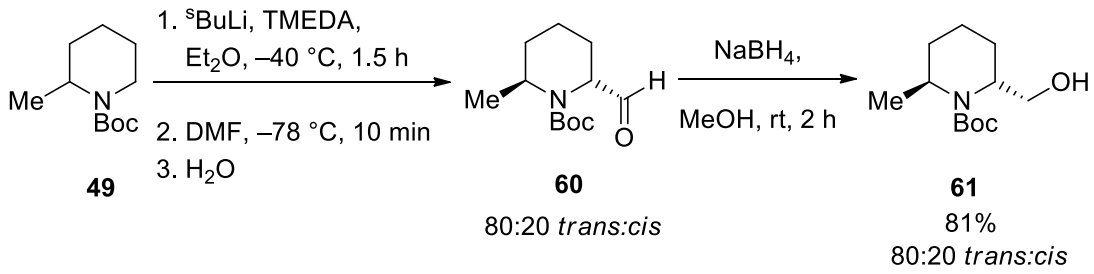

Scheme 3.26

The lithiation-trapping of 2-methyl piperidine **49** with DMF was therefore repeated, but rather than cooling to –78 °C and adding the electrophile we explored addition the electrophile at –40 °C and leaving the mixture to warm to room temperature overnight. This gave an 80:20 mixture of disubstituted aldehydes *cis*-**60** and *trans*-**60** by ^{1}H NMR spectroscopy of the crude reaction mixture. Assignment was based on comparison to literature[92], *J* values for all diagnostic protons could not be obtained due to poor resolution. Reduction of the crude aldehyde mixture **60** with sodium borohydride gave an 80:20 mixture of inseparable disubstituted alcohols *cis*-**61** and *trans*-**61** in 30% yield over two steps (Scheme 3.27). Interestingly, the *cis*-diastereomer was now the major product.

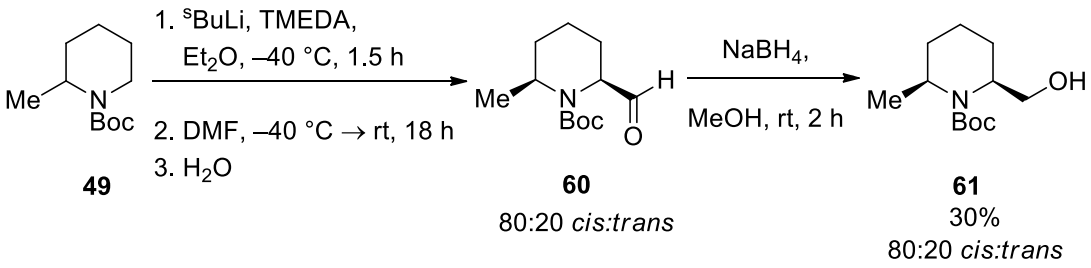

Scheme 3.27

Beak observed a similar *in situ* epimerisation of an 89:11 mixture of *trans*-**60** and *cis*-**60** on silica during purification to give an 83:17 mixture of *cis*-**60** and *trans*-**60**.[81] This could be explained by the conformation of the different products. Due to the avoidance of $A^{1,3}$ strain, it is postulated that the lowest energy conformer will put the aldehyde group in the axial position to give *cis*-**60** (Scheme 3.28).[79,85] These reactions show that electrophile trapping at a lower temperature preferentially gives the *trans*-aldehyde, the kinetic product, whereas electrophile trapping at a higher temperature gives the *cis*-aldehyde, the thermodynamic product.

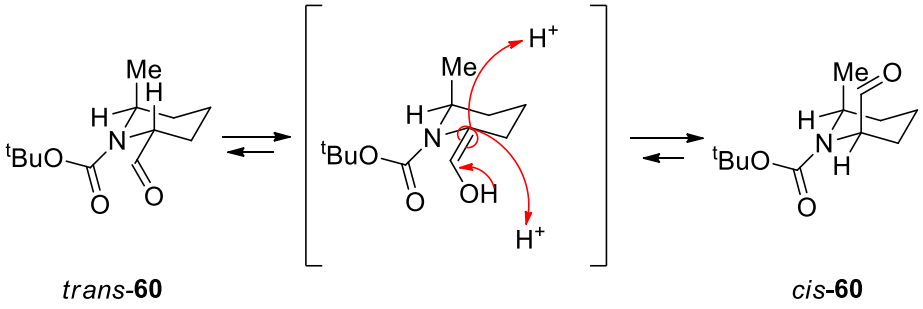

Scheme 3.28

Although the formation of both of the diastereomers is favourable for synthetic versatility and in relation to the desired fragments **A16**, **A19** and **A20**, the difficulty in separation of the different diastereomers meant that an alternative method for the synthesis of the fragments was sought. Fortunately, lithiation-trapping of *N*-Boc 2-methyl piperidine **49** with CO_2 yielded the 2,6-disubstituted piperidine *trans*-**62** as a single diastereomer, by ^{1}H NMR spectroscopy, in 82% yield (Scheme 3.29). This 2,6-disubstituted piperidine *trans*-**62** was then reacted with Me_3Si-diazomethane to give methyl ester *trans*-**63** in 93% yield (Scheme 3.29). Alternatively, 2,6-disubstituted piperidine *trans*-**62** was reacted with potassium carbonate and methyl iodide in DMF to give methyl ester **63** in 97% yield. This reaction is more amenable to larger scale synthesis (Scheme 3.29).

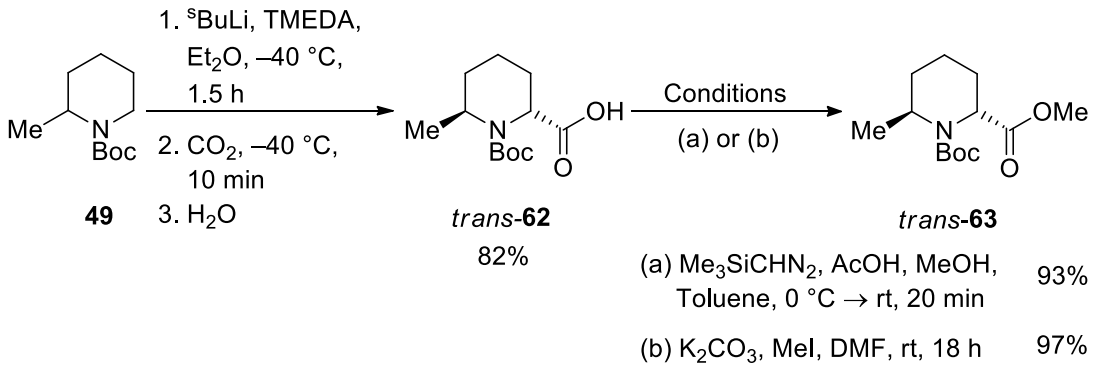

Scheme 3.29

With methyl ester piperidine *trans*-**63** in hand, the final functionalisation was carried out to give 2,6-disubstituted piperidine **A16**. 2,6-Disubstituted ester *trans*-**63** was deprotected with HCl, generated *in situ* from acetyl chloride and ethanol, to give deprotected disubstituted piperidine *trans*-**43.HCl** (Scheme 3.30).

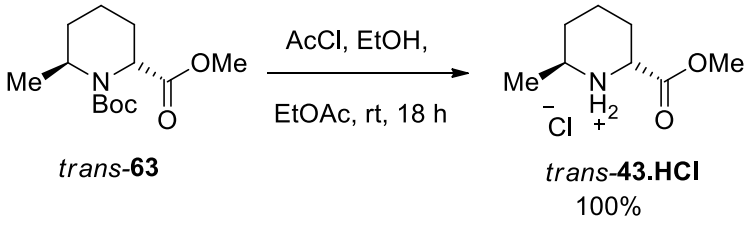

Scheme 3.30

Piperidine salt **43.HCl** was then converted into the piperidine acetamide *trans*-**64** through reaction with acetyl chloride in the presence of triethylamine to give the acetamide in 96% yield (Scheme 3.31). Subsequent reduction using lithium borohydride conditions gave acetamide alcohol fragment **A16** in 66% yield (Scheme 3.31).

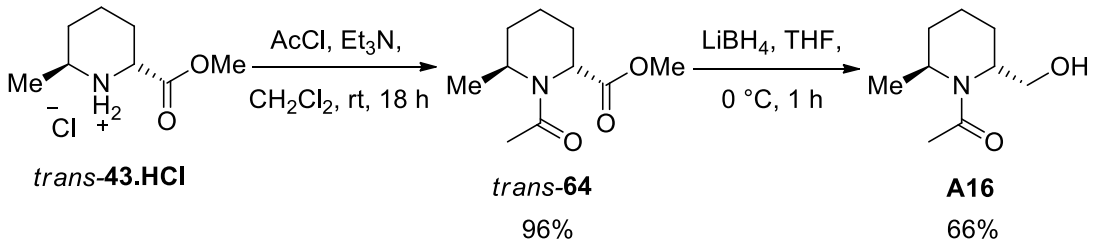

Scheme 3.31

We have successfully synthesised selected fragment **A16** in good yield in five steps from *N*-Boc 2-methylpiperidine. This synthesis is amenable to scale up and provides the intermediate piperidine ester *trans*-**63** which could be derivatised further if fragment **A16** proved interesting. It is envisaged that the intermediate piperidine ester *trans*-**63** could be epimerised to give the piperidine ester *cis*-**63**, the precursor to fragments **A19** and **A20**. Treatment of piperidine ester *trans*-**63** with sodium methoxide in methanol could give piperidine ester *cis*-**63** (Scheme 3.32). Deprotection with HCl, generated *in situ* from acetyl chloride and ethanol would give the piperidine ester *cis*-**43.HCl** (Scheme 3.32).

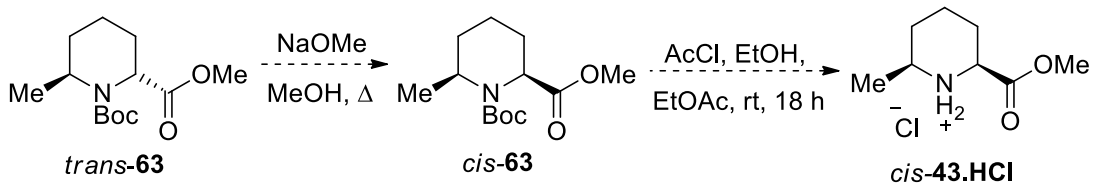

Scheme 3.32

Functionalisation with methanesulfonyl chloride or acetyl chloride using our *N*-functionalisation conditions and subsequent reduction of the ester would furnish the two final fragments **A19** and **A20** (Scheme 3.33).

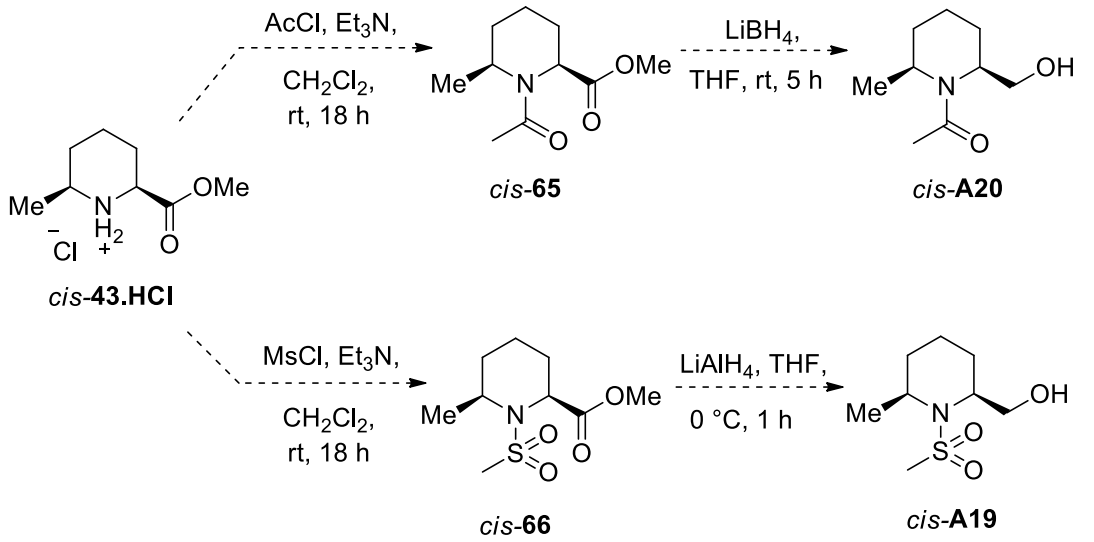

Scheme 3.33

3.5 Synthesis of 2-hydroxymethyl, 3-methyl disubstituted piperidines

The synthesis of fragments bearing a 2,3-substitution pattern such as fragments **A71** and **A72** (Figure 3.9) has not been reported extensively in the literature. Therefore, the synthesis of related disubstituted piperidines bearing ester or carboxylic acid groups in the 2-position and alkyl or aryl groups in the 3-position is briefly summarised here.

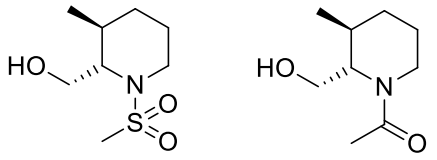

A71 **A72**

Figure 3.9: The two selected 2-hydroxymethyl, 3-methyl disubstituted piperidine fragments.

In 2002, Burke and co-workers reported a synthesis of an enantiomerically pure *N*-Fmoc protected 3-phenylpipecolic acid for use as a constrained phenylalanine analogue.[93,94] This synthesis employed commercially available Evans auxiliary **67** to install the desired stereochemistry. The diastereoselective 1,4-addition of allylmagnesium bromide using a copper bromide dimethyl sulfide complex to **67** gave an alkene, which after hydroboration gave alcohol **68** in 65% over two steps (Scheme 3.34).[93] Next, alcohol **68** was protected using *tert*-butyldimethylsilyl chloride. This compound was then subjected to asymmetric azidation to give **69** in 92% yield. In order for cyclisation to occur deprotection of the TBS ether was undertaken using HF·pyridine to yield alcohol **72** in 95% yield. Synthesis of the piperidine was then attempted using imine formation to help cyclisation. Alcohol **72** was subjected to Swern oxidation which was then ring closed by reductive amination to give methyl ester piperidine **70** in 52% yield. This was then converted into the desired Fmoc piperidine **71** in 40% yield (Scheme 3.34) over a total of nine synthetic steps.[93]

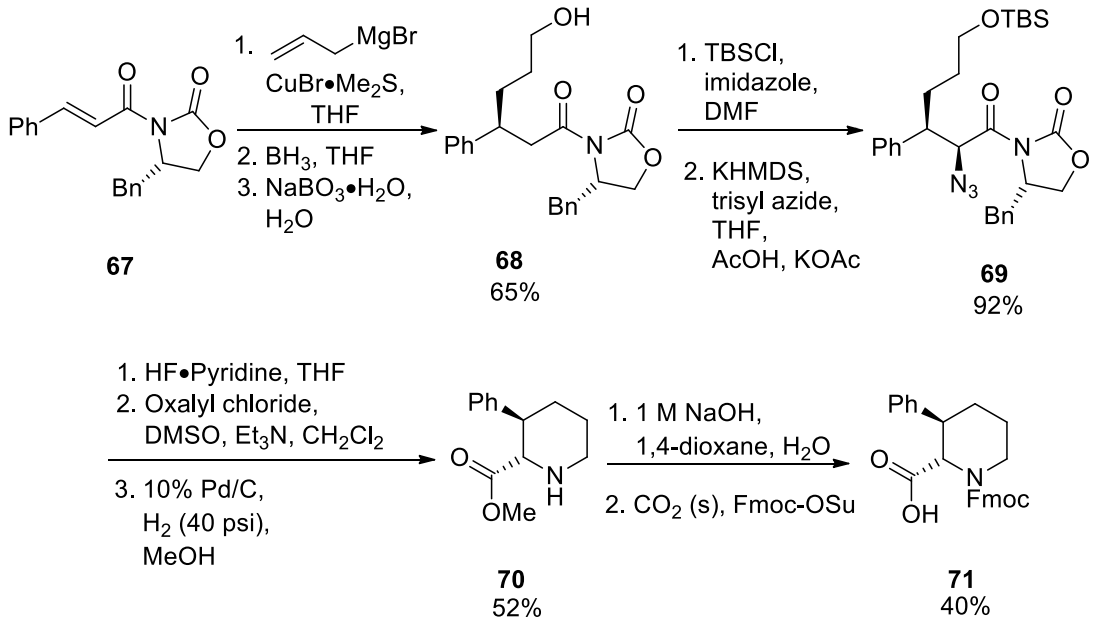

Scheme 3.34

Synthesis of 3-substituted pipecolic methyl esters for use as conformationally constrained analogues of peptide-based protease inhibitors was also reported by Mallamo and colleagues.[95] Here, catalytic hydrogenation proved crucial in obtaining *cis*-disubstituted piperidine **75.** Triflate **73** was converted into 3-methyl, 2-ester pyridine **74** through a Stille coupling in 50% yield. This pyridine was then converted into 3-methyl, 2-ester piperidine **75** by high pressure catalytic hydrogenation in quantitative yield (Scheme 3.35). The hydrogenation selectively gave the *cis*-diastereomer, which was confirmed by coupling constants observed in the ^{1}H NMR spectrum.

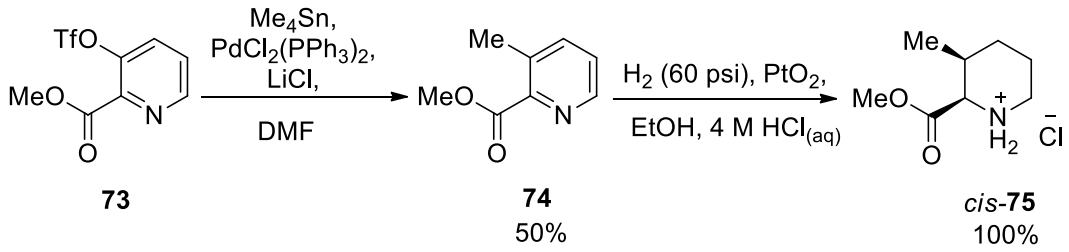

Scheme 3.35

During an investigation into the uses of iridium-catalysed asymmetric allylic substitution, Takemoto reported the synthesis of pipecolic acid derivatives and 2,3-disubstituted piperidine **70**.[96] Allyl-ester **76** was easily converted into pipecolic acid derivative **77** (Scheme 3.36) with a ring closing metathesis reaction as the key step.

Conversion of pipecolic acid derivative **77** into *trans*-disubstituted piperidine **70** was achieved by hydrogenation in 52% yield (Scheme 3.36).[96]

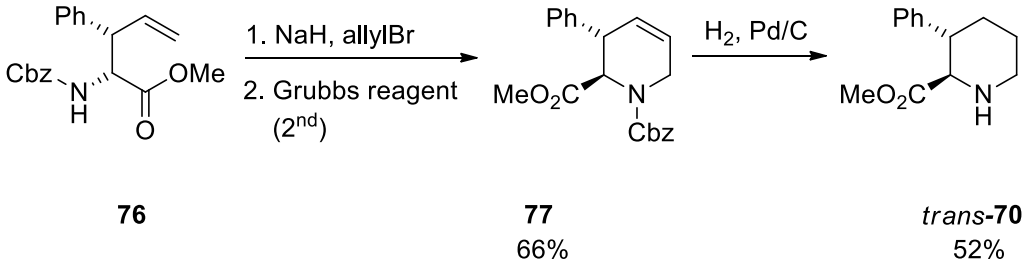

76 **77** 66% *trans*-**70** 52%

Scheme 3.36

2-Ester, 3-methyl disubstituted piperidines can also be synthesised using amino zinc enolate carbocyclisation reactions. Such reactions were reported by Normant and colleagues in the development of methodology for the synthesis of polysubstituted piperidines. For example, amino-ester **78** was deprotonated with LDA in Et_2O and then transmetallated with zinc bromide to obtain the *Z*-amino zinc enolate. A 6-exo-trig cyclisation *via* intramolecular carbo-metallation occurs upon warming to room temperature to give piperidine intermediate **79**. This intermediate can be treated with various electrophiles. In this case, protonation gave disubstituted piperidine *cis*-**80** (Scheme 3.37).[97]

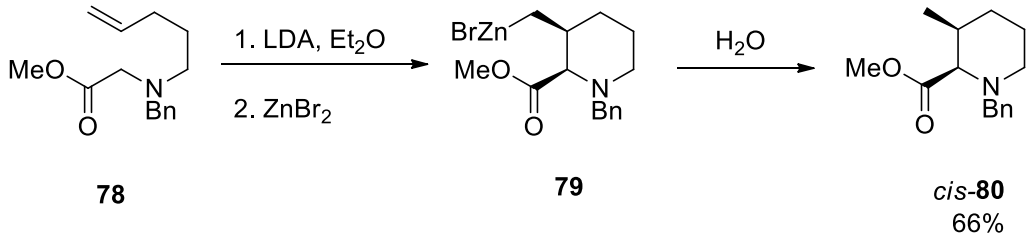

78 **79** *cis*-**80** 66%

Scheme 3.37

The reaction gives selectively *cis*-disubstituted piperidines which can be explained by the chair-like transition state of the oxygen-centred zinc-enolate-ene-type reactive intermediate. The electrophilic double bond occupies a pseudoaxial position and the *Z*-α-amino zinc enolate and the double bond are gauche to each other as shown in Figure 3.10.[97,98]

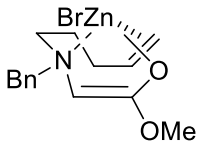

Figure 3.10

An epimerisation for the conversion of disubstituted piperidine *cis*-**80** into disubstituted piperidine *trans*-**80** was also reported by Normant (Scheme 3.38).[97] Deprotonation with LDA at low temperature (–78 °C) and then reprotonation at room temperature gave a 35:65 mixture of *cis*-**80** and *trans*-**80**. These unusual conditions employ a kinetic protonation to give the more stable *trans*-diastereomer, compared to a more typical epimerisation *via* thermodynamic equilibration.

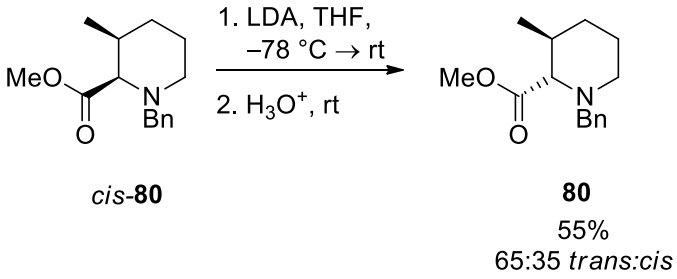

cis-**80**

80
55%
65:35 *trans:cis*

Scheme 3.38

Based on this somewhat limited literature precedent, we decided to investigate the use of Normant's amino zinc enolate carbocyclisation methodology in our synthesis towards fragments **A71** and **A72**. The lengthy asymmetric synthetic route described by Burke and the need for high pressure hydrogenation in Mallamo's synthesis suggested that Normant's route would be a more favourable way to access disubstituted piperidines. In addition, the option to trap with a number of different electrophiles after cyclisation opened up the opportunity for further functionalisation of the fragments.

The required amino-ester **78** was synthesised in two steps from benzylamine following literature procedures.[97] Firstly, benzylamine and 5-bromopentene **81** were reacted in the presence of sodium iodide to give *N*-benzyl-*N*-pentenylamine **82** in 47% yield. Subsequent reaction of amine **82** with methyl α-bromoacetate in a nucleophilic substitution reaction gave amino ester **78** in 87% yield (Scheme 3.39).

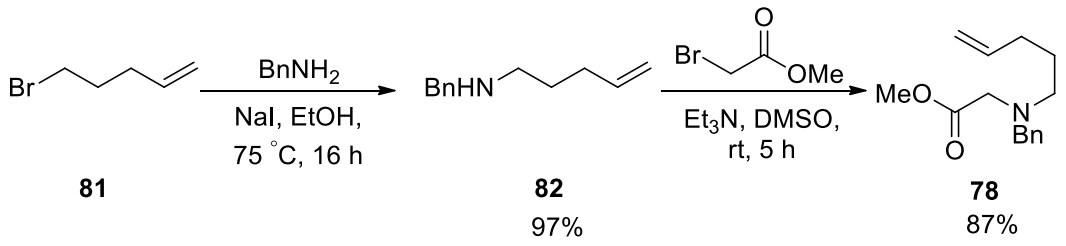

81 **82** 97% **78** 87%

Scheme 3.39

With amino-ester **78** in hand, the amino-zinc enolate carbocyclisation reaction was undertaken using similar conditions to those reported by Normant.[97] Reaction of amino-ester **78** with LHMDS gave the lithium enolate which was subsequently reacted with zinc bromide and warmed to room temperature to give cyclised intermediate **79**. Hydrolysis selectively gave the disubstituted piperidine *cis*-**80** in varying yields (15 to 40%, Table 3.4).

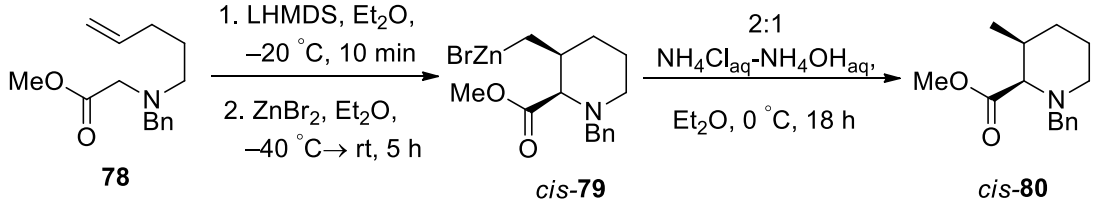

78 *cis*-**79** *cis*-**80**

Entry	Description	Scale / mmol	Yield / %
1	Standard reaction	0.8	15
2	Sonication for 10 minutes after addition to reaction mixture	4.04	40
3	Sonication for 10 minutes every 1 h after addition of enolate	2.02	39
4	Vigorous stirring of zinc bromide in Et_2O for 1 h before addition	40.4	32

Table 3.4: Different conditions used in the $ZnBr_2$ step.

These varying yields were thought to be related to the solubility of the zinc bromide in Et_2O. A standard reaction gave a 15% yield of *cis*-**80** (Entry 1). Zinc bromide has poor solubility in Et_2O and the reaction mixture was a suspension. Since we believed the poor solubility of zinc bromide was hindering the reaction, sonication was used to help with solubility. Two different sonication procedures were investigated: the reaction mixture was sonicated for 10 minutes after addition of the zinc bromide (Entry 2) and the reaction mixture was sonicated for 10 minutes every hour during the 5 hours stirring at room temperature (Entry 3). The sonication of the reaction mixture in both of these cases increased the yield to 40% (Entry 2) and 39% (Entry 3). However, it was noticed if the zinc bromide was stirred vigorously in Et_2O for one hour before

addition to the reaction mixture the zinc bromide was fully solubilised. A similar yield (32%, Entry 4) was obtained using this easier procedure.

The fragments selected for the library subset are the *trans*-diastereomers and therefore the reported epimerisation was undertaken next.[97] Reaction of disubstituted piperidine *cis*-**80** with LDA in Et_2O, followed by reprotonation gave a 60:40 mixture of *cis*-**80** and *trans*-**80** from the ^1H NMR spectrum of the crude reaction product. The diagnostic signals are the doublet at δ 3.41 with a *J* value of 5.0 Hz corresponding to *cis*-**80** and the doublet at δ 2.64 with a *J* value of 9.0 Hz corresponding the larger coupling of *trans*-**80**. They were then separated by column chromatography to give *trans*-**80** in 57% yield and *cis*-**80** in 40% yield (Scheme 3.40).

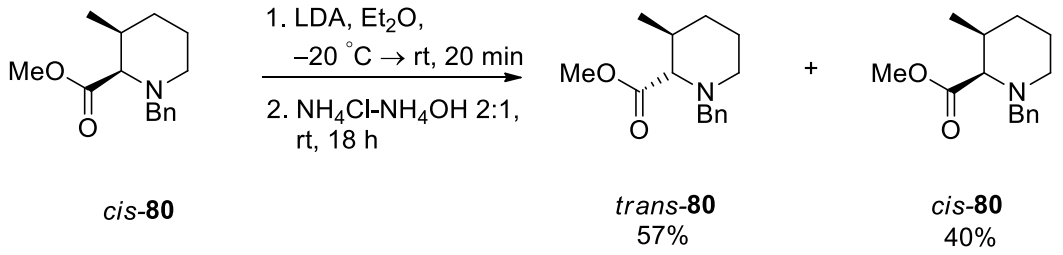

Scheme 3.40

Deprotection of *trans*-**80** using transfer hydrogenation conditions with palladium hydroxide and ammonium formate gave free amine *trans*-**75** in quantitative yield (Scheme 3.41).[99]

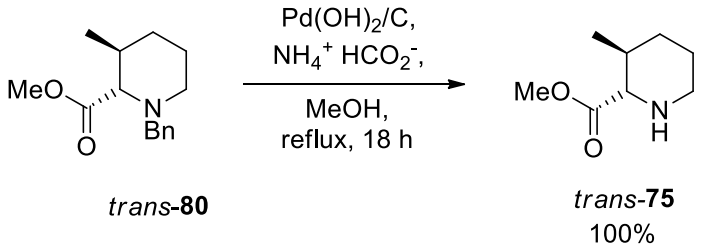

Scheme 3.41

With *trans*-**75** in hand, using the conditions described in Section 3.2 for functionalisation and reduction would be carried out to give fragments **A71** and **A72** (Scheme 3.42). However, due to time constraints, this was not completed.

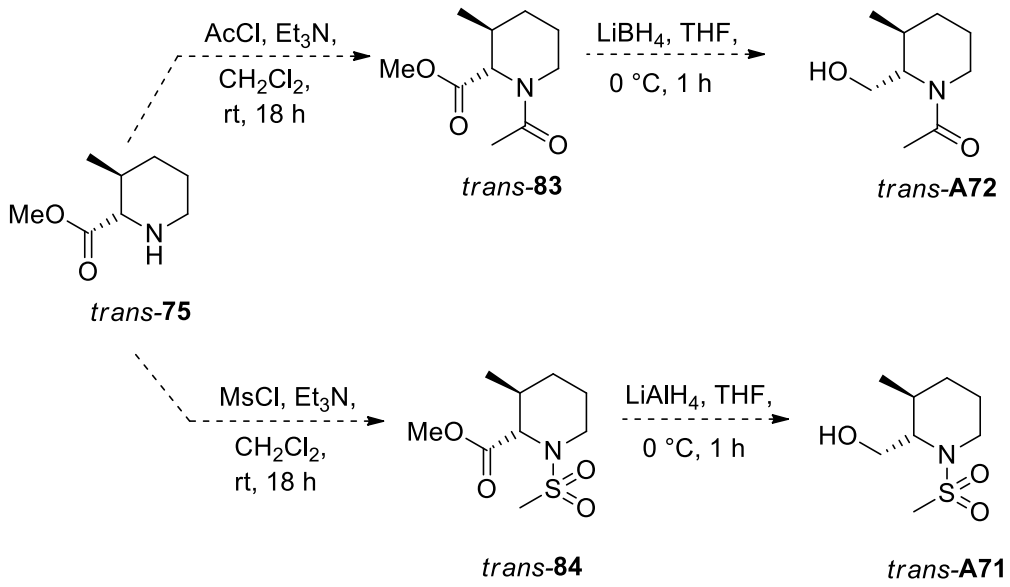

Scheme 3.42

This amino-zinc cyclisation methodology has furnished the desired precursor fragments **A71** and **A72** in good yield. This methodology is also very versatile. Both diastereomers can be obtained and the opportunity to trap the zinc-enolate with different electrophiles opens up the possibility of synthetic variation and fragment development. The use of the methyl-ester fits well with our *N*-functionalisation strategy and also opens up a route to the synthesis of different fragments.

3.6 Synthesis of 3-hydroxymethyl, 4-methyl and 4-hydroxymethyl, 5-methyl disubstituted piperidines

Given the success with the amino zinc enolate carbocyclisation methodology described in Section 3.5, we reasoned that the same approach could also be used to synthesise fragments **A65**, **A66** and **A89**, as all of these fragments bear an adjacent hydroxymethyl and methyl motif (Figure 3.11).

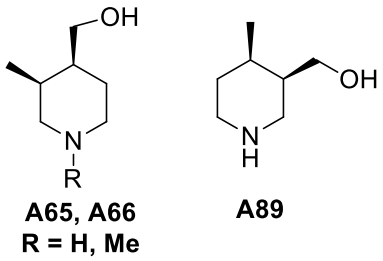

Figure 3.11

It was envisaged that with synthesis of suitable amino-esters **85** and **87**, carbocyclisation reactions would give the desired disubstituted piperidines *cis*-**86** and *cis*-**88** respectively (Scheme 3.43).

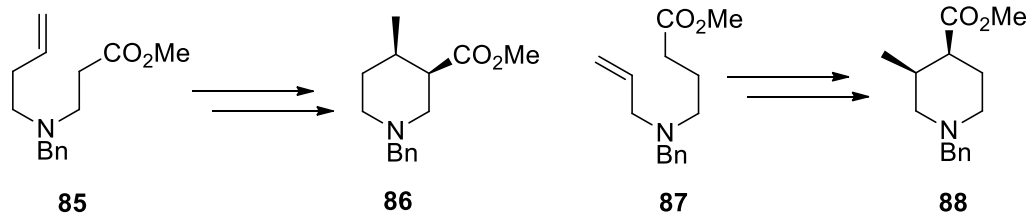

Scheme 3.43

Amino esters **85** and **87** were prepared following established routes. Reaction of benzylamine with 4-bromobut-1-ene **89** in the presence of sodium iodide and potassium carbonate gave *N*-benzylbut-3-en-1-amine **90** in 38% yield.[97] Subsequent reaction of this with methyl acrylate in the presence of DBU gave the desired amine-ester precursor **85** in 74% yield (Scheme 3.44).

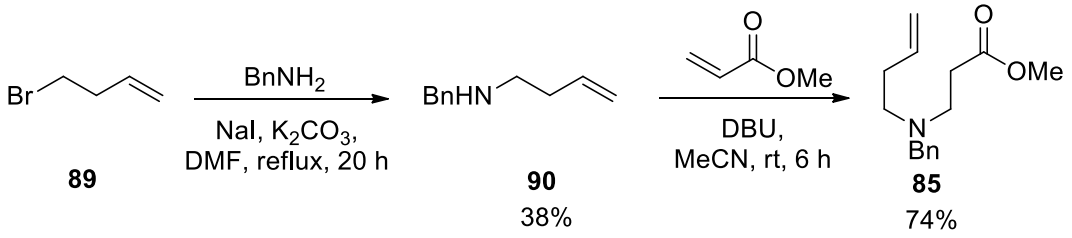

89 90 38% 85 74%

Scheme 3.44

Synthesis of *N*-benzylprop-2-en-1-amine **92** was undertaken by nucleophilic substitution of benzyl bromide with an excess of allylamine **91** in the presence of potassium carbonate to give a yield of 50% of amine **92**.[100] *N*-Benzylprop-2-en-1-amine **92** was then reacted with methyl 4-bromobutyrate and potassium carbonate to give the amino-ester **87** in 56% yield (Scheme 3.45).

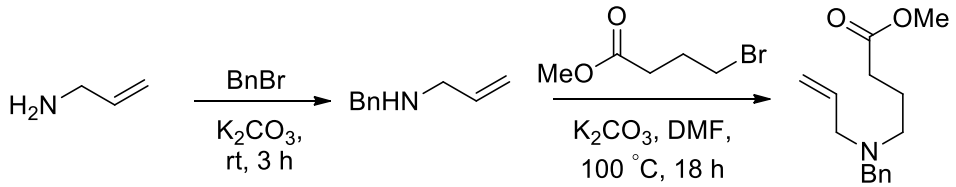

91 92 50% 87 56%

Scheme 3.45

With the suitable amino esters in hand, the conditions with pre-stirring of zinc bromide in Et_2O used in the synthesis of disubstituted piperidine *cis*-**80** (Section 3.5) were employed in the attempted synthesis of disubstituted piperidines *cis*-**86** and *cis*-**88**. Amino-ester **87** was deprotonated with LHMDS and subsequently reacted with zinc bromide, warmed to room temperature and then protonated. Unfortunately, no desired product **88** was obtained in this case (Scheme 3.46). However, a Claisen condensation product **93** was obtained and identified. The Claisen condensation product is formed from the initially generated lithium enolate self-condensing with the ester (Scheme 3.46). The structure of the Claisen condensation by-product was determined using a number of analytical techniques. The presence of two carbonyl peaks in both the ^{13}C NMR spectrum (δ 205.3 and δ 170.4) and the IR spectrum (1743 cm^{-1} and 1713 cm^{-1}) were indicative of a condensation product. The increased proton count and the dd at δ 3.59 in the ^{1}H NMR spectrum also suggested the condensation product, which the peak at $[M + H]^+ = 463$ in the mass spectrum confirmed.

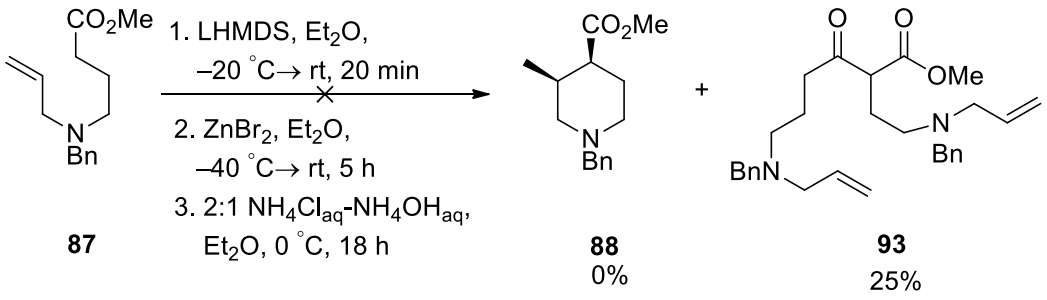

Scheme 3.46

Reverse addition of the amino-ester **87** to a solution of LHMDS may reduce the possibility of Claisen condensation. Addition of LHMDS into the ester solution means that the enolate is formed in the presence of a large amount of ester, allowing for condensation to occur. However, addition of the ester into a solution of LHMDS ensures that the ester concentration remains low compared to the concentration of enolate, reducing the chance of condensation. This reaction was attempted, but only the condensation product **93** was obtained in 40% yield and none of the desired product was observed (Scheme 3.47).

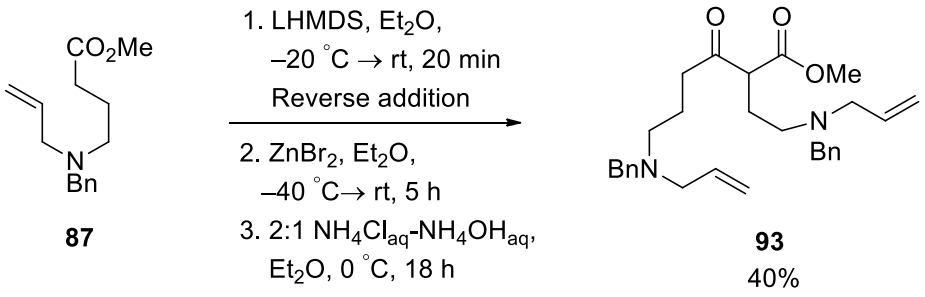

Scheme 3.47

Despite the unsuccessful results with amino-ester **87**, the amino zinc enolate carbocyclisation of amino ester **85** was next attempted. The LHMDS conditions as above, with vigorous stirring of zinc bromide before addition were used on amino-ester **85**. Unfortunately, no desired or identifiable product was obtained in this case (Scheme 3.48).

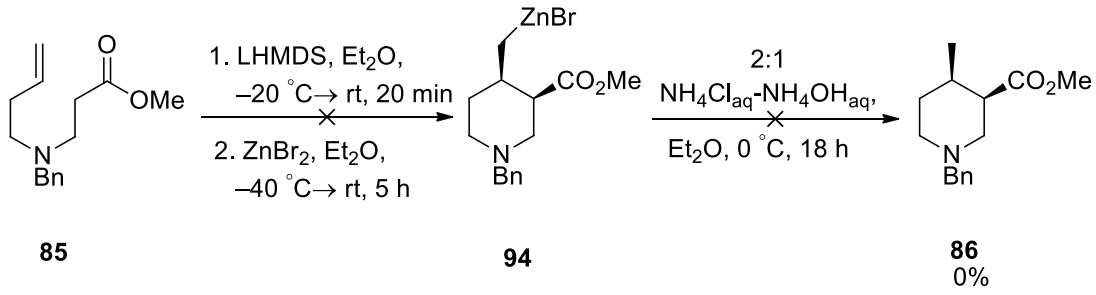

Scheme 3.48

Although we had no evidence that Claisen condensation is the issue with amino-ester **85**, we decided to explore whether a more sterically hindered ester could supress side reactions and therefore *tert*-butyl ester **95** was investigated. Synthesis of *tert*-butyl amino ester **95** was undertaken. Reaction of amine **89** with *tert*-butyl acrylate gave amino ester **95** in 67% yield (Scheme 3.49).

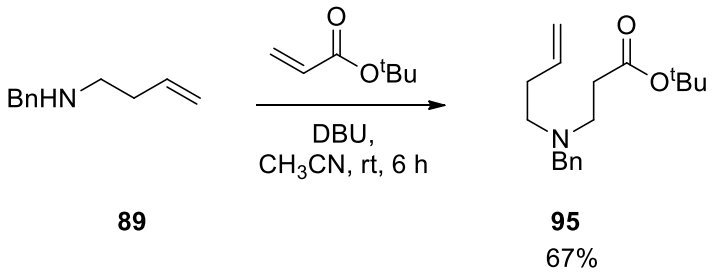

Scheme 3.49

This amino ester **95** was then subjected to LHMDS conditions as above and with the zinc bromide stirred vigorously before reaction. Deprotonation with LHMDS and subsequent reaction with zinc bromide followed by protonation gave no desired product **97** or any other identifiable products (Scheme 3.50).

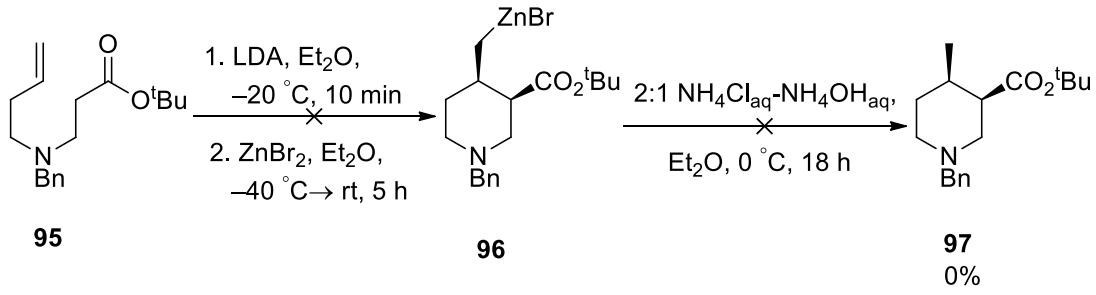

Scheme 3.50

Despite our efforts neither of the cyclisations gave the desired disubstituted piperidines. Amino-ester **87** gave the Claisen self-condensation product which was not observed in Section 3.5 for amino-ester **78**. This might be explained by the more

hindered enolate disfavouring intermolecular reaction. Therefore, the use of a more hindered ester may reduce the chance of Claisen condensation. The second amino-ester (**85**) produced no identifiable products, which would suggest that Claisen self-condensation may not be an issue here. However, Normant reported that competitive β-elimination was observed in the synthesis of different isomers of disubstituted pyrrolidines and led to recovery of amine **92** (Scheme 3.51).[98,101] This type of product, however, was not observed in our reaction.

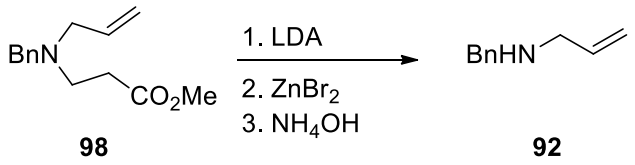

98 **92**

Scheme 3.51

This methodology has not been reported as a synthetic route towards the synthesis of disubstituted piperidines and therefore an alternative route is needed for synthesis of fragments **A65**, **A66** and **A89**.

3.7 Synthesis of 2-methyl, 3-hydroxymethyl disubstituted piperidines

Fragments **A38**, **A40**, **A41** and **A42** all bear a 2-methyl, 3-hydroxymethyl substitution pattern (Figure 3.12). Synthesis of piperidines with these substituents has not been previously reported. However, synthesis of closely related 2-methyl 3-ester disubstituted piperidines is known and a number of routes are briefly summarised below.

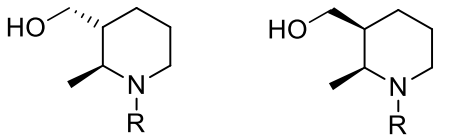

A38, A40
R = Me, Ac

A41, A42
R = H, Me

Figure 3.12: The four selected 2-methyl, 3-hydroxymethyl piperidine fragments

Work by Terashima and co-workers, reported in 1968, focused on the hydrogenation of pyridines. It was found that after *N*-alkylation, 2,3-disubstituted pyridinium salts readily underwent hydrogenation to give disubstituted piperidines.[102] Terashima reported that reaction of ethyl 2-methylnicotinate **99** with methyl *p*-toluenesulfonate gave methylated pyridinium salt **100**. This was subsequently hydrogenated at room temperature and atmospheric pressure in the presence of a palladium catalyst to give the 2,3-disubstituted piperidine **101** in 88% yield (Scheme 3.52). It was expected that the *cis* diastereomer would be formed, although this was not confirmed.

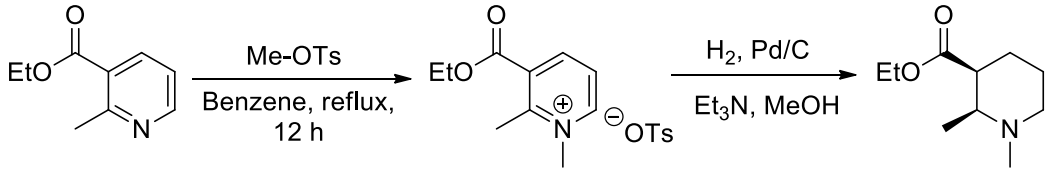

99

100
77%

101
88%

Scheme 3.52

The synthesis of 2-methyl, 3-ester disubstituted piperidine was described by Albertson in 1950. This synthesis relied on the Michael condensation of acrylonitriles and β-ketoesters with subsequent reduction of the cyano esters in the presence of Raney nickel to yield solely disubstituted piperidines.[103] In the example most relevant to our fragments, the condensation of acrylonitrile with ethyl acetoacetate gave ethyl (2-cyano-ethyl)-acetoacetate **102** in 63% yield. This nitrile reduction using Raney nickel

and cyclisation gave disubstituted piperidine **103** in 86% yield, with no comment on the ratio of diastereomers (Scheme 3.53). [103]

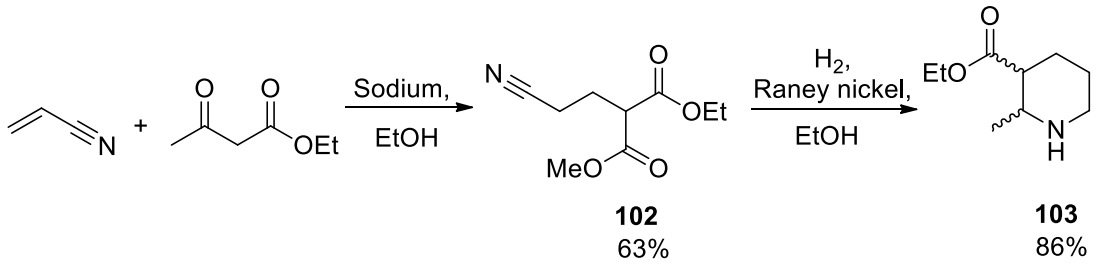

Scheme 3.53

In more recent work, Lhommet reported in 2005, the synthesis of disubstituted piperidine via β-enamino carbonyl substructures. The key step of this synthesis involves the condensation of *(S)*-phenylglycinol with prepared tricarbonyl compounds to give *β*-enamino carbonyl derivatives. These can then be converted easily into disubstituted piperidines **107**.[104] A range of tricarbonyl compounds can be synthesised from activated methylene compounds and *α,β*-unsaturated carbonyl compounds. Tricarbonyl compound **104** was prepared by Michael reaction of a dicarbonyl compound with acrolein on solid Al_2O_3.[104] The tricarbonyl compound **104** can then be reacted with *(S)*-phenylglycinol in CH_2Cl_2 to give the *β*-enamino carbonyl derivative **105** in 96% yield as a 40:60 mixture of diastereomers (Scheme 3.54).[104]

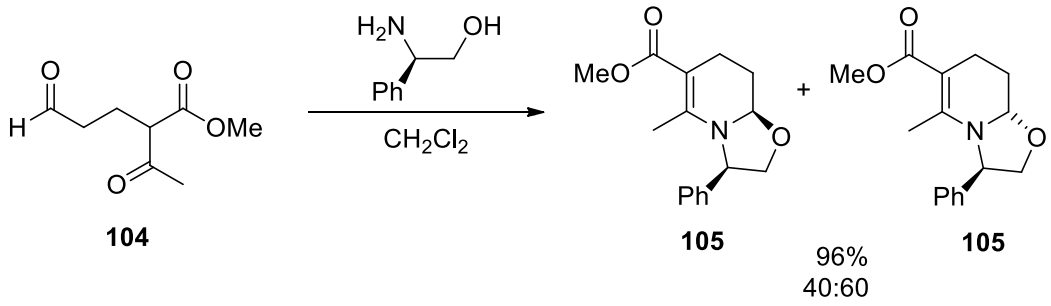

Scheme 3.54

In a subsequent paper, Lhommet and co-workers reported a number of methods to manipulate the *β*-enamino carbonyl derivative **105**. Treatment of *β*-enamino carbonyl derivative **105** with sodium triacetoxy borohydride gave disubstituted piperidine **106** in 93% yield (Scheme 3.55). In this reaction, the double bond is diastereoselectively reduced and the oxazolidine ring-opened. Subsequent hydrogenolysis and Boc protection gave piperidine *cis*-**107** in 96% yield (Scheme 3.55).[105] Hydrogenolysis of *β*-enamino carbonyl derivative **105** in the presence of platinum on carbon gave directly

the deprotected piperidine *cis*-**108**, which was subsequently treated with Boc_2O to yield protected piperidine *cis*-**107** in 70% overall yield (Scheme 3.55).[105]

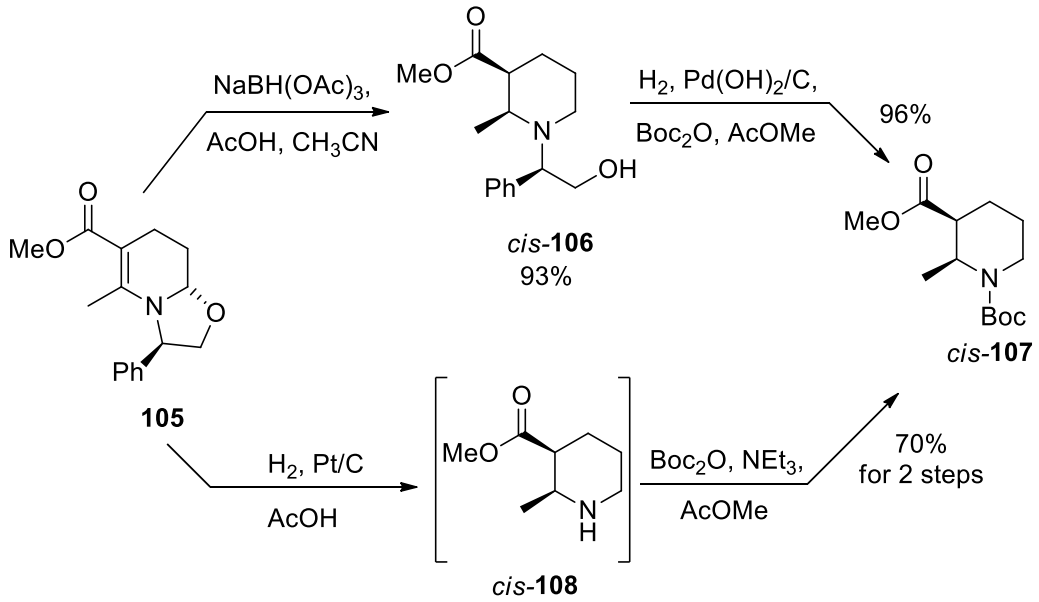

Scheme 3.55

Finally, hydrogenolysis of *β*-enamino carbonyl derivative **105** in the presence of PtO_2 gave a mixture of bicycles **109** in 78% yield. Subsequent treatment with sodium triacetoxy borohydride cleaved the oxazolidine ring to give piperidine **110** in 93% yield. Alternatively, cleavage and deprotection of the bicycles **109** with hydrogen and palladium hydroxide and then treatment with Boc_2O gave protected piperidine *cis*-**107** in 89% yield (Scheme 3.56).[105] This variety of methods for manipulation of the *β*-enamino carbonyl derivative **105** gives a greater opportunity for synthetic development.

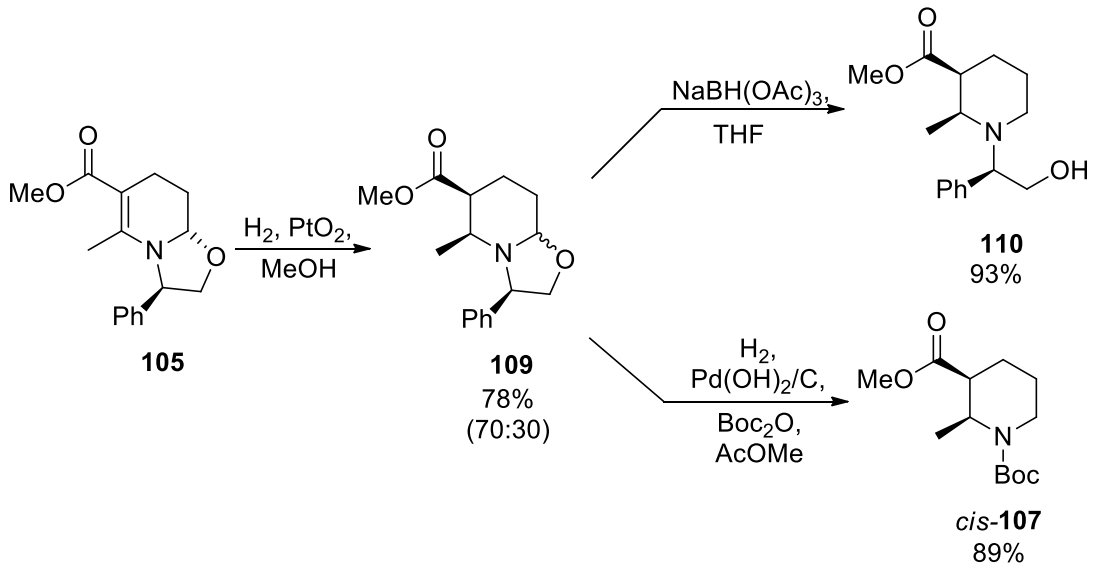

Scheme 3.56

Hebbe and co-workers have reported a condensation and aza-annulation approach in the synthesis of *β*-enamino derivatives and δ-lactams in a number of publications.[106,107] Here, Hebbe uses an aza-annulation reaction of β-enaminocarbonyl compounds bearing a hydroxyl function which can act as an internal nucleophile. The condensation reaction of (*S*)-phenylglycinol and methyl acetoacetate gave β-enaminoester **111**, which can subsequently undergo aza-anulation.[106] Reaction of β-enaminoester **111** with acryloyl chloride **112** gave bicycle **113** in 85% yield as a mixture of diastereomers (ratio not reported). The two diastereomers were separated using silica gel chromatography, but individual yields were not reported (Scheme 3.57).

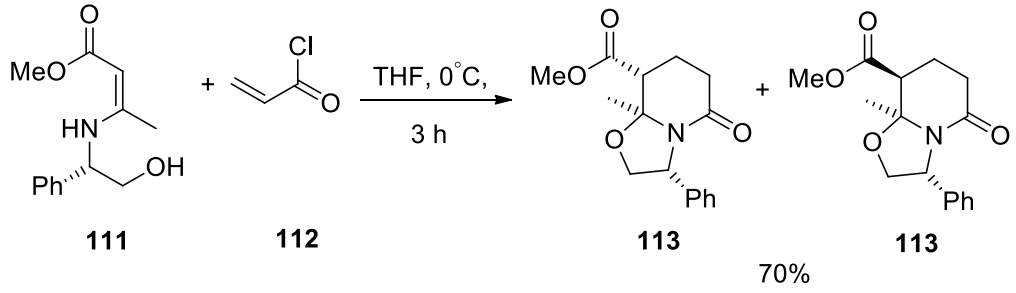

Scheme 3.57

Hebbe described the importance of the methyl group in the aza-annulation reaction, suggesting that the methyl group enhances the electron density on the α-carbon promoting reaction. Following formation of the bicycle **113**, Hebbe and colleagues investigated the reduction of the lactam and opening of the oxazolidine ring. Treatment

of *cis*-**113** with borane dimethylsulfide gave the disubstituted piperidine *cis*-**110** in 61% yield (Scheme 3.58). The deprotected piperidine *cis*-**108** was obtained after hydrogenolysis in 69% yield (Scheme 3.58). The same synthetic route was applied to the *trans*-diastereomer.

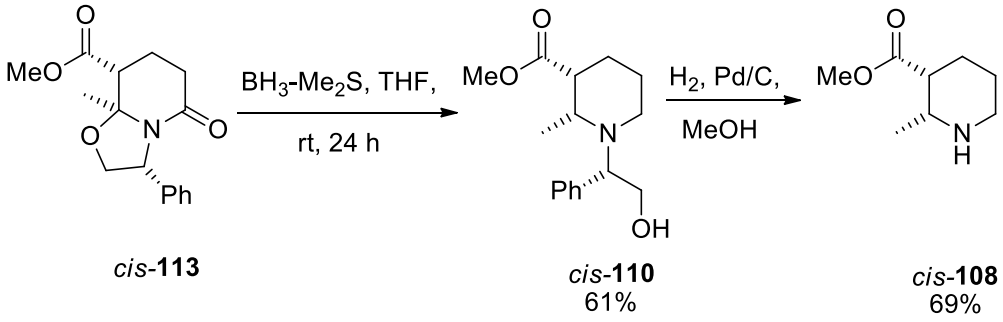

Scheme 3.58

The high yields and the short linear sequence of Hebbe's route led us to pursue this route for the synthesis of the disubstituted piperidines desired for our library sub-set. However, racemic phenyl glycinol was used for this synthesis as racemic mixtures of the selected fragments were desired. This methodology did, however, give the option for asymmetric synthesis should it be required at a later stage.

The β-enaminoester **111** was synthesised following Hebbe's method with the condensation reaction of phenylglycinol **114** and methyl acetoacetate **115** in quantitative yield and used without purification (Scheme 3.59).[106]

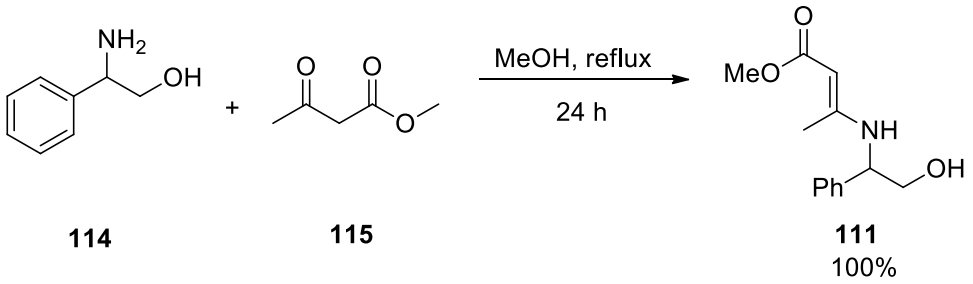

Scheme 3.59

The aza-annulation step to form the bicyclic lactam by reaction of β-enaminoester **111** and acryloyl chloride **112** proceeded in 57% yield to give an inseparable 75:25 mixture of *cis*-**113** and *trans*-**113** (Scheme 3.60). The diastereomers were assigned by analogy with Hebbe's results, with diagnostic signals in the ^{1}H NMR spectrum at δ 4.55 (*cis*-

113) and δ 4.39 (*trans*-**113**) and δ 3.99 (*cis*-**113**) and δ 3.93 (*trans*-**113**) for the protons adjacent to the oxygen in the oxazolidine ring. Despite a number of different attempts, we were unable to separate the two diastereomers.

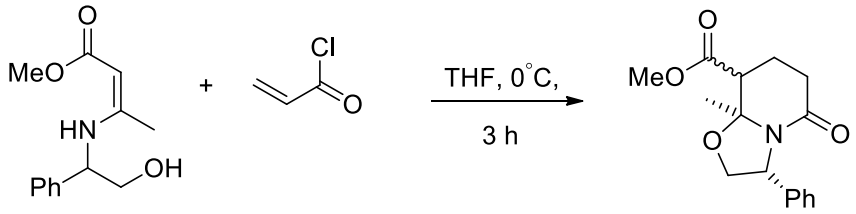

111 **112** **113**
57%
75:25 *cis:trans*

Scheme 3.60

The lactam was reduced and the oxazolidine ring was opened after treatment of the bicycle **113** with borane dimethylsulfide to give a 70:30 mixture of diastereomers *cis*-**110** and *trans*-**110** in 42% yield. Unfortunately, again despite our best efforts, we were unable to separate the different diastereomers (Scheme 3.61).

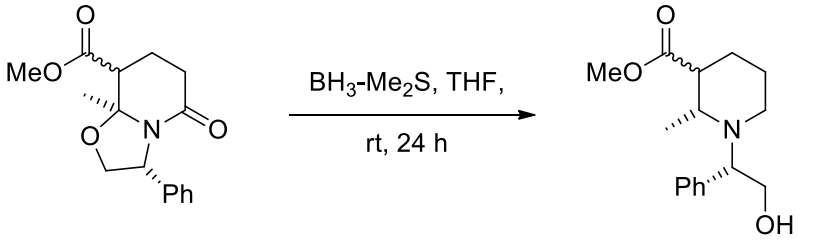

113 **110**
42%
70:30 *cis:trans*

Scheme 3.61

Therefore, hydrogenolysis to remove the nitrogen protecting group and then treatment with Boc_2O gave the *N*-Boc disubstituted piperidine *cis*-**107** and *trans*-**107** in 40% and 30% yield respectively (Scheme 3.62). The diastereomers were assigned using ^{1}H NMR spectroscopy in an analogous way to Hebbe.[106] The *trans*-diastereomer was assigned based on the ^3J coupling between the proton at the 3-position and the proton at the 2-position (12.5 Hz). Unfortunately, due to the poor resolution of the ^{1}H NMR spectrum of the *cis*-diastereomer, a small coupling of the 3-position proton signal at δ 2.42-2.38 could not be determined.

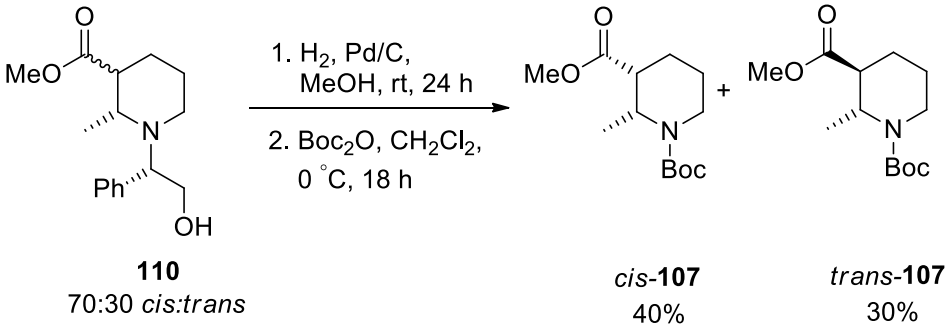

110
70:30 *cis:trans*

cis-**107**
40%

trans-**107**
30%

Scheme 3.62

This route has provided us with the precursors for fragments **A38**, **A40**, **A41** and **A42**, and the procedures described earlier for nitrogen functionalisation and ester reduction could be used to obtain the final fragments (Scheme 3.63).

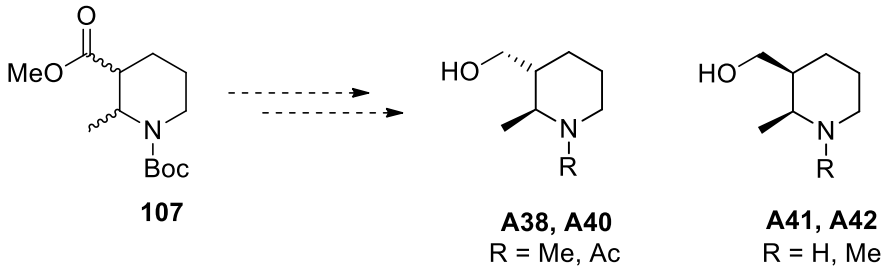

107

A38, A40
R = Me, Ac

A41, A42
R = H, Me

Scheme 3.63

The route, however, has proved challenging at a number of points. Both diastereomers are accessible with this methodology, which is ideal for accessibility to different diastereomers, but their separation is very difficult, even after a number of attempts. There are a number of steps in the route and yields are generally quite low, but reaction optimisation might improve this. This methodology does, however, benefit from an asymmetric version that could be useful for fragment optimisation or development if required.

3.8 Synthetic approach to *cis*-disubstituted piperidine fragments

Fragments **A25**, **A26**, **A65**, **A66** and **A89** are all *cis*-disubstituted piperidines (Figure 3.13) and therefore it was thought desirable to try and synthesise these compounds with the same methodology. We postulated that hydrogenation of disubstituted pyridines may provide a strategy for the synthesis of these types of compounds.

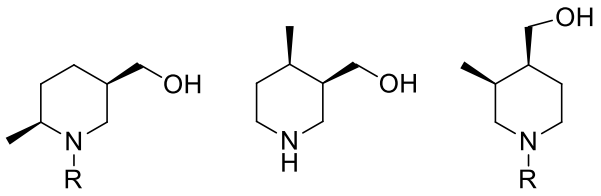

A25, A26
R = H, Me

A89

A65, A66
R = H, Me

Figure 3.13

A number of disubstituted pyridine hydrogenations have been reported in the literature,[108,109] A high pressure hydrogenation reaction was reported in the synthesis of 3-methyl, 4-ester disubstituted piperidine *cis*-**117** by Saunders and colleagues. 3,4-Disubstituted pyridine **116** was treated with H_2 in the presence of platinum oxide to give *cis*-disubstituted piperidine **117**, although the yield was not reported (Scheme 3.64).[110] A range of different methyl and ester disubstituted pyridines would provide access to the fragments shown in Figure 3.13.

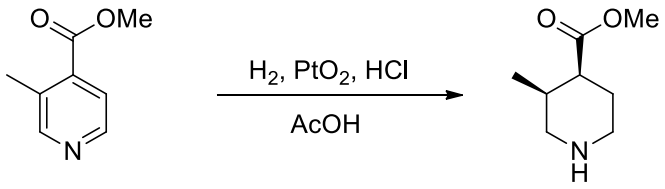

116

cis-**117**

Scheme 3.64

A possible alternative approach to the synthesis of disubstituted piperidines from pyridines could be *via* tetrahydropyridines. Thomas and colleagues reported that treatment of 3-ester, 4-phenyl pyridine **118** with ethyl iodide and subsequent reduction with sodium borohydride gave the tetrahydropyridine **119** (Scheme 3.65). Simple hydrogenation of **119** with a palladium catalyst gave a mixture of *cis* and *trans* disubstituted piperidines **120** (Scheme 3.65).[111]

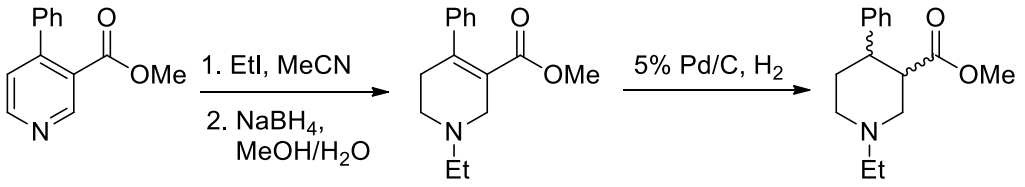

118 **119** **120**

Scheme 3.65

In a similar fashion, Baker and colleagues accessed a 2,5-tetrahydropyridine **123** from methyl 6-methylnicotinate **121**. The synthesis involves the formation of quaternary ammonium salt **122** and subsequent reduction with sodium borohydride to give tetrahydropyridine **123** (Scheme 3.66).[112] Although not reported, the hydrogenation method as reported by Thomas could be used to give a 2,5-disubstituted piperidine.

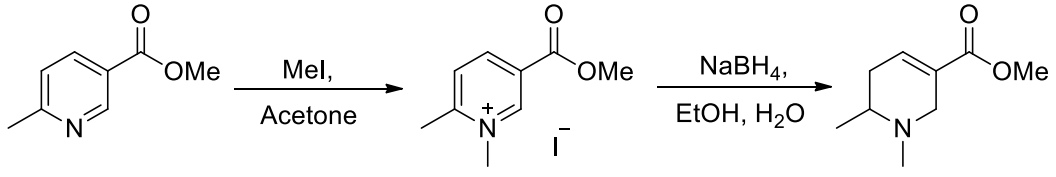

121 **122** **123**

Scheme 3.66

With the literature precedence and as pyridine reduction would provide rapid and easy access to a range of disubstituted piperidines, this is the route we investigated first.

The availability and ease of preparation of the 3-methyl, 4-ester pyridine meant that the hydrogenation reaction was carried out on this system. The desired pyridine was prepared from pyridine **124** through hydrolysis of the nitrile to give carboxylic acid **125** and subsequent methyl ester **126** formation as described by Grygorenko (Scheme 3.67).[113]

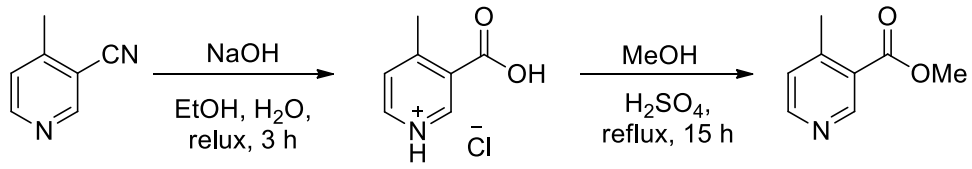

124 **125.HCl** 59% **126** 100%

Scheme 3.67

With the suitable disubstituted piperidine **126** in hand the hydrogenation could be undertaken. The atmospheric pressure hydrogenation with platinum oxide as the catalyst was attempted. However, none of the desired product was obtained and only starting material was recovered (Scheme 3.68). The hydrogenation was then repeated at a high pressure in the presence of a palladium catalyst at a high temperature. Again only starting material was recovered and none of the desired product obtained (Scheme 3.68). Another attempt with both a palladium and platinum catalyst at high pressure also gave no desired product and full recovery of starting material (Scheme 3.68). It was decided after this attempt had failed that an alternative route for the synthesis of these types of compounds from pyridines would be explored.

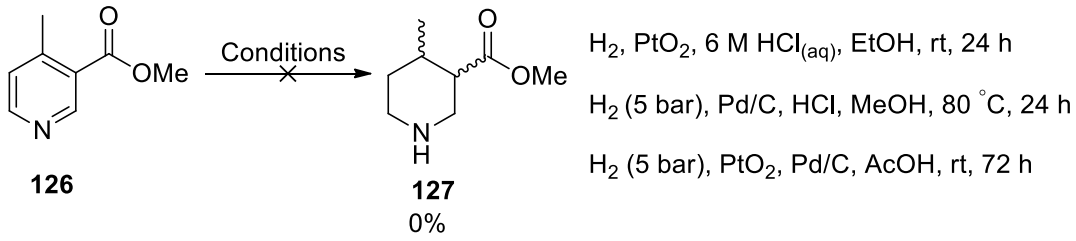

Scheme 3.68

Before synthesis was attempted on the disubstituted pyridines, a model study based on the literature routes to find suitable conditions was undertaken.[114,115] Benzyl bromide was chosen as the nitrogen substituent, due to ease of manipulation later in the synthesis. Reaction of 1 equivalent of benzyl bromide with methylnicotinate **128** at reflux gave full conversion into pyridinium salt **129**. Pyridinium salt **129** was then reacted with 9 equivalents of sodium borohydride at low temperature to give tetrahydropyridine **130** in 21% yield (Scheme 3.69).

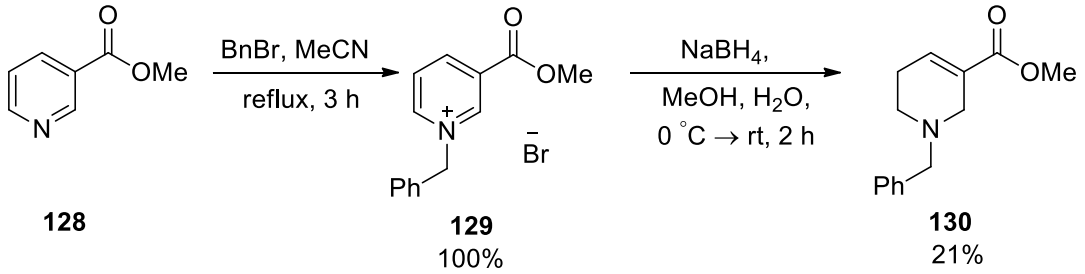

Scheme 3.69

With suitable conditions in hand, reduction of 3,4-disubstituted pyridine **126** was attempted. Treatment with benzyl bromide and subsequent reduction gave the disubstituted tetrahydropyridine **132** in 44% yield (Scheme 3.70).

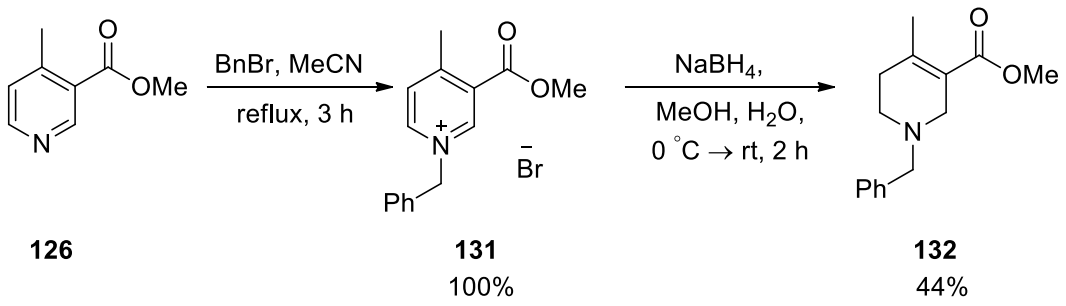

126 **131** 100% **132** 44%

Scheme 3.70

Finally, the reduction of 2,5-disubstituted pyridine **121** was attempted. Treatment, as before, with benzyl bromide gave the pyridinium salt **133**, and subsequent treatment with sodium borohydride gave 2,5-tetrahydropyridine **134** in 29% yield (Scheme 3.71).

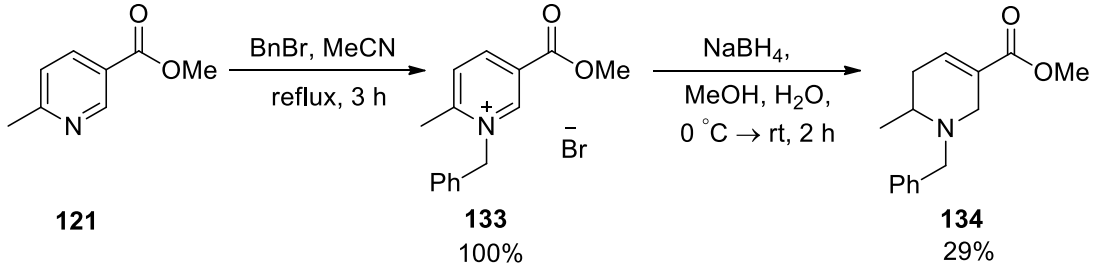

121 **133** 100% **134** 29%

Scheme 3.71

We have thus been able to successfully synthesise two tetrahydropyridines, which, following hydrogentation using the conditions described by Thomas would give desirable disubstituted piperidines. Unfortunately, due to time constraints this was not completed. The final fragments **A25**, **A26** and **A89** could be obtained following ester reduction, deprotection and *N*-functionalisation.

This initial work has shown that reduction of pyridines to piperidines is a viable method for fragment synthesis. The synthetic route *via* tetrahydropyridines has shown promise, but further optimisation is required to increase yields and explore substrate scope. The availability and accessibility of different pyridines offers increased synthetic scope and may offer a route to the more challenging targets. The double bond may also offer an additional synthetic handle for fragment generation in the future.

3.9 Conclusions and Overview

We have presented the synthesis towards a number of the selected disubstituted piperidine fragments. We were able to group fragments in order to reduce the number of different synthetic routes required. This worked well for some fragments. For example, we were able to apply enolate alkylation chemistry in the synthesis of five geminal disubstituted piperidines. We also made initial progress to investigate pyridine reduction as a method to synthesise a number of different piperidines and early results look promising. We have tried to keep the number of different synthetic steps to a minimum and developed a general route for *N*-functionalisation starting from an *N*-Boc ester piperidine. Generally, yields have been moderate to good and some routes are amenable to larger scale synthesis. It has been important to also use routes that allow for different functionalisation and fragment generation. For example, in some cases, changing the electrophile would allow installation of different groups. This work has shown that although disubstituted piperidine is a simple scaffold, the synthesis of this type of compound is not trivial and development of robust methodology to access these compounds needs further work.

Chapter 4: Lead-oriented Synthesis, Design and 3-Dimensional Shape Evaluation of a Virtual Lead-like Library

In this part of the project, we aimed to design and enumerate a virtual library of lead-like compounds, with particular focus on more 3-dimensional compounds to access new areas of chemical space. As discussed earlier, the prevalence of saturated heterocyclic ring structures in approved drug molecules, their interesting 3-dimensional structure and the expertise already developed in the O'Brien group relating to the synthesis of saturated heterocycles led to the investigation of these types of compounds. It was felt that these type of compounds would also be suitable for use as interesting synthetic building blocks.

It was planned that pyrrolidine, piperidine and piperazine-based cores which offer points for diversification would be investigated (Figure 4.1). Different functional groups in these positions would offer a variety of properties and interactions and handles for further development of these compounds during lead optimisation. These functional groups are also shown in Figure 4.1.

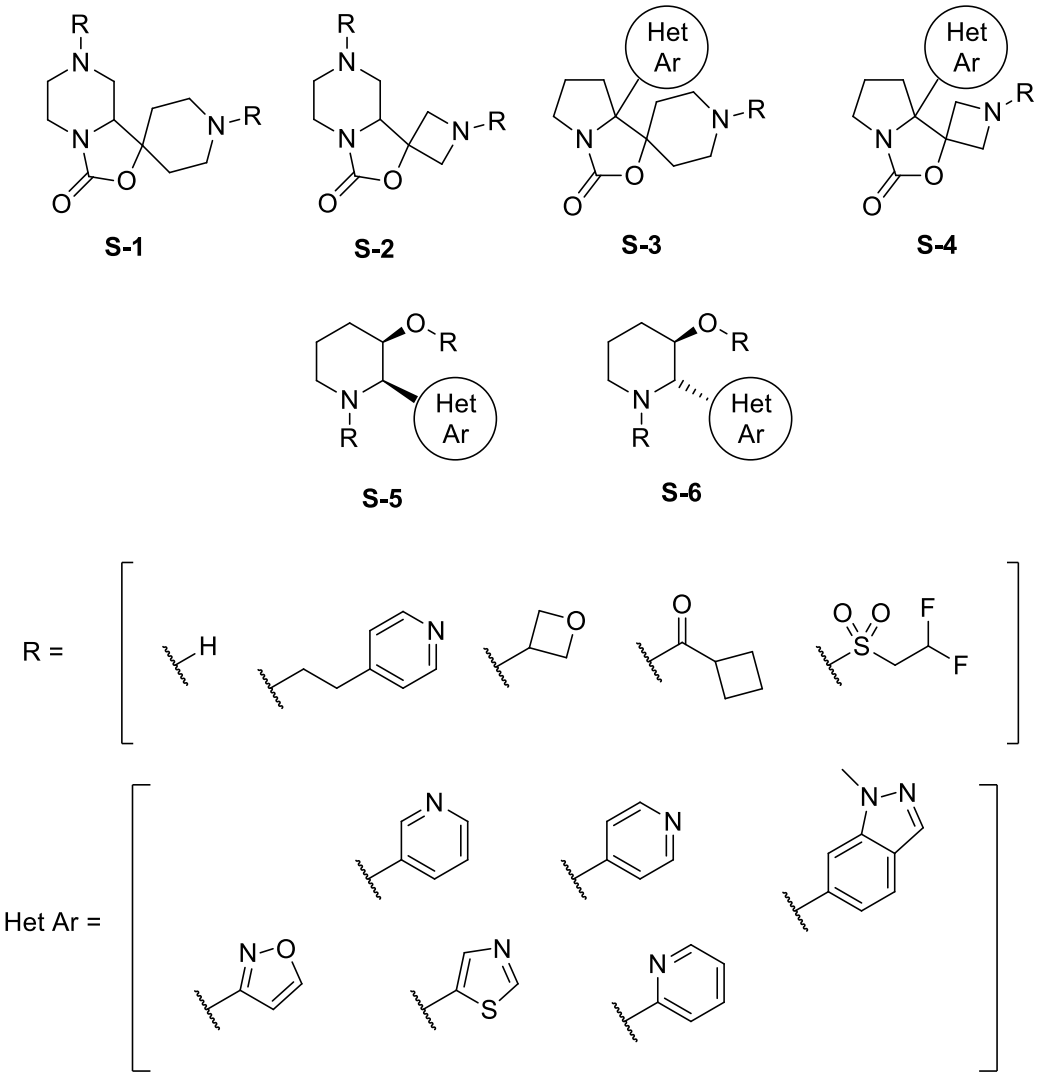

Figure 4.1: The six different lead-like scaffolds, showing points of diversification and the chosen groups for functionalisation.

The structures generated from these different combinations would then be analysed for shape diversity and 3-dimensionality using PMI plots, in order to analyse the spread of these compounds across chemical space. We also planned to evaluate the physicochemical properties in relation to the properties that are desirable for lead-like compounds.

4.1 Overview of lead-oriented synthesis

The drug discovery process is challenging in many aspects and, as discussed earlier (Chapter 1), new approaches are being constantly developed to meet the needs of more challenging targets and areas.[116] Molecular and physical properties play a very significant role in the success of compounds through the drug development process. Different parameters and criteria have been developed to summarise the requirements of different compounds, such as Lipinski's "Rule of five" for orally bioavailable drugs. These have helped medicinal chemists to focus efforts during lead optimisation. A number of groups have highlighted that, although these criteria are highly valuable during development, the selection of high quality lead compounds is vital to success.

It has been highlighted in a number of reports that the lead optimisation process often causes an increase in molecular weight and lipophilicity, which are thought to be the main reason for attrition in later drug development and testing stages.[6,7,65] Nadin and colleagues from GlaxoSmithKline reported that compounds with *c*LogP < 3 and a polar surface area > 75 $Å^2$ have a better safety profile in pre-clinical studies and molecules with a molecular weight < 400 and *c*LogP < 4 are more successful in drug-like character assays, such as solubility, bioavailability, plasma-protein binding and *in vivo* clearance assays.[65] It is also widely reported that the more lipophilic the compound, the more promiscuous a compound is, giving more off-target activity and toxicity.[65]

Therefore, in a similar way to fragment-based drug discovery described in Section 1.1, it can be desirable to start with smaller compounds to allow for expansion during lead optimisation. This is exemplified in Figure 4.2 as reported by Nadin and colleagues.[65]

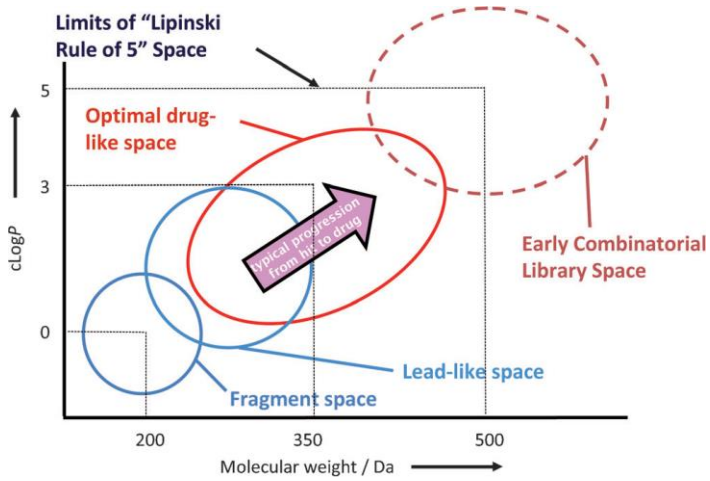

Figure 4.2: Diagram showing the "Lead-like" area of chemical space compared to the Lipinski's "Rule of 5" and fragment space.[65]

As with fragment libraries, there are a number of advantages to screening smaller lead-like compounds compared to current HTS libraries. These smaller compounds are able to sample chemical space more efficiently which results in a higher probability of finding hits. There is also more chance of successful binding as smaller compounds have less chance of mis-match and clashes with the active site. Along with making compounds smaller, Nadin suggested that shape should be a key consideration when designing lead-like compounds.[65] As discussed, increased lipophilicity is a key cause of attrition and therefore reducing or restricting the number of aromatic rings in lead-like compounds could help to prevent issues further in development. Increased sp^3 character has also been reported as a positive characteristic for screening compounds. Work by Lovering showed that compounds that have successfully progressed through the different stages of drug development have more sp^3 character.[40]

All of these different physical properties and parameters have been drawn together to give a set of criteria specifically for lead-like compounds. These are as follows:

- $14 \leq$ Heavy atoms ≤ 26 (giving a molecular weight range of around 200 to 350 Da).
- $-1 \leq \text{LogP} \leq 3$
- Aromatic rings ≤ 3
- Avoid reactive and unfavourable groups

A number of groups have analysed different compound collections against these criteria to assess the lead-likeness of compound collections.[65,117] An analysis of commercially available compounds showed that more than 99% of compounds did not fit these criteria and in a separate analysis it was found that a large proportion of compounds reported in synthetic methodology papers fall outside of these guidelines. This and the uneven sampling of chemical space synthetically has led to a call to develop synthetic methodologies to prepare more relevant lead-like compounds, ie. Lead-oriented synthesis.

Nelson and co-workers noted that the poor availability of diverse lead-like compounds comes from an inherent lack of good synthetic methods to synthesise these types of compounds.[117,118] Therefore both current methodology and new methodology needs to be developed and adapted for use in lead-oriented synthesis. Initially, Nadin and colleagues highlighted the need for a similar approach to synthesis as that used in diversity-oriented synthesis, first reported by Schreiber and colleagues.[65,119] Although diversity-oriented synthesis produces a large number of diverse compounds using elegant routes and cascades, the molecular weight and physical properties are generally not suitable for lead-like compounds and do not routinely produce compounds in drug-like chemical space. Lead-oriented synthesis is concerned with the production of a number of compounds with specific molecular properties with utility in the drug discovery and optimisation process, as defined by Nadin and colleagues.[65]

Nadin and colleagues highlighted a simple set of guidelines that lead-oriented synthesis should meet.[65] These are:

- Produce a wide range of lead-like chemical structures,
- Efficiently produce compounds using cheap reagents and mild conditions amenable for use in array formats,
- Tolerate a wide range of polar functional groups,
- Produce molecules without multiple residual reactive centres.

With this in mind, Nelson and co-workers highlighted that although the synthetic methods used in diversity-oriented synthesis may not be practical for lead-like compound synthesis, the principles may be applied, such as the combinatorial variation of the molecular scaffold. They reported that the "build, couple, pair" process used in diversity-oriented synthesis can be readily applied to simpler starting materials, giving lead-like compounds after linking and cyclisation.[117] In a separate report, they applied this methodology to the synthesis of 52 different lead-like scaffolds. They employed a simple two- or three-step synthesis (Scheme 4.1). The first step involves the reaction of an allylic carbonate **135** with an amine **136** to furnish a cyclisation precursor **137**. These cyclisation precursors can then be cyclised either once or twice depending on functional groups available for reaction. Late-stage functionalisation of the cyclisation products then yielded a wide range of compounds with lead-like properties. [118]

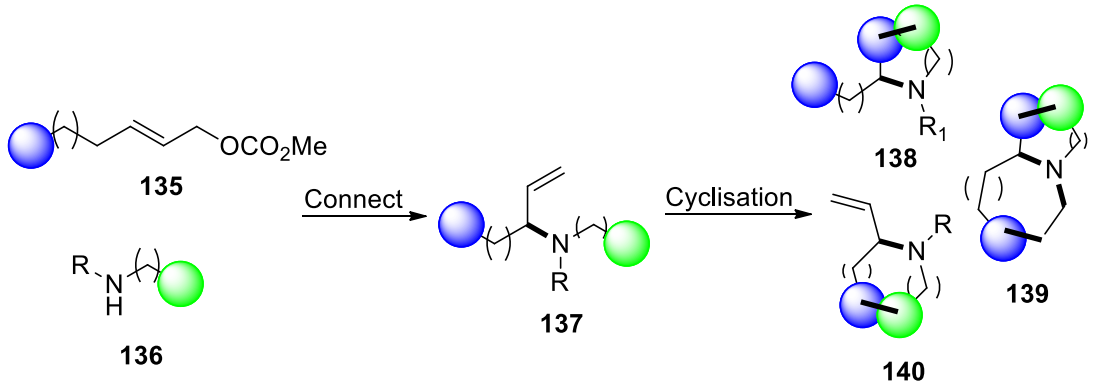

Scheme 4.1

After preparation of the 52 scaffolds, the late-stage functionalisation was carried out virtually, with 59 different medicinally relevant capping groups. This gave a total of 19 530 compounds in the virtual library. Representative protected scaffolds are shown in Figure 4.3. Subsequent analysis of these compounds found that 59% had lead-like molecular properties as defined earlier and that after analysis of sp^3 centres it was found that a high number of compounds had a diverse shape. This method provided medicinal chemically relevant compounds, with suitable properties for use in lead-like screening libraries. [118]

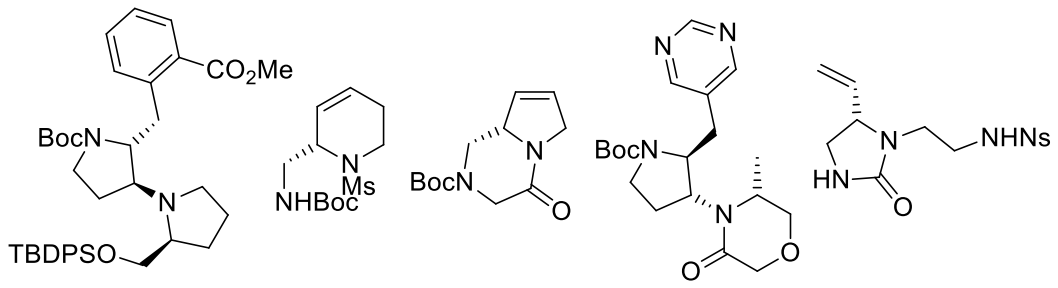

Figure 4.3: Example of some of the 52 scaffolds prepared in one or two cyclisation steps. Deprotection and functionalisation would give a range of lead-like compounds.

Lead-oriented synthesis has received more attention in recent times and a number of groups have adopted a similar approach for the synthesis of lead-like compounds. For example, Marsden, Nelson and co-workers reported the aminomethylhydroxylation of alkenes as a method to synthesise small molecules[120] and Nortcliffe and Moody synthesised a number of azepanes and oxepanes for use in drug discovery.[121] A report by Clausen and co-workers employed a 3-component cascade reaction in the synthesis of over 500 compounds based on trisubstituted γ-lactams.[122] These recent reports highlight the values of this method as a viable approach for the synthesis of lead-like compounds for use in drug discovery.

4.2 Organometallic routes to lead-like compounds: O'Brien group chemistry

Lead-oriented synthesis aims to provide a simple and effective method to produce diverse lead-like compounds. It was envisaged that organolithium-mediated routes would provide good methodology to access the desired library of compounds. This synthesis work was undertaken by others in the O'Brien group and is presented in a publication from 2015[99]. A summary of the synthetic routes used by others to furnish the different scaffolds is presented briefly below.

Scaffolds **S1** and **S2** were synthesised by α-lithiation of *N*-Boc piperazine **141**, originally reported by Beak.[76] It was found by earlier workers that the diamine-free lithiation reported by O'Brien[90] was suitable for this lithiation. The lithiation with 1.3 equivalents of *s*-BuLi of *N*-Boc piperazine in THF, followed by trapping with cyclic ketones **142** or **143** and stirring at room temperature for 24 hours gave the carbamates **144** or **145** in 64% and 42% yields respectively (Scheme 4.2). Warming to room temperature and stirring promoted the attack of the alkoxide onto the Boc group to give the cyclic carbamate. By using *N*-Boc protected ketones as the electrophile and orthogonally protecting the two nitrogens of the piperazine, differential deprotection and further functionalisation of the products was possible.

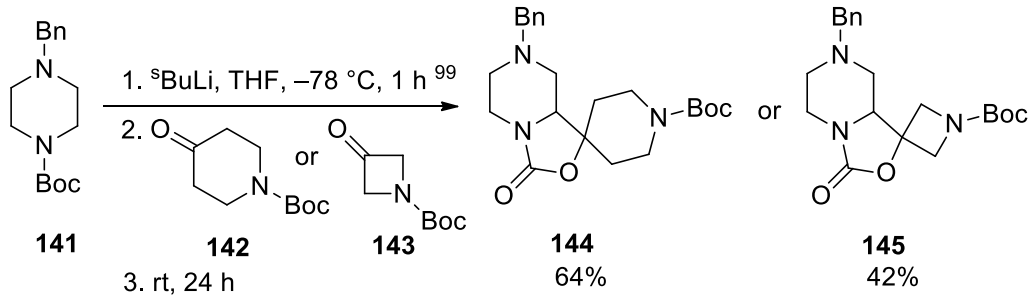

Scheme 4.2

In a similar approach to the piperazine above, pyridinyl *N*-Boc pyrrolidine **146** was subjected to a lithiation-trapping process by earlier workers. In this case, however, the reaction site is benzylic and therefore different lithiation conditions were employed, as developed by a number of groups.[123-125] Generally, a higher temperature was employed in order to allow for Boc rotamer interconversion and *n*-BuLi was used in order to selectively deprotonate the more acidic benzylic proton. Therefore, lithiation was carried out using *n*-BuLi at –50 °C for 30 minutes in THF. *N*-Benzyl piperidine-

4-one or *N*-Boc azetidine-4-one were used to trap the lithiated intermediate and cyclisation onto the Boc group gave the pyrrolidine spirocyclic compounds **147** and **148** (Scheme 4.3). These scaffolds can then be subjected to deprotection and further *N*-functionalisation.

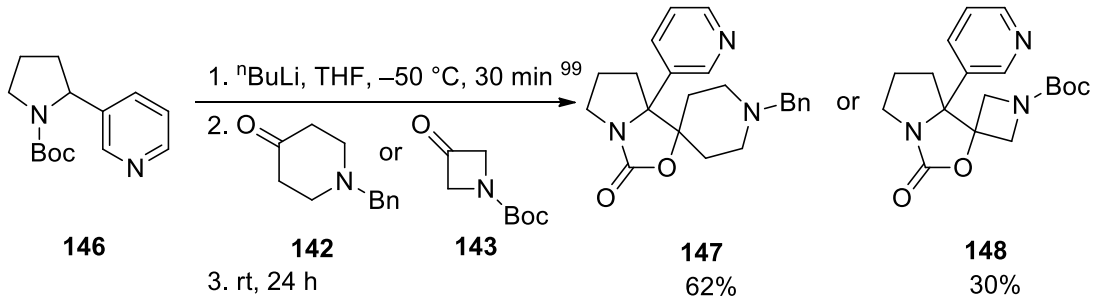

Scheme 4.3

The final scaffold was a 2,3-disubstituted piperidine which was synthesised, by earlier workers, from *N*-benzyl amino alcohols *syn*-**152** and *anti*-**152**. These *N*-benzyl amino alcohols were prepared in a three-step synthesis from *N*-Boc pyrrolidine **149** (Scheme 4.4). Lithiation-trapping using 3-pyridine carboxaldehyde gave a 70:30 mixture of diastereomers *syn*-**150** and *anti*-**150**, which upon deprotection with TFA gave the free amine **151** as a 70:30 mixture. As the later ring expansion required a nucleophilic *N*-alkyl substituent reductive amination was carried out to give the *N*-benzyl protected amino alcohols *syn*-**152** and *anti*-**152** both in 30% yield (Scheme 4.4).

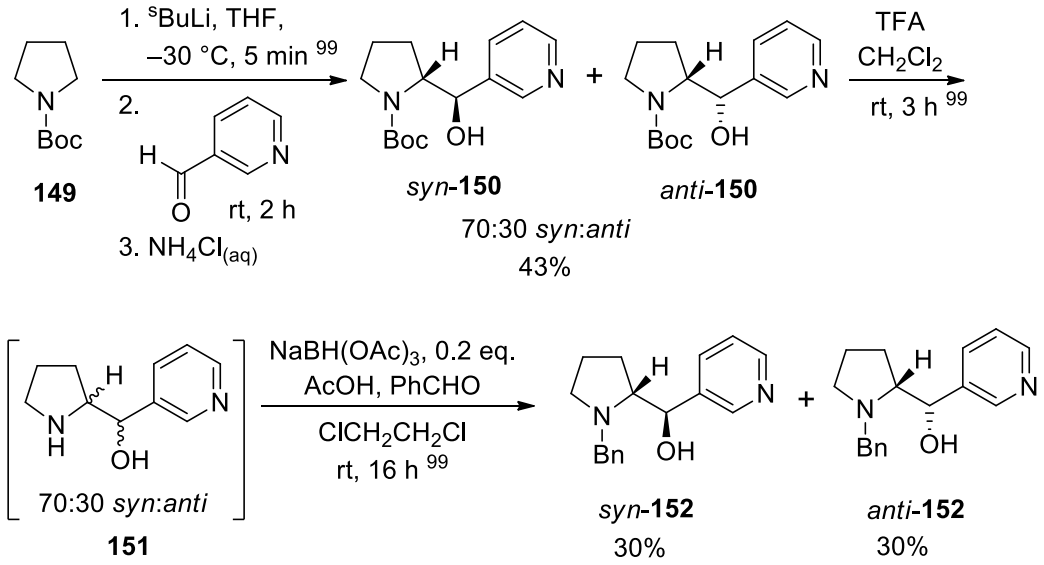

Scheme 4.4

Next, the aziridinium ion-based ring expansion was carried out, by earlier workers, on each of the diastereomers *syn*-**152** and *anti*-**152**. Trifluoroacetylation and ring expansion over 48 hours with subsequent hydrolysis with NaOH gave the desired piperidines *syn*-**153** and *anti*-**153** in 76% and 79% yields respectively (Scheme 4.5).

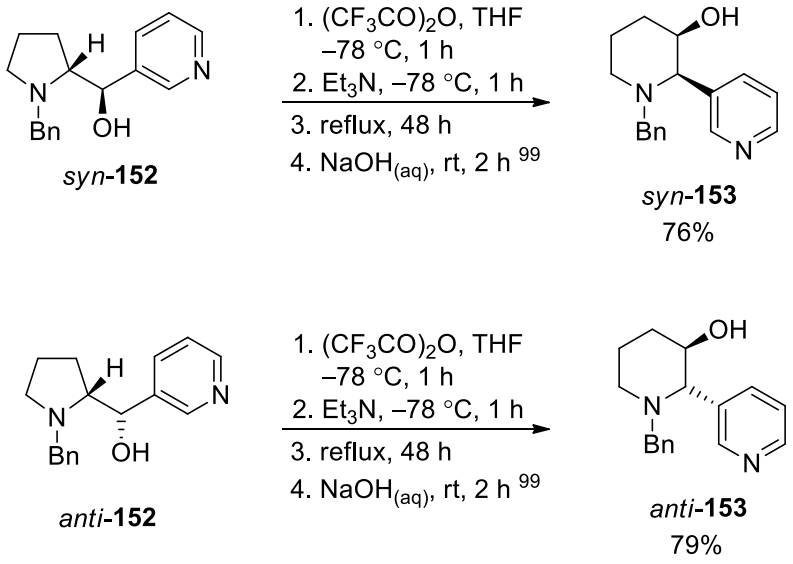

Scheme 4.5

4.3 Computational analysis of 3-dimensional shape

The scaffolds **S1** to **S6** and the different functionalisation groups described above can be combined and enumerated to generate a virtual lead-like compound library, with designed synthesis of such compounds in place. It was envisaged that the compounds could then be analysed for shape diversity and coverage of chemical space. The virtual library was enumerated as shown in Figure 4.4, by combining the different scaffolds with the different substituents.

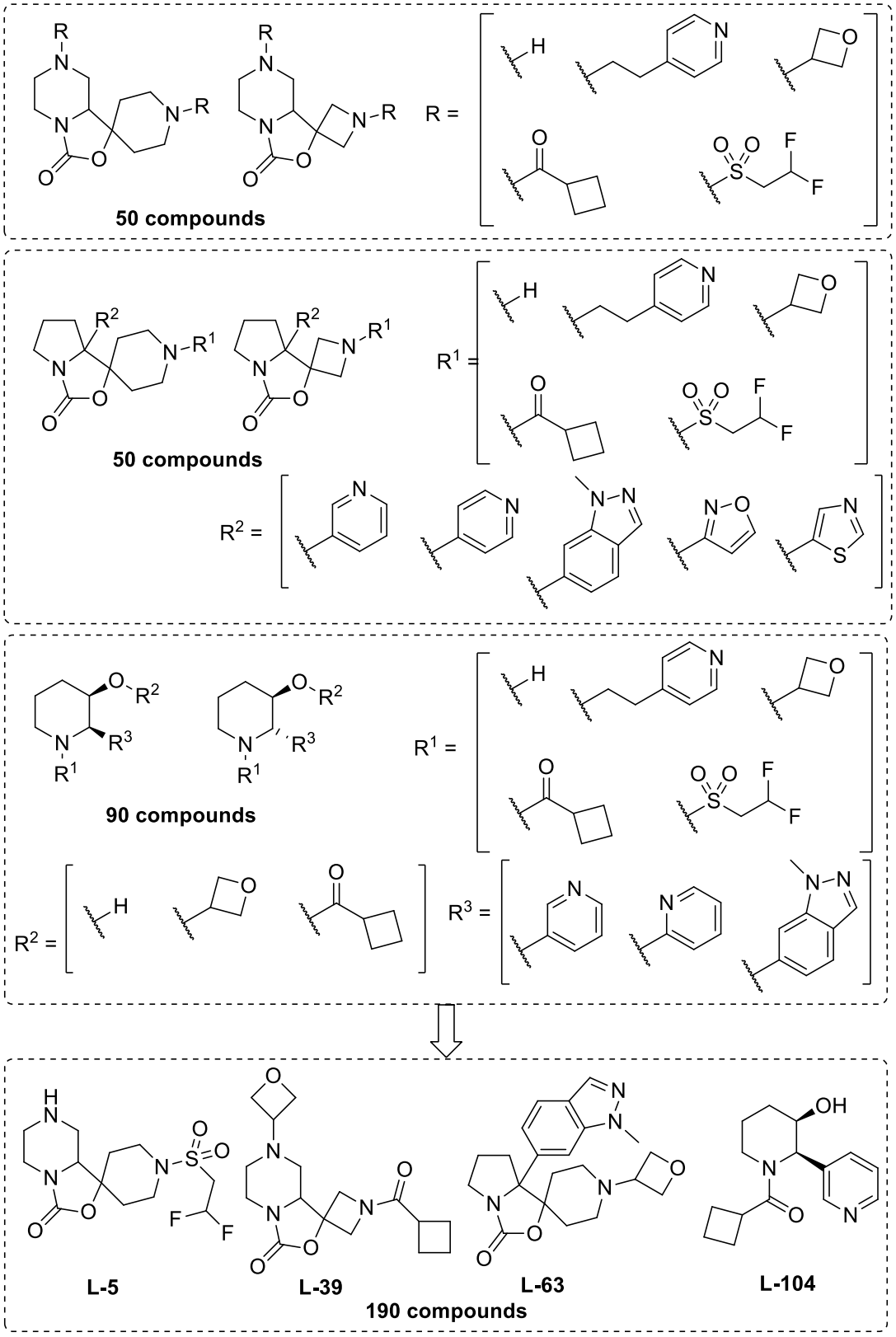

Figure 4.4: The different scaffolds, substituents and how they will be combined to give a virtual lead-like compound library.

The lowest energy conformation of each of the virtual 190 compounds was then generated and subsequent PMI analysis was carried out using a Pipeline Pilot protocol (details in Section 6.1.5). Firstly, the unprotected scaffolds were analysed and the PMI plot is shown in Figure 4.5, with labels to highlight where each scaffold appears on the PMI plot. It was decided that only the lowest energy conformation of these compounds would be investigated, this was to make this analysis more distinctive from the analysis described in previous chapters. Also, generally, only analysis of the lowest energy conformation is presented in the literature.

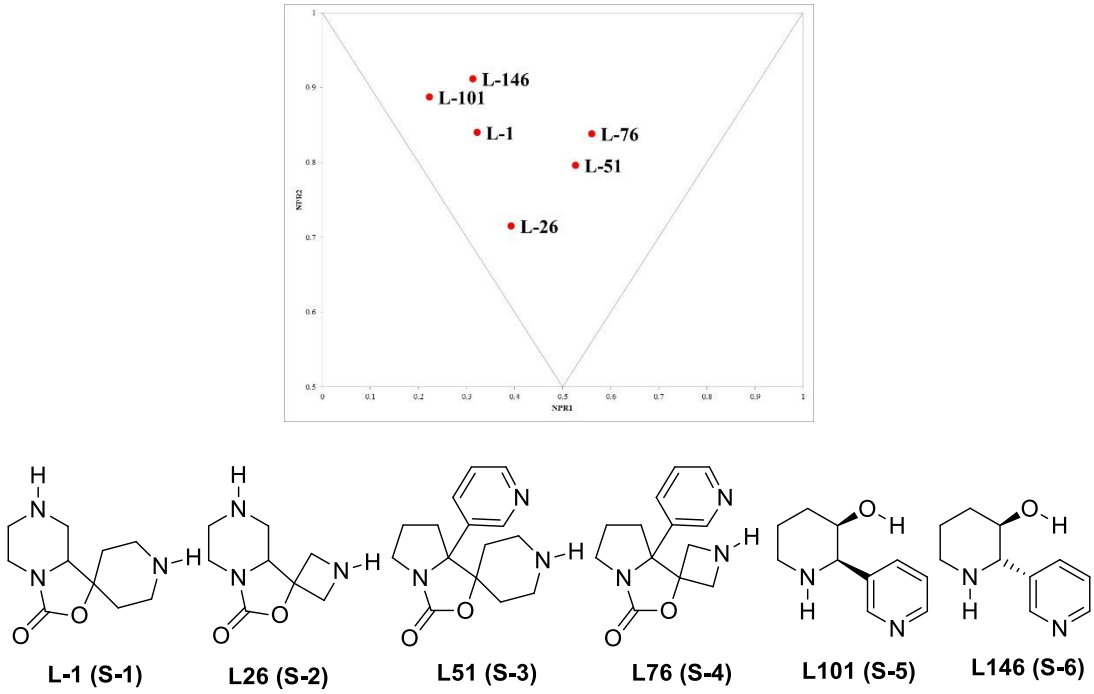

Figure 4.5: PMI plot showing the lowest energy conformation of each of the six scaffolds.

This plot shows that the different scaffolds occupy quite different areas of the plot, with **L-51** and **L-76** providing the most 3-dimensional shape. There also appears to be quite a difference in position of the two piperazine fragments **L-1** and **L-26**. This is interesting as there is only the side ring that differs between the two structures. These also lie quite close to the rod-disc axis, suggesting a flatter, less 3-dimensional conformation.

Each of the scaffolds was then analysed in turn. Firstly, the spirocyclic fused piperazine group of compounds based on **S-1** and **S-2** (**L-1** to **L-50**). The PMI plots are shown in Figure 4.6 (a) and (b).

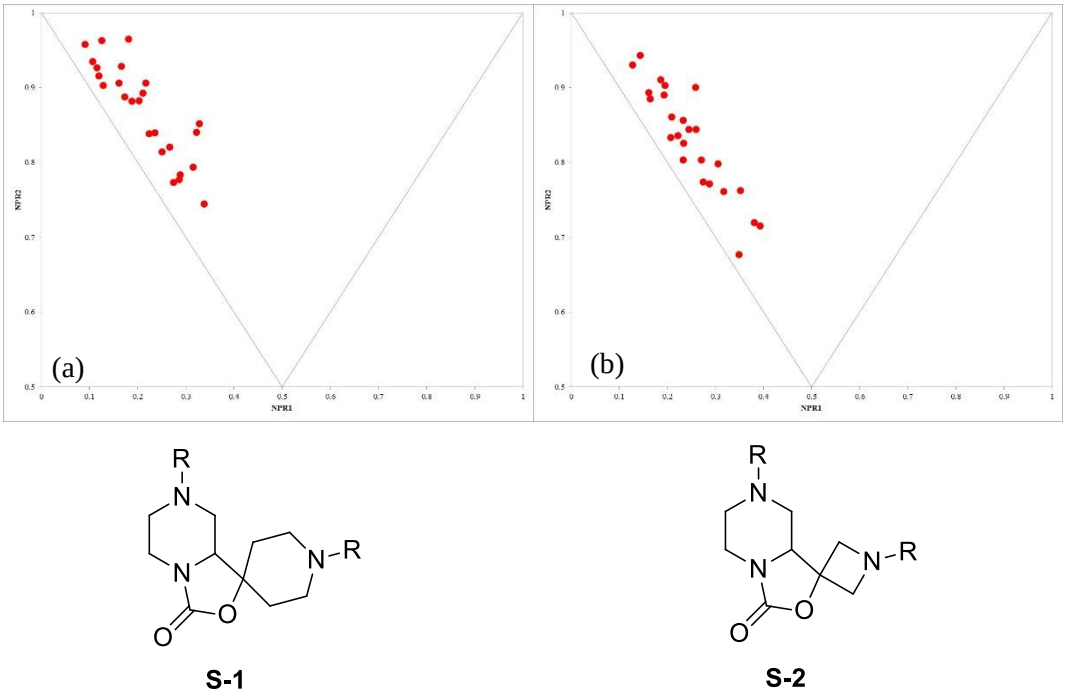

Figure 4.6: PMI plots showing the lowest energy conformations of the lead-like compounds derived from scaffold **S-1** (a) and **S-2** (b).

This plot clearly shows that both of these sets of compounds lie very close to the rod-disc axis, and are surprisingly flat and less 3-dimensional. This result is unusual as the spirocyclic nature of these compounds was expected to give quite architecturally interesting and 3-dimensional shapes.

Figure 4.7 shows the two PMI plots for each of the 25-member compound sets derived from **S-3** and **S-4**. The fully unprotected version of these scaffolds (**L-51** and **L-76**) gave conformations in the most 3-dimensional areas of the plot. Therefore, it was hoped that after functionalisation, a large coverage of chemical space would be achieved. These compounds have more of a spread across the plot, with compounds from **S-4** (**L-76** to **L-100**) having more compounds towards the right side of the plot. These compounds generally have a larger spread across the plot compared to the piperazine compounds (**L-1** to **L-50**) above, suggesting more diversity in shape.

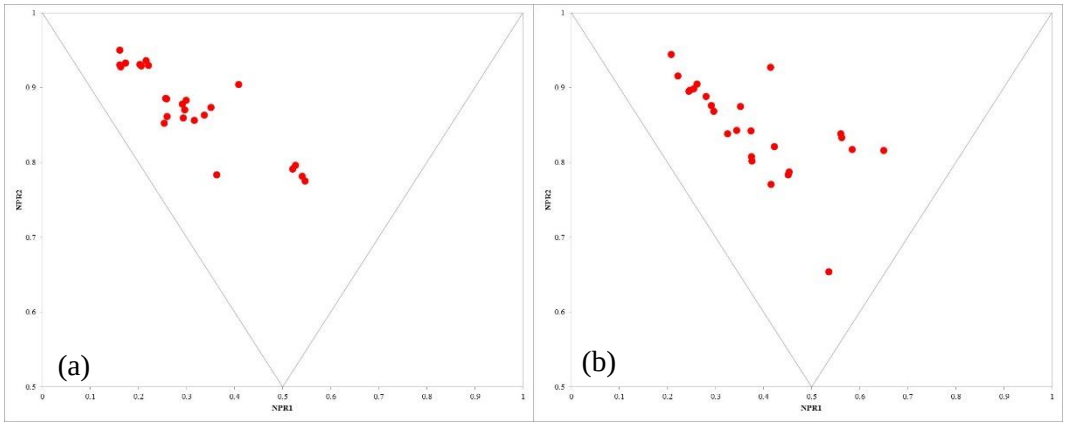

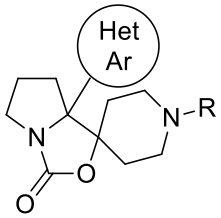

S-3

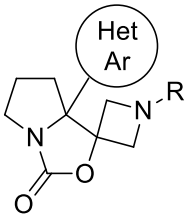

S-4

Figure 4.7: PMI plots showing the lowest energy conformations of the lead-like compounds derived from scaffolds **S-3** (a) and **S-4** (b).

Finally, the piperidine compounds generated from the ring expansion of *N*-benzyl pyrrolidine, scaffolds **S-5** and **S-6** (**L-101** to **L-190**), were analysed. The PMI plots in Figure 4.8 shows the two PMI plots for each of the 45-member compound sets.

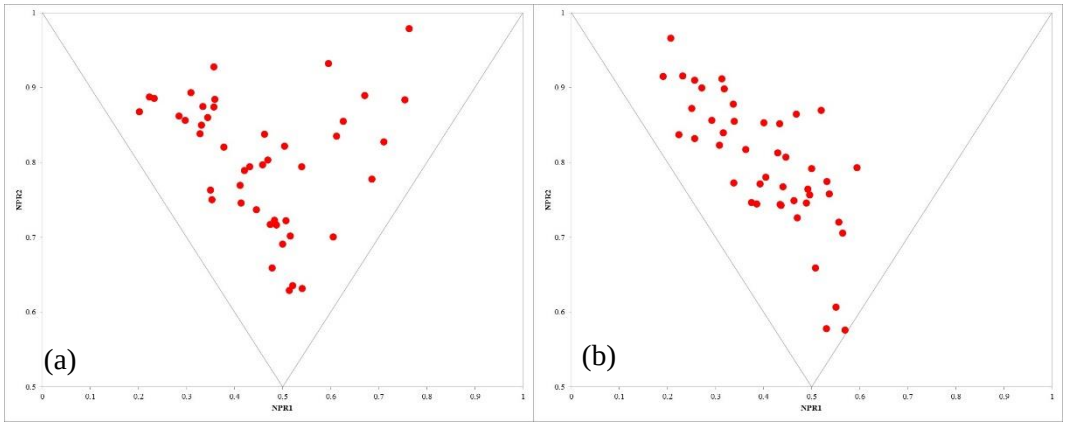

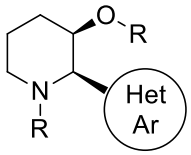

S-5

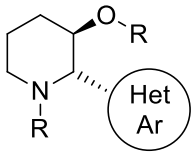

S-6

Figure 4.8: PMI plots showing the lowest energy conformations of the lead-like compounds derived from scaffolds **S-5** (a) and **S-6** (b).

These plots show that these compounds have a much larger spread across the plot and access more 3-dimensional areas of space. This is quite different to the unprotected compounds shown in Figure 4.5. The compounds produced from the *syn*-piperidines (Figure 4.8 (a)) have a number of compounds in the top right of the plot, whereas the *anti*-piperidine compounds spread more towards the bottom part of the plot, towards the disc vertex (Figure 4.8 (b). These results are quite surprising as these scaffolds, on paper, appear the most simple.

The PMI plots were then combined to give an overall impression of the full 190-member virtual lead-like library produced from these scaffolds. The PMI plot is shown in Figure 4.9.

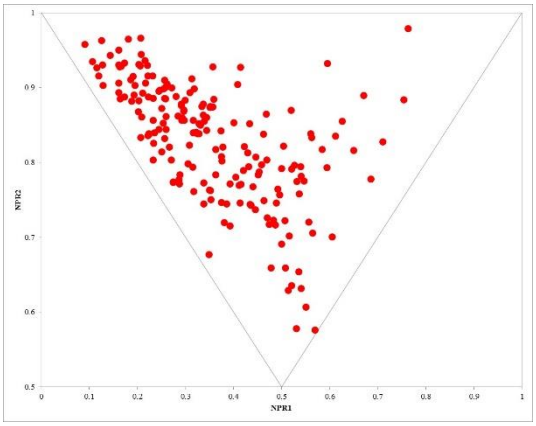

Figure 4.9: PMI plot showing the lowest energy conformations of all the 190 lead-like compounds.

Further analysis was carried out to determine the number of compounds that are in the more 3-dimensional area of the plot. It was decided that this more 3-dimensional area of the plot could be defined as the area where a conformer's NPR1 value is ≥ 0.35 and NPR2 value is ≥ 0.7.

Table 4.1 shows the total number of compounds in the selected area for each of the different scaffolds and the full 190-member library.

	Scaffold	**Number of Compounds with NPR1 ≥ 0.35 and NPR2 ≥ 0.7**	**Total number of compounds**
1	**S-1**	0	25
2	**S-2**	3	25
3	**S-3**	7	25
4	**S-4**	13	25
5	**S-5**	29	45
6	**S-6**	25	45
7	Full 190-member library	77	190

Table 4.1: The number of compounds from each scaffold in the desirable 3-dimensional area of the plot.

These data highlight the difference between each of the scaffolds, clearly showing how the piperidine compounds provide the most 3-dimensional compounds. This also highlights how despite the idea to design more 3-dimensional fragments, and although they look 3-dimensional on paper, analysis of the conformer shape shows that these compounds are generally quite flat and close to the undesirable rod-disc axis of the PMI plot. This should not detract, however, from the more 3-dimensional lead-like compounds that access new and interesting areas of chemical space.

4.4 Analysis of the lead-like nature of compounds in the virtual library

As discussed above, it is desirable that lead-like compounds fit within certain physicochemical parameters in order to offer the best properties for further elaboration and development in drug discovery programmes. These criteria are defined as:

- $-1 \leq \text{AlogP} \leq 3$
- $14 \leq$ number of heavy atoms ≤ 26
- Total polar surface area ≥ 50 Å^2

These properties were assessed for the enumerated virtual lead-like library. A Pipeline Pilot protocol was used to determine a range of different properties. It is therefore important to look at the library as a whole and analyse the spread of values across the library.

The full 190-member compound library was analysed and the average, smallest and largest values were determined (Table 4.2).

	Data	MW (HAC)	ALogP	Molecular PSA / Å^2	H Bond Acceptor	H Bond Donor
1	Average	331.55 (23.5)	0.627	66.6	4.22	0.589
2	Smallest	179.24 (13)	-3.54	43.8	2	0
3	Largest	467.46 (32)	4.08	121.1	6	2

Table 4.2: Analysis of the different physicochemical properties of the full 190-member library.

This shows that the average for each of the properties fall within the desirable range for lead-like compounds. The smallest and largest values from the whole library, however, fall quite far out of these criteria and therefore the spread of the number of compounds across the different property ranges was investigated.

Heavy atom count gives a good indication of molecular weight and therefore the spread of heavy atom count was analysed as a representation of the spread of molecular weight for the whole library (Table 4.3). Table 4.3 shows a spread of compounds across the different heavy atom counts, with only a few compounds in the extreme groups. It is desirable for lead-like compounds to have between 14 and 26 heavy atoms and most of the compounds fit within this range. Although there are some

compounds that fall outside this and these may be too heavy to be considered for the library.

Heavy atom number range	10 to 13	14 to 17	18 to 21	22 to 25	26 to 29	30 to 33
Percentage of total library / %	3	8	23	34	27	6

Table 4.3: The percentage of compounds in the library in different heavy atom count groups.

Most compounds have an AlogP between 0 and 1, which is ideal for lead-like compounds, as shown in Table 4.4.

ALogP Range	-4	-3	-2	-1	0	1	2	3	4
Percentage of total library / %	1	7	7	15	29	23	12	5	1

Table 4.4: The percentage of compounds in the library in different AlogP groups.

The polar surface area of the compounds in the virtual library was also assessed and the results in Table 4.5 show most compounds have a polar surface area greater than the desirable 50 $Å^2$ for lead-like compounds and only a small number below 50 $Å^2$ or greater than 100 $Å^2$, which is very promising for our library.

PSA Range / $Å^2$	40 to 49	50 to 59	60 to 69	70 to 79	80 to 89	90 to 99	100 to 109	110 to 119	120 to 129
Percentage of total library / %	14	33	22	8	13	8	1	1	1

Table 4.5: The percentage of compounds in the library in different polar surface area groups.

A number of groups have discussed the importance of monitoring the number of aromatic rings in lead-like compounds, some specifically suggesting that there should be no more than 3 present. Therefore, our virtual library was assessed for this, with results in Table 4.6, shows that all compounds have 3 or fewer aromatic rings. This may be as a result of targeting more architecturally interesting compounds.

Number of aromatic rings	0	1	2	3
Percentage of total library / %	17	51	28	4

Table 4.6: The percentage of compounds in the library with 0, 1, 2, or 3 aromatic rings.

A summary of the number of compounds that match each of the criteria is shown in Table 4.7. This table shows that for individual properties a large proportion of compounds fit within the desired criteria. However, when all of the criteria are taken into consideration only 34% of the library fits within the defined criteria, which increases to 48% when only heavy atom count is used as a weight restrictor. This is slightly disappointing as the compounds were designed with lead-criteria in mind. However, these criteria could be used to help focus synthesis in the direction of the most desirable compounds.

		MW	**HAC**	**ALogP**	**Molecular PSA / Å²**	**Aromatic Rings**	**All Criteria**
1	**Number of compounds**	108	137	150	160	190	64
2	**Percentage of total library**	57	72	79	84	100	34

Table 4.7: The number of compounds and percentage of the library that fit with the desirable lead-like compound criteria.

4.5 Combination of 3-dimensional compounds and suitable physicochemical properties

As discussed above, another main consideration when selecting compounds for a lead-like library and subsequent screening is not only the physicochemical properties but the 3-dimensional shape of the compounds. In Section 4.3, the compounds in our virtual lead-like library were assessed for their spread across chemical space and for their shape diversity. This analysis can now be combined with the analysis of physicochemical properties. In Section 4.3, 77 compounds (41%) were in the most spherical area of the plot (NPR1 $\geq$ 0.35 and NPR2 $\geq$ 0.7) and in Section 4.4, 64 compounds (34%) had suitable lead-like properties. However, only 42 compounds (22%) fit with all the physicochemical criteria *and* the 3-dimensional criteria. If molecular weight is not used as an additional size criteria there are 46 compounds (24%) of compounds that fit. These 42 compounds are shown on the PMI plot in Figure 4.10. Figure 4.11 shows the structures of the four most spherical lead-like compounds.

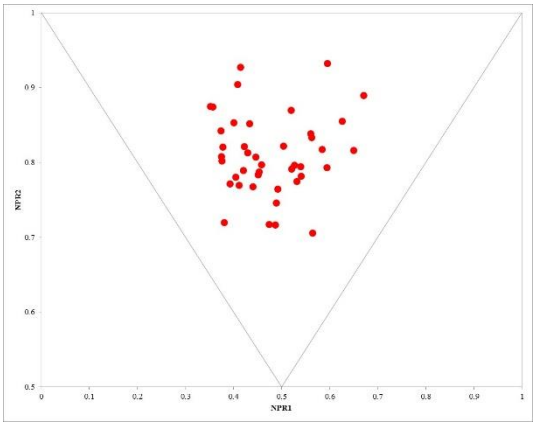

Figure 4.10: PMI plot of the lowest energy conformation of the 42 compounds that fit both the 3-dimensional criteria and the lead-like physicochemical properties.

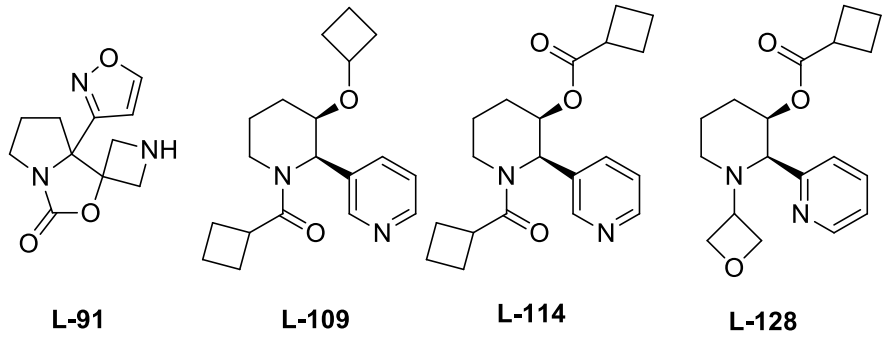

Figure 4.11: The four most spherical lead-like compounds that satisfy the lead-like physicochemical properties too.

The PMI plot in Figure 4.10 clearly shows that our enumerated virtual lead-like library contains some relevant lead-like compounds that cover a large area of chemical space. It should be highlighted that only 22 compounds with the desirable lead-like physical properties are in the most 3-dimensional area of chemical space. This is a promising result suggesting that it is possible to design compounds that have desirable physical properties and are architecturally interesting and diverse. By narrowing down and selecting compounds with desirable shape and physical properties, it also helps to focus synthesis in the direction of the most favourable compounds.

4.6 Conclusion and future work

We aimed to develop a small range of synthetic methods for use in lead-oriented synthesis to produce a range of lead-like compound scaffolds. We then wanted to enumerate a virtual library based on these scaffolds and analyse for lead-like properties and for 3-dimensional structure. Specifically, saturated heterocycles were investigated and pyrrolidine, piperidine and piperazine scaffolds were developed. These scaffolds were then virtually functionalised in a number of ways with a number of medicinally chemically relevant groups, which offered key interaction points and handles for further functionalisation. The enumerated library was then analysed for coverage of chemical space using PMI plots, and was found to cover a large area, with 41% of compounds in the more desirable 3-dimensional area of chemical space. The physicochemical properties of the virtual library were analysed and it was found that on average the values for the library fell within the desired criteria. This was further investigated and it was found that the 34% of compounds fit within all the criteria. Combining these analyses gave 22% of compounds that fit both criteria. This gives a good starting point to enumerate synthesis too, focussing on the most desirable compounds.

The most notable finding throughout this analysis is the difficulty in designing 3-dimensional compounds on paper. Some of the spirocyclic scaffolds that we expected to be most 3-dimensional actually appeared in the more unfavourable, 2-dimensional area of the plot. The piperidine-based scaffolds actually produced the most 3-dimensional compounds, possibly due to vectors accessed from the chair conformation of this scaffold. This may also suggest that the simpler scaffolds provide more architecturally interesting compounds and conformations.

We have developed some interesting lead-like compounds that access new areas of pharmaceutical space and have applied organolithium chemistry in a lead-oriented synthesis setting. This approach to design and analyse compounds could be applied to new or different synthetic methodology. The computational methods to generate and analyse virtual libraries can be applied to help focus the synthesis of the most desirable

lead-like compounds and build up structurally and architecturally diverse lead-like compound libraries with suitable physicochemical properties.

Chapter 5: Conclusions and Future Work

We have presented a new and innovative method to design, computationally assess and select 3-dimensional fragments to explore pharmaceutical space and the subsequent synthesis of some of these fragments. Our method, to design and assess the shape diversity of different fragments before synthesis, is novel compared to current literature methods. The investigation of different conformations of a given fragment also sets our work apart. We sought to investigate the use of saturated heterocycles as a means to introduce structural and shape diversity into fragment libraries and access under-represented areas of chemical space. Our approach focussed on medicinally relevant, different-sized, saturated nitrogen heterocycles with two substituents.

In order to analyse these compound sets, we customised a computational pipeline pilot workflow through a series of iterations to analyse the shape diversity. By using a computational method, we were able to avoid any bias and create an efficient method that works for any size data set. We used principal moments of inertia (PMI) plots to analyse the structural diversity of all the isomers of the six different compound sets and, from these, developed selection criteria and rules to select the compounds that accessed the under-represented, 3-dimensional area of chemical space. We found that a suitable number of compounds were selected from very similar cut-offs for all of the systems. Using the generated PMI plots and associated data, we have demonstrated that shape diversity can be obtained from simple scaffolds and that the selection criteria and rules could be employed in the selection of small sub-set libraries. These libraries focussed on the more under-represented, 3-dimensional area of the PMI plot and new areas of pharmaceutical space and move away from the undesirable rod-disc axis.

The different selected substituent and scaffold sub-set libraries were combined and compared to both the full library and to a commercially available library, the Maybridge “Rule of 3” core 1000 fragment library. This analysis highlighted that our fragments access more of the under-represented, 3-dimensional area of chemical space than a current commercial library. Although we expected the physicochemical

properties to be in-line with the "Rule of 3" guidelines, the physicochemical properties were computationally generated and analysed. It was found that in general our fragments fit within the "Rule of 3" guidelines. The properties also offered flexibility to further develop and grow the fragments while still maintaining good physicochemical properties, ideal for further stages of the drug development process.

From our computational analysis, we demonstrated that shape diversity can be obtained from simple scaffolds and that using saturated compounds allowed access to more 3-dimensional and complex shapes as well as favourable physicochemical properties for fragment development. The computational protocol now works well for a number of different scaffolds and compound types and could be employed in the analysis of different fragments, and it is currently being used in the group to assess different fragment structures. The selection criteria focussed on the 3-dimensional area of the PMI plot and could be used or further developed to choose fragments in very specific areas of the plot, for example disc-shaped fragments. The introduction of different energy conformations is a novel approach and could be investigated in other shape analyses, such as plane of best fit. The use of different shape analysis techniques to carry out a similar analysis and selection method would also be a very interesting comparison, especially to see if similar conformations are generated and how the definition of 3-dimensionality varies between these different techniques for our specific fragments. The selection of smaller sub-sets of compounds has made synthesis more amenable. However, the computational protocol could be further developed to focus on specifically shaped fragments and then highlight closely related shaped neighbours. This approach could be used to focus synthesis on distinct chemical shapes, but allows for synthesis of closely related shape analogues if required.

After selection of our sub-set libraries, the synthesis of the hydroxymethyl piperidine fragments was attempted and we have presented the synthesis towards a number of these disubstituted piperidine fragments. Our focus was to develop routes to access the compounds in the minimum number of steps and synthesise a number of different compounds using similar methodology. We were initially able to group the geminal disubstituted piperidines together and synthesised five final fragments (**A1**, **A2**, **A5**,

A6 and **A9**) using enolate alkylation chemistry (Scheme 5.1). We were able to synthesise intermediates to fragments **A71**, **A72** using amino zinc enolate carbocyclisation methodology (Scheme 5.2), but this route was not successful for the synthesis of fragments **A65**, **A66** and **A89**. Initial work on the reduction of different pyridines looks promising as a method to access a number of different piperidines, including fragment **A89** (Scheme 5.3). We were able to develop a general route for *N*-functionalisation starting from an *N*-Boc ester piperidine that furnishes the final fragment compounds in moderate to good yields in the minimum number of steps. We have been able to employ some routes that are amenable to larger scale synthesis, allowing selected intermediates to be prepared in larger quantities. It has also been possible to use routes that allow access to different analogues. For example, in the amino zinc enolate carbocyclisation methodology the electrophile used can be varied, giving access to a number of different disubstituted piperidines. This ability allows for fragment development and growth as well as rapid synthesis of close analogues.

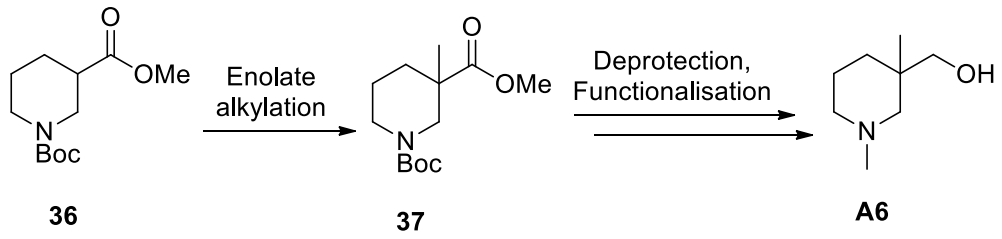

Scheme 5.1

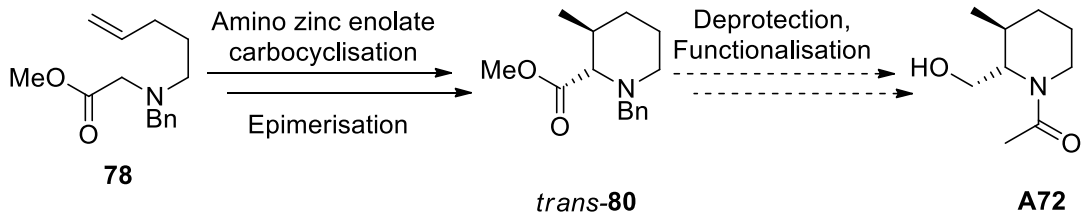

Scheme 5.2

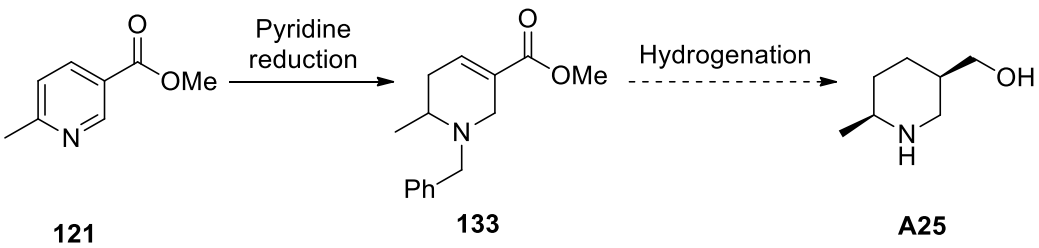

Scheme 5.3

This synthetic work has highlighted that although disubstituted piperidine is a simple scaffold, the synthesis is not trivial. Despite the simplicity of these compounds a significant number have not previously been reported in the literature and there is limited reports of synthetic methodology to access known compounds. This combined with the difficulty of handling low molecular weight, saturated and often polar compounds makes the synthesis very challenging. The development of robust methodology to access these compounds and similar simple saturated nitrogen heterocycles and for their as building blocks needs further work. Development of simple methodology, such as reduction of pyridines, to yield saturated heterocycles would provide access to a number of fragments from simple, readily available material in a few steps and this should be investigated in the future. Epimerisation of different stereocentres would also provide easy access to different diastereomers and would reduce the need for different synthetic routes to access different diastereomers. It is hoped that fragments such as **A19** and **A20** could be synthesised using this method (Scheme 5.4).

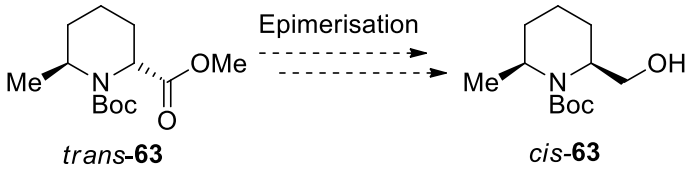

trans-**63** *cis*-**63**

Scheme 5.4

After synthesis, it is important to test the stability of the compounds. Unfortunately, due to time restraints, we were unable to do this for the fragments synthesised. This stability in different solvents and under different conditions is very important before screening is undertaken in order to ensure erroneous results are avoided. Ultimately, it is hoped that these fragments would be tested against different targets. Combining the fragments into current libraries would give a good comparison of these selected 3-dimensional fragments to current fragments.

We were able to apply our novel computational workflow to the shape analysis of lead-like compounds. Other work in the O'Brien group led to the synthesis of six lead-like scaffolds using organolithium chemistry, which were virtually enumerated into a range of lead-like compounds. Conformations of the enumerated library were

generated and the shape diversity and coverage of chemical space was analysed using PMI plots. Our analysis found that 41% of the compounds were in the more desirable 3-dimensional area of the PMI plot. An interesting and somewhat unexpected finding was that what were thought to be the most 3-dimensional fragments on paper did not always fall in the more 3-dimensional area of the plot. Some of the spirocyclic scaffolds, for example, appeared in the more unfavourable, 2-dimensional area of the plot. However, the more simple piperidine-based scaffolds were the most 3-dimensional compounds. This may be due to the different vectors accessed from the chair conformation of this scaffold. It was actually the simpler scaffolds that provided more architecturally interesting compounds.

The physicochemical properties of the virtual library were also analysed. We found that 34% of compounds fit within all the lead-like criteria. Although, further analysis showed that 22% of compounds fit both the 3-dimensional criteria and the lead-like physical properties. Although this is not a particularly high proportion of the compounds, this information could help to focus the synthesis to the most desirable lead-like compounds.

We have been able to employ our computational protocol to lead-like compounds, making the analysis of the shape diversity of the virtual library quick and easy. This approach to design and analyse compounds could be applied to different synthetic methodology and different enumerated libraries. The computational analysis of the shape diversity and physicochemical properties can be applied to help focus the synthesis of the most desirable lead-like compounds. The computational approach can be used build up structurally and architecturally diverse lead-like compound libraries with suitable physicochemical properties.

Using our customised computational workflow to analyse shape diversity of different compounds, both fragments and lead-like compounds, it has been possible to demonstrate that simple compounds can give diverse compound shapes, with good physical properties. In both stages, we have been able to highlight the most 3-

dimensional compounds with the most suitable physical properties. This type of analysis is highly beneficial if carried out before starting synthesis, as it can help to focus the synthesis on the most suitable compounds, negating the unnecessary synthesis of compounds with poor properties. This is important for many reasons: it helps to reduce cost, makes processes more efficient and decreases the impact on the environment. The analysis is rapid and efficient and can be used to direct synthesis of similar compounds if hits are found. That said, the synthesis of these simple compounds is challenging and there is a need to develop more efficient methods to access such simple compounds if this approach is to be successful and taken up by others.

Chapter 6: Experimental

6.1 Computational Methods

Computational analysis and protocol development was carried out in collaboration with Paul Bond and Rod Hubbard at York Structural Biology Laboratory (YSBL).[62] Coding and programming was carried out by Paul Bond. Pipeline pilot protocol workflow designed by Mary Wheldon in collaboration with Paul Bond. Data analysis carried out by Mary Wheldon.

6.1.1 General methods

Shape analysis

A SMILES file containing the SMILES strings for all fragment compounds was generated using ChemDraw 12.0.

3-Dimensional structures were generated Pipeline Pilot 8.5.0.200, 2011, Accelrys Software Inc. Generated conformations were used to generate the three Principal Moments of Inertia (I1, I2 and I3) which were then normalised by dividing the two lower values by the largest (I1/I3 and I2/I3) using Pipeline Pilot built-in components.

Principal moments of inertia (PMI) about the principal axes of a molecule were calculated according to the following rules:[126]

1. The moments of inertia are computed for a series of straight lines through the centre of mass.
2. Distances are established along each line proportional to the reciprocal of the square root of I on either side of the centre of mass. The locus of these distances forms an ellipsoidal surface. The principal moments are associated with the principal axes of the ellipsoid.

The PMI plots were then generated with these data in Excel 2013.

Molecular properties

All physical properties were calculated using Pipeline Pilot built-in components.

ALogP component: calculates ALogP using the Ghose and Crippen octanol-water partition coefficient method.[127]

Number of hydrogen donors component: number of heteroatoms (oxygen, nitrogen, sulfur, or phosphorus) with one or more lone pairs, excluding atoms with positive formal charges, amide and pyrrole-type nitrogens, and aromatic oxygen and sulfur atoms in heterocyclic rings.

Number of hydrogen acceptors component: number of heteroatoms (oxygen, nitrogen, sulfur, or phosphorus) with one or more attached Hydrogen atoms.

Molecular polar surface area component: Calculates the polar surface area for each molecule using a 2-dimensional approximation using a method based on the published method of Selzer and co-workers.[128]

6.1.2 Initial protocol

Prior to conformer generation a wash step was performed, which involved ionising the molecule at pH 7.4, converting to the canonical tautomer and adding hydrogens. 3-dimensional coordinates were then generated using the built-in Conformation Generator component from the Discovery Studio Component Collection. The conformation method was set to BEST with an energy threshold of 20 kcal mol^{-1}, maximum of 255 conformers for each compound. Within the same Conformation Generator component the conformations were minimised using 1000 steps of Steepest Descent with a RMS gradient tolerance of 3 and 200 steps of Conjugate Gradient with a RMS gradient tolerance of 0.1. A CHARMm forcefield with Momany-Rone partial charges was used for the minimisations. Initial minimisations were performed without

an implicit solvent model, but a Generalised Born solvent model was later added. Similar conformations were then filtered using a chosen RMSD threshold of 0, 0.5 or 1. Finally, conformations were filtered based on a chosen maximum relative energy threshold of 7 or 20 kcal mol^{-1}.

6.1.3 Analysis of enantiomers

Prior to conformer generation a wash step was performed, which involved ionising the molecule at pH 7.4, converting to the canonical tautomer and adding hydrogens. 3-dimensional coordinates were then generated using the built-in Conformation Generator component from the Discovery Studio Component Collection. Two copies of the molecule were generated, the original and mirror image. Conformers were generated using the BEST method in Catalyst using the rel option, run directly on the server and not through the built-in Conformation Generator component with a chosen maximum relative energy threshold of 20 kcal mol^{-1}, maximum of 255 conformers for each compound. Conformations were read and mirrored if the wrong enantiomer is generated. Duplicates were filtered with a chosen RMSD threshold of 0.1. Minimisation was performed using the CHARMm forcefield with Momany-Rone partial charge estimation and a Generalised Born implicit solvent model. Duplicates are filtered again with a RMSD threshold of 0.1.

6.1.4 New version of protocol

Prior to conformer generation a wash step was performed, which involved stripping salts and ionising the molecule at pH 7.4. Any stereocentre created here was left with undefined stereochemistry. SMILES strings were converted to their canonical representation. A list of allowed chirality at each centre is generated and a SMILES file with all possible stereoisomers was written. Conformers were generated using the BEST method in Catalyst using the rel option, run directly on the server and not through the built-in Conformation Generator component with a chosen maximum relative energy threshold of 20 kcal mol^{-1}, maximum of 255 conformers for each compound. Conformations were read, ones that cannot be represented by the canonical SMILES are discarded, with the remaining ones standardised to a single enantiomer.

Duplicates were filtered with a RMSD threshold of 0.1. Minimisation with 200 steps of Conjugate Gradient minimisation with an RMS gradient tolerance of 0.1 was performed using the CHARMm forcefield with Momany-Rone partial charge estimation and a Generalised Born implicit solvent model. Duplicates were filtered again with a RMSD threshold of 0.1.

6.1.5 Analysis of lead-like library

Prior to conformer generation a wash step was performed, which involved ionising the molecule at pH 7.4, adding explicit hydrogens and outputting the canonical tautomer. Conformers were generated using the BEST method in Catalyst with a maximum relative energy threshold of 20 kcal mol^{-1}. These conformations were then minimised using 1000 steps of Steepest Descent with a RMS gradient tolerance of 3 and 200 steps of Conjugate Gradient with an RMS gradient tolerance of 0.1. Minimisation was performed using the CHARMm forcefield with Momany-Rone partial charge estimation and a Generalised Born implicit solvent model. The lowest energy conformer was selected.

6.2 Synthetic Methods

6.2.1 General Methods

All non-aqueous reactions were carried out under oxygen-free Ar using flame-dried glassware. Et_2O and THF were freshly distilled from sodium and benzophenone respectively. Alkyllithiums were titrated against *N*-benzylbenzamide before use.[129] TMEDA, Me_3SiCl and methyl iodide used in lithiations were distilled over CaH_2 before use. Dimethylformamide was obtained from the dry solvent still and CO_2 was dried over $CaCl_2$ before use in lithiation reactions. Petrol refers to the fraction of petroleum ether boiling in the range of 40-60 °C and was purchased in Winchester quantities. Brine refers to a saturated solution. Water is distilled water.

Flash column chromatography was carried out using Fluka Chemie GmbH silica (220-440 mesh). Thin layer chromatography was carried out using commercially available Merk F_{254} aluminium backed silica plates. Proton (400 MHz) and carbon (100.6 MHz) NMR spectra were recorded on a Jeol ECX-400 instrument using an internal deuterium lock. For samples recorded in $CDCl_3$, chemical shifts are quoted in parts per million relative to $CHCl_3$ (δ_H 7.26) and $CDCl_3$ (δ_C 77.0, central line of triplet). For samples recorded in DMSO-*d*$_6$, chemical shifts are quoted on parts per million relative to DMSO (δ_H 2.50, central line of quintet) and DMSO-*d*$_6$ (δ_C 39.52, central line of septet). Carbon NMR spectra were recorded with broad band decoupling and assigned using DEPT experiments. Coupling constants (*J*) are quoted in Hertz. Melting points were carried out on a Gallenkamp melting point apparatus. Infrared spectra were recorded on an ATI Mattson Genesis FT-IR spectrometer. Electrospray high and low resonance mass spectra were recorded at room temperature on a Bruker Daltronics micrOTOF spectrometer.

6.2.2 General Procedures

General Procedure A: Methyl ester formation and Boc protection

Thionyl chloride (3.09 mL, 42.6 mmol, 1.1 eq.) was added dropwise over 5 min to a stirred solution of the carboxylic acid (38.7 mmol, 1.0 eq.) in MeOH (50 mL) at 0 °C under Ar. The resulting solution was stirred and heated at reflux for 1 h. The mixture was then allowed to cool to rt and the solvent was evaporated under reduced pressure to give the crude methyl ester. Triethylamine (5.40 mL, 38.7 mmol, 1.0 eq.) was added to a stirred solution of crude methyl ester in CH_2Cl_2 (25 mL) at rt under Ar. Then, a solution of di-*tert*-butyl dicarbonate (8.45 g, 38.7 mmol, 1.0 eq.) in CH_2Cl_2 (25 mL) was added. The resulting solution was stirred at rt for 18 h. The solids were removed by filtration and the filtrate was evaporated under reduced pressure to give a wet solid. The wet solid was dissolved in Et_2O (50 mL) and washed with 1 M $HCl_{(aq)}$ (2 x 25 mL) and saturated $NaHCO_{3(aq)}$ (10 mL). The organic layer was dried ($MgSO_4$) and evaporated under reduced pressure to give the crude product.

General Procedure B: Reduction of methyl esters

A solution of the methyl ester (4.11 mmol, 1.0 eq.) in THF (20 mL) was added dropwise to a stirred suspension of lithium aluminium hydride (156 mg, 4.11 mmol, 1.0 eq.) in THF (30 mL) at 0 °C under Ar. The resulting mixture was stirred at 0 °C for 1 h and then H_2O (0.7 mL), 20% $NaOH_{(aq)}$ (1.4 mL) and H_2O (0.7 mL) were carefully added. The mixture was allowed to warm to rt and the solids were removed by filtration through Celite. H_2O (20 mL) was then added to the filtrate and the mixture was extracted with Et_2O (3 x 50 mL). The combined organic extracts were dried ($MgSO_4$) and evaporated under reduced pressure to give the crude product.

General Procedure C: *N*-Boc deprotection using HCl in Et_2O

Hydrogen chloride (0.93 mL of a 2.0 M solution in Et_2O, 1.86 mmol, 4.0 eq.) was added to a stirred solution of the *N*-Boc amine (0.46 mmol, 1.0 eq.) in Et_2O (1 mL) at rt under Ar. The resulting solution was stirred at rt for 18 h. The solvent was then evaporated under reduced pressure to give the crude product.

General Procedure D: *N*-Boc deprotection using HCl in EtOAc

Acetyl chloride (0.93 mL, 13.2 mmol, 4.0 eq.) was added dropwise (CARE - exothermic, vigorous reaction) to a stirred solution of *N*-Boc methyl ester **16** (3.29 mmol, 1.0 eq.) and EtOH (0.77 mL, 13.2 mmol, 4.0 eq.) in EtOAc (20 mL) at rt under Ar. The resulting solution was stirred at rt or stirred and heated at reflux for 18 h. The solvent was then evaporated under reduced pressure to give the crude product.

General Procedure E: Reduction of *N*-Boc to *N*-Me

A solution of the *N*-Boc piperidine (0.88 mmol, 1.0 eq.) in THF (20 mL) was added dropwise to a stirred suspension of lithium aluminium hydride (165 mg, 4.36 mmol, 5.0 eq.) in THF (30 mL) at 0 °C under Ar. The resulting mixture was allowed to warm to rt for 30 min and then stirred at heated at reflux for 24 h. After being allowed to cool to rt, the mixture was cooled to 0 °C then H_2O (1.4 mL), 20% $NaOH_{(aq)}$ (2.8 mL) and H_2O (1.4 mL) were carefully added. The mixture was allowed to warm to rt and the solids were removed by filtration through Celite. The filtrate was evaporated under reduced pressure to give the crude product.

General Procedure F: *N*-Acetylation

Acetyl chloride (0.12 mL, 1.67 mmol, 3.0 eq.) was added to a stirred solution of the amine hydrochloride salt (0.557 mmol, 1.0 eq.) and triethylamine (0.23 mL, 1.67 mmol, 3.0 eq.) in CH_2Cl_2 (2 mL) at rt under Ar. The resulting solution was stirred at rt for 18 h. H_2O (2 mL) was added and the reaction mixture was extracted with CH_2Cl_2 (3 x 10 mL). The combined organic extracts were dried ($MgSO_4$) and evaporated under reduced pressure to give the crude product.

General Procedure G: *N*-Sulfonation

Methanesulfonyl chloride (0.13 mL, 1.67 mmol, 3.0 eq.) was added to a stirred solution of the amine hydrochloride salt (0.56 mmol, 1.0 eq.) and triethylamine (0.23 mL, 1.67 mmol, 3.0 eq.) in CH_2Cl_2 (2 mL) at rt under Ar. The resulting solution was stirred at rt for 18 h. H_2O (2 mL) was added and the reaction mixture was extracted

with CH_2Cl_2 (3 x 10 mL). The combined organic extracts were dried ($MgSO_4$) and evaporated under reduced pressure to give the crude product.

General Procedure H: Enolate alkylation

Lithium bis(trimethylsilyl)amide (1.0 M solution in THF, 0.750 mmol, 1.5 eq.) or potassium bis(trimethylsilyl)amide (0.5 M solution in toluene, 0.750 mmol, 1.5 eq.) was added to a stirred solution of methyl ester (122 mg, 0.50 mmol, 1.0 eq.) (and *N*,*N*′-dimethylpropylene urea (0.75 mL, 1.5 eq.) if used) in THF (0.93 mL or 10 mL) at –78 °C under Ar. The resulting mixture was stirred at –78 °C for 1 h. Then, methyl iodide (0.75 mmol, 1.5 eq.) was added. The resulting solution was allowed to warm to rt over 4 h and then stirred at rt for 16 h. Saturated $NH_4Cl_{(aq)}$ (0.5 mL) was added and the mixture was extracted with Et_2O (3 x 5 mL). The combined organic extracts were dried ($MgSO_4$) and evaporated under reduced pressure to give the crude product.

General procedure I: Methyl ester reduction with $LiBH_4$

Lithium borohydride (4.0 M solution in THF, 8.00 mmol, 8.0 eq.) was added to a stirred solution of methyl ester (1.00 mmol, 1.0 eq.) in THF (10 mL) at rt under Ar. The resulting solution was stirred at rt for 3-5 h. H_2O (5 mL) was added and the mixture was extracted with EtOAc (3 x 10 mL). The combined organic extracts were dried ($MgSO_4$) and evaporated under reduced pressure to give the crude product.

General procedure J: Amino zinc enolate carbocyclisation reaction

Lithium bis(trimethylsilyl)amide (1.0 M solution in THF, 40.4 mmol, 2.0 eq.) was added to a stirred solution of ester-alkene **78** (20.2 mmol, 1.0 eq.) in Et_2O (300 mL) at –20 °C under Ar. The resulting solution was stirred at –20 °C for 10 min and then allowed to warm to rt for 20 min. The mixture was then cooled to –40 °C. A solution of zinc bromide (9.10 g, 40.4 mmol, 2.0 eq.) in dry Et_2O (40.4 mL) (NOTE: zinc bromide should be stirred vigorously in Et_2O for 1 h before reaction to aid dissolution) was added. The resulting mixture was allowed to warm to rt and stirred at rt for 5 h. The mixture was then cooled to 0 °C and a 2:1 solution of saturated $NH_4Cl_{(aq)}$-

$NH_4OH_{(aq)}$ (40 mL) was added. The resulting mixture was then allowed to warm to rt and stirred at rt for 18 h. The mixture was extracted with Et_2O (3 x 50 mL). The combined organic extracts were dried ($MgSO_4$) and evaporated under reduced pressure to give the crude product.

General procedure K: Methyl ester formation

Concentrated H_2SO_4 (2.54 mL, 46.7 mmol, 3.7 eq.) was added to a stirred solution of pyridine carboxylic acid **125** (12.7 mmol, 1.0 eq.) in MeOH (20 mL) at rt under air. The resulting solution was stirred and heated at reflux for 20 h. After being allowed to cool to rt, the solvent was evaporated under reduced pressure. H_2O (20 mL) and cold saturated $K_2CO_{3(aq)}$ (20 mL) was added until pH > 10 was reached and the mixture was extracted with CH_2Cl_2 (3 x 15 mL). The combined organic extracts were dried ($MgSO_4$) and evaporated under reduced pressure to give the crude product.

General procedure L: Benzylation of pyridine ester

Benzyl bromide (0.86 mL, 7.29 mmol, 1.0 eq.) was added to a stirred solution of pyridine ester **128** (7.29 mmol, 1.0 eq.) in MeCN (18 mL) at rt under air. The resulting solution was stirred and heated at reflux for 3 h. After being allowed to cool to rt, the solvent was evaporated under reduced pressure to give the crude benzyl pyridinium bromide.

General procedure M: Pyridine reduction using sodium borohydride

Sodium borohydride (2.48 g, 65.6 mmol, 9.0 eq.) was added portionwise (CARE - vigorous reaction) to a stirred solution of benzyl pyridinium bromide (7.29 mmol, 1.0 eq.) in MeOH (20 mL) and H_2O (10 mL) at 0 °C under air. The resulting yellow solution was allowed to warm to rt and stirred at rt for 2 h. The solvent was then evaporated under reduced pressure to give a thick yellow oil. H_2O (10 mL) was added and the mixture was extracted with CH_2Cl_2 (3 x 10 mL). The combined organic extracts were dried ($MgSO_4$) and evaporated under reduced pressure to give the crude product.

6.2.3 Experimental procedures and characterisation data

1-*tert*-Butyl 2-methyl piperidine-1,2-dicarboxylate 16

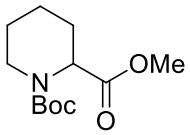

16

Using general procedure A, thionyl chloride (3.09 mL, 42.6 mmol, 1.1 eq.), pipecolic acid **15** (5.00 g, 38.7 mmol, 1.0 eq.) in MeOH (50 mL) and then triethylamine (5.40 mL, 38.7 mmol, 1.0 eq.) in CH_2Cl_2 (25 mL) and di-*tert*-butyl dicarbonate (8.45 g, 38.7 mmol, 1.0 eq.) in CH_2Cl_2 (25 mL) gave the crude product. Purification by flash chromatography on silica with 80:20 hexane-Et_2O as eluent gave methyl ester **16** (8.88 g, 94%) as a colourless oil, R_F (80:20 hexane-Et_2O) 0.2; ^{1}H NMR (400 MHz, $CDCl_3$) (50:50 mixture of rotamers) δ 4.89 (br s, 0.5H, NCHCO), 4.72 (br s, 0.5H, NCHCO), 4.05-3.87 (m, 1H, NCH), 3.723 (s, 1.5H, OMe), 3.721 (s, 1.5H, OMe), 2.96 (br dd, *J* = 13.0, 13.0 Hz, 0.5H, NCH), 2.86 (br dd, *J* = 13.0, 13.0 Hz, 0.5H. NCH), 2.19 (br d, *J* = 12.0 Hz, 1H, CH), 1.73-1.57 (m, 4H, CH), 1.45 (s, 9H, CMe_3), 1.29-1.15 (m, 1H, CH); ^{13}C NMR (101.6 MHz, $CDCl_3$) (rotamers) δ 172.4 (C=O), 155.5 (C=O), 79.9 (*C*Me_3), 55.0 (NCH), 53.7 (NCH), 52.0 (OMe), 42.1 (NCH_2), 41.0 (NCH_2), 28.3 (C*Me*$_3$), 26.8 (CH_2), 24.8 (CH_2), 20.8 (CH_2). Spectroscopic data consistent with those reported in the literature.[68]

Lab book reference: mcw/3/44/1

***tert*-Butyl 2-(hydroxymethyl)piperidine-1-carboxylate 17**

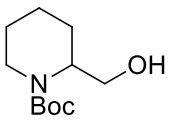

17

A solution of 2-piperidine methanol **18** (1.00 g, 8.68 mmol, 1.0 eq.) in CH_2Cl_2 (25 mL) and triethylamine (4.36 mL, 31.3 mmol, 3.6 eq.) was added dropwise to a stirred solution of di-*tert*-butyl dicarbonate (2.27 g, 10.4 mmol, 1.2 eq.) in CH_2Cl_2 (25 mL) at 0 °C under Ar. The resulting solution was allowed to warm to rt and stirred at rt for

16 h. H_2O (20 mL) was added and the mixture was extracted with CH_2Cl_2 (3 x 15 mL). The combined organic extracts were dried ($MgSO_4$) and evaporated under reduced pressure to give the crude product. Purification by flash chromatography on silica with 90:10 petrol-Et_2O as eluent gave *N*-Boc piperidine **17** (1.49 g, 80%) as a white solid, mp 61-64 °C (lit.,[21] 76-77 °C); R_F (9:1 Et_2O-petrol) 0.3; ^{1}H NMR (400 MHz, $CDCl_3$) δ 4.31-4.25 (m, 1H, NCH), 3.93 (br d, *J* = 13.0 Hz, 1H, NCH), 3.81 (dd, *J* = 11.0, 9.0 Hz, 1H, C*H*OH), 3.60 (dd, *J* = 11.0, 5.5 Hz, 1H, C*H*OH), 2.94-2.77 (m, 1H, NCH), 2.08 (br s, 1H, CH), 1.72-1.38 (m, 5H, CH), 1.46 (s, 9H, CMe_3); ^{13}C NMR (101.6 MHz, $CDCl_3$) δ 156.2 (C=O), 79.8 (*C*Me_3), 61.7 (CH_2OH), 52.5 (NCH), 39.8 (NCH_2), 28.4 (C*Me*$_3$), 25.2 (CH_2), 25.1 (CH_2), 19.6 (CH_2). Spectroscopic data consistent with those reported in the literature.[68]

Lab Book Reference: mcw/1/82

Using general procedure B, methyl ester **16** (1.00 g, 4.11. mmol, 1.0 eq.) and lithium aluminium hydride (156 mg, 4.11 mmol, 1.0 eq.) in THF (50 mL) gave the crude product. Purification by flash chromatography on silica with 60:40 hexane-Et_2O and then Et_2O as eluent gave amino alcohol **17** (781 mg, 88%) as a white solid.

Lab Book Reference: mcw/3/41/2

2-(Hydroxymethyl)piperidine hydrochloride salt 18.HCl

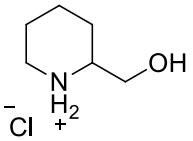

18.HCl

Using general procedure D, hydrogen chloride (0.93 mL of a 2.0 M solution in Et_2O, 1.86 mmol, 4.0 eq.) and *N*-Boc amino alcohol **17** (100 mg, 0.46 mmol, 1.0 eq.) in Et_2O (1 mL) gave amine hydrochloride salt **18** (76 mg, quant) as a yellow oil, IR (ATR) 3368 (OH or NH), 2949, 2754, 1652, 1402, 1324, 1050, 568 cm^{-1}; ^{1}H NMR (400 MHz, DMSO-d_6) δ 8.73 (br s, 1H, NH), 8.42 (br s, 1H, NH), 5.37 (dd, *J* = 4.5, 4.5 Hz, 1H, OH), 3.57 (ddd, *J* = 11.0, 4.0, 4.0 Hz, 1H), 3.49-3.42 (m, 1H), 3.17 (br d, *J* = 12.0 Hz, 1H), 3.02 (br s, 1H), 2.82 (br dd, *J* = 12.0, 12.0 Hz, 1H), 1.77-1.66 (m, 3H, CH), 1.61-1.33 (m, 3H, CH); ^{13}C NMR (101.6 MHz, DMSO-d_6) δ 61.4 (OCH_2), 57.3 (NCH),

43.7 (NCH_2), 24.7 (CH_2), 21.9 (CH_2), 21.3 (CH_2); MS (ESI) *m/z* 116 [M^+, 100]; HMRS (ESI) *m/z* calcd for $C_6H_{14}NO\,M^+$ 116.1070, found 116.1067 (+2.5 ppm error).

Lab Book Reference: mcw/3/58/c

(1-Methylpiperidin-2-yl)methanol 19

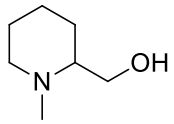

19

Using general procedure E, *N*-Boc piperidine **16** (243 mg, 1.00 mmol, 1.0 eq.) in THF (20 mL) and lithium aluminium hydride (189 mg, 5.00 mmol, 5.0 eq.) in THF (30 mL) gave *N*-methyl piperidine **19** (106 mg, 82%) as a colourless oil; IR (ATR) 3349 (OH), 2931, 2855, 2791, 1444, 1144, 1025, 749 cm^{-1}; ^1H NMR (400 MHz, $CDCl_3$) δ 3.84 (dd, *J* = 11.0, 4.0 Hz, 1H, C*H*OH), 3.39 (dd, *J* = 11.0, 2.0 Hz, 1H, C*H*OH), 2.87 (br d, *J* = 11.5 Hz, 1H, NCH), 2.28 (s, 3H, Me), 2.13 (ddd, *J* = 11.5, 11.5, 3.0 Hz, 1H, NCH), 1.98-1.92 (m, 1H, NCH), 1.78-1.72 (m, 1H, CH), 1.64-1.56 (m, 3H, CH), 1.55-1.43 (m, 1H, CH), 1.33-1.20 (m, 1H, CH); ^{13}C NMR (101.6 MHz, $CDCl_3$) δ 64.0 (NCH), 63.2 (OCH_2), 56.6 (NCH_2), 42.8 (NMe), 28.4 (CH_2), 25.5 (CH_2), 24.1 (CH_2); MS (ESI) *m/z* 130 [$(M + H)^+$, 100]; HMRS (ESI) *m/z* calcd for $C_7H_{15}NO$ $(M + H)^+$ 130.1226, found 130.1232 (–3.9 ppm error).

Lab Book Reference: mcw/3/79

2-(Methoxycarbonyl)piperidine hydrochloride salt 20.HCl

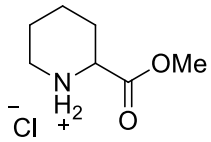

20.HCl

Using general procedure C, acetyl chloride (0.93 mL, 13.2 mmol, 4.0 eq), *N*-Boc methyl ester **16** (800 mg, 3.29 mmol, 1.0 eq.) and EtOH (0.77 mL, 13.2 mmol, 4.0 eq.) in EtOAc (20 mL) gave amine hydrochloride salt **20** (485 mg, 82%) as a white solid, mp 196-198 °C; IR (ATR) 2906, 2707, 2420, 1745 (C=O), 1430, 1136, 1230, 1017, cm^{-1}; ^{1}H NMR (400 MHz, $CDCl_3$) δ 9.90 (br s, 2H, NH_2), 3.95 (dd, *J* = 10.0, 4.0 Hz, 1H, NCH), 3.84 (s, 3H, OMe), 3.64 (ddd, *J* = 12.0, 4.0, 4.0, Hz, 1H, NCH), 3.10 (ddd, *J* = 12.0, 10.0, 4.0 Hz, 1H, NCH), 2.33-2.21 (m, 1H, CH), 2.16-1.96 (m, 2H, CH), 1.94-1.75 (m, 2H, CH), 1.66-1.53 (m, 1H, CH); ^{13}C NMR (101.6 MHz, $CDCl_3$) δ 168.7 (C=O), 56.7 (NCH), 53.2 (OMe), 43.7 (NCH_2), 25.6 (CH_2), 21.63 (CH_2), 21.59 (CH_2); MS (ESI) *m/z* 144 [M^+, 100]; HMRS (ESI) *m/z* calcd for $C_7H_{14}NO_2$ M^+ 144.1019, found 144.1015 (+2.6 ppm error).

Lab Book reference: mcw/3/43/c

Methyl 1-acetylpiperidine-2-carboxylate 21

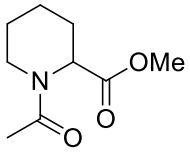

21

Using general procedure F, acetyl chloride (0.12 mL, 1.67 mmol, 3.0 eq.), methyl ester **20** (100 mg, 0.56 mmol, 1.0 eq.) and triethylamine (0.23 mL, 1.67 mmol, 3.0 eq.) in CH_2Cl_2 (2 mL) gave the crude product. Purification by flash chromatography on silica with 80:20 Et_2O-hexane and then Et_2O as eluent gave acetamide **21** (102 mg, 99%) as a colourless oil, R_F (80:20 Et_2O-hexane) 0.2; IR (ATR) 2944, 2861, 1736 (C=O, ester), 1639 (C=O, amide), 1419, 1261, 1204, 999 cm^{-1}; ^{1}H NMR (400 MHz, $CDCl_3$) (80:20 mixture of rotamers) δ 5.38 (d, *J* = 5.5 Hz, 0.8H, NCHCO), 4.58-4.49 (m, 0.4H, NCH), 3.76 (s, 0.6H, OMe), 3.72 (s, 2.4H, OMe), 3.72-3.70 (m,

0.8H, NCH), 3.27 (ddd, *J* = 13.0, 13.0, 3.0 Hz, 0.8H, NCH), 2.60 (ddd, *J* = 13.0, 13.0, 3.0 Hz, 0.2H, NCH), 2.28-2.21 (m, 1H, CH), 2.13 (s, 2.4H, Me), 2.07 (s, 0.6H, Me), 1.77-1.55 (m, 3H, CH), 1.52-1.23 (m, 2H, CH); ^{1}H NMR (400 MHz, DMSO-*d*$_6$) (70:30 mixture of rotamers) δ 5.12 (d, *J* = 5.0 Hz, 0.7H, NCHCO), 4.78 (d, *J* = 5.0 Hz, 0.3H, NCHCO), 4.31 (d, *J* = 12.5 Hz, 0.3H, NCH), 3.74 (br d, *J* = 12.5 Hz, 0.7H, NCH), 3.69 (s, 0.9H, OMe), 3.65 (s, 2.1H, OMe), 3.10 (ddd, *J* = 12.5, 12.5, 3.0 Hz, 0.7H, NCH), 2.42 (ddd, *J* = 12.5, 12.5, 3.0 Hz, 0.3H, NCH), 2.18-2.05 (m, 1H, CH), 2.03 (s, 2.1H, OMe), 1.96 (s, 0.9H, OMe), 1.70-1.13 (m, 5H); ^{13}C NMR (101.6 MHz, $CDCl_3$) (rotamers) δ 171.9 (C=O), 171.4 (C=O), 170.6 (C=O), 170.4 (C=O), 56.8 (OMe), 52.5 (NCH), 52.2 (NCH), 44.2 (NCH_2), 39.2 (NCH_2), 27.2 (CH_2), 26.6 (CH_2), 25.3 (CH_2), 24.4 (CH_2), 21.6 (Me), 21.5 (Me), 20.9 (CH_2), 20.7 (CH_2); MS (ESI) *m/z* 208 [$(M + Na)^+$, 100], 186 [$(M + H)^+$, 10]; HMRS (ESI) *m/z* calcd for $C_9H_{15}NO_3$ $(M + Na)^+$ 208.0944, found 208.0953 (–4.2 ppm error).

Lab Book Reference: mcw/3/50/1

1-(2-(Hydroxymethyl)piperidin-1-yl)ethanone 22

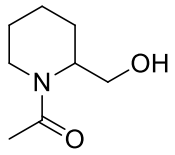

22

Using general procedure B, acetamide **21** (50 mg, 0.27 mmol, 1.0 eq.) in THF (2 mL) and lithium aluminium hydride (10.2 mg, 0.27 mmol, 1.0 eq.) in THF (4 mL) gave the crude product. Purification by flash chromatography on silica with 80:20 Et_2O-hexane and then Et_2O as eluent gave amino alcohol **22** (9 mg, 19%) as a colourless oil, R_F (80:20 Et_2O-hexane) 0.2; ^{1}H NMR (400 MHz, $CDCl_3$) (60:40 mixture of rotamers) δ 4.81-4.69 (m, 0.6H, NCH), 4.54 (br d, *J* = 13.5 Hz, 0.4H, NCH), 4.07-3.95 (m, 0.8H), 3.85-3.72 (m, 0.6H), 3.69-3.59 (m, 1H), 3.56 (dd, *J* = 10.0, 3.5 Hz, 0.4H), 3.20 (ddd, *J* = 12.5, 12.5, 3.5 Hz, 0.6H), 2.62 (br dd, *J* = 12.0, 12.0 Hz, 0.6H), 2.15 (s, 1.2H, Me), 2.12 (s, 1.8H, Me), 1.77-1.21 (m, 6H, CH); ^{13}C NMR (101.6 MHz, $CDCl_3$) (rotamers) δ 171.6 (C=O), 170.8 (C=O), 62.2 (OCH_2), 60.7 (OCH_2), 55.4 (NCH), 51.0 (NCH), 42.7 (NCH_2), 36.6 (NCH_2), 26.1 (CH_2), 25.5 (CH_2), 25.2 (CH_2), 25.1 (CH_2), 22.0

(Me), 21.9 (Me), 19.63 (CH_2), 19.57 (CH_2); MS (ESI) *m/z* 180 [$(M + Na)^+$, 100], 158 [$(M + H)^+$, 15]; HMRS (ESI) *m/z* calcd for $C_8H_{15}NO_2$ $(M + Na)^+$ 180.0995, found 180.0988 (+3.9 ppm error).

Lab Book Reference: mcw/3/61

Using general procedure I, lithium borohydride (1.62 mL of a 4.0 M solution in THF, 6.47 mmol, 8.0 eq.) and methyl ester **21** (150 mg, 0.81 mmol, 1.0 eq.) in THF (10 mL) for 5 h gave the crude product. Purification by flash chromatography on silica with 50:50 EtOAc-hexane and then EtOAc as eluent gave alcohol **22** (36 mg, 29%) as a colourless oil.

Lab book reference: mcw/4/47

Methyl 1-(methylsulfonyl)piperidine-2-carboxylate 23

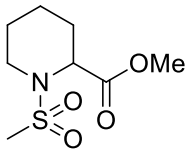

23

Using general procedure G, methanesulfonyl chloride (0.13 mL, 1.67 mmol, 3.0 eq.), methyl ester **20** (100 mg, 0.56 mmol, 1.0 eq.) and triethylamine (0.23 mL, 1.67 mmol, 3.0 eq.) in CH_2Cl_2 (2 mL) gave the crude product. Purification by flash chromatography on silica with 80:20, 50:50, 20:80 hexane-Et_2O and then Et_2O as eluent gave sulfonamide **23** (107 mg, 87%) as a white solid, mp 79-81 °C; R_F (80:20 hexane-Et_2O) 0.2; IR (ATR) 2954, 2851, 1730 (C=O), 1317 (S=O), 1302, 1148 (S=O), 966, 769, 519 cm^{-1}; ^1H NMR (400 MHz, $CDCl_3$) δ 4.75 (d, *J* = 5.0 Hz, 1H, NCHCO), 3.76 (s, 3H, OMe), 3.75-3.69 (m, 1H, NCH), 3.18 (ddd, *J* = 12.5, 12.5, 3.0 Hz, 1H, NCH), 2.94 (s, 3H, Me), 2.29-2.21 (m, 1H, CH), 1.87-1.67 (m, 3H, CH), 1.65-1.52 (m, 1H, CH), 1.31-1.18 (m, 1H, CH); ^{13}C NMR (101.6 MHz, $CDCl_3$) δ 171.9 (C=O), 55.7 (OMe), 52.3 (NCH), 42.4 (NCH_2), 38.8 (Me), 28.0 (CH_2), 24.9 (CH_2), 20.5 (CH_2); MS (ESI) *m/z* 244 [$(M + Na)^+$, 100], 222 [$(M + H)^+$, 10]; HMRS (ESI) *m/z* calcd for $C_8H_{15}NO_4S$ $(M + Na)^+$ 244.0614, found 244.0608 (+2.5 ppm error).

Lab Book Reference mcw/3/51/2

(1-(Methylsulfonyl)piperidin-2-yl)methanol 24

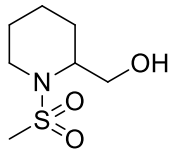

24

Using general procedure B, sulfonamide **23** (50 mg, 0.23 mmol, 1.0 eq.) in THF (2 mL) and lithium aluminium hydride (8.6 mg, 0.23 mmol, 1.0 eq.) in THF (4 mL) gave the crude product. Purification by flash chromatography on silica with 80:20 hexane-Et_2O as eluent gave amino alcohol **24** (42 mg, 85%) as a colourless oil, R_F (80:20 hexane-Et_2O) 0.2; IR (ATR) 3500 (OH), 2932, 2868, 1311 (S=O), 1142 (S=O), 1061, 963, 769, 586 cm^{-1}; ^1H NMR (400 MHz, $CDCl_3$) δ 4.07-3.99 (m, 1H, NCH), 3.91 (dd, *J* = 11.0, 11.0 Hz, 1H, C*H*OH), 3.73-3.66 (m, 1H, NCH), 3.58 (dd, *J* = 11.0, 5.0 Hz, 1H, C*H*OH), 3.11-3.02 (m, 1H, NCH), 2.95 (s, 3H, Me), 2.31 (br s, 1H, OH), 1.76-1.61 (m, 4H, CH), 1.58-1.42 (m, 2H, CH); ^{13}C NMR (101.6 MHz, $CDCl_3$) δ 60.7 (OCH_2), 54.9 (NCH), 40.9 (NCH_2), 40.0 (Me), 26.0 (CH_2), 25.2 (CH_2), 19.4 (CH_2); MS (ESI) *m/z* 216 [$(M + Na)^+$, 100], 194 [$(M + H)^+$, 15]; HMRS (ESI) *m/z* calcd for $C_7H_{15}NO_3S$ $(M + Na)^+$ 216.0665, found 216.0666 (–0.9 ppm error).

Lab Book Reference: mcw/3/60/1

1-*tert*-Butyl 2-methyl 2-methylpiperidine-1,2-dicarboxylate 25

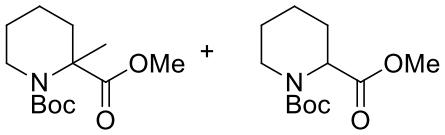

25 **16**

(Table 3.1, Entry 1)

Using general procedure H, lithium bis(trimethylsilyl)amide (0.75 mL of a 1.0 M solution in THF, 0.75 mmol, 1.5 eq.), methyl ester **16** (122 mg, 0.50 mmol, 1.0 eq.) in THF (0.93 mL) and then methyl iodide (0.05 mL, 0.75 mmol, 1.5 eq.) gave the crude product as a 91:9 mixture (by ^1H NMR spectroscopy) of methylated methyl ester **25** and starting methyl ester **16** (95 mg, 68% of methylated ester **25** and 7% of starting ester **16**) as a colourless oil.

Lab Book Reference: mcw/3/34

(Table 3.1, Entry 2)

Using general procedure H, potassium bis(trimethylsilyl)amide (1.5 mL of a 0.5 M solution in toluene, 0.75 mmol, 1.5 eq.) and methyl ester **16** (122 mg, 0.50 mmol, 1.0 eq.) in THF (0.93 mL) and then methyl iodide (0.05 mL, 0.75 mmol, 1.5 eq.) gave the crude product as a 98:2 mixture (by ^{1}H NMR spectroscopy) of methylated methyl ester **25** and starting methyl ester **16** (126 mg, 96% of methylated ester **25** and 2% of starting ester **16**) as a colourless oil.

Lab Book Reference: mcw/3/35

(Table 3.1, Entry 3)

Using general procedure H, lithium bis(trimethylsilyl)amide (0.75 mL of a 1.0 M solution in THF, 0.75 mmol, 1.5 eq.), methyl ester **16** (122 mg, 0.50 mmol, 1.0 eq.) and *N,N′*-dimethylpropylene urea (0.09 mL, 0.75 mL, 1.5 eq.) in THF (0.93 mL) and then methyl iodide (0.05 mL, 0.75 mmol, 1.5 eq.) gave the crude product as a 42:58 mixture (by ^{1}H NMR spectroscopy) of methylated methyl ester **25** and starting methyl ester **16** (141 mg, 72% of methylated ester **25** and 40% of starting ester **16**) as a colourless oil.

Lab Book Reference: mcw/3/36

Using general procedure H, potassium bis(trimethylsilyl)amide (15 mL of a 0.5 M solution in toluene, 7.50 mmol, 1.5 eq.) and methyl ester **16** (1.22 mg, 5.00 mmol, 1.0 eq.) in THF (10 mL) and then methyl iodide (0.47 mL, 7.50 mmol, 1.5 eq.) gave the crude product as a 95:5 mixture (by ^{1}H NMR spectroscopy) of methylated methyl ester **25** and starting methyl ester **16** (1.26 g, 94% of methylated ester **25** and 5% of starting ester **16**) as a colourless oil, R_F (80:20 hexane-Et_2O) 0.2; ^{1}H NMR (400 MHz, $CDCl_3$) for **25**: δ 3.84 (ddd, *J* = 13.5, 4.0, 4.0 Hz, 1H, NCH), 3.70 (s, 3H, OMe), 2.95 (br dd, *J* = 13.5, 13.5 Hz, 1H, NCH), 1.92-1.77 (m, 1H, CH), 1.75-1.53 (m, 5H, CH), 1.40 (s, 9H, CMe_3).^{13}C NMR (101.6 MHz, $CDCl_3$) for **16**: δ 175.6 (C=O, CO_2Me), 155.5 (C=O, Boc), 79.9 (*C*Me_3), 60.3 (NCH_2), 52.0 (OMe), 41.0 (CH_2), 34.8 (CH_2), 28.2 (C*Me*$_3$), 23.7 (Me), 18.4 (CH_2). Spectroscopic data for **25** consistent with those reported in the literature.[68]

Lab Book Reference: mcw/3/49/1

tert-Butyl 2-(hydroxymethyl)-2-methylpiperidine-1-carboxylate 34

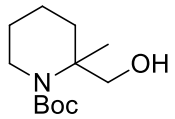

34

Using general procedure B, a 95:5 mixture of methyl esters **25** and **16** (200 mg, 190 mg of **25** (0.74 mmol) and 10 mg of **16** (0.041 mmol)) in THF (5 mL) and lithium aluminium hydride (30 mg, 0.78 mmol, 1.0 eq.) in THF (30 mL) gave the crude product. Purification by flash chromatography on silica with 70:30 and then 50:50 hexane-Et_2O as eluent gave methylated amino alcohol **34** (111 mg, 65% from **25**) as a colourless oil, R_F (50:50 hexane-Et_2O) 0.4; ^{1}H NMR (400 MHz, $CDCl_3$) δ 4.70 (br s, 1H, OH), 3.85 (br ddd, J = 12.0, 4.0, 4.0 Hz, 1H, NCH), 3.67-3.59 (m, 2H, C*H*OH), 2.96 (ddd, J = 13.5, 12.0, 3.0 Hz, 1H, NCH), 1.68-1.56 (m, 5H, CH), 1.44 (s, 9H. CMe_3), 1.36-1.31 (m, 1H, CH), 1.23 (s, 3H, Me); ^{13}C NMR (101.6 MHz, $CDCl_3$) δ 156.4 (C=O), 80.0 (*C*Me_3), 71.4 (OCH_2), 59.5 (*C*Me), 42.5 (NCH_2), 35.4 (CH_2), 28.4 (C*Me*$_3$), 24.9 (CH_2), 19.6 (CH_2), 18.2 (Me) and amino alcohol **17** (8 mg, 100% from **16**). Spectroscopic data for **34** consistent with those reported in the literature.[68]

Lab Book Reference: mcw/3/56/1

2-(Hydroxymethyl)-2-methylpiperidine hydrochloride salt A1.HCl

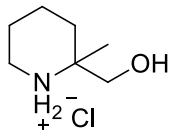

A1.HCl

Using general procedure D, hydrogen chloride (3.49 mL of a 1.0 M solution in Et_2O, 3.49 mmol, 8.0 eq.) and *N*-Boc amino alcohol **34** (100 mg, 0.44 mmol, 1.0 eq.) in Et_2O (1.75 mL) gave amine hydrochloride salt **A1.HCl** (68 mg, 94%) as a white solid, mp 120-122 °C; IR (ATR) 3345 (OH or NH), 2943, 2870, 2747, 1671, 1394, 1274, 1253, 1156, 1049 cm^{-1}; ^{1}H NMR (400 MHz, DMSO-d_6) δ 8.95 (s, 1H, NH), 8.46 (s, 1H,

NH), 3.96 (br s, 1H, OH), 3.55 (d, *J* = 11.5 Hz, 1H, C*H*OH), 3.39 (d, *J* = 11.5 Hz, 1H, C*H*OH), 2.97-2.89 (m, 2H, NCH), 1.65-1.54 (m, 5H, CH), 1.46-1.42 (m, 1H, CH), 1.22 (s, 3H, Me); ^{13}C NMR (101 MHz, DMSO-d_6) δ 65.0 (OCH_2), 57.3 (*C*Me), 39.0 (NCH_2), 29.45 (CH_2), 21.5 (CH_2), 18.1 (Me), 17.6 (CH_2); MS (ESI) *m/z* 130 [M^+, 100]; HMRS (ESI) *m/z* calcd for $C_7H_{16}NO$ M^+ 130.1226, found 130.1231 (–3.9 ppm error).

Lab Book Reference: mcw/5/15/c

(1,2-Dimethylpiperidin-2-yl)methanol A2

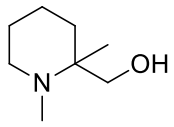

A2

Using general procedure E, *N*-Boc piperidine **34** (200 mg, 0.88 mmol, 1.0 eq.) in THF (20 mL) and lithium aluminium hydride (165 mg, 4.36 mmol, 5.0 eq.) in THF (30 mL) gave *N*-methyl piperidine **A2** (96 mg, 76%) as a colourless oil, IR (ATR) 3350 (OH), 2930, 2862, 1450, 1371, 1106, 1051, 669 cm^{-1}; ^{1}H NMR (400 MHz, $CDCl_3$) δ 3.55 (d, *J* = 10.5 Hz, 1H, C*H*OH), 3.08 (d, *J* = 10.5 Hz, 1H, C*H*OH), 2.65 (br d, *J* = 12.0, 1H, NCH), 2.44 (ddd, *J* = 12.0, 12.0, 3.0 Hz, 1H, NCH), 2.17 (s, 3H, NMe), 1.88-1.78 (m, 1H, CH), 1.62-1.57 (m, 2H, CH), 1.49-1.40 (m, 2H), 1.32-1.24 (m, 1H, CH), 0.86 (s, 3H, Me); ^{13}C NMR (101.6 MHz, $CDCl_3$) (*C*Me not resolved) δ 62.8 (OCH_2), 50.8 (NCH_2), 37.3 (NMe), 34.1 (CH_2), 29.8 (CH_2), 20.5 (CH_2), 11.7 (Me); MS (ESI) *m/z* 144 [$(M + H)^+$, 100]; HMRS (ESI) *m/z* calcd for $C_8H_{17}NO$ $(M + H)^+$ 144.1383, found 144.1384 (–0.6 ppm error).

Lab book reference: mcw/3/98

1-*tert*-Butyl 3-methyl piperidine-1,3-dicarboxylate 36

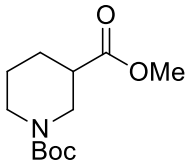

36

Using general procedure A, thionyl chloride (1.85 mL, 25.5 mmol, 1.1 eq.), carboxylic acid **35** (3.00 g, 23.2 mmol, 1.0 eq.) in MeOH (40 mL) and then triethylamine (3.24 mL, 23.2 mmol, 1.0 eq.) in CH_2Cl_2 (20 mL) and di-*tert*-butyl dicarbonate (5.07 g, 23.2 mmol, 1.0 eq.) in CH_2Cl_2 (20 mL) gave the crude product. Purification by flash chromatography on silica with 80:20 hexane-Et_2O as eluent gave methyl ester **36** (4.56 g, 81%) as a yellow solid, mp 43-45 °C; R_F (80:20 hexaneEt_2O) 0.2; ^{1}H NMR (400 MHz, $CDCl_3$) δ 4.07 (br s, 1H, NCH), 3.89 (br d, *J* = 13.0 Hz, 1H, NCH), 3.66 (s, 3H, OMe), 2.96 (br s, 1H, NCH), 2.79 (ddd, *J* = 13.0, 11.0, 3.0 Hz, 1H, NCH), 2.43 (dddd, *J* = 10.5, 10.5, 3.5, 3.5 Hz, 1H, C*H*CO_2Me), 2.06-1.98 (m, 1H, CH), 1.72-1.62 (m, 1H, CH), 1.61-1.51 (m, 1H, CH), 1.49-1.35 (m, 10H, CH and CMe_3); ^{13}C NMR (101.6 MHz, $CDCl_3$) δ 173.8 (C=O, CO_2Me), 154.6 (C=O, Boc), 79.6 (*C*Me_3), 51.7 (OMe), 45.4 (NCH_2), 43.6 (NCH_2), 41.3 (CH), 28.4 (C*Me*$_3$), 27.3 (CH_2), 24.2 (CH_2). Spectroscopic data consistent with those reported in the literature.[130]

Lab Book reference: mcw/3/15/2

1-*tert*-Butyl 3-methyl 3-methylpiperidine-1,3-dicarboxylate 37

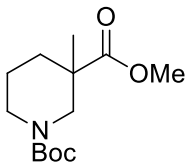

37

Using general procedure H, potassium bis(trimethylsilyl)amide (15 mL of a 0.5 M solution in toluene, 7.50 mmol, 1.5 eq.) and methyl ester **36** (1.22 mg, 5.00 mmol, 1.0 eq.) in THF (10 mL) and then methyl iodide (0.47 mL, 7.50 mmol, 1.5 eq.) gave the crude product. Purification by flash chromatography on silica with 80:20 hexane-Et_2O as eluent gave methylated piperidine **37** (1.25 g, 97%) as a colourless oil, IR (ATR)

2974, 2863, 1731 (C=O, CO_2Me), 1689 (C=O, Boc), 1422, 1364, 1277, 1152, 1001, 866 cm^{-1}; ^1H NMR (400 MHz, $CDCl_3$) δ 3.84 (d, *J* = 13.0 Hz, 1H, NCH), 3.67 (s, 3H, OMe), 3.49-3.38 (m, 1H, NCH), 3.28-3.18 (m, 1H, NCH), 3.11 (d, *J* = 13.0 Hz, 1H, NCH), 2.06-1.97 (m, 1H, CH), 1.62-1.52 (m, 2H, CH), 1.46-1.40 (m, 1H, CH), 1.44 (s, 9H, CMe_3), 1.15 (s, 3H, Me); ^{13}C NMR (101.6 MHz, $CDCl_3$) (NCH_2 signal not resolved) δ 176.3 (C=O, CO_2Me), 154.7 (C=O, Boc), 79.3 (*C*Me_3), 51.8 (OMe), 42.6 (NCH_2), 33.6 (CH_2), 28.4 (C*Me*$_3$), 22.1 (Me), 21.8 (CH_2); MS (ESI) *m/z* 280 [(M + $Na)^+$, 100], 258 [(M + $H)^+$, 15]; HMRS (ESI) *m/z* calcd for $C_{13}H_{23}NO_4$ (M + $Na)^+$ 280.1519, found 280.1512 (+2.7 ppm error).

Lab Book Reference: mcw/3/72/1

tert-Butyl 3-(hydroxymethyl)-3-methylpiperidine-1-carboxylate 38

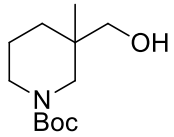

38

Using general procedure B, methyl ester **37** (400 mg, 1.55 mmol, 1.0 eq.) in THF (5 mL) and lithium aluminium hydride (59 mg, 1.55 mmol, 1.0 eq.) in THF (25 mL) gave the crude product. Purification by flash chromatography on silica with 50:50 hexane-Et_2O as eluent gave amino alcohol **38** (323 mg, 91%) as a colourless oil, R_F (50:50 Et_2O-hexane) 0.3; IR (ATR) 3446 (OH), 2933, 2862, 1663 (C=O), 1426, 1364, 1245, 1156, 766 cm^{-1}; ^1H NMR (400 MHz, $CDCl_3$) δ 3.83 (d, *J* = 11.5 Hz, 1H, CH), 3.53 (dd, *J* = 11.5, 3.0 Hz, 1H, CH), 3.46-2.80 (m, 3H, CH), 2.51 (d, *J* = 12.5 Hz, 1H, CH), 1.69 (br s, 1H, CH), 1.57-1.39 (m, 2H, CH), 1.46 (s, 9H, CMe_3), 1.38-1.28 (m, 1H, CH), 0.91 (s, 3H, Me); ^{13}C NMR (101.6 MHz, $CDCl_3$) δ 156.2 (C=O), 79.8 (*C*Me_3), 66.0 (OCH_2), 50.2 (NCH_2), 45.4 (NCH_2), 35.9 (*C*Me(CH_2OH)), 33.5 (CH_2), 28.4 (C*Me*$_3$), 23.2 (Me), 21.6 (CH_2); MS (ESI) *m/z* 252 [(M + $Na)^+$, 100]; HMRS (ESI) *m/z* calcd for $C_{12}H_{23}NO_3$ (M + $Na)^+$ 252.1570, found 252.1561 (+3.8 ppm error).

Lab Book Reference: mcw/4/35

3-(Hydroxymethyl)-3-methylpiperidine hydrochloride salt A5.HCl

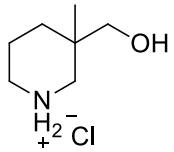

A5.HCl

Using general procedure D, hydrogen chloride (1.74 mL of a 2.0 M solution in Et_2O, 3.49 mmol, 8.0 eq.) and *N*-Boc amino alcohol **38** (100 mg, 0.44 mmol, 1.0 eq.) in Et_2O (1 mL) gave amine hydrochloride salt **A5.HCl** (72 mg, 100%) as a thick colourless oil, IR (ATR) 3362 (OH or NH), 2943, 2805, 2729, 1595, 1451, 1027, 519 cm^{-1}; ^1H NMR (400 MHz, DMSO-d_6) δ 8.51 (br s, 2H, NH_2), 4.86 (br s, 1H, OH), 3.25 (d, *J* = 10.5 Hz, 1H, C*H*OH), 3.20 (d, *J* = 10.5 Hz, 1H, C*H*OH), 2.98 (ddd, *J* = 12.5, 5.0, 5.0 Hz, 1H, NCH), 2.88-2.80 (m, 2H, CH), 2.75 (d, *J* = 12.5 Hz, 1H, NCH), 1.69-1.62 (m, 2H, CH), 1.55-1.47 (m, 1H, CH), 1.51 (ddd, *J* = 12.5, 5.0, 5.0, 1H, CH), 0.92 (s, 3H, Me); ^{13}C NMR (101.6 MHz, DMSO-d_6) δ 67.2 (OCH_2), 49.2 (NCH_2), 43.3 (NCH_2), 33.9 (*C*Me), 29.8 (CH_2), 20.8 (Me), 18.2 (CH_2); MS (ESI) *m/z* 130 [M^+, 100]; HMRS (ESI) *m/z* calcd for $C_7H_{16}NO$ M^+ 130.1226, found 130.1231 (–3.5 ppm error).

Lab Book Reference: mcw/5/11

(1,3-Dimethylpiperidin-3-yl)methanol A6

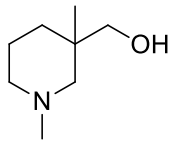

A6

Using general procedure E, *N*-Boc piperidine **37** (257 mg, 1.00 mmol, 1.0 eq.) in THF (20 mL) and lithium aluminium hydride (190 mg, 5.00 mmol, 5.0 eq.) in THF (30 mL) gave *N*-methyl piperidine **A6** (138 mg, 96%) as a colourless oil, IR (ATR) 3337 (OH), 2934, 2777, 1447, 1211, 1054, 811 cm^{-1}; ^1H NMR (400 MHz, $CDCl_3$) δ 3.62 (dd, *J* = 10.5, 1.5 Hz, 1H, C*H*OH), 3.56 (dd, *J* = 10.5, 1.5 Hz, 1H, C*H*OH), 2.67 (br s, 2H, NCH), 2.20 (s, 3H, NMe), 2.11-2.01 (m, 1H, CH), 1.96 (br d, *J* = 10.5 Hz, 2H, NCH), 1.65-1.54 (m, 2H, CH), 1.26-1.14 (m, 1H, CH), 0.77 (s, 3H, Me); ^{13}C NMR (101.6 MHz, $CDCl_3$) δ 74.3 (OCH_2), 62.8 (NCH_2), 55.9 (NCH_2), 46.4 (Me), 34.9 (CH_2), 34.4

(*C*Me), 29.9 (CH_2), 23.1 (Me); MS (ESI) *m/z* 144 [$(M + H)^+$, 100]; HMRS (ESI) *m/z* calcd for $C_8H_{17}NO$ $(M + H)^+$ 144.1383, found 144.1379 (+2.7 ppm error).

Lab Book Reference: mcw/3/80

1-*tert*-Butyl 4-methyl piperidine-1,4-dicarboxylate 31

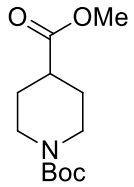

31

Using general procedure A, thionyl chloride (3.09 mL, 42.6 mmol, 1.1 eq.), carboxylic acid **38** (5.00 g, 38.7 mmol, 1.0 eq.) in MeOH (50 mL) and then triethylamine (5.40 mL, 38.7 mmol, 1.0 eq.) in CH_2Cl_2 (25 mL) and di-*tert*-butyl dicarbonate (8.45g, 38.7 mmol, 1.0 eq.) in CH_2Cl_2 (25 mL) gave the crude product. Purification by flash chromatography on silica with 80:20 hexane-Et_2O as eluent gave methyl ester **31** (7.98 g, 85%) as a colourless oil, R_F (80:20 hexaneEt_2O) 0.1; IR (ATR) 2953, 2860, 1734 (C=O, CO_2Me), 1689 (C=O, Boc), 1448, 1419, 1365, 1158, 1038, 768 cm^{-1}; ^1H NMR (400 MHz, $CDCl_3$) δ 4.01 (br d, *J* = 13.5 Hz, 2H, NCH), 3.68 (s, 3H, OMe), 2.81 (ddd, *J* = 13.5, 11.5, 3.0 Hz, 2H, NCH), 2.44 (tt, *J* = 11.0, 4.0 Hz, 1H, C*H*CO_2Me), 1.91-1.81 (m, 2H, CH), 1.67-1.55 (m, 2H, CH), 1.45 (s, 9H, CMe_3); ^{13}C NMR (101.6 MHz, $CDCl_3$) δ 175.0 (C=O, CO_2Me), 154.7 (C=O, Boc), 79.6 (*C*Me_3), 51.8 (OMe), 43.1 (NCH_2), 41.0 (CH), 28.4 (C*Me*$_3$), 27.9 (CH_2); MS (ESI) *m/z* 266 [$(M + Na)^+$, 100]; HMRS (ESI) *m/z* calcd for $C_{12}H_{21}NO_4$ $(M + Na)^+$ 266.1363, found 266.1355 (+2.6 ppm error).

Lab Book Reference: mcw/3/3/2

1-*tert*-Butyl 4-methyl 4-methylpiperidine-1,4-dicarboxylate 33

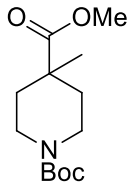

33

Using general procedure H, potassium bis(trimethylsilyl)amide (15 mL of a 0.5 M solution in toluene, 7.50 mmol, 1.5 eq.) and methyl ester **31** (1.22 mg, 5.00 mmol, 1.0 eq.) in THF (10 mL) and then methyl iodide (0.47 mL, 7.50 mmol, 1.5 eq.) gave the crude product. Purification by flash chromatography on silica with 80:20 hexane-Et_2O as eluent gave methylated piperidine ester **33** (1.29 g, 100%) as a colourless oil, R_F (80:20 hexane-Et_2O) 0.3; IR (ATR) 2971, 2872, 1729 (C=O, CO_2Me), 1691 (C=O, Boc), 1459, 1419, 1169, 1147, 1110, 872 cm^{-1}; ^1H NMR (400 MHz, $CDCl_3$) δ 3.79-3.71 (m, 2H, NCH), 3.70 (s, 3H, OMe), 2.98 (br dd, J = 11.0, 11.0 Hz, 2H, NCH), 2.09-2.02 (m, 2H, CH), 1.45 (s, 9H, CMe_3), 1.35 (ddd, J = 14.5, 11.0, 4.5 Hz, 2H, CH), 1.20 (s, 3H, Me); ^{13}C NMR (101.6 MHz, $CDCl_3$) δ 177.0 (C=O, CO_2Me), 154.9 (C=O, Boc), 79.4 (CMe_3), 51.9 (OMe), 41.7 (CMe), 41.2 (NCH_2), 34.6 (CH_2), 28.4 (CMe_3), 25.8 (Me); MS (ESI) *m/z* 280 [$(M + Na)^+$, 100]; HMRS (ESI) *m/z* calcd for $C_{13}H_{23}NO_4$ $(M + Na)^+$ 280.1519, found 280.1510 (+3.1 ppm error).

Lab Book Reference: mcw/3/5/1

***tert*-Butyl 4-(hydroxymethyl)-4-methylpiperidine-1-carboxylate 39**

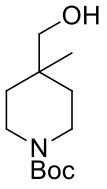

39

Using general procedure B, methyl ester **33** (200 mg, 0.78 mmol, 1.0 eq.) in THF (5 mL) and lithium aluminium hydride (29.5 mg, 0.78 mmol, 1.0 eq.) in THF (30 mL) gave the crude product. Purification by flash chromatography on silica with 50:50 hexane-Et_2O as eluent gave amino alcohol **39** (268 mg, 100%) as a colourless oil, R_F

(50:50 Et_2O-hexane) 0.3; IR (ATR) 3435 (OH), 2972, 2817, 1666 (C=O), 1423, 1247, 1158, 1047, 860, 735 cm^{-1}; ^1H NMR (400 MHz, $CDCl_3$) δ 3.67 (br d, *J* = 10.5 Hz, 2H, NCH), 3.37 (s, 2H, C*H*$_2$OH), 3.12 (ddd, *J* = 13.5, 10.5, 3.0 Hz, 2H, NCH), 1.53-1.40 (m, 11H, CH and CMe_3), 1.32-1.23 (m, 2H, CH), 0.98 (s, 3H, Me); ^{13}C NMR (101.6 MHz, $CDCl_3$) δ 154.9 (C=O), 79.3 (*C*Me_3), 71.7 (OCH_2), 39.9 (NCH_2), 33.8 (*C*Me), 33.1 (CH_2), 28.4 (C*Me*$_3$), 20.5 (Me); MS (ESI) *m/z* 252 [$(M + Na)^+$, 100], 230 [$(M + H)^+$, 10]; HMRS (ESI) *m/z* calcd for $C_{12}H_{23}NO_3$ $(M + Na)^+$ 252.1570, found 252.1567 (+1.1 ppm error).

Lab Book Reference: mcw/3/73/1

4-(Hydroxymethyl)-4-methylpiperidine hydrochloride salt A9.HCl

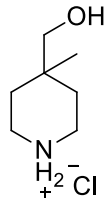

A9.HCl

Using general procedure D, hydrogen chloride (1.74 mL of a 2.0 M solution in Et_2O, 3.49 mmol, 8.0 eq.) and *N*-Boc amino alcohol **39** (100 mg, 0.44 mmol, 1.0 eq.) in Et_2O (1 mL) gave amine hydrochloride salt **A9·HCl** (72 mg, 100%) as a white solid, mp 120-122 °C; IR (ATR) 3193 (OH or NH), 2984, 2744, 2665, 1610, 1468, 1027, 701, 611 cm^{-1}; ^1H NMR (400 MHz, DMSO-d_6) δ 8.50 (s, 2H, NH_2), 3.17 (d, *J* = 5.0 Hz, 2H, C*H*$_2$OH), 3.06 (ddd, *J* = 12.5, 4.0, 4.0 Hz, 2H, NCH), 2.96 (ddd, *J* = 12.5, 10.0, 4.0 Hz, 2H, NCH), 1.62 (ddd, *J* = 14.5, 10.0, 4.0 Hz, 2H, CH), 1.38 (br s, 1H, OH), 1.34 (ddd, *J* = 14.5, 4.0, 4.0 Hz, 2H, CH); ^{13}C NMR (101.6 MHz, DMSO-d_6) δ 68.9 (OCH_2), 32.6 (NCH_2), 29.8 (CH_2), 28.1 (*C*Me), 21.2 (Me); MS (ESI) *m/z* 130 [M^+, 100]; HMRS (ESI) *m/z* calcd for $C_7H_{16}NO$ M^+ 130.1226, found 130.1228 (–1.5 ppm error).

Lab Book Reference: mcw/5/12

***tert*-Butyl 2-((triisopropylsilyloxy)methyl)piperidine-1-carboxylate 55**

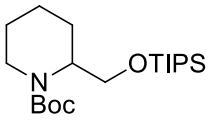

55

Triisopropylsilyl chloride (0.60 mL, 2.79 mmol, 1.2 eq.) was added dropwise to a stirred solution of *N*-Boc piperidine **17** (500 mg, 2.32 mmol, 1.0 eq.) and imidazole (395 mg, 5.81 mmol, 2.5 eq.) in DMF (6 mL) at rt under Ar. The resulting mixture was stirred at rt for 16 h. Saturated $NH_4Cl_{(aq)}$ (10 mL) was added and the mixture was extracted with Et_2O (3 x 5 mL). The combined organic extracts were dried ($MgSO_4$) and evaporated under reduced pressure to give the crude product. Purification by flash chromatography on silica with 95:5 petrol-EtOAc as the eluent gave protected *N*-Boc piperidine **55** (794 mg, 92%) as a colourless oil, R_F (9:1 petrol-EtOAc) 0.4; IR (ATR) 2940, 2865, 1693 (C=O), 1407, 1364, 1170, 1138, 1112, 882, 680, 658 cm^{-1}; ^1H NMR (400 MHz, $CDCl_3$) δ 4.18 (br s, 1H, NCH), 3.99 (d, *J* = 12.5 Hz, 1H, NCH), 3.78 (dd, *J* = 9.5, 9.5 Hz, 1H, OCH), 3.65 (dd, *J* = 9.5, 5.5 Hz, 1H, OCH), 2.74 (dd, *J* = 12.5, 12.5 Hz, 1H, NCH), 1.95-1.90 (m, 1H, CH), 1.68-1.35 (m, 5H, CH), 1.43 (s, 9H, CMe_3) 1.11-1.01 (m, 21H, $Si(CHMe_2)_3$); ^{13}C NMR (101.6 MHz, $CDCl_3$) δ 155.2 (C=O), 79.2 (*C*Me_3), 61.0 (OCH_2), 51.7 (NCH), 40.0 (NCH_2), 28.5 (C*Me*$_3$), 25.3 (CH_2), 24.4 (CH_2), 19.1 (CH_2), 18.0 (SiCH*Me*$_2$), 11.9 (SiCH); MS (ESI) *m/z* 394 [(M + Na)$^+$, 100], 372 [(M + H)$^+$, 10]; HMRS (ESI) *m/z* calcd for $C_{20}H_{41}NO_3Si$ (M + Na)$^+$ 394.2748, found 394.2748 (+0.3 ppm error).

Lab Book Reference: mcw/2/8

***tert*-Butyl 2-methyl-6-((triisopropylsilyloxy)methyl)piperidine-1-carboxylate *trans*-56**

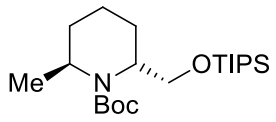

trans-**56**

s-BuLi (0.72 mL of a 1.3 M solution in hexane, 0.94 mmol, 1.3 eq.) was added dropwise to a stirred solution of *N*-Boc piperidine **55** (268 mg, 0.72 mmol, 1.0 eq.) and TMEDA (0.14 mL, 0.94 mmol, 1.3 eq.) in Et_2O (8 mL) at –50 °C under Ar. The resulting yellow solution was stirred at –50 °C for 1 h. Then, Me_2SO_4 (0.14 mL, 1.44 mmol, 2.0 eq.) was added. The resulting solution was stirred at –50 °C for 10 min before being allowed to warm to rt over 4 h and stirred at rt for 14 h. Saturated $NH_4Cl_{(aq)}$ (10 mL) was added and the mixture was extracted with Et_2O (3 x 10 mL). The combined organic extracts were dried ($MgSO_4$) and evaporated under reduced pressure to give the crude product. Purification by flash chromatography on silica with 98:2, 97:3 and 95:5 petrol-EtOAc as eluent gave disubstituted piperidine *trans*-**56** (115 mg, 41%) as a colourless oil, R_F (97:3 petrol-EtOAc) 0.2; IR (ATR) 2942, 2866, 1691 (C=O), 1386, 1363, 1177, 1161, 1087, 881, 680 cm^{-1}; ^1H NMR (400 MHz, $CDCl_3$) δ 4.03-3.93 (m, 1H, NCH), 3.86-3.79 (m, 1H, NCH), 3.74 (dd, *J* = 9.5, 4.0 Hz, 1H, OCH), 3.56 (dd, *J* = 9.5, 9.5 Hz, 1H, OCH), 2.05-1.96 (m, 1H, CH), 1.88-1.73 (m, 2H, CH), 1.70-1.49 (m, 4H, CH), 1.44 (s, 9H, CMe_3), 1.22 (d, *J* = 6.5 Hz, 3H, CH*Me*), 1.09-1.01 (m, 20H, $Si(CHMe_2)_3$); ^{13}C NMR (101.6 MHz, $CDCl_3$) δ 155.1 (C=O), 79.0 (*C*Me_3), 64.2 (OCH_2), 52.8 (NCH), 46.7 (NCH), 28.5 (C*Me*$_3$), 27.0 (CH_2), 20.6 (CH_2), 20.5 (Me), 18.0 (SiCH*Me*$_2$), 13.3 (CH_2), 12.3 (SiCH); MS (ESI) *m/z* 408 [$(M + Na)^+$, 100], 386 [$(M + H)^+$, 5]; HMRS (ESI) *m/z* calcd for $C_{21}H_{43}NO_3Si$ $(M + H)^+$ 386.3085, found 386.3088 (–0.7 ppm error) and recovered starting material **55** (152 mg, 57%) as a colourless oil.

Lab Book Reference: mcw/1/96

s-BuLi (1.0 mL of a 1.3 M solution in hexane, 1.3 mmol, 1.3 eq.) was added dropwise to a stirred solution of *N*-Boc piperidine **55** (372 mg, 1.0 mmol, 1.0 eq.) and TMEDA (0.195 mL, 1.3 mmol, 1.3 eq.) in Et_2O (10 mL) at –78 °C under Ar. The resulting

yellow solution was stirred at –78 °C for 3 h. Then, Me_2SO_4 (0.19 mL, 2.0 mmol, 2.0 eq.) was added. The resulting solution was stirred at –78 °C for 10 min before being allowed to warm to rt over 4 h and stirred at rt for 14 h. Saturated $NH_4Cl_{(aq)}$ (10 mL) was added and the mixture was extracted with Et_2O (3 x 10 mL). The combined organic extracts were dried ($MgSO_4$) and evaporated under reduced pressure to give the crude product. Purification by flash chromatography on silica with 98:2, 97:3 and 95:5 petrol-EtOAc as eluent gave disubstituted piperidine **56** (101 mg, 29%) as a colourless oil and recovered starting material **55** (191 mg, 52%) as a colourless oil.

Lab Book Reference: mcw/1/95

tert-Butyl 2-methylpiperidine-1-carboxylate 49

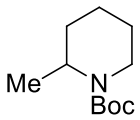

49

2-Methyl piperidine **58** (5.0 mL, 42.5 mmol, 1.0 eq.) was added dropwise to a stirred solution of di-*tert*-butyl dicarbonate (10.2 g, 46.8 mmol, 1.1 eq.) in CH_2Cl_2 (200 mL) at 0 °C under Ar. The resulting solution was allowed to warm to rt and stirred at rt for 16 h. H_2O (20 mL) was added and the mixture was extracted with CH_2Cl_2 (3 x 15 mL). The combined organic extracts were dried ($MgSO_4$) and evaporated under reduced pressure to give the crude product. Purification by flash chromatography on silica with 90:10 petrol-Et_2O as eluent gave *N*-Boc methyl piperidine **49** (7.6 g, 82%) as a colourless oil, R_F (90:10 petrol-Et_2O) 0.3; ^{1}H NMR (400 MHz, $CDCl_3$) δ 4.41-4.30 (m, 1H, NCH), 3.90 (dd, *J* = 13.5, 3.0 Hz, 1H, NCH), 2.79 (ddd, *J* = 13.5, 13.5, 2.5 Hz, 1H, NCH), 1.68-1.45 (m, 5H CH), 1.44 (s, 9H, CMe_3), 1.40-1.32 (m, 1H, CH), 1.10 (d, *J* = 7.0 Hz, 3H, Me); ^{13}C NMR (101.6 MHz, $CDCl_3$) δ 155.0 (C=O), 79.0 (*C*Me_3), 46.0 (NCH), 38.6 (NCH_2), 30.1 (CH_2), 28.5 (C*Me*$_3$), 25.7 (CH_2), 18.7 (CH_2), 15.7 (Me). Spectroscopic data consistent with those reported in the literature.[131]

Lab Book Reference: mcw/2/2

(2*S,6*R**)-*tert*-Butyl 2-methyl-6-(trimethylsilyl)piperidine-1-carboxylate *trans*-59**

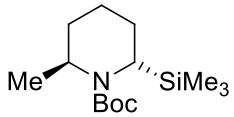

trans-**59**

(Table 3.3, Entry 5)

s-BuLi (1.0 mL of a 1.3 M solution in hexane, 1.3 mmol, 1.3 eq.) was added dropwise to a stirred solution of *N*-Boc piperidine **49** (199 mg, 1.0 mmol, 1.0 eq.) and TMEDA (0.19 mL, 1.3 mmol, 1.3 eq.) in Et_2O (7 mL) at –40 °C under Ar. The resulting yellow solution was stirred at –40 °C for 1.5 h. Then, trimethylsilyl chloride (0.16 mL, 1.3 mmol, 1.3 eq.) was added. The resulting solution was stirred at –40 °C for 10 min before being allowed to warm to rt over 4 h and stirred at rt for 14 h. Saturated $NH_4Cl_{(aq)}$ (10 mL) was added and the mixture was extracted with Et_2O (3 x 10 mL). The combined organic extracts were dried ($MgSO_4$) and evaporated under reduced pressure to give the crude product. Purification by flash chromatography on silica with 95:5 and then 50:50 hexane-Et_2O as eluent gave disubstituted piperidine *trans*-**59** (230 mg, 85%) as a colourless oil, R_F (95:5 hexane-Et_2O) 0.6; IR (ATR) 2974, 2929, 2861, 1685 (C=O), 1418, 1296, 1244, 1170, 1107, 835, 636 cm^{-1}; ^1H NMR (400 MHz, $CDCl_3$) δ 4.33-4.20 (m, 1H, NCH), 2.45 (br d, J = 10.5 Hz, 1H, NCH), 1.70-1.51 (m, 4H, CH), 1.43 (s, 9H, CMe_3), 1.40-1.35 (m, 2H), 1.17 (d, J = 7.0 Hz, 3H, Me), 0.04 (s, 9H, $SiMe_3$); ^{13}C NMR (101.6 MHz, $CDCl_3$) δ 155.3 (C=O), 78.6 (*C*Me_3), 48.2 (NCH), 42.2 (NCH), 30.0 (CH_2), 28.5 (C*Me*$_3$), 26.4 (CH_2), 20.5 (CH_2), 17.0 (Me), –0.3 ($SiMe_3$); MS (ESI) *m/z* 294 [$(M + Na)^+$, 100], 272 [$(M + H)^+$, 5]; HMRS (ESI) *m/z* calcd for $C_{14}H_{29}NO_2Si$ $(M + H)^+$ 294.1860, found 294.1857 (+7.1 ppm error).

Lab Book Reference: mcw/2/92/1

(Table 3.3, entry 1)

s-BuLi (1.0 mL of a 1.3 M solution in hexane, 1.3 mmol, 1.3 eq.) was added dropwise to a stirred solution of *N*-Boc piperidine **49** (199 mg, 1.0 mmol, 1.0 eq.) and TMEDA (0.19 mL, 1.3 mmol, 1.3 eq.) in Et_2O (7 mL) at –78 °C under Ar. The resulting yellow solution was stirred at –78 °C for 3 h. Then, trimethylsilyl chloride (0.16 mL, 1.3

mmol, 1.3 eq.) was added. The resulting solution was stirred at –78 °C for 10 min before being allowed to warm to rt over 4 h and stirred at rt for 14 h. Saturated $NH_4Cl_{(aq)}$ (10 mL) was added and the mixture was extracted with Et_2O (3 x 10 mL). The combined organic extracts were dried ($MgSO_4$) and evaporated under reduced pressure to give the crude product. Purification by flash chromatography on silica with 95:5 and 50:50 hexane-Et_2O as eluent gave disubstituted piperidine *trans*-**59** (171 mg, 63%) as a colourless oil.

(Table 3.3, Entry 2)

s-BuLi (1.0 mL of a 1.3 M solution in hexane, 1.3 mmol, 1.3 eq.) was added dropwise to a stirred solution of *N*-Boc piperidine **49** (199 mg, 1.0 mmol, 1.0 eq.) and TMEDA (0.19 mL, 1.3 mmol, 1.3 eq.) in Et_2O (7 mL) at –78 °C under Ar. The resulting yellow solution was stirred at –78 °C for 1 h. Then, trimethylsilyl chloride (0.16 mL, 1.3 mmol, 1.3 eq.) was added. The resulting solution was stirred at –78 °C for 10 min before being allowed to warm to rt over 4 h and stirred at rt for 14 h. Saturated $NH_4Cl_{(aq)}$ (10 mL) was added and the mixture was extracted with Et_2O (3 x 10 mL). The combined organic extracts were dried ($MgSO_4$) and evaporated under reduced pressure to give the crude product. Purification by flash chromatography on silica with 95:5 and 50:50 hexane-Et_2O as eluent gave disubstituted piperidine *trans*-**59** (78.6 mg, 30%) as a colourless oil.

(Table 3.3, Entry 3)

s-BuLi (1.0 mL of a 1.3 M solution in hexane, 1.3 mmol, 1.3 eq.) was added dropwise to a stirred solution of *N*-Boc piperidine **49** (199 mg, 1.0 mmol, 1.0 eq.) and TMEDA (0.19 mL, 1.3 mmol, 1.3 eq.) in Et_2O (7 mL) at –50 °C under Ar. The resulting yellow solution was stirred at –40 °C for 1 h. Then, trimethylsilyl chloride (0.16 mL, 1.3 mmol, 1.3 eq.) was added. The resulting solution was stirred at –50 °C for 10 min before being allowed to warm to rt over 4 h and stirred at rt for 14 h. Saturated $NH_4Cl_{(aq)}$ (10 mL) was added and the mixture was extracted with Et_2O (3 x 10 mL). The combined organic extracts were dried ($MgSO_4$) and evaporated under reduced pressure to give the crude product. Purification by flash chromatography on silica with 95:5 and 50:50 hexane-Et_2O as eluent gave disubstituted piperidine *trans*-**59** (190 mg, 70%) as a colourless oil.

(Table 3.3, Entry 4)

s-BuLi (1.0 mL of a 1.3 M solution in hexane, 1.3 mmol, 1.3 eq.) was added dropwise to a stirred solution of *N*-Boc piperidine **49** (199 mg, 1.0 mmol, 1.0 eq.) and TMEDA (0.19 mL, 1.3 mmol, 1.3 eq.) in Et_2O (7 mL) at –40 °C under Ar. The resulting yellow solution was stirred at –40 °C for 1 h. Then, trimethylsilyl chloride (0.16 mL, 1.3 mmol, 1.3 eq.) was added. The resulting solution was stirred at –40 °C for 10 min before being allowed to warm to rt over 4 h and stirred at rt for 14 h. Saturated $NH_4Cl_{(aq)}$ (10 mL) was added and the mixture was extracted with Et_2O (3 x 10 mL). The combined organic extracts were dried ($MgSO_4$) and evaporated under reduced pressure to give the crude product. Purification by flash chromatography on silica with 95:5 and 50:50 hexane-Et_2O as eluent gave disubstituted piperidine *trans*-**59** (185 mg, 68%) as a colourless oil.

***tert*-Butyl 2-formyl-6-methylpiperidine-1-carboxylate 60**

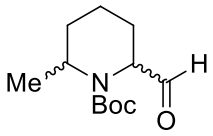

60

s-BuLi (1.0 mL of a 1.3 M solution in hexane, 1.30 mmol, 1.3 eq.) was added dropwise to a stirred solution of *N*-Boc methyl piperidine **49** (199 mg, 1.00 mmol, 1.0 eq.) and TMEDA (0.19 mL, 1.30 mmol, 1.3 eq.) in Et_2O (7 mL) at –40 °C under Ar. The resulting yellow solution was stirred at –40 °C for 2 h. The solution was then cooled to –78 °C before addition of dimethylformamide (0.16 mL, 2.00 mmol, 2.0 eq.). The resulting solution was stirred at –78 °C for 10 min before addition of H_2O (10 mL). The resulting mixture was then allowed to warm to rt over 1 h. The mixture was extracted with Et_2O (3 x 10 mL). The combined organic extracts were dried ($MgSO_4$) and evaporated under reduced pressure to give the crude product which contained an 80:20 mixture (by ^1H NMR spectroscopy) of aldehydes *trans*-**60** and *cis*-**60** (214 mg) as a colourless oil, ^1H NMR (400 MHz, $CDCl_3$) δ 9.61 (d, *J* = 1.0 Hz, 0.2H, CHO), 9.29 (d, *J* = 4.5 Hz, 0.8H, CHO), 4.56 (br d, *J* = 4.5 Hz, 0.2H, NCH), 4.27 (br s, 0.8H, NCH), 3.63 (ddd, *J* = 11.5, 11.5, 4.5 Hz, 0.8H, NCH), 3.54 (ddd, *J* = 12.0, 2.5, 2.5, 0.2H, NCH), 1.76-1.52 (m, 6H, CH), 1.46 (s, 9H, CMe_3), 1.12 (d, *J* = 7.0 Hz, 2.4H, Me), 1.07 (d, *J* = 7.0 Hz, 0.6H, Me).

Lab Book Reference: mcw/2/97

s-BuLi (1.0 mL of a 1.3 M solution in hexane, 1.30 mmol, 1.3 eq.) was added dropwise to a stirred solution of *N*-Boc methyl piperidine **49** (199 mg, 1.00 mmol, 1.0 eq.) and TMEDA (0.19 mL, 1.30 mmol, 1.3 eq.) in Et_2O (7 mL) at –40 °C under Ar. The resulting yellow solution was stirred at –40 °C for 2 h. Then, dimethylformamide (0.16 mL, 2.00 mmol, 2.0 eq.) was added. The resulting solution was stirred at –40 °C for 30 min before allowing to warm to rt for 2 h and stirred at rt for 16 h. H_2O (10 mL) was added and the mixture extracted with Et_2O (3 x 10 mL). The combined organic extracts were dried ($MgSO_4$) and evaporated under reduced pressure to give the crude product which contained a 80:20 mixture (by ^{1}H NMR spectroscopy) of aldehydes *cis*-**60** and *trans*-**60** (143 mg) as a colourless oil,^{1}H NMR (400 MHz, $CDCl_3$) δ 9.61 (d, *J* = 1.0 Hz, 0.8H, CHO), 9.29 (d, *J* = 4.0 Hz, 0.2H, CHO), 4.56 (d, *J* = 5.0 Hz, 0.8H, NCH), 4.41-4.32 (m, 0.8H, NCH), 4.27 (br s, 0.2H, NCH), 3.63 (ddd, *J* = 12.0, 4.0, 4.0, 0.2H, NCH), 1.75-1.55 (m, 6H, CH), 1.48 (s, 9H, CMe_3), 1.12 (d, *J* = 7.0 Hz, 0.6H, Me), 1.07 (d, *J* = 7.0 Hz, 2.4H, Me).

Lab Book Reference: mcw/2/98

tert-Butyl 2-(hydroxymethyl)-6-methylpiperidine-1-carboxylate 61

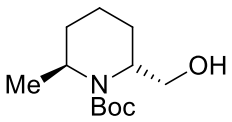

61

Sodium borohydride (107 mg, 2.84 mmol, 3.0 eq.) was added to a stirred solution of an 80:20 mixture of aldehydes *trans*-**60** and *cis*-**60** (214 mg, 0.95 mmol, 1.0 eq.) in MeOH (3 mL) at 0 °C under Ar. The resulting mixture was allowed to warm to rt and stirred at rt for 18 h. The reaction mixture was poured carefully into H_2O (10 mL). The mixture was extracted with EtOAc (3 x 10 mL). The combined organic extracts were washed with brine (10 mL), dried ($MgSO_4$) and evaporated under reduced pressure to give the crude product. Purification by flash chromatography on silica with 80:20 and then 50:50 hexane-Et_2O as eluent gave an 80:20 mixture (by ^{1}H NMR spectroscopy) of diastereomeric disubstituted piperidines *trans*-**61** and *cis*-**61** (186 mg, 81%) as a colourless oil, R_F (50:50 hexane-Et_2O) 0.1; IR (ATR) 3460 (OH), 3412 (OH), 2969,

2943, 2872, 1657 (C=O), 1397, 1365, 1167, 1056, 876 cm^{-1}; ^{1}H NMR (400 MHz, $CDCl_3$) δ 4.31-4.24 (m, 0.8H, NCH), 4.24-4.17 (m, 0.2H, NCH), 3.80-3.73 (m, 0.8H, C*H*OH), 3.72-3.69 (m, 0.8H, C*H*OH), 3.68-3.61 (m, 1.4H, C*H*OH and NCH), 2.95 (br s, 1H, OH), 1.80-1.48 (m, 6H, CH), 1.47-1.44 (m, 9H, CMe_3), 1.19 (d, *J* = 7.0 Hz, 2.4H, Me), 1.15 (d, *J* = 7.0 Hz, 0.6H, Me); ^{13}C NMR (101.6 MHz, $CDCl_3$) δ 156.6 and 154.3 (C=O), 80.1 and 79.8 (*C*Me_3), 66.5 (OCH_2), 54.3 and 51.6 (NCH), 48.5 and 45.9 (NCH), 30.1 (CH_2), 28.6 and, 28.1 (C*Me*$_3$), 25.6 and 25.1 (CH_2), 22.6 and 20.6 (Me), 18.5 and 16.1 (CH_2), 14.4 (CH_2); MS (ESI) *m/z* 252 [$(M + Na)^+$, 100]. 230 [$(M + H)^+$, 5]; HMRS (ESI) *m/z* calcd for $C_{12}H_{23}NO_3$ $(M + Na)^+$ 252.1570 found 252.1559 (+4.1 ppm error).

Lab Book Reference: mcw/2/99/3

(2*S*,6*S*)-1-(*tert*-Butoxycarbonyl)-6-methylpiperidine-2-carboxylic acid *trans*-62

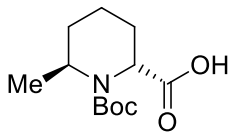

62

s-BuLi (1.0 mL of a 1.3 M solution in hexane, 1.3 mmol, 1.3 eq.) was added dropwise to a stirred solution of *N*-Boc piperidine **49** (199 mg, 1.0 mmol, 1.0 eq.) and TMEDA (0.19 mL, 1.3 mmol, 1.3 eq.) in Et_2O (7 mL) at –40 °C under Ar. The resulting yellow solution was stirred at –40 °C for 1.5 h. Then, CO_2 (excess) was bubbled through the reaction mixture at –40 °C for 10 min. H_2O (10 mL) was added. 1 M $HCl_{(aq)}$ (15 mL) was added and the mixture extracted with Et_2O (3 x 10 mL). The combined organic extracts were dried ($MgSO_4$) and evaporated under reduced pressure to give the crude product. Purification by flash chromatography on silica with 90:10 CH_2Cl_2-Et_2O and 0.5% acetic acid and then 70:30 CH_2Cl_2-Et_2O and 0.5% acetic acid as eluent gave piperidine carboxylic acid *trans*-**62** (199 mg, 82%) as a white solid, mp 82-84 °C; R_F (90:10 CH_2Cl_2-Et_2O) 0.2; IR (ATR) 2977, 2944, 1698 (C=O), 1445, 1380, 1365, 1227, 868, 779, 512 cm^{-1}; ^{1}H NMR (400 MHz, $CDCl_3$) δ 4.24-4.18 (m, 1H, NCH), 4.18 (dd, *J* = 7.0, 5.0 Hz, 1H, NCH), 2.09-1.80 (m, 3H, CH), 1.69-1.49 (m, 3H, CH), 1.45 (s, 9H, CMe_3), 1.18 (d, *J* = 7.0 Hz, 3H, Me); ^{13}C NMR (101.6 MHz, $CDCl_3$) δ 178.3 (C=O, CO_2Me), 156.4 (C=O, Boc), 80.9 (*C*Me_3), 53.8 (NCH), 47.6 (NCH), 28.3

(C*Me*$_3$), 27.7 (CH_2), 25.6 (CH_2), 18.8 (Me), 15.0 (CH_2); MS (ESI) *m/z* 266 [$(M + Na)^+$, 100], 244 [$(M + H)^+$, 5]; HMRS (ESI) *m/z* calcd for $C_{12}H_{21}NO_4$ $(M + Na)^+$ 266.1363, found 266.1355 (+2.9 ppm error).

Lab Book Reference: mcw/2/95/2 and mcw/3/57/2

(2*R,6*S**)-1-*tert*-Butyl 2-methyl 6-methylpiperidine-1,2-dicarboxylate *trans*-63**

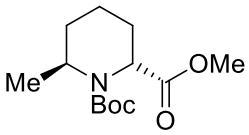

63

Potassium carbonate (2.56 g, 18.5 mmol, 3.0 eq) was added to a stirred solution of piperidine carboxylic acid **62** (1.50 g, 61.7 mmol, 1.0 eq.) in dimethylformamide (20 mL) at rt under Ar. The resulting suspension was stirred at rt for 30 min before the addition of methyl iodide (1.15 mL, 18.5 mmol, 3.0 eq.). The mixture was then stirred at rt for 18 h. The solvent was evaporated under reduced pressure and H_2O (10 mL) and EtOAc (10 mL) were added. The mixture was extracted with EtOAc (3 x 20 mL). The combined organic extracts were washed with 10% $Na_2S_2O_{3(aq)}$ (15 mL) and the mixture extracted with EtOAc (20 mL). The combined organic extracts were dried ($MgSO_4$) and evaporated under reduced pressure to give the crude product. Purification by flash chromatography on silica with 80:20 hexane-Et_2O as eluent gave piperidine methyl ester *trans*-**63** (1.55 g, 97%) as a yellow oil, R_F (80:20 hexane-Et_2O) 0.2; IR (ATR) 2972, 2950, 1746 (C=O, CO_2Me), 1692 (C=O, Boc), 1390, 1364, 1163, 1112, 735 cm^{-1}; ^1H NMR (400 MHz, $CDCl_3$) δ 4.26-4.17 (m, 1H, NCH), 4.12 (dd, *J* = 7.0, 5.0 Hz, 1H, NCH), 3.72 (s, 3H, OMe), 2.04-1.92 (m, 1H, CH), 1.91-1.78 (m, 2H, CH), 1.67-1.48 (m, 3H, CH), 1.43 (s, 9H, CMe_3), 1.16 (d, *J* = 7.0 Hz, 3H, Me); ^{13}C NMR (101.6 MHz, $CDCl_3$) δ 173.8 (C=O, CO_2Me), 156.0 (C=O, Boc), 80.1 (*C*Me_3), 54.1 (NCH), 52.0 (OMe), 47.5 (NCH), 28.3 (C*Me*$_3$), 28.0 (CH_2), 26.2 (CH_2), 18.8 (Me), 15.5 (CH_2); MS (ESI) *m/z* 280 [$(M + Na)^+$, 100], 258 [$(M + H)^+$, 15]; HMRS (ESI) *m/z* calcd for $C_{13}H_{23}NO_4$ $(M + Na)^+$ 280.1519, found 280.1507 (+4.2 ppm error).

Lab Book Reference: mcw/3/59/1

(Trimethylsilyl)diazomethane (0.31 mL of a 2.0 M solution in hexane, 0.62 mmol, 3.0 mmol) was added to a stirred solution of piperidine carboxylic acid **62** (50 mg, 0.21 mmol, 1.0 eq.) in MeOH (1 mL) and toluene (2.5 mL) at 0 °C, under Ar. The resulting solution was stirred at 0 °C for 20 min. Then, acetic acid (0.02 mL, 0.412 mmol, 2.0 eq.) was added. The solvent was evaporated under reduced pressure to give the crude product. Purification by flash chromatography on silica with 90:10 hexane-Et_2O as eluent gave piperidine methyl ester *trans*-**63** (49 mg, 93%) as a colourless oil.

Lab Book Reference: mcw/2/77/2

2- *trans*-(Methoxycarbonyl)-6-methylpiperidine hydrochloride salt 43.HCl

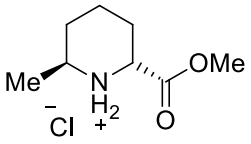

43.HCl

Using general procedure C, acetyl chloride (0.66 mL, 9.32 mmol, 4.0 eq), *N*-Boc methyl ester **63** (600 mg, 2.33 mmol, 1.0 eq.) and EtOH (0.54 mL, 9.32 mmol, 4.0 eq.) in EtOAc (15 mL), heated at reflux, gave amine hydrochloride salt **43.HCl** (451 mg, 100%) as a white solid, mp 132-133 °C; IR (ATR) 3336 (NH), 3038, 1680 (C=O), 1604, 1287, 1173, 1003, 848 cm^{-1}; ^1H NMR (400 MHz, DMSO-d_6) δ 9.38 (s, 2H, NH_2), 4.38 (dd, *J* = 5.0, 5.0 Hz, 1H, $NCHCO_2Me$), 3.77 (s, 3H, OMe), 3.48-3.40 (m, 1H, NC*H*Me), 2.02-1.87 (m, 2H, CH), 1.80-1.64 (m, 2H, CH), 1.51-1.33 (m, 2H, CH), 1.27 (d, *J* = 6.5 Hz, 3H, Me); ^{13}C NMR (101.6 MHz, DMSO-d_6) δ 169.1 (C=O), 53.0 (NCH), 52.7 (NCH), 48.9 (OMe), 28.5 (CH_2), 24.4 (CH_2), 18.2 (CH_2), 17.2 (Me); MS (ESI) *m/z* 158 [M^+, 100]; HMRS (ESI) *m/z* calcd for $C_8H_{16}NO_2$ M^+ 158.1176, found 158.1181 (–3.4 ppm error).

Lab book reference: mcw/4/64

Methyl *trans*-1-acetyl-6-methylpiperidine-2-carboxylate 64

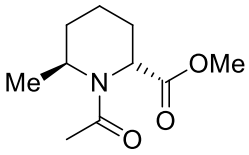

trans-**64**

Using general procedure F, acetyl chloride (0.33 mL, 4.65 mmol, 3.0 eq.), amine hydrochloride salt **43** (300 mg, 1.54 mmol, 1.0 eq.) and triethylamine (0.64 mL, 4.65 mmol, 3.0 eq.) in CH_2Cl_2 (5 mL) gave the crude product. Purification by flash chromatography on silica with 70:30 EtOAc-hexane and then EtOAc as eluent gave acetamide **64** (307 mg, 96%) as a colourless oil, R_F (EtOAc) 0.3; IR (ATR) 2954, 2872, 1737 (C=O, CO_2Me), 1642 (C=O, amide), 1404, 1199, 1172, 1010 cm^{-1}; ^1H NMR (400 MHz, $CDCl_3$) (85:15 mixture of rotamers) δ 4.40 (br s, 0.15H, NCH), 4.33 (br s, 0.15H, NCH), 4.21 (dd, *J* = 7.5, 5.0 Hz, 0.85H, NCH) 4.17-4.08 (m, 0.85H, NCH), 3.72 (s, 3H, OMe), 2.17 (s, 0.45H, COMe), 2.15 (s, 2.55, COMe), 2.06-1.82 (m, 3H, CH), 1.76-1.53 (m, 3H, CH), 1.25 (d, *J* = 6.5 Hz, 3H, Me); ^{13}C NMR (101.6 MHz, $CDCl_3$) (rotamers) δ 173.0 (C=O), 171.8 (C=O), 52.9 (NCH), 52.14 (NCH), 52.08 (NCH), 49.0 (NCH), 30.3 (OMe), 27.7 (CH_2), 25.6 (CH_2), 21.3 (CO*Me*), 19.6 (Me), 15.1 (CH_2); MS (ESI) *m/z* 222 [$(M + Na)^+$, 100], 200 [$(M + H)^+$, 5]; HMRS (ESI) *m/z* calcd for $C_{10}H_{17}NO_3$ $(M + Na)^+$ 222.1101, found 222.1103 (–0.8 ppm error).

Lab book reference: mcw/4/52

1-(*trans*-2-(Hydroxymethyl)-6-methylpiperidin-1-yl)ethanone A16

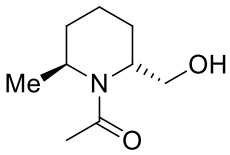

A16

Using general procedure I, lithium borohydride (2.0 mL of a 4.0 M solution in THF, 8.0 mmol, 8.0 eq.) and methyl ester **64** (200 mg, 1.00 mmol, 1.0 eq.) in THF (10 mL) for 3 h gave the crude product. Purification by flash chromatography on silica with 50:50 EtOAc-hexane and then EtOAc as eluent gave recovered methyl ester **64 (**130

mg, 65%) as a colourless oil and alcohol **A16** (37 mg, 22%, 66%, based on recovery of piperidine ester **64**) as a colourless oil, R_F (EtOAc) 0.2; IR (ATR) 3285 (OH), 2932, 2871, 1614 (C=O), 1419, 1052, 697, 600 cm^{-1}; ^1H NMR (400 MHz, $CDCl_3$) (90:10 mixture of rotamers) δ 4.77 (br s, 0.1H, NCH), 4.62 (br s, 0.9H, NCH), 4.04 (br s, 0.9H, NCH), 3.77 (br s, 2H, C*H*$_2$OH), 3.68 (br d, *J* = 7.5 Hz, 0.1H, NCH), 2.17 (s, 0.3H, COMe), 2.15 (s, 2.7H, COMe), 1.84-1.57 (m, 6H, CH), 1.30 (d, *J* = 7.0 Hz, 3H, Me); ^{13}C NMR (101.6 MHz, $CDCl_3$) δ 171.6 (C=O), 65.8 (CH_2OH), 55.1 (NCH), 50.9 (NCH), 28.6 (CH_2), 25.6 (CH_2), 23.1 (CO*Me*), 18.6 (Me), 16.4 (CH_2); MS (ESI) *m/z* 194 [$(M + Na)^+$, 100], 172 [$(M + H)^+$, 25]; HMRS (ESI) *m/z* calcd for $C_9H_{17}NO_2$ ($M + Na)^+$ 194.1151, found 194.1147 (+2.4 ppm error).

Lab book reference: mcw/5/9

***N*-Benzylpent-4-en-1-amine 82**

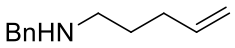

82

Sodium iodide (158 mg, 1.05 mmol, 0.05 eq.) was added to a stirred solution of benzylamine (11.5 mL, 106 mmol, 5.0 eq.) and 5-bromopent-1-ene **81** (2.5 mL, 21.1 mmol, 1.0 eq.) in EtOH (50 mL) at rt, under Ar. The resulting suspension was then stirred and heated at 75 °C for 16 h. After being allowed to cool to rt, the solvent was evaporated under reduced pressure. Then, 1 M $KOH_{(aq)}$ (50 mL) was added and the mixture was extracted with CH_2Cl_2 (3 x 20 mL). The combined organic extracts were dried ($MgSO_4$) and evaporated under reduced pressure to give the crude product. Purification by flash chromatography on silica with 80:20 EtOAc-hexane and then EtOAc as eluent gave amine **82** (3.58 g, 97%) as a yellow oil, R_F (EtOAc) 0.2; ^1H NMR (400 MHz, $CDCl_3$) δ 7.37-7.19 (m, 5H, Ph), 5.81 (ddt, *J* = 17.0, 10.0, 6.5 Hz, 1H, =CH), 5.00 (ddt, *J* = 17.0, 2.0, 2.0 Hz, 1H, =CH), 4.95 (ddt, *J* = 10.0, 2.0, 1.0 Hz, 1H, =CH), 3.79 (s, 2H, NCH_2Ph), 2.65 (t, *J* = 7.0 Hz, 2H, N*CH*$_2$$CH_2$), 2.17-2.04 (m, 2H, CH_2), 1.62 (tt, *J* = 7.0, 7.0 Hz, 2H, CH_2); ^{13}C NMR (101.6 MHz, $CDCl_3$) δ, 140.5 (*ipso*-Ph), 138.5 (=CH), 128.4 (Ph), 128.1 (Ph), 126.9 (Ph), 114.6 (=CH_2), 54.0 (NCH_2), 48.9 (NCH_2), 31.5 (CH_2), 29.2 (CH_2). Spectroscopic data consistent with those reported in the literature.[97]

Lab Book Reference: mcw/4/62

Methyl 2-(benzyl(pent-4-en-1-yl)amino)acetate 78

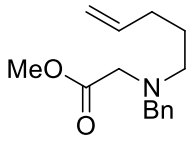

78

Methyl α-bromo acetate (1.94 mL, 20.5 mmol, 1.2 eq.), was added to a stirred solution of amine **82** (3.00 g, 17.1 mmol, 1.0 eq.) and triethylamine (2.86 mL, 20.5 mmol, 1.2 eq.) in DMSO (420 mL) at rt under Ar. The resulting solution was stirred at rt for 5 h. A solution of 2:1 saturated $NH_4Cl_{(aq)}$-$NH_4OH_{(aq)}$ (100 mL) was added and the mixture was extracted with Et_2O (3 x 100 mL). The combined organic extracts were washed with brine (25 mL), dried ($MgSO_4$) and evaporated under reduced pressure to give the crude product. Purification by flash chromatography on silica with 70:30 hexane-Et_2O as eluent gave ester-alkene amine **78** (3.70 g, 87%) as a colourless oil, R_F (70:30 hexane-Et_2O) 0.3; ^{1}H NMR (400 MHz, $CDCl_3$) δ 7.37-7.20 (m, 5H, Ph), 5.80 (ddt, *J* = 16.5, 10.0, 7.0 Hz, 1H, =CH), 4.99 (ddt, *J* = 16.0, 1.5, 1.5 Hz, 1H, =CH), 4.96-4.90 (m, 1H, =CH), 3.77 (s, 2H, CH_2CO_2Me), 3.68 (s, 3H, OMe), 3.31 (s, 2H, NCH_2Ph), 2.64 (t, *J* = 7.0 Hz, 2H, NCH_2), 2.07 (br dt, *J* = 7.0, 7.0 Hz, 2H, CH_2), 1.59 (tt, *J* = 7.0, 7.0 Hz, 2H, CH_2); ^{13}C NMR (101.6 MHz, $CDCl_3$) δ 172.0 (C=O), 139.0 (*ipso*-Ph), 138.5 (=CH), 128.9 (Ph), 128.2 (Ph), 127.0 (Ph), 114.5 (=CH_2), 58.2 (NCH_2), 54.0 (NCH_2), 53.3 (NCH_2), 51.2 (OMe), 31.3 (CH_2), 26.8 (CH_2). Spectroscopic data consistent with those reported in the literature.[97]

Lab book reference: mcw/4/15/2

Methyl *cis*-1-benzyl-3-methylpiperidine-2-carboxylate 80

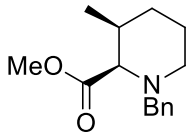

cis-**80**

(Table 3.4, Entry 1)

Lithium bis(trimethylsilyl)amide (1.62 mL of a 1.0 M solution in THF, 1.62 mmol, 2.0 eq.) was added to a stirred solution of ester-alkene **78** (200 mg, 0.80 mmol, 1.0 eq.) in Et_2O (13 mL) at –20 °C under Ar. The resulting solution was stirred at –20 °C for 10 min and then allowed to warm to rt for 20 min. The mixture was then cooled to –40 °C. The lithium enolate solution was added dropwise via cannula transfer to a stirred solution of zinc bromide (365 mg, 1.62 mmol, 2.0 eq.) in dry Et_2O (1.62 mL) at –40 °C under Ar. The resulting mixture was allowed to warm to rt and stirred at rt for 5 h. The mixture was then cooled to 0 °C and a 2:1 solution of saturated $NH_4Cl_{(aq)}$-$NH_4OH_{(aq)}$ (5 mL) was added. The resulting mixture was then allowed to warm to rt and stirred at rt for 18 h. The mixture was extracted with Et_2O (3 x 10 mL). The combined organic extracts were dried ($MgSO_4$) and evaporated under reduced pressure to give the crude product. Purification by flash chromatography on silica with 90:10 hexane-Et_2O as eluent gave piperidine *cis*-**80** (53.4 mg, 15%) as a colourless oil.

Lab book reference: mcw/3/90

(Table 3.4, Entry 2)

Lithium bis(trimethylsilyl)amide (8.08 mL of a 1.0 M solution in THF, 8.08 mmol, 2.0 eq.) was added to a stirred solution of ester-alkene **78** (1.00 g, 4.04 mmol, 1.0 eq.) in Et_2O (20 mL) at –20 °C under Ar. The resulting solution was stirred at –20 °C for 10 min and then allowed to warm to rt for 20 min. The mixture was then cooled to –40 °C. The lithium enolate solution was added dropwise to a stirred solution of zinc bromide (1.82 g, 8.08 mmol, 2.0 eq.) in dry Et_2O (40 mL) at –40 °C under Ar. The resulting mixture was then sonicated for 5 minutes to encourage dissolution of zinc bromide and then was allowed to warm to rt and stirred at rt for 5 h. The mixture was then cooled to 0 °C and a 2:1 solution of saturated $NH_4Cl_{(aq)}$-$NH_4OH_{(aq)}$ (5 mL) was

added. The resulting mixture was then allowed to warm to rt and stirred at rt for 18 h. The mixture was extracted with Et_2O (3 x 10 mL). The combined organic extracts were dried ($MgSO_4$) and evaporated under reduced pressure to give the crude product. Purification by flash chromatography on silica with 90:10 hexane-Et_2O as eluent gave piperidine *cis*-**80** (394 mg, 40%) as a colourless oil.

Lab book reference: mcw/4/8

(Table 3.4, Entry 3)

Lithium bis(trimethylsilyl)amide (4.04 mL of a 1.0 M solution in THF, 4.04 mmol, 2.0 eq.) was added to a stirred solution of ester-alkene **78** (500 mg, 2.02 mmol, 1.0 eq.) in Et_2O (10 mL) at –20 °C under Ar. The resulting solution was stirred at –20 °C for 10 min and then allowed to warm to rt for 20 min. The mixture was then cooled to –40 °C. The lithium enolate solution was added dropwise to a stirred solution of zinc bromide (910 mg, 4.04 mmol, 2.0 eq.) in dry Et_2O (20 mL) at –40 °C under Ar. The resulting mixture was then was allowed to warm to rt. The mixture was sonicated for 10 minutes every hour to aid dissolution of zinc bromide for 5 h,. The mixture was then cooled to 0 °C and a 2:1 solution of saturated $NH_4Cl_{(aq)}$-$NH_4OH_{(aq)}$ (5 mL) was added. The resulting mixture was then allowed to warm to rt and stirred at rt for 18 h. The mixture was extracted with Et_2O (3 x 10 mL). The combined organic extracts were dried ($MgSO_4$) and evaporated under reduced pressure to give the crude product. Purification by flash chromatography on silica with 90:10 hexane-Et_2O as eluent gave piperidine *cis*-**80** (194 mg, 39%) as a colourless oil.

Lab book reference: mcw/4/11

(Table 3.4, Entry 4)

Using general procedure J, lithium bis(trimethylsilyl)amide (1.0 M solution in THF, 40.4 mmol, 2.0 eq.), ester-alkene **78** (5.00 g, 20.2 mmol, 1.0 eq.) in Et_2O (300 mL), zinc bromide (9.10 g, 40.4 mmol, 2.0 eq.) in Et_2O (40 mL) and a 2:1 solution of saturated $NH_4Cl_{(aq)}$-$NH_4OH_{(aq)}$ (40 mL) gave the crude product. Purification by flash chromatography on silica with 90:10 hexane-Et_2O as eluent gave piperidine *cis*-**80** (1.62 g, 32%) as a colourless oil, R_F (90:10 hexane-Et_2O) 0.2; ^{1}H NMR (400 MHz, $CDCl_3$) δ 7.28-7.17 (m, 5H, Ph), 3.65 (s, 3H, OMe), 3.57 (d, J = 13.5 Hz, 1H, NCHPh), 3.52 (d, J = 13.5 Hz, 1H, NCHPh), 3.41 (d, J = 5.0 Hz, 1H, NCH), 2.95-2.88 (m, 1H,

NCH), 2.46 (ddd, *J* = 11.5, 4.0, 4.0 Hz, 1H, NCH), 1.99-1.89 (m, 1H, CH), 1.66-1.60 (m, 1H, CH), 1.55-1.41 (m, 3H, CH), 0.86 (d, *J* = 7.0 Hz, 3H, Me); ^{13}C NMR (101.6 MHz, $CDCl_3$) δ 172.9 (C=O), 139.0 (*ipso*-Ph), 128.7 (Ph), 128.1 (Ph), 126.9 (Ph), 66.1 (NCH), 60.1 (NCH_2), 50.4 (OMe), 46.8 (CH_2), 33.0 (*C*HMe), 27.7 (CH_2), 25.0 (CH_2), 18.1 (Me). Spectroscopic data consistent with those reported in the literature.[97]

Lab book reference: mcw/4/80

Methyl 1-benzyl-3-methylpiperidine-2-carboxylate, *trans*-80 and *cis*-80

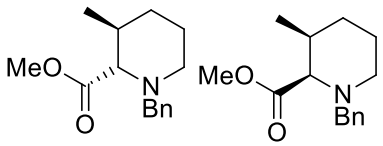

trans-**80** *cis*-**80**

n-BuLi (0.736 mL of a 2.2 M solution in hexane, 1.62 mmol, 4.0 eq.) was added dropwise to a stirred solution of diisopropylamine (0.36 mL, 1.62 mmol, 4.0 eq.) in THF (0.97 mL) at 0 °C under Ar. The resulting solution was stirred at 0 °C for 30 min. The LDA solution was added dropwise to a stirred solution of *cis*-piperidine *cis*-**80** (100 mg, 0.40 mmol, 1.0 eq.) in Et_2O (20 mL) at –20 °C under Ar. The resulting solution was allowed to warm to rt over 20 min and then stirred at rt for 20 min. The mixture was cooled to 0 °C and a 2:1 solution of saturated $NH_4Cl_{(aq)}$-$NH_4OH_{(aq)}$ (10 mL) was added. The resulting mixture was then allowed to warm to rt over 30 min and stirred at rt for 18 h. The mixture was extracted with Et_2O (3 x 20 mL). The combined organic extracts were washed with brine (10 mL), dried ($MgSO_4$) and evaporated under reduced pressure to give the crude product. Purification by flash chromatography on silica with 90:10 and then 50:50 hexane-Et_2O as eluent gave recovered piperidine *cis*-**80** (39 mg, 40%) and *trans*-piperidine *trans*-**80** (57 mg, 57%) as a colourless oil, R_F (90:10 hexane-Et_2O) 0.1; ^{1}H NMR (400 MHz, $CDCl_3$) δ 7.35-7.21 (m, 5H, Ph), 3.76 (s, 3H, OMe), 3.71 (d, *J* = 13.0 Hz, 1H, NCHPh), 3.25 (d, *J* = 13.0 Hz, 1H, NCHPh), 2.87 (ddd, *J* = 11.5, 4.0, 4.0 Hz, 1H, NCH), 2.64 (d, *J* = 9.0 Hz, 1H, $NCHCO_2Me$), 1.95-1.86 (m, 2H, CH), 1.78-1.68 (m, 1H, CH), 1.62-1.53 (m, 2H, CH), 1.06-0.93 (m, 1H, CH), 0.90 (d, *J* = 6.5 Hz, 3H, Me); ^{13}C NMR (101.6 MHz, $CDCl_3$) δ 174.2 (C=O), 137.5 (*ipso*-Ph), 129.4 (Ph), 128.1 (Ph), 127.1 (Ph), 73.6 (NCH), 61.0 (NCH_2), 51.7 (OMe), 51.2 (NCH_2), 34.2 (*C*HMe), 31.9 (CH_2), 24.4

(CH_2), 18.7 (Me). Spectroscopic data of *trans*-**80** consistent with those reported in the literature.[97]

Lab book reference: mcw/4/17/2

Methyl *trans*-3-methylpiperidine-2-carboxylate *trans*-75

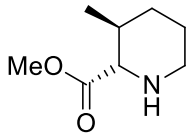

trans-**75**

10% $Pd(OH)_2/C$ (23 mg, 0.032 mmol, 0.1 eq.) was added to a stirred solution of piperidine *trans*-**80** (80 mg, 0.32 mmol, 1.0 eq.) and ammonium formate (408 mg, 6.47 mmol, 20 eq.) in MeOH (30 mL) at rt, under Ar. The resulting suspension was stirred and heated at reflux for 18 h. After being allowed to cool to rt, the solids were removed by filtration through Celite and washed with MeOH (50 mL). The filtrate was evaporated under reduced pressure to give amine *trans*-**75** (51 mg, 100%) as a pale yellow oil, IR (ATR) 2956, 2697, 1741 (C=O) 1578, 1436, 1273, 1210, 765 cm^{-1}; ^1H NMR (400 MHz, $CDCl_3$) δ 3.77 (s, 3H, OMe), 3.42 (br d, *J* = 12.5 Hz, 1H, NCH), 3.30 (d, *J* = 10.5 Hz, 1H, $NCHCO_2Me$), 2.81 (ddd, *J* = 12.5, 12.5, 5.0 Hz, 1H, NCH), 1.98-1.77 (m, 4H, CH), 1.35-1.20 (m, 1H, CH), 1.00 (d, *J* = 6.5 Hz, 3H, Me); ^{13}C NMR (101.6 MHz, $CDCl_3$) δ 170.4 (C=O), 63.5 (NCH), 52.5 (OMe), 43.8 (NCH_2), 32.9 (*C*HMe), 31.8 (CH_2), 22.9 (CH_2), 18.4 (Me); MS (ESI) *m/z* 158 [$(M + H)^+$, 100]; HMRS (ESI) *m/z* calcd for $C_8H_{15}NO_2$ $(M + H)^+$ 158.1176, found 158.1173 (+1.7 ppm error).

Lab book reference: mcw/5/10/c

***N*-Benzylbut-3-en-1-amine 90**

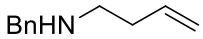

90

Sodium iodide (13.5 g, 90.0 mmol, 1.5 eq.) was added to a stirred suspension of benzylamine (6.55 mL, 60.0 mmol, 1.0 eq.), potassium carbonate (12.4 g, 90.0 mmol, 1.5 eq.) and 4-bromobut-1-ene **89** (7.31 mL, 72.0 mmol, 1.2 eq.) in dimethylformamide (190 mL) at rt under Ar. The resulting suspension was stirred and heated at reflux for 20 h. After being allowed to cool to rt, H_2O (50 mL) was added and the mixture was extracted with Et_2O (3 x 50 mL). The combined organic extracts were washed with brine (50 mL), dried ($MgSO_4$) and evaporated under reduced pressure to give the crude product. Purification by flash chromatography on silica with 80:20 EtOAc-hexane as eluent gave amine **90** (3.70 g, 38%) as a yellow oil, R_F (80:20 EtOAc-hexane) 0.2; ^{1}H NMR (400 MHz, $CDCl_3$) δ 7.31-7.15 (m, 5H, Ph), 5.73 (ddt, *J* = 17.0, 10.0, 7.0 Hz, 1H, =CH), 5.03 (ddt, *J* = 17.0, 1.5, 1.5, 1H, =CH), 4.98 (br d, *J* = 10.0 Hz, 1H, =CH), 3.74 (s, 2H, NCH_2Ph), 2.65 (t, *J* = 7.0 Hz, 2H, NCH_2), 2.23 (br dt, *J* = 7.0, 7.0 Hz, 2H, CH_2); ^{13}C NMR (101.6 MHz, $CDCl_3$) δ 140.3 (*ipso*-Ph), 136.4 (=CH), 128.4 (Ph), 128.1 (Ph), 126.9 (Ph), 116.4 (=CH_2), 53.8 (NCH_2), 48.2 (NCH_2), 34.2 (CH_2). Spectroscopic data consistent with those reported in the literature.[132]

Lab book reference: mcw/4/23

Methyl 3-(benzyl(but-3-en-1-yl)amino)propanoate 85

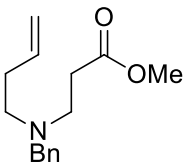

85

1,8-Diazabicyclo[5.4.0]undec-7-ene (1.85 mL, 12.4 mmol, 0.5 eq.) was added to a stirred solution of methylacrylate (3.35 mL, 37.2 mmol, 1.5 eq.) and amine **90** (4.00 g, 24.8 mmol, 1.0 eq.) in MeCN (15 mL) at rt under Ar. The resulting mixture was stirred at rt for 6 h. The solvent was then evaporated under reduced pressure to give

the crude product. Purification by flash chromatography on silica with 50:50 EtOAc-hexane as eluent gave ester-alkene **85** (4.55 g, 74%) as a colourless oil, R_F (50:50 EtOAc-hexane) 0.5; IR (ATR) 3064, 2949, 2805, 1736 (C=O), 1435, 1193, 1174, 910, 734 cm^{-1}; ^1H NMR (400 MHz, $CDCl_3$) δ 7.30-7.16 (m, 5H, Ph), 5.73 (ddt, *J* = 17.0, 10.5, 7.0 Hz, 1H, =CH), 4.98 (ddt, *J* = 17.0, 1.5, 1.5, 1H, =CH), 4.93 (br dd, *J* = 10.5, 1.5 Hz, 1H, =CH), 3.61 (s, 3H, OMe), 3.56 (s, 2H, NCH_2), 2.78 (t, *J* = 7.0 Hz, 2H, NCH_2), 2.48 (t, *J* = 7.0 Hz, 2H, NCH_2), 2.44 (t, *J* = 7.0 Hz, 2H, CH_2CO_2Me), 2.20 (br dt, *J* = 7.0, 7.0 Hz, 2H, CH_2); ^{13}C NMR (101.6 MHz, $CDCl_3$) δ 173.1 (C=O), 139.4 (*ipso*-Ph), 136.8 (=CH), 128.7 (Ph), 128.1 (Ph), 126.9 (Ph), 115.5 ($=CH_2$), 58.3 (NCH_2), 53.1 (NCH_2), 51.5 (OMe), 49.2 (NCH_2), 32.5 (CH_2), 31.5 (CH_2); MS (ESI) *m/z* 248 [$(M + H)^+$, 100]; HMRS (ESI) *m/z* calcd for $C_{15}H_{21}NO_2$ $(M + H)^+$ 248.1645, found 248.1624 (+1.4 ppm error).

Lab book reference: mcw/4/5

N-Benzylprop-2-en-1-amine 92

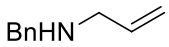

92

Benzyl bromide (6.0 mL, 50.5 mmol, 1.0 eq.) was added dropwise over 30 min to a stirred suspension of potassium (8.37 g, 60.5 mmol, 1.2 eq.) in allylamine **91** (30.2 mL, 404 mmol, 8.0 eq.) at rt under Ar. The resulting mixture was stirred at rt for 3 h. The solids were removed by filtration through Celite and the filtrate was evaporated under reduced pressure to give the crude product. Purification by Kügelrohr short path distillation gave **92** (3.66 g, 50%) as a colourless oil, bp 69-71 °C / 991 mbar; ^1H NMR (400 MHz, $CDCl_3$) δ 7.36-7.22 (m, 5H, Ph), 5.94 (ddt, *J* = 16.5, 10.0, 6.0 Hz, 1H, =CH), 5.21 (ddt, *J* = 16.5, 1.5, 1.5 Hz, 1H, =CH), 5.12 (br dd, *J* = 10.0, 1.5 Hz, 1H, =CH), 3.80 (s, 2H, NCH_2Ph), 3.29 (ddd, *J* = 6.0, 1.5, 1.5 Hz, 2H, NCH_2), 1.50 (br s, 1H, NH); ^{13}C NMR (101.6 MHz, $CDCl_3$) δ 140.2 (*ispo*-Ph), 136.7 (=CH), 128.4 (Ph), 128.2 (Ph), 126.9 (Ph), 116.0 ($=CH_2$), 53.2 (NCH_2), 51.7 (NCH_2). Spectroscopic data consistent with those reported in the literature.[133]

Lab book reference: mcw/4/6/1

Methyl 4-(allyl(benzyl)amino)butanoate 87

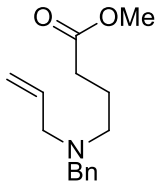

87

Methyl 4-bromobutyrate (2.57 mL, 20.4 mmol, 1.0 eq.) was added to a stirred suspension of potassium carbonate (5.63 g, 40.8 mmol, 2.0 eq.) and amine **92** (3.00 g, 20.4 mmol, 1.0 eq.) in DMF (40 mL) at rt under Ar. The resulting mixture was stirred and heated at 100 °C for 18 h. After being allowed to cool to rt, H_2O (20 mL) was added and the mixture was extracted with EtOAc (3 x 20 mL). The combined organic extracts were dried ($MgSO_4$) and evaporated under reduced pressure to give the crude product. Purification by flash chromatography on silica with 70:30 hexane-Et_2O as eluent gave ester-alkene amine **87** (2.86 g, 56%) as a colourless oil, R_F (70:30 hexane-Et_2O) 0.3; IR (ATR) 2949, 2799, 1736 (C=O), 1435, 1251, 1170, 736, 698 cm^{-1}; ^1H NMR (400 MHz, $CDCl_3$) δ 7.37-7.17 (m, 5H, Ph), 5.85 (ddt, *J* = 17.0, 10.0, 6.5 Hz, 1H, =CH), 5.17 (ddt, *J* = 17.0, 1.5, 1.5, 1H, =CH), 5.12, (ddt, *J* = 10.0, 1.5, 1.5, 1H, =CH), 3.64 (s, 2H, OMe), 3.55 (s, 2H, NCH_2Ph), 3.05 (ddd, *J* = 6.5, 1.5, 1.5, 1H, NCH_2), 2.44 (t, *J* = 7.0 Hz, 2H, NCH_2), 2.33 (t, *J* = 7.0 Hz, 2H, CH_2CO_2Me), 1.80 (tt, *J* = 7.0, 7.0, 2H, CH_2); ^{13}C NMR (101.6 MHz, $CDCl_3$) δ 174.2 (C=O), 139.6 (*ipso*-Ph), 135.9 (=CH), 128.8 (Ph), 128.1 (Ph), 126.8 (Ph), 117.2 (=CH_2), 58.1 (NCH_2), 56.6 (NCH_2), 52.3 (NCH_2), 51.4 (OMe), 31.7 (CH_2), 22.4 (CH_2); MS (ESI) *m/z* 248 [$(M + H)^+$, 100]; HMRS (ESI) *m/z* calcd for $C_{15}H_{21}NO_2$ $(M + H)^+$ 248.1645, found 248.1646 (–0.5 ppm error).

Lab book reference: mcw/4/7

Methyl 6-(allyl(benzyl)amino)-2-(2-(allyl(benzyl)amino)ethyl)-3-oxohexanoate 93

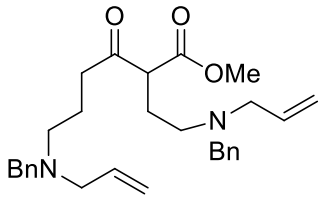

93

Using general procedure J, lithium bis(trimethylsilyl)amide (8.08 mL of a 1.0 M solution in THF, 8.08 mmol, 2.0 eq.), ester-alkene **87** (1.00 g, 4.04 mmol, 1.0 eq.) in Et_2O (52 mL), zinc bromide (1.82 g, 8.08 mmol, 2.0 eq.) in Et_2O (8 mL) and a 2:1 solution of saturated $NH_4Cl_{(aq)}$-$NH_4OH_{(aq)}$ (20 mL) gave the crude product. Purification by flash chromatography on silica with 50:50 and then 80:20 Et_2O-hexane as eluent gave Claisen product **93** (232 mg, 25%) as a colourless oil, R_F (50:50 hexane-Et_2O) 0.1; IR (ATR) 3063, 2949, 2800, 1743 (C=O, CO_2Me), 1713 (C=O, ketone), 1452, 1251, 1073, 917 cm^{-1}; ^1H NMR (400 MHz, $CDCl_3$) δ 7.34-7.17 (m, 10H, Ph), 5.87-5.76 (m, 2H, =CH), 5.22-5.07 (m, 4H, $=CH_2$), 3.64 (s, 3H, OMe), 3.59 (dd, *J* = 7.0, 7.0 Hz, 1H, (C=O)CH(CO_2Me)), 3.53 (s, 2H, NCH_2Ph), 3.51 (s, 2H, NCH_2Ph), 3.06-3.01 (m, 4H, NCH_2), 2.53 (ddd, *J* = 18.0, 7.0, 7.0 Hz, 1H, NCH), 2.45-2.34 (m, 5H, CH), 1.99 (dt, *J* = 7.0, 7.0 Hz, 2H, CH), 1.72 (tt, *J* = 7.0, 7.0 Hz, 2H, CH_2); ^{13}C NMR (101.6 MHz, CDC_3) δ 205.3 (C=O, ketone), 170.4 (C=O, CO_2Me), 139.6 (*ipso*-Ph), 139.2 (*ipso*-Ph), 135.8 (=CH), 135.6 (=CH), 129.0 (Ph), 128.8 (Ph), 128.18 (Ph), 128.15 (Ph), 127.0 (Ph), 126.8 (Ph), 117.6 ($=CH_2$), 117.3 ($=CH_2$), 66.7 (CH), 58.1 (NCH_2), 57.9 (NCH_2), 56.6 (NCH_2), 56.4 (OMe), 52.23 (NCH_2), 52.20 (NCH_2), 50.7 (NCH_2), 39.9 (CH_2), 25.7 (CH_2), 20.8 (CH_2); MS (ESI) *m/z* 463 [$(M + H)^+$, 100]; HMRS (ESI) *m/z* calcd for $C_{29}H_{38}N_2O_3$ $(M + H)^+$ 463.2955, found 463.2941 (+3.2 ppm error).

Lab book reference: mcw/4/9

Attempted synthesis of methyl 1-benzyl-4-methylpiperidine-3-carboxylate 97

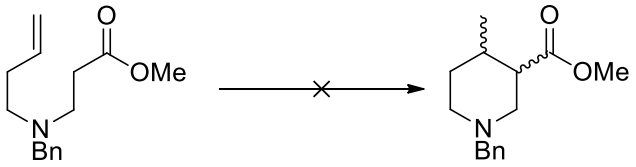

85 **86**

Using general procedure J, lithium bis(trimethylsilyl)amide (1.0 M solution in THF, 4.04 mmol, 2.0 eq.), ester-alkene **85** (500 mg, 2.02 mmol, 1.0 eq.) in Et_2O (30 mL), zinc bromide (910 mg, 4.04 mmol, 2.0 eq.) in Et_2O (4.04 mL) and a 2:1 solution of saturated $NH_4Cl_{(aq)}$-$NH_4OH_{(aq)}$ (10 mL) gave no identifiable product.

Lab book reference: mcw/4/14

***tert*-Butyl 3-(benzyl(but-3-en-1-yl)amino)propanoate 95**

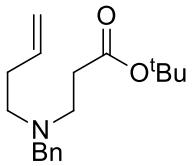

95

1,8-Diazabicyclo[5.4.0]undec-7-ene (1.39 mL, 9.30 mmol, 0.5 eq.) was added to a stirred solution of *tert*-butyl acrylate (4.09 mL, 27.9 mmol, 1.5 eq.) and amine **89** (3.00 g, 18.6 mmol, 1.0 eq.) in MeCN (9 mL) at rt under Ar. The resulting mixture was stirred at rt for 6 h. The solvent was then evaporated under reduced pressure to give the crude product. Purification by flash chromatography on silica with 50:50 EtOAc-hexane as eluent gave ester-alkene **95** (3.61 g, 67%) as a colourless oil, R_F (50:50 hexane-Et_2O) 0.2; IR (ATR) 2977, 2931, 1726 (C=O), 1453, 1366, 1252, 1151, 734, 697 cm^{-1}; ^1H NMR (400 MHz, $CDCl_3$) δ 7.29-7.15 (m, 5H, Ph), 5.71 (ddt, *J* = 17.0, 10.5, 7.0 Hz, 1H, =CH), 4.95 (ddt, *J* = 17.0, 1.5, 1.5, 1H, $=CH_2$), 4.93-4.88 (m, 1H, $=CH_2$), 3.53 (s, 2H, CH_2Ph), 2.74 (t, *J* = 7.0 Hz, 2H, NCH_2), 2.45 (t, *J* = 7.0 Hz, 2H, NCH_2), 2.33 (t, *J* = 7.0 Hz, 2H, CH_2), 2.21-2.14 (m, 2H, CH_2), 1.39 (s, 9H, O^{t}Bu); ^{13}C NMR (101 MHz, $CDCl_3$) δ 172.1 (C=O), 139.6 (*ipso*-Ph), 136.9 (=CH), 128.7 (Ph), 128.1 (Ph), 126.8 (Ph), 115.4 ($=CH_2$), 80.2 (CMe_3), 58.3 (CH_2), 53.0 (CH_2), 49.5 (CH_2), 33.8 (CH_2), 31.5 (CH_2), 28.1 (CMe_3); MS (ESI) *m/z* 290 [$(M + H)^+$, 100];

HMRS (ESI) *m/z* calcd for $C_{18}H_{27}NO_2$ $(M + H)^+$ 290.2115, found 290.2110 (+1.7 ppm error).

Lab book reference: mcw/4/25

Attempted synthesis of *tert*-butyl 1-benzyl-4-methylpiperidine-3-carboxylate 97

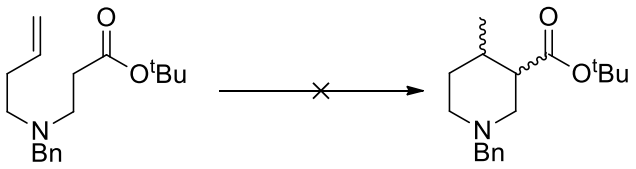

95 **97**

Using general procedure J, lithium bis(trimethylsilyl)amide (1.0 M solution in THF, 6.91 mmol, 2.0 eq.), ester-alkene **95** (1.00 g, 3.45 mmol, 1.0 eq.) in Et_2O (20 mL), zinc bromide (1.55 g, 6.91 mmol, 2.0 eq.) in Et_2O (30 mL) and a 2:1 solution of saturated $NH_4Cl_{(aq)}$-$NH_4OH_{(aq)}$ (15 mL) gave no identifiable product.

Lab book reference: mcw/4/30

(*E*)-Methyl 3-((2-hydroxy-1-phenylethyl)amino)but-2-enoate 111

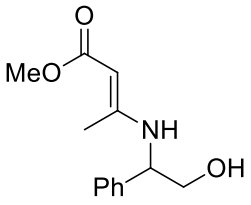

111

Methyl acetoacetate **115** (2.16 mL, 20.0 mmol, 1.1 eq.) was added to a stirred solution of phenylglycinol **114** (2.50 g, 18.2 mmol, 1.0 eq.) in MeOH (90 mL) at rt under Ar. The resulting solution was stirred and heated at reflux for 24 h. After being allowed to cool to rt, the solvent was evaporated under reduced pressure to give crude enaminoester **111** (4.28 g, 100%) as a pale yellow solid, mp 92-93 °C (lit.[106] 61 °C), ^{1}H NMR (400 MHz, $CDCl_3$) δ 9.22 (d, *J* = 8.0 Hz, 1H, NH), 7.40-7.24 (m, 5H, Ph), 4.67 (ddd, *J* = 8.0, 7.0, 4.0, 1H, NCH), 4.56 (s, 1H, =CH), 3.87 (dd, *J* = 11.0, 4.0 Hz, 1H, CH), 3.79 (dd, *J* = 11.0, 7.0 Hz, 1H, CH), 3.67 (s, 3H, OMe), 1.93 (br s, 1H, OH),

1.82 (s, 3H, Me); ^{13}C NMR (101.6 MHz, $CDCl_3$) δ 171.1 (C=O), 161.9 (=C), 139.7 (*ipso*-Ph), 128.9 (Ph), 127.8 (Ph), 126.4 (Ph), 84.1 (=CH), 67.3 (CH_2OH), 59.1 (NCH), 50.2 (OMe), 19.8 (Me). Spectroscopic data consistent with those reported in the literature.[106]

Lab book reference: mcw/4/3

Methyl 8a-methyl-5-oxo-3-phenylhexahydro-2H-oxazolo[3,2-a]pyridine-8-carboxylate *cis*-113 and *trans*-113

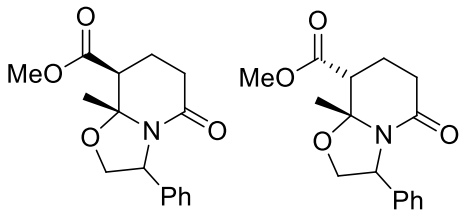

cis-**113** *trans*-**113**

Acryloyl chloride **112** (1.38 mL, 17.0 mmol, 1.0 eq.) was added to a stirred solution of enamino ester **111** (4.00 g, 17.0 mmol 1.0 eq.) in THF (180 mL) at 0 °C under Ar. The resulting solution was stirred at 0 °C for 3 h. Saturated $NaHCO_{3(aq)}$ (30 mL) was added and the mixture was extracted with Et_2O (3 x 25 mL). The combined organic extracts were dried ($MgSO_4$) and evaporated under reduced pressure to give the crude product. Purification by flash chromatography on silica with 60:40, 30:70 hexane-EtOAc as eluent gave a 75:25 mixture (by ^{1}H NMR spectroscopy) of oxazololactams *cis*-**113** and *trans*-**113** (1.61 g, 57%) as a yellow oil, R_F (60:40 hexane-EtOAc) 0.1; ^{1}H NMR (400 MHz, $CDCl_3$) δ 7.37-7.19 (m, 5H, Ph), 5.34 (dd, *J* = 8.0, 8.0 Hz, 0.75H, CHPh), 5.31-5.27 (m, 0.25H, CHPh), 4.55 (dd, *J* = 8.0, 8.0, 0.75H, CHO), 4.39 (dd, *J* = 8.0, 8.0 Hz, 0.25H, CHO), 3.99 (dd, *J* = 9.0, 8.0 Hz, 0.75H, CHO), 3.93 (dd, *J* = 9.0, 8.0 Hz, 0.25H, CHO), 3.78 (s, 2.25H, OMe), 3.71 (s, 0.75H, OMe), 3.16 (dd, *J* = 4.0, 4.0 Hz, 0.25H, $CHCO_2Me$), 2.79-2.74 (m, 0.75H, CH), 2.73-2.71 (m, 0.25H, CH), 2.70-2.65 (m, 0.75H, CH), 2.56-2.43 (m, 1H, CH), 2.22-2.11 (m, 2H, CH_2), 1.55 (s, 0.75H, Me), 1.48 (s, 2.25H, Me); ^{13}C NMR (101.6 MHz, $CDCl_3$) δ 171.5 (C=O, *trans*), 171.4 (C=O, *cis*), 169.2 (C=O, *trans*), 168.4 (C=O, *cis*), 139.6 (*ipso*-Ph, *trans*), 139.2 (*ipso*-Ph, *cis*), 128.7 (Ph, *cis*), 128.6 (Ph, *trans*), 127.4 (Ph, *cis*), 127.3 (Ph, *trans*), 125.7 (Ph, *trans*), 125.5 (Ph, *cis*), 93.9 (*C*Me, *cis*), 93.8 (*C*Me, *trans*), 70.1 (OCH_2, *cis*), 70.1 (OCH_2, *trans*), 59.4 (NCH, *trans*), 58.6 (NCH, *cis*), 52.4 (OMe, *cis*), 51.9

(OMe, *trans*), 50.1 (CH, *cis*), 47.0 (CH, *trans*), 29.7 (CH_2, *cis*), 27.5 (CH_2, *trans*), 25.9 (Me, *trans*), 20.5 (Me, *cis*), 20.2 (CH_2, *cis*), 19.9 (CH_2, *trans*). Spectroscopic data consistent with those reported in the literature.[106]

Lab book reference: mcw/4/54

Methyl 1-(2-hydroxy-1-phenylethyl)-2-methylpiperidine-3-carboxylate *cis*-110 and *trans*-110

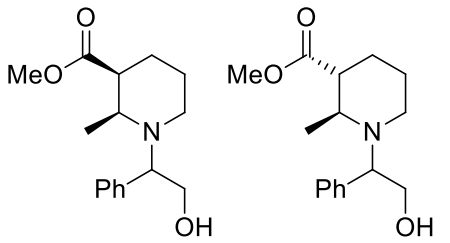

cis-**110** *trans*-**110**

$BH_3 \cdot Me_2S$ (6.91 mL of a 2 M solution in THF, 13.8 mmol, 4.0 eq.) was added to a stirred solution of a 75:25 mixture of oxazololactams *cis*-**113** and *trans*-**113** (1.00 g, 3.45 mmol, 1.0 eq.) in THF (40 mL) at rt under Ar. The resulting solution was stirred at rt for 24 h. H_2O (20 mL) was added carefully (CARE - vigorous reaction) and the mixture was extracted with Et_2O (3 x 25 mL). The combined organic extracts were dried ($MgSO_4$) and evaporated under reduced pressure to give the crude product. Purification by flash chromatography on silica with 60:40 hexane-EtOAc and then EtOAc as eluent gave a 70:30 mixture (by ^{1}H NMR spectroscopy) of piperidines *cis*-**110** and *trans*-**110** (402 g, 42%) as a yellow oil, R_F (60:40 hexane-EtOAc) 0.1; ^{1}H NMR (400 MHz, $CDCl_3$) δ 7.38-7.13 (m, 5H, Ph), 4.29 (dd, *J* = 10.5, 5.0 Hz, 0.3H, CHO), 3.98 (dd, *J* = 10.5, 10.5 Hz, 0.3H, CHO), 3.92 (dd, *J* = 6.5, 6.5 Hz, 0.7H, CHPh), 3.87-3.74 (m, 1.4H, CHO), 3.67 (s, 0.9H, OMe), 3.62 (s, 2.1H, OMe), 3.58 (dd, *J* = 10.5, 5.0 Hz, 0.3H, CHPh), 3.20-3.12 (m, 0.7H, NCH), 2.90 (ddd, *J* = 12.0, 4.0, 4.0 Hz, 0.3H, NCH), 2.82-2.64 (m, 2H, NCH), 2.39-2.28 (m, 1H, CH), 1.90-1.62 (m, 3H, CH), 1.55-1.36 (m, 1H, CH), 1.25 (d, *J* = 6.5 Hz, 0.9H, Me), 1.03 (d, *J* = 6.5 Hz, 2.1H, Me); ^{13}C NMR (101.6 MHz, $CDCl_3$) δ 175.3 (C=O, *trans*), 174.1 (C=O, *cis*), 138.8 (*ipso*-Ph, *trans*), 135.6 (*ipso*-Ph, *cis*), 128.7 (Ph, *trans*), 128.5 (Ph, *cis*), 128.3 (Ph, *trans*), 128.2 (Ph, *cis*), 127.8 (Ph, *trans*), 127.6 (Ph, *cis*), 64.0 (NCH, *cis*), 61.8 (OCH_2, *cis*), 60.9 (NCH, *trans*), 59.4 (OCH_2, *trans*), 54.5 (OMe, *trans*), 52.7

(OMe, *cis*), 51.6 (NCH, *trans*), 51.4 (NCH, *cis*), 51.0 (CH, *trans*), 46.4 (CH, *cis*), 45.0 (NCH_2, *trans*), 43.7 (NCH_2, *cis*), 27.8 (CH_2, *trans*), 25.0 (CH_2, *trans*), 23.8 (CH_2, *cis*), 23.6 (CH_2, *cis*), 12.0 (Me, *cis*), 18.4 (Me, *trans*). Spectroscopic data consistent with those reported in the literature.[106]

Methyl 2-methylpiperidine-3-carboxylate *trans*-107 and *cis*-107

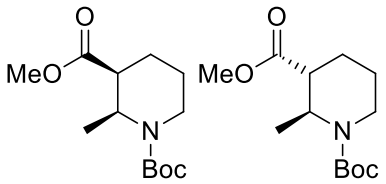

cis-**107** *trans*-**107**

10% Pd/C (192 mg, 0.18 mmol, 0.5 eq.) was added to a stirred solution of a 70:30 mixture of piperidines *cis*-**110** and *trans*-**110** (100 mg, 0.36 mmol, 1.0 eq.) in MeOH (9 mL) at rt under Ar. The reaction flask was evacuated under reduced pressure and back-filled with Ar three times. After the final evacuation, H_2 was charged and the reaction mixture stirred at rt under a H_2 atmosphere for 24 h. The solids were removed by filtration through Celite and washed with MeOH (15 mL). The filtrate was evaporated under reduced pressure to give deprotected piperidine **108** as shown by ^{1}H NMR spectroscopy. Di-*tert*-butyl dicarbonate (218 mg, 0.10 mmol, 1.45 eq.) was added to a stirred solution of the crude deprotected piperidine **108** in CH_2Cl_2 (5 mL) at 0 °C under Ar. The solution was then allowed to warm to rt over 3 h and stirred at rt for 30 h. H_2O (2 mL) was added and the mixture was extracted with CH_2Cl_2 (3 x 5 mL). The combined organic extracts were dried ($MgSO_4$) and evaporated under reduced pressure to give the crude product. Purification by flash chromatography on silica with 80:20 and then 50:50 hexane-Et_2O as eluent gave *N*-boc-piperidine *cis*-**107** (51 mg, 40%) as a clear oil, R_F (50:50 hexane-Et_2O) 0.3; IR (ATR) 2972, 1735 (C=O, CO_2Me), 1687 (C=O, Boc), 1413, 1363, 1174, 1147, 1130 cm^{-1}; ^{1}H NMR (400 MHz, $CDCl_3$) δ 4.87 (br q, *J* = 7.0 Hz, 1H, NCH), 3.94 (br dd, *J* = 13.5, 4.0 Hz, 1H, NCH_2), 3.69 (s, 3H, OMe), 2.81 (ddd, *J* = 13.5, 13.5, 3.5 Hz, 1H, NCH), 2.42-2.38 (m, 1H, CH), 2.04 (br dd, *J* = 13.5, 3.5 Hz, 1H, CH), 1.82-1.58 (m, 3H, CH), 1.45 (s, 9H, CMe_3), 1.21 (d, *J* = 7.0 Hz, 3H, Me); ^{13}C NMR (101.6 MHz, $CDCl_3$) δ 173.9 (C=O, CO_2Me), 154.8 (C=O, Boc), 79.2 (*C*Me_3), 51.8 (OMe), 47.2 (NCH), 43.8

(*CH*CO_2Me), 37.7 (NCH_2), 28.4 (C*Me*$_3$), 21.8 (CH_2), 20.5 (CH_2), 16.5 (Me); MS (ESI) *m/z* 280 [$(M + Na)^+$, 100]; HMRS (ESI) *m/z* calcd for $C_{13}H_{23}NO_4$ $(M + Na)^+$ 280.1519, found 280.1525 (–2.3 ppm error) and *N*-boc-piperidine *trans*-**107** (38 mg, 30%) as a clear oil, R_F (50:50 hexane-Et_2O) 0.2; IR (ATR) 2950, 1736 (C=O, CO_2Me), 1687 (C=O, Boc), 1407, 1364, 1240, 1146, 1000, 832 cm^{-1}; ^{1}H NMR (400 MHz, $CDCl_3$) (50:50 mixture of rotamers) δ 4.83 (br s, 0.5H, NCH), 4.63 (br s, 0.5H, NCH), 3.99 (br d, *J* = 11.5 Hz, 0.5H, NCH), 3.85 (br d, *J* = 11.5 Hz, 0.5H, NCH), 3.70 (s, 1.5H, OMe), 3.67 (s, 1.5H, OMe), 2.87-2.68 (m, 1H, NCH), 2.62 (ddd, *J* = 12.5, 4.5, 4.5 Hz, 1H, C*H*CO_2Me), 1.91-1.61 (m, 4H, CH), 1.46 (s, 9H, CMe_3), 1.02 (d, *J* = 7.0 Hz, 3H, Me); ^{13}C NMR (101.6 MHz, $CDCl_3$) (rotamers) δ 173.4 (C=O, CO_2Me), 154.6 (C=O, Boc), 79.6 (*C*Me_3), 53.4 (NCH_2), 51.7 (NCH), 51.6 (NCH), 47.9 (OMe), 46.7 (OMe), 45.2 (CH), 44.8 (CH), 38.5 (CH_2), 37.4 (CH_2), 30.3 (C*Me*$_3$), 28.4 (C*Me*$_3$), 24.8 (CH_2), 24.5 (CH_2), 20.5 (CH_2), 12.2 (Me), 12.0 (Me); MS (ESI) *m/z* 280 [$(M + Na)^+$, 100]; HMRS (ESI) *m/z* calcd for $C_{13}H_{23}NO_4$ $(M + Na)^+$ 280.1519, found 280.1516 (+1.1 ppm error).

Lab book reference: mcw/4/75

3-Carboxy-4-methylpyridin-1-ium chloride 125.HCl

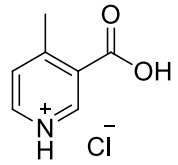

125.HCl

Sodium hydroxide (3.00 g, 74.5 mmol, 4.4 eq.) was added to a stirred solution of cyano-4-methylpyridine **124** (2.00 g, 16.9 mmol, 1.0 eq.) in EtOH (140 mL) and H_2O (60 mL) at rt under air. The solution was stirred and heated at reflux for 3 h. After being allowed to cool to rt, the solvent was evaporated under reduced pressure. H_2O (20 mL) was added to the residue and then 1 M $HCl_{(aq)}$ (75 mL) was added. The water was evaporated under reduced pressure. Hot EtOH (40 mL) was added and the solids were removed by filtration. The filtrate was evaporated under reduced pressure to give the crude product. Purification by flash chromatography on silica with 90:10 EtOAc-MeOH as eluent gave pyridine carboxylic acid **125.HCl** (1.74 g, 59%) as a white solid,

mp 150-151 °C, R_F (90:10 EtOAc-MeOH) 0.2; IR (ATR) 3044, 1665 (C=O), 1597, 1427, 1382, 1059, 839, 669 cm^{-1}; ^1H NMR (400 MHz, DMSO-d_6) δ 8.52 (s, 1H, Ar), 8.45 (d, J = 5.0 Hz, 1H, Ar), 7.93 (br s, 1H, OH), 7.57 (br s, 1 H, NH), 7.28 (d, J = 5.0 Hz, 1H, Ar), 2.38 (s, 3H, Me); ^{13}C NMR (101.6 MHz, DMSO-d_6) δ 168.8 (C=O), 150.0 (Ar), 147.6 (Ar), 144.9 (*ipso*-Ar), 132.7 (*ipso*-Ar), 125.6 (Ar), 19.0 (Me).

Lab book reference: mcw/4/40

Methyl 4-methylnicotinate 126

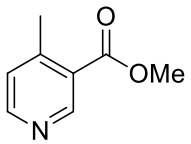

126

Using general procedure K, concentrates H_2SO_4 (2.54 mL, 46.7 mmol, 3.7 eq.) and pyridine carboxylic acid **125.HCl** (1.74 g, 10.0 mmol, 1.0 eq.) in MeOH (20 mL) gave the crude product. Purification by flash chromatography on silica with EtOAc as eluent gave methyl 4-methylnicotinate **126** (1.51 g, 100%) as a clear oil, R_F (EtOAc) 0.5; ^1H NMR (400 MHz, $CDCl_3$) δ 9.05 (s, 1H, Ar), 8.54 (d, J = 5.0 Hz, 1H, Ar), 7.16 (d, J = 5.0 Hz, 1H, Ar), 3.91 (s, 3H, OMe), 2.60 (s, 3H, Me); ^{13}C NMR (101.6 MHz, $CDCl_3$) δ 166.5 (C=O), 152.1 (Ar), 151.6 (Ar), 149.4 (*ipso*-Ar), 126.4 (Ar), 125.7 (*ipso*-Ar), 52.1 (OMe), 21.2 (Me). Spectroscopic data consistent with those reported in the literature.[134]

Lab book referemce: mcw/4/44

Attempted synthesis of methyl 4-methylpiperidine-3-carboxylate 127

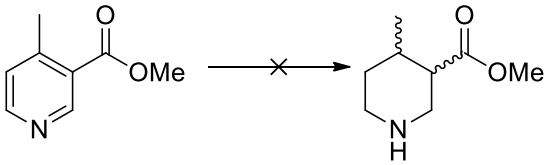

126 **127**

Platinum oxide (4.5 mg, 0.02 mmol, 0.006 eq.) was added to a stirred solution of methyl 4-methylnicotinate **126** (500 mg, 3.31 mmol, 1.0 eq.) in EtOH (5.48 mL) and 6 M $HCl_{(aq)}$ (1 mL) at rt under Ar. The reaction flask was evacuated under reduced pressure and back-filled with Ar three times. After the final evacuation, H_2 was charged and the reaction mixture was stirred vigorously at rt under a H_2 atmosphere for 24 h. The solids were removed by filtration through Celite and washed with the MeOH (20 mL). The filtrate was evaporated under reduced pressure. Then, the residue was dissolved in 2 M $NH_4OH_{(aq)}$ (10 mL) and the aqueous layer was extracted with CH_2Cl_2 (3 x 10 mL). The combined organic extracts were dried ($MgSO_4$) and evaporated under reduced pressure to give recovered methyl 4-methylnicotinate **126** (490 mg, 98%) as a yellow oil.

10% Pd/C (105 mg, 0.10 mmol, 0.03 eq.) was added to a stirred solution of methyl 4-methylnicotinate **126** (500 mg, 3.31 mmol, 1.0 eq.) in concentrated $HCl_{(aq)}$ (0.31 mL) and MeOH (20 mL) under air in a high pressure pot reactor. After evacuation, H_2 was charged at 5 bar and the reaction mixture was stirred and heated at 80 °C for 18 h. After being allowed to cool to rt, the solids were removed by filtration through Celite and washed with MeOH (20 mL). The filtrate was evaporated under reduced pressure. ^{1}H NMR spectroscopy of the crude product showed that none of the desired product had been formed.

Platinum oxide (59.2 mg, 2.61 mmol, 0.09 eq.) and 10% Pd/C (41.3 mg, 0.04 mmol, 0.013 eq.) was added to a stirred solution of methyl 4-methylnicotinate **126** (438 mg, 2.89 mmol, 1.0 eq.) in glacial acetic $acid_{(aq)}$ (13 mL) under air in a high pressure pot reactor. After evacuation, H_2 was charged at 5 bar and the reaction mixture stirred at rt for 72 h. The solids were removed by filtration through Celite and washed with

MeOH (20 mL). The filtrate was then evaporated under reduced pressure. ^{1}H NMR spectrospcopy of the crude product showed that none of the desired product had been formed.

1-Benzyl-3-(methoxycarbonyl)pyridin-1-ium bromide 129

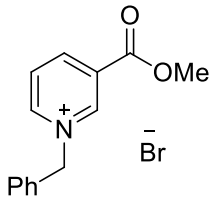

129

Using general procedure L, benzyl bromide (0.86 mL, 7.29 mmol, 1.0 eq.) and methyl nicotinate **128** (1.00 g, 7.29 mmol, 1.0 eq.) in MeCN (18 mL) gave benzyl pyridinium bromide **129** (2.24 g, 100%) as a yellow oil, ^{1}H NMR (400 MHz, $CDCl_3$) δ 10.09 (br d, *J* = 6.0 Hz, 1H, Ar), 9.68 (s, 1H, Ar), 8.85 (br d, *J* = 8.0 Hz, 1H, Ar), 8.26 (dd, *J* = 8.0, 6.0 Hz, 1H, Ar), 7.71-7.67 (m, 2H, Ph), 7.40-7.34 (m, 3H, Ph), 6.47 (s, 2H, NCH_2Ph), 3.97 (s, 3H, OMe); ^{13}C NMR (101.6 MHz, $CDCl_3$) δ 161.4 (C=O), 148.8 (Ar), 145.3 (Ar), 145.1 (Ar), 132.4 (*ipso*-Ar), 130.3 (*ipso*-Ar), 130.1 (Ar), 129.8 (Ar), 129.7 (Ar), 128.6 (Ar), 64.7 (NCH_2), 53.8 (OMe). Spectroscopic data consistent with those reported in the literature.[135]

Lab book reference: mcw/4/76

Methyl 1-benzyl-1,2,5,6-tetrahydropyridine-3-carboxylate 130

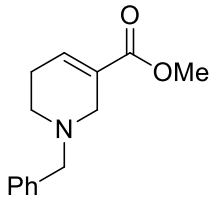

130

Using general procedure M, sodium borohydride (2.48 g, 65.6 mmol, 9.0 eq.) and benzyl pyridinium bromide **129** (2.24 g, 7.29 mmol, 1.0 eq.) in MeOH (20 mL) and H_2O (10 mL) gave the crude product. Purification by flash chromatography on silica with 70:30 and then 50:50 hexane-EtOAc as eluent gave tetrahydropyridine **130** (355

mg, 21%) as a pale yellow oil, R_F (50:50 hexane-EtOAc) 0.2; ^{1}H NMR (400 MHz, $CDCl_3$) δ 7.37-7.23 (m, 5H, Ph), 7.03-6.99 (m, 1H, =CH), 3.71 (s, 3H, OMe), 3.65 (s, 2H, NCH_2Ph), 3.24-3.20 (m, 2H, NCH_2), 2.53 (t, J = 6.0 Hz, 2H, NCH_2), 2.36-2.29 (m, 2H, CH_2); ^{13}C NMR (101.6 MHz, $CDCl_3$) δ 166.3 (C=O), 138.0 (*ipso*-Ph), 137.9 (=CH), 129.1 (=C), 129.0 (Ph), 128.3 (Ph), 127.1 (Ph), 62.4 (NCH_2), 51.6 (NCH_2), 51.5 (OMe), 48.3 (CH_2), 26.5 (CH_2). Spectroscopic data consistent with those reported in the literature.[136]

Lab book reference: mcw/4/77

1-Benzyl-3-(methoxycarbonyl)-4-methylpyridin-1-ium bromide 131

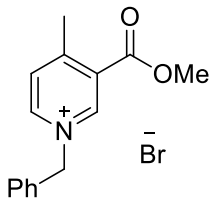

131

Using general procedure L, benzyl bromide (0.4 mL, 3.30 mmol, 1.0 eq.) and methyl 4-methylnicotinate **126** (500 mg, 3.30 mmol, 1.0 eq.) in MeCN (8 mL) gave benzyl pyridinium bromide **131** (1.06 g, 100%) as an orange oil, ^{1}H NMR (400 MHz, $CDCl_3$) δ 9.85 (dd, J = 6.0, 1.0 Hz, 1H, Ar), 9.48 (d, J = 1.0 Hz, 1H, Ar), 7.93 (d, J = 6.0 Hz, 1H, Ar), 7.67-7.63 (m, 2H, Ph), 7.44-7.38 (m, 3H, Ph), 6.36 (s, 2H, NCH_2Ph), 4.00 (s, 3H, OMe), 2.85 (s, 3H, Me); ^{13}C NMR (101.6 MHz, $CDCl_3$) δ 162.1 (C=O), 161.0 (*ipso*-Ar), 146.5 (Ar), 145.5 (Ar), 132.4 (*ipso*-Ar), 131.1 (Ar), 130.2 (Ar), 129.74 (Ar), 129.67 (Ar), 129.2 (*ipso*-Ar), 64.2 (NCH_2), 53.6 (OMe), 22.5 (Me); MS (ESI) *m/z* 242 [M^+, 100]; HMRS (ESI) *m/z* calcd for $C_{15}H_{25}NO_2\,M^+$ 242.1176, found 242.1177 (–0.4 ppm error).

Lab book reference: mcw/4/98

Methyl 1-benzyl-4-methyl-1,2,5,6-tetrahydropyridine-3-carboxylate 132

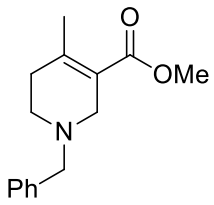

132

Using general procedure M, sodium borohydride (1.12 g, 29.7 mmol, 9.0 eq.) and benzyl pyridinium bromide **131** (1.06 g, 3.30 mmol, 1.0 eq.) in MeOH (6 mL) and H_2O (3 mL) gave the crude product. Purification by flash chromatography on silica with 80:20 and then 50:50 hexane-EtOAc as eluent gave 4-methyl tetrahydropyridine **132** (436 mg, 44%) as a pale yellow oil, R_F (50:50 hexane-EtOAc) 0.2; IR (ATR) 2948, 2764, 1714 (C=O), 1433, 1243, 1216, 1061, 737, 697 cm^{-1}; ^1H NMR (400 MHz, $CDCl_3$) δ 7.38-7.20 (m, 5H, Ph), 3.69 (s, 3H, OMe), 3.61 (br s, 2H, NCH_2Ph), 3.25-3.18 (m, 2H, NCH_2), 2.50 (br t, J = 6.0 Hz, 2H, NCH_2), 2.29-2.25 (m, 2H, CH_2), 2.09 (s, 3H, Me); ^{13}C NMR (101.6 MHz, $CDCl_3$) δ 167.2 (C=O), 147.4 (=C), 138.1 (*ipso*-Ph), 129.1 (Ph), 128.3 (Ph), 127.1 (Ph), 122.3 (=C), 62.4 (NCH_2Ph), 53.3 (NCH_2), 51.1 (OMe), 48.9 (NCH_2), 34.4 (CH_2), 21.4 (Me); MS (ESI) *m/z* 246 [$(M + H)^+$, 100]; HMRS (ESI) *m/z* calcd for $C_{15}H_{19}NO_2$ $(M + H)^+$ 246.1489, found 246.1481 (+1.7 ppm error).

Lab book reference: mcw/5/2

1-Benzyl-5-(methoxycarbonyl)-2-methylpyridin-1-ium bromide 133

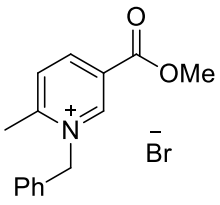

133

Using general procedure L, benzyl bromide (0.4 mL, 3.30 mmol, 1.0 eq.) and methyl 6-methylnicotinate **121** (500 mg, 3.30 mmol, 1.0 eq.) in MeCN (8 mL) gave benzyl pyridinium bromide **133** (1.06 g, 100%) as a yellow oil, ^1H NMR (400 MHz, $CDCl_3$) δ 9.47 (d, J = 1.0 Hz, 1H, Ar), 8.80 (dd, J = 8.0, 1.0 Hz, 1H, Ar), 8.15 (d, J = 8.0 Hz,

1H, Ar), 7.44-7.40 (m, 3H, Ph), 7.38-7.33 (m, 2H, Ph), 6.31 (s, 2H, NCH_2Ph), 3.99 (s, 3H, OMe), 3.15 (s, 3H, Me); ^{13}C NMR (101.6 MHz, $CDCl_3$) δ 161.6 (C=O), 160.5 (*ipso*-Ar), 146.6 (Ar), 144.8 (Ar), 130.9 (Ar), 130.8 (*ipso*-Ar), 129.9 (Ar), 129.8 (Ar), 128.6 (Ar), 128.4 (*ipso*-Ar), 63.0 (NCH_2), 53.7 (OMe), 22.5 (Me). Spectroscopic data consistent with those reported in the literature.[135]

Lab book reference: mcw/4/78

Methyl 1-benzyl-6-methyl-1,2,5,6-tetrahydropyridine-3-carboxylate 134

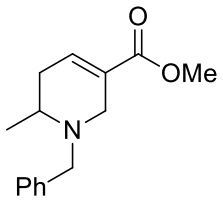

134

Using general procedure M, sodium borohydride (1.12 g, 29.7 mmol, 9.0 eq.) and benzyl pyridinium bromide **133** (1.06 g, 3.30 mmol, 1.0 eq.) in MeOH (6 mL) and H_2O (3 mL) gave the crude product. Purification by flash chromatography on silica with 80:20 and then 50:50 hexane-EtOAc as eluent gave 2-methyl tetrahydropyridine **134** (234 mg, 29%) as a pale yellow oil, R_F (50:50 hexane-EtOAc) 0.4; IR (ATR) 2950, 2803, 1711 (C=O), 1435, 1255, 1116, 722, 697 cm^{-1}; ^1H NMR (400 MHz, $CDCl_3$) δ 7.39-7.21 (m, 5H, Ph), 7.03-6.94 (m, 1H, =CH), 3.77 (d, *J* = 13.5 Hz, 1H, CHPh), 3.70 (s, 3H, OMe), 3.55 (d, *J* = 13.5 Hz, 1H, CHPh), 3.27-3.23 (m, 2H, NCH), 2.94 (m, 1H, NC*H*Me), 2.54-2.45 (m, 1H, CH), 2.08-1.99 (m, 1H, CH), 1.05 (d, *J* = 6.5 Hz, 3H, Me); ^{13}C NMR (101.6 MHz, $CDCl_3$) δ 166.3 (C=O), 138.9 (*ipso*-Ph), 137.2 (=CH), 128.8 (Ph), 128.3 (Ph), 128.2 (=C), 127.0 (Ph), 57.6 (NCH_2Ph), 51.5 (OMe), 49.8 (NCH), 47.1 (NCH_2), 32.7 (CH_2), 14.0 (Me); MS (ESI) *m/z* 246 [$(M + H)^+$, 100]; HMRS (ESI) *m/z* calcd for $C_{15}H_{19}NO_2$ $(M + H)^+$ 246.1489, found 246.1486 (–0.8 ppm error).

Lab book reference: mcw/4/79

Abbreviations

Δ	Heat
$A^{1,3}$	Allylic 1,3-Strain
aq	Aqueous
Bn	Benzyl
Boc	*t*-Butoxycarbonyl
br	Broad
cbz	Carboxybenzyl
CHARMm	Chemistry at HARvard Macromolecular Mechanics
cm^{-1}	Wavenumber
d	Doublet
Da	Dalton(s)
DABCO	1,4-Diazabicyclo[2.2.2]octane
DBU	1,8-Diazabicyclo[5.4.0]undec-7-ene
DMF	Dimethylformamide
DMPU	*N,N′*-Dimethylpropylene urea
DMSO	Dimethylsulfoxide
E^+	Electrophile
Eq.	Equivalents
ESI	Electrospray ionisation
Et_2O	Diethyl ether
EtOAc	Ethyl acetate
FBDD	Fragment based drug discovery
FDA	Food and drug administration
Fmoc	Fluorenylmethyloxycarbonyl

H bond	Hydrogen bond
HAC	Heavy atom count
Het Ar	Heteroaryl
HRMS	High resolution mass spectrometry
HTS	High throughput screening
IR	Infra-red
J	Coupling constant in Hz
KHMDS	Potassium bis(trimethylsilyl)amide
LDA	Lithium diisopropylamide
LHMDS	Lithium bis(trimethylsilyl)amide
m	Multiplet
M	Molar
m/z	Mass to charge ratio
M^+	Molecular ion
Me	Methyl
MS	Mass spectrometry
Ms	Mesyl
MW	Molecular weight
NMR	Nuclear Magnetic Resonance
npr	Normalised PMI ratio
O-Su	*N*-Hydroxysuccinimide
PAINS	Pan-assay interference compounds
PBF	Plane of Best Fit
Petrol	Petroleum Ether (fraction which boils at 40-60 °C)
PhF	9-Phenyl-9-fluorenyl

PMI	Principal moment of inertia
ppm	Parts per million
PrATs	Promiscuous 2-AminoThiazoles
PSA	Polar surface area
q	Quartet
R_F	Retention Factor
RMS	Root Mean Square
RMSD	Root Mean Square Deviation
ROCS	Rapid Overlay of Chemical Structures
rt	Room Temperature
s	Singlet
SMILES	Simplified molecular-input line-entry system
SPR	Surface plasmon resonance
t	Triplet
TBS	*tert*-Butyldimethylsilyl
TFA	Trifluoroacetic acid
THF	Tetrahydrofuran
TIPS	triisopropylsilyl
TMEDA	*N,N,N',N'*-Tetramethylethylenediamine
Trisyl	2,4,6-Triisopropylbenzenesulfonyl
VT NMR	Variable Temperature Nuclear Magnetic Resonance
δ	Chemical Shift

References

(1) Murray, C. W.; Rees, D. C. *Nat. Chem.* **2009**, *1*, 187.
(2) Chessari, G.; Woodhead, A. J. *Drug Discovery Today* **2009**, *14*, 668.
(3) Carr, R. A. E.; Congreve, M.; Murray, C. W.; Rees, D. C. *Drug Discovery Today* **2005**, *10*, 987.
(4) Zartler, E. R.; Shapiro, M. J. *Curr. Opin. Chem. Biol.* **2005**, *9*, 366.
(5) Murray, C. W.; Verdonk, M. L.; Rees, D. C. *Trends Pharmacol. Sci.* **2012**, *33*, 224.
(6) Wenlock, M. C.; Austin, R. P.; Barton, P.; Davis, A. M.; Leeson, P. D. *J. Med. Chem.* **2003**, *46*, 1250.
(7) Leeson, P. D.; Springthorpe, B. *Nat. Rev. Drug Discovery* **2007**, *6*, 881.
(8) Shuker, S. B.; Hajduk, P. J.; Meadows, R. P.; Fesik, S. W. *Science* **1996**, *274*, 1531.
(9) Congreve, M.; Carr, R.; Murray, C.; Jhoti, H. *Drug Discovery Today* **2003**, *8*, 876.
(10) Jhoti, H.; Williams, G.; Rees, D. C.; Murray, C. W. *Nat. Rev. Drug Discovery* **2013**, *12*, 644.
(11) Lipinski, C. A.; Lombardo, F.; Dominy, B. W.; Feeney, P. J. *Adv. Drug Delivery Rev.* **2001**, *46*, 3.
(12) Congreve, M.; Chessari, G.; Tisi, D.; Woodhead, A. J. *J. Med. Chem.* **2008**, *51*, 3661.
(13) Hall, R. J.; Mortenson, P. N.; Murray, C. W. *Prog. Biophys. Mol. Biol.* **2014**, *116*, 82.
(14) Baker, M. *Nat. Rev. Drug Discovery* **2013**, *12*, 5.
(15) Lau, W.; Withka, J.; Hepworth, D.; Magee, T.; Du, Y.; Bakken, G.; Miller, M.; Hendsch, Z.; Thanabal, V.; Kolodziej, S.; Xing, L.; Hu, Q.; Narasimhan, L.; Love, R.; Charlton, M.; Hughes, S.; van Hoorn, W.; Mills, J. *J. Comput.-Aided Mol. Des.* **2011**, *25*, 621.
(16) Hajduk, P. J.; Galloway, W. R. J. D.; Spring, D. R. *Nature* **2011**, *470*, 42.
(17) Hann, M. M.; Leach, A. R.; Harper, G. *J. Chem. Inf. Comput. Sci.* **2001**, *41*, 856.
(18) Leach, A. R.; Hann, M. M. *Curr. Opin. Chem. Biol.* **2011**, *15*, 489.
(19) Keserű, G. M.; Erlanson, D. A.; Ferenczy, G. G.; Hann, M. M.; Murray, C. W.; Pickett, S. D. *J. Med. Chem.* **2016**.
(20) Bembenek, S. D.; Tounge, B. A.; Reynolds, C. H. *Drug Discovery Today* **2009**, *14*, 278.
(21) Blomberg, N.; Cosgrove, D.; Kenny, P.; Kolmodin, K. *J. Comput.-Aided Mol. Des.* **2009**, *23*, 513.
(22) Davis, B. J.; Erlanson, D. A. *Bioorg. Med. Chem. Lett.* **2013**, *23*, 2844.
(23) Warr, W. A. *J. Comput.-Aided Mol. Des.* **2009**, *23*, 453.
(24) Scott, D. E.; Coyne, A. G.; Hudson, S. A.; Abell, C. *Biochemistry* **2012**, *51*, 4990.
(25) Chen, I.-J.; Hubbard, R. E. *J. Comput.-Aided Mol. Des.* **2009**, *23*, 603.
(26) Siegal, G.; Ab, E.; Schultz, J. *Drug Discovery Today* **2007**, *12*, 1032.
(27) Murray, C. W.; Rees, D. C. *Angew. Chem., Int. Ed.* **2016**, *55*, 488.
(28) Schulz, M. N.; Landström, J.; Bright, K.; Hubbard, R. E. *J. Comput.-Aided Mol. Des.* **2011**, *25*, 611.
(29) Baell, J. B.; Holloway, G. A. *J. Med. Chem.* **2010**, *53*, 2719.
(30) Baell, J. W., M.A. *Nature* **2014**, *513*, 481.

(31) Devine, S. M.; Mulcair, M. D.; Debono, C. O.; Leung, E. W. W.; Nissink, J. W. M.; Lim, S. S.; Chandrashekaran, I. R.; Vazirani, M.; Mohanty, B.; Simpson, J. S.; Baell, J. B.; Scammells, P. J.; Norton, R. S.; Scanlon, M. J. *J. Med. Chem.* **2015**, *58*, 1205.
(32) Irwin, J. J.; Duan, D.; Torosyan, H.; Doak, A. K.; Ziebart, K. T.; Sterling, T.; Tumanian, G.; Shoichet, B. K. *J. Med. Chem.* **2015**, *58*, 7076.
(33) Sun, C.; Petros, A.; Hajduk, P. *J. Comput.-Aided Mol. Des.* **2011**, *25*, 607.
(34) Blomberg, N.; Cosgrove, D. A.; Kenny, P. W.; Kolmodin, K. *J. Comput.-Aided Mol. Des.* **2009**, *23*, 513.
(35) Cox, O. B.; Krojer, T.; Collins, P.; Monteiro, O.; Talon, R.; Bradley, A.; Fedorov, O.; Amin, J.; Marsden, B. D.; Spencer, J.; von Delft, F.; Brennan, P. E. *Chem. Sci.* **2016**, *7*, 2322.
(36) Aldeghi, M.; Malhotra, S.; Selwood, D. L.; Chan, A. W. E. *Chem. Biol. Drug Des.* **2014**, *83*, 450.
(37) Morley, A. D.; Pugliese, A.; Birchall, K.; Bower, J.; Brennan, P.; Brown, N.; Chapman, T.; Drysdale, M.; Gilbert, I. H.; Hoelder, S.; Jordan, A.; Ley, S. V.; Merritt, A.; Miller, D.; Swarbrick, M. E.; Wyatt, P. G. *Drug Discovery Today* **2013**, *18*, 1221.
(38) Over, B.; Wetzel, S.; Grütter, C.; Nakai, Y.; Renner, S.; Rauh, D.; Waldmann, H. *Nat. Chem.* **2013**, *5*, 21.
(39) James, T.; MacLellan, P.; Burslem, G. M.; Simpson, I.; Grant, J. A.; Warriner, S.; Sridharan, V.; Nelson, A. *Org. Biomol. Chem.* **2014**, *12*, 2584.
(40) Lovering, F.; Bikker, J.; Humblet, C. *J. Med. Chem.* **2009**, *52*, 6752.
(41) Hung, A. W.; Ramek, A.; Wang, Y.; Kaya, T.; Wilson, J. A.; Clemons, P. A.; Young, D. W. *Proc. Natl. Acad. Sci.* **2011**, *108*, 6799.
(42) Erlanson, D. A.; Fesik, S. W.; Hubbard, R. E.; Jahnke, W.; Jhoti, H. *Nat. Rev. Drug Discovery* **2016**, *15*, 605.
(43) Bollag, G.; Hirth, P.; Tsai, J.; Zhang, J.; Ibrahim, P. N.; Cho, H.; Spevak, W.; Zhang, C.; Zhang, Y.; Habets, G.; Burton, E. A.; Wong, B.; Tsang, G.; West, B. L.; Powell, B.; Shellooe, R.; Marimuthu, A.; Nguyen, H.; Zhang, K. Y. J.; Artis, D. R.; Schlessinger, J.; Su, F.; Higgins, B.; Iyer, R.; D/'Andrea, K.; Koehler, A.; Stumm, M.; Lin, P. S.; Lee, R. J.; Grippo, J.; Puzanov, I.; Kim, K. B.; Ribas, A.; McArthur, G. A.; Sosman, J. A.; Chapman, P. B.; Flaherty, K. T.; Xu, X.; Nathanson, K. L.; Nolop, K. *Nature* **2010**, *467*, 596.
(44) Tsai, J.; Lee, J. T.; Wang, W.; Zhang, J.; Cho, H.; Mamo, S.; Bremer, R.; Gillette, S.; Kong, J.; Haass, N. K.; Sproesser, K.; Li, L.; Smalley, K. S. M.; Fong, D.; Zhu, Y.-L.; Marimuthu, A.; Nguyen, H.; Lam, B.; Liu, J.; Cheung, I.; Rice, J.; Suzuki, Y.; Luu, C.; Settachatgul, C.; Shellooe, R.; Cantwell, J.; Kim, S.-H.; Schlessinger, J.; Zhang, K. Y. J.; West, B. L.; Powell, B.; Habets, G.; Zhang, C.; Ibrahim, P. N.; Hirth, P.; Artis, D. R.; Herlyn, M.; Bollag, G. *Proc. Natl. Acad. Sci.* **2008**, *105*, 3041.
(45) Oltersdorf, T.; Elmore, S. W.; Shoemaker, A. R.; Armstrong, R. C.; Augeri, D. J.; Belli, B. A.; Bruncko, M.; Deckwerth, T. L.; Dinges, J.; Hajduk, P. J.; Joseph, M. K.; Kitada, S.; Korsmeyer, S. J.; Kunzer, A. R.; Letai, A.; Li, C.; Mitten, M. J.; Nettesheim, D. G.; Ng, S.; Nimmer, P. M.; O'Connor, J. M.; Oleksijew, A.; Petros, A. M.; Reed, J. C.; Shen, W.; Tahir, S. K.; Thompson, C. B.; Tomaselli, K. J.; Wang, B.; Wendt, M. D.; Zhang, H.; Fesik, S. W.; Rosenberg, S. H. *Nature* **2005**, *435*, 677.
(46) Park, C.-M.; Bruncko, M.; Adickes, J.; Bauch, J.; Ding, H.; Kunzer, A.; Marsh, K. C.; Nimmer, P.; Shoemaker, A. R.; Song, X.; Tahir, S. K.; Tse, C.; Wang,

X.; Wendt, M. D.; Yang, X.; Zhang, H.; Fesik, S. W.; Rosenberg, S. H.; Elmore, S. W. *J. Med. Chem.* **2008**, *51*, 6902.
(47) Souers, A. J.; Leverson, J. D.; Boghaert, E. R.; Ackler, S. L.; Catron, N. D.; Chen, J.; Dayton, B. D.; Ding, H.; Enschede, S. H.; Fairbrother, W. J.; Huang, D. C. S.; Hymowitz, S. G.; Jin, S.; Khaw, S. L.; Kovar, P. J.; Lam, L. T.; Lee, J.; Maecker, H. L.; Marsh, K. C.; Mason, K. D.; Mitten, M. J.; Nimmer, P. M.; Oleksijew, A.; Park, C. H.; Park, C.-M.; Phillips, D. C.; Roberts, A. W.; Sampath, D.; Seymour, J. F.; Smith, M. L.; Sullivan, G. M.; Tahir, S. K.; Tse, C.; Wendt, M. D.; Xiao, Y.; Xue, J. C.; Zhang, H.; Humerickhouse, R. A.; Rosenberg, S. H.; Elmore, S. W. *Nat. Med.* **2013**, *19*, 202.
(48) Evin, G. *BioDrugs* **2016**, *30*, 173.
(49) Zhu, Z.; Sun, Z.-Y.; Ye, Y.; Voigt, J.; Strickland, C.; Smith, E. M.; Cumming, J.; Wang, L.; Wong, J.; Wang, Y.-S.; Wyss, D. F.; Chen, X.; Kuvelkar, R.; Kennedy, M. E.; Favreau, L.; Parker, E.; McKittrick, B. A.; Stamford, A.; Czarniecki, M.; Greenlee, W.; Hunter, J. C. *J. Med. Chem.* **2010**, *53*, 951.
(50) Wang, Y.-S.; Strickland, C.; Voigt, J. H.; Kennedy, M. E.; Beyer, B. M.; Senior, M. M.; Smith, E. M.; Nechuta, T. L.; Madison, V. S.; Czarniecki, M.; McKittrick, B. A.; Stamford, A. W.; Parker, E. M.; Hunter, J. C.; Greenlee, W. J.; Wyss, D. F. *J. Med. Chem.* **2010**, *53*, 942.
(51) Sauer, W. H. B.; Schwarz, M. K. *J. Chem. Inf. Comput. Sci.* **2003**, *43*, 987.
(52) Koutsoukas, A.; Paricharak, S.; Galloway, W. R. J. D.; Spring, D. R.; Ijzerman, A. P.; Glen, R. C.; Marcus, D.; Bender, A. *J. Chem. Inf. Model.* **2014**, *54*, 230.
(53) Firth, N. C.; Brown, N.; Blagg, J. *J. Chem. Inf. Model.* **2012**, *52*, 2516.
(54) Grant, J. A.; Gallardo, M. A.; Pickup, B. T. *J. Comput. Chem.* **1996**, *17*, 1653.
(55) Timmermans, J. *Nature* **1954**, *174*, 235.
(56) Meyer, A. Y. *J. Comput. Chem.* **1986**, *7*, 144.
(57) Meyer, A. Y. *Chem. Soc. Rev.* **1986**, *15*, 449.
(58) Taylor, R. D.; MacCoss, M.; Lawson, A. D. G. *J. Med. Chem.* **2014**, *57*, 5845.
(59) Barreiro, E. J.; Kümmerle, A. E.; Fraga, C. A. M. *Chem. Rev.* **2011**, *111*, 5215.
(60) Schönherr, H.; Cernak, T. *Angew. Chem., Int. Ed.* **2013**, *52*, 12256.
(61) Sauer, W. H. B.; Schwarz, M. K. *J. Chem. Inf. Comput. Sci.* **2003**, *43*, 987.
(62) Bond, P.; Hubbard, R. E. *Collaboration between Paul Bond and Rod Hubbard at York Structural Biology Laboratory (YSBL). Pipeline Pilot licensed to YSBL.* **2014**.
(63) Roughley, S. D.; Hubbard, R. E. *Unpublished results* **2014**.
(64) *Maybridge Rule of 3 Library Core 1000 fragments* **2014**.
(65) Nadin, A.; Hattotuwagama, C.; Churcher, I. *Angew. Chem., Int. Ed.* **2012**, *51*, 1114.
(66) Confalone, P. N.; Huie, E. M.; Ko, S. S.; Cole, G. M. *J. Org. Chem.* **1988**, *53*, 482.
(67) De Costa, B. R.; Dominguez, C.; He, X. S.; Williams, W.; Radesca, L.; Bowen, W. *J. Med. Chem.* **1992**, *35*, 4334.
(68) Sato, T.; Yamazaki, T.; Nakanishi, Y.; Uenishi, J.-i.; Ikeda, M. *J. Chem. Soc., Perkin Trans. 1* **2002**, 1438.
(69) Kirira, P. G.; Kuriyama, M.; Onomura, O. *Chem. - Eur. J* **2010**, *16*, 3970.
(70) Nelson, T. D.; Rosen, J. D.; Smitrovich, J. H.; Payack, J.; Craig, B.; Matty, L.; Huffman, M. A.; McNamara, J. *Org. Lett.* **2005**, *7*, 55.
(71) Coppola, G. M.; Damon, R. E.; Eskesen, J. B.; France, D. S.; Paterniti Jr, J. R. *Bioorg. Med. Chem. Lett.* **2002**, *12*, 2439.

(72) Renslo, A. R.; Atuegbu, A.; Herradura, P.; Jaishankar, P.; Ji, M.; Leach, K. L.; Huband, M. D.; Dermyer, M. R.; Wu, L.; Vara Prasad, J. V. N.; Gordeev, M. F. *Bioorg. Med. Chem. Lett.* **2007**, *17*, 5036.
(73) Beck, A. K.; Seebach, D.; Nikonov, G. In *Encyclopedia of Reagents for Organic Synthesis*; John Wiley & Sons, Ltd: 2001.
(74) Gebauer, J.; Dewi, P.; Blechert, S. *Tetrahedron Lett.* **2005**, *46*, 43.
(75) Swarbrick, M. E.; Gosselin, F.; Lubell, W. D. *J. Org. Chem.* **1999**, *64*, 1993.
(76) Beak, P.; Lee, W.-K. *Tetrahedron Lett.* **1989**, *30*, 1197.
(77) Hart, D. J.; Wu, W.-L.; Kozikowski, A. P. *J. Am. Chem. Soc.* **1995**, *117*, 9369.
(78) Pissarnitski, D. A.; Asberom, T.; Bara, T. A.; Buevich, A. V.; Clader, J. W.; Greenlee, W. J.; Guzik, H. S.; Josien, H. B.; Li, W.; McEwan, M.; McKittrick, B. A.; Nechuta, T. L.; Parker, E. M.; Sinning, L.; Smith, E. M.; Song, L.; Vaccaro, H. A.; Voigt, J. H.; Zhang, L.; Zhang, Q.; Zhao, Z. *Bioorg. Med. Chem. Lett.* **2007**, *17*, 57.
(79) Wilkinson, T. J.; Stehle, N. W.; Beak, P. *Org. Lett.* **1999**, *2*, 155.
(80) Beng, T. K.; Gawley, R. E. *Heterocycles* **2012**, *84*, 697.
(81) Beak, P.; Lee, W. K. *J. Org. Chem.* **1993**, *58*, 1109.
(82) Beak, P.; Lee, W. K. *J. Org. Chem.* **1990**, *55*, 2578.
(83) Ashweek, N. J.; Coldham, I.; Haxell, T. F. N.; Howard, S. *Org. Biomol. Chem.* **2003**, *1*, 1532.
(84) Coldham, I.; Copley, R. C. B.; Haxell, T. F. N.; Howard, S. *Org. Lett.* **2001**, *3*, 3799.
(85) Hoffmann, R. W. *Chem. Rev.* **1989**, *89*, 1841.
(86) Firth, J. D. *PhD Thesis, University of York* **2014**.
(87) Adamo, M. F. A.; Aggarwal, V. K.; Sage, M. A. *Synth. Commun.* **1999**, *29*, 1747.
(88) Chackalamannil, S.; Davies, R. J.; Wang, Y.; Asberom, T.; Doller, D.; Wong, J.; Leone, D.; McPhail, A. T. *J. Org. Chem.* **1999**, *64*, 1932.
(89) Chackalamannil, S.; Davies, R.; McPhail, A. T. *Org. Lett.* **2001**, *3*, 1427.
(90) Barker, G.; O'Brien, P.; Campos, K. R. *Org. Lett.* **2010**, *12*, 4176.
(91) Stead, D.; Carbone, G.; O'Brien, P.; Campos, K. R.; Coldham, I.; Sanderson, A. *J. Am. Chem. Soc.* **2010**, *132*, 7260.
(92) Hart, D. J.; Li, J.; Wu, W.-L.; Kozikowski, A. P. *J. Org. Chem.* **1997**, *62*, 5023.
(93) Liu, D.-G.; Gao, Y.; Wang, X.; Kelley, J. A.; Burke, T. R. *J. Org. Chem.* **2002**, *67*, 1448.
(94) Liu, D.-G.; Wang, X.-Z.; Gao, Y.; Li, B.; Yang, D.; Burke Jr, T. R. *Tetrahedron* **2002**, *58*, 10423.
(95) Subramanyam, C.; Chattarjee, S.; Mallamo, J. P. *Tetrahedron Lett.* **1996**, *37*, 459.
(96) Kanayama, T.; Yoshida, K.; Miyabe, H.; Kimachi, T.; Takemoto, Y. *J. Org. Chem.* **2003**, *68*, 6197.
(97) Lorthiois, E.; Marek, I.; Normant, J. F. *J. Org. Chem.* **1998**, *63*, 566.
(98) Sliwinski, É.; Prian, F.; Denes, F.; Chemla, F.; Normant, J.-F. *C. R. Chim.* **2003**, *6*, 67.
(99) Lüthy, M.; Wheldon, M. C.; Haji-Cheteh, C.; Atobe, M.; Bond, P. S.; O'Brien, P.; Hubbard, R. E.; Fairlamb, I. J. S. *Bioorg. Med. Chem.* **2015**, *23*, 2680.
(100) Petersen, M. T.; Nielsen, T. E. *Org. Lett.* **2013**, *15*, 1986.
(101) Perez-Luna, A.; Botuha, C.; Ferreira, F.; Chemla, F. *New J. Chem.* **2008**, *32*, 594.

(102) Wenkert, E.; Dave, K. G.; Haglid, F.; Lewis, R. G.; Oishi, T.; Stevens, R. V.; Terashima, M. *J. Org. Chem.* **1968**, *33*, 747.
(103) Albertson, N. F. *J. Am. Chem. Soc.* **1950**, *72*, 2594.
(104) Noël, R.; Vanucci-Bacqué, C.; Fargeau-Bellassoued, M.-C.; Lhommet, G. *J. Org. Chem.* **2005**, *70*, 9044.
(105) Noël, R.; Vanucci-Bacqué, C.; Fargeau-Bellassoued, M.-C.; Lhommet, G. *Eur. J. Org. Chem.* **2007**, *2007*, 476.
(106) Agami, C.; Dechoux, L.; Ménard, C.; Hebbe, S. *J. Org. Chem.* **2002**, *67*, 7573.
(107) Agami, C.; Dechoux, L.; Hebbe, S.; Ménard, C. *Tetrahedron* **2004**, *60*, 5433.
(108) DeNinno, M. P.; Wright, S. W.; Visser, M. S.; Etienne, J. B.; Moore, D. E.; Olson, T. V.; Rocke, B. N.; Andrews, M. P.; Zarbo, C.; Millham, M. L.; Boscoe, B. P.; Boyer, D. D.; Doran, S. D.; Houseknecht, K. L. *Bioorg. Med. Chem. Lett.* **2011**, *21*, 3095.
(109) Huang, J.; Orac, C. M.; McKay, S.; McKay, D. B.; Bergmeier, S. C. *Bioorg. Med. Chem.* **2008**, *16*, 3816.
(110) Snow, R. J.; Baker, R.; Herbert, R. H.; Hunt, I. J.; Merchant, K. J.; Saunders, J. *J. Chem. Soc., Perkin Trans. 1* **1991**, 409.
(111) Augelli-Szafran, C. E.; Blankley, C. J.; Jaen, J. C.; Moreland, D. W.; Nelson, C. B.; Penvose-Yi, J. R.; Schwarz, R. D.; Thomas, A. J. *J. Med. Chem.* **1999**, *42*, 356.
(112) Showell, G. A.; Gibbons, T. L.; Kneen, C. O.; MacLeod, A. M.; Merchant, K.; Saunders, J.; Freedman, S. B.; Patel, S.; Baker, R. *J. Med. Chem.* **1991**, *34*, 1086.
(113) Yaremenko, A. G.; Volochnyuk, D. M.; Shelyakin, V. V.; Grygorenko, O. O. *Tetrahedron* **2013**, *69*, 6799.
(114) Moos, W. H.; Bergmeier, S. C.; Coughenour, L. L.; Davis, R. E.; Hershenson, F. M.; Kester, J. A.; McKee, J. S.; Marriott, J. G.; Schwarz, R. D.; Tecle, H.; Thomas, A. J. *J. Pharm. Sci.* **1992**, *81*, 1015.
(115) Lyle, R. E.; Perlowski, E. F.; Troscianiec, H. J.; Lyle, G. G. *J. Org. Chem.* **1955**, *20*, 1761.
(116) Nelson, A.; Roche, D. *Bioorg. Med. Chem.* **2015**, *23*, 2613.
(117) Doveston, R.; Marsden, S.; Nelson, A. *Drug Discovery Today* **2014**, *19*, 813.
(118) Doveston, R. G.; Tosatti, P.; Dow, M.; Foley, D. J.; Li, H. Y.; Campbell, A. J.; House, D.; Churcher, I.; Marsden, S. P.; Nelson, A. *Org. Biomol. Chem.* **2015**, *13*, 859.
(119) Schreiber, S. L. *Science* **2000**, *287*, 1964.
(120) Colomer, I.; Adeniji, O.; Burslem, G. M.; Craven, P.; Rasmussen, M. O.; Willaume, A.; Kalliokoski, T.; Foster, R.; Marsden, S. P.; Nelson, A. *Bioorg. Med. Chem.* **2015**, *23*, 2736.
(121) Nortcliffe, A.; Moody, C. J. *Bioorg. Med. Chem.* **2015**, *23*, 2730.
(122) Petersen, M. Å.; Mortensen, M. A.; Cohrt, A. E.; Petersen, R.; Wu, P.; Fleury-Brégeot, N.; Morgentin, R.; Lardy, C.; Nielsen, T. E.; Clausen, M. H. *Bioorg. Med. Chem.* **2015**, *23*, 2695.
(123) Xiao, D.; Lavey, B. J.; Palani, A.; Wang, C.; Aslanian, R. G.; Kozlowski, J. A.; Shih, N.-Y.; McPhail, A. T.; Randolph, G. P.; Lachowicz, J. E.; Duffy, R. A. *Tetrahedron Lett.* **2005**, *46*, 7653.
(124) Beng, T. K.; Woo, J. S.; Gawley, R. E. *J. Am. Chem. Soc.* **2012**, *134*, 14764.
(125) Sheikh, N. S.; Leonori, D.; Barker, G.; Firth, J. D.; Campos, K. R.; Meijer, A. J. H. M.; O'Brien, P.; Coldham, I. *J. Am. Chem. Soc.* **2012**, *134*, 5300.
(126) In *Accerlrys Software Inc.* 2011.

(127) Ghose, A. K.; Viswanadhan, V. N.; Wendoloski, J. J. *The Journal of Physical Chemistry A* **1998**, *102*, 3762.
(128) Ertl, P.; Rohde, B.; Selzer, P. *J. Med. Chem.* **2000**, *43*, 3714.
(129) Burchat, A. F.; Chong, J. M.; Nielsen, N. *J. Organomet. Chem.* **1997**, *542*, 281.
(130) Liljeblad, A.; Kavenius, H.-M.; Tähtinen, P.; Kanerva, L. T. *Tetrahedron: Asymmetry* **2007**, *18*, 181.
(131) Julian, L. D.; Hartwig, J. F. *J. Am. Chem. Soc.* **2010**, *132*, 13813.
(132) Dobbs, A. P.; Guesne, S. J. J.; Parker, R. J.; Skidmore, J.; Stephenson, R. A.; Hursthouse, M. B. *Org. Biomol. Chem.* **2010**, *8*, 1064.
(133) Cheng, C.; Brookhart, M. *J. Am. Chem. Soc.* **2012**, *134*, 11304.
(134) Sugimori, A.; Tobita, E.; Kumagai, Y.; Sat; ocirc; P., G. *Bull. Chem. Soc. Jpn.* **1981**, *54*, 1761.
(135) Christian, N.; Aly, S.; Belyk, K. *J. Am. Chem. Soc.* **2011**, *133*, 2878.
(136) Long, S.; Stefani, F. R.; Biondi, S.; Ghiselli, G.; Panunzio, M. *Bioorg. Med. Chem.* **2013**, *21*, 5811.